Dissertation

# Atmospheric influence on warm water intrusions into Filchner Trough in the 21st century

by
Vanessa Teske

A thesis submitted in partial fulfillment of the requirements of the degree of doctor rerum naturalium (Dr. rer. nat.)

in Faculty 1 - Physics/Electrical Engineering
submitted to the
University of Bremen

Date of colloquium:
31 January 2025


1. Reviewer:
Prof. Dr. Thomas Jung
**Alfred Wegener Institute**, Helmholtz Center for Polar and Marine Research, Bremerhaven
Climate Dynamics
**University of Bremen**

2. Reviewer:
Prof. Dr. Torsten Kanzow
**Alfred Wegener Institute**, Helmholtz Center for Polar and Marine Research, Bremerhaven
Physical Oceanography of the Polar Seas
**University of Bremen**

This dissertation was written in the section of Climate Dynamics of the Alfred Wegener Institute, Helmholtz Center for Polar and Marine Research, Bremerhaven and part of the project *Regional high-resolution Downscaling of Climate Change in the Antarctic* (REDOCCA), funded by the Deutsche Forschungsgemeinschaft.

# Erklärung

Ich erkläre, dass

- die vorliegende Arbeit ohne unerlaubte fremde Hilfe angefertigt wurde,
- keine anderen Hilfmittel und Quellen als die angegebenen benutzt wurden,
- und die den benutzten Werken wörtlich oder inhaltlich entnommenen Stellen als solche kenntlich gemacht wurden.

---

Ort, Datum Vanessa Teske

**Abstract**

Heat transport between the deep ocean and the southern Weddell Sea continental shelf plays a key role in a potential future melting of the western Antarctic ice sheet. Recent studies have highlighted the Filchner Trough as an area for a potential cold-to-warm tipping point in the ocean circulation, governed by the density gradient across the shelf break, influenced by sea ice formation and wind stress.

This thesis firstly explores the representation of on-shore heat transport in the Filchner Trough in climate simulations for a suite of carbon dioxide emission scenarios from high-mitigation to high-emission for the 21st century. The model reproduces observed seasonal pulses of warm water transport into the Filchner Trough, mainly driven by seasonally increased Dense Shelf Water (DSW) formation and export, and a wind driven shoaling of the thermocline at the shelf break. The two high-emission scenarios suggest a strongly increased heat transport onto the continental shelf before the year 2100. Over the course of the 21st century, seasonal pulses increase in temperature and duration until a tipping point is reached and the regime shift occurs.

The effect of sea ice and DSW formation on the continental shelf, as well as the position of the thermocline at the shelf break, are regulated by the atmospheric conditions. Especially temperature and wind fields influence the sea ice formation in coastal polynyas – areas of open ocean surrounded by sea ice, adjacent to the coast and with high sea ice productivity – on the continental shelf of the southern Weddell Sea. While a reference ocean simulation forced with atmospheric data from a high-emission climate simulation does not produce a regime shift, dynamic downscaling of the atmospheric data to 15 km decreases the DSW formation on the shelf enough for a regime shift to be initiated. The better resolution of orographic features decreases the wind speed of the westerlies crossing the peninsula, while stronger offshore winds can be found along several sectors of the coastline of the southern Weddell Sea. The combination of reduced wind-driven sea ice export and higher summer air temperatures decreases the density of the shelf waters at an accelerated rate compared to the reference simulation, making a regime shift possible.

The Antarctic Slope Front prevents the transport of saline Warm Deep Water onto the continental shelf. In the southern Weddell Sea, the density distribution of the front takes on the form of a distinct V-shape, formed by the interplay of Ekman downwelling and DSW export. With the occurrence of a regime shift, the V-shape is temporarily disturbed and confined to the upper ocean afterwards. This shows that a weakening of the Slope Front in the upper ocean is no indicator for an imminent regime shift in the Filchner Trough.

In summary, this thesis examines controls of the heat transport into Filchner Trough for present and future climate and shows that the possibility for a regime shift in the Filchner Trough is high with current climate policies in effect. However, a regime shift might be avoided if global warming is kept below the 2°C limit.

# CONTENTS

CHAPTER

# ONE

# INTRODUCTION

## 1.1 Motivation

Over the last decades, West Antarctica and the Antarctic Peninsula have experienced rapid climate changes with more frequent climate extremes. In February 2022, the Antarctic Peninsula saw a new extreme warm event with record-high melt rates in line with the recent temperature records from 2015 and 2020 (González-Herrero et al., 2023; Gorodetskaya et al., 2023; Turner et al., 2021), followed by an unprecedented heat wave over East Antarctica in March 2022 (Blanchard-Wrigglesworth et al., 2023). However, only small changes have been observed in East Antarctica, where natural variability and the Southern Annular Mode mask much of the climate signal (Jones et al., 2019). In February 2023, a new record minimum in Antarctic sea-ice coverage was reached (Purich and Doddridge, 2023). On top of these isolated events, surface wind speeds above the Southern Ocean have increased and the maximum in the wind speed has shifted southward (Young and Ribal, 2019), precipitation at higher latitudes has increased (Manton et al., 2020), and evaporation over the Southern Ocean decreased (Boisvert et al., 2020).

Antarctica is an important component of the global climate system. The continent plays a pivotal role in the Earth's energy budget, and water masses produced on its shelves are important components of the meridional overturning circulation. Through this close connection to the global circulation, Antarctica has the ability to drive global sea-level rise through ice melting. Along the continental shelves of Antarctica important water masses are formed that are pivotal for the thermohaline circulation (Foldvik et al., 1985).

Over the last one hundred years, global mean sea level has risen by approx. 21 cm (Church and White, 2011). In recent years, increased basal melting and the acceleration of the mass loss of the West Antarctic ice sheet have already contributed 7.9 millimeters of global sea level rise alone between 1992 and 2017 (Shepherd et al., 2018), and this trend might accelerate with continuing climate change (Naughten et al., 2023). Coastal areas are some of the most densely populated areas in the world. The IPCC (IPCC, 2019) estimated in 2019 that approx. 680 million people currently live in low-lying coastal zones. Studies differ between an estimated 187 million people (Nicholls et al., 2011) and up to

649 million people (Hinkel et al., 2014) living in areas flooded by rising sea levels until 2100, depending on sea level estimates and assumed population growths (McMichael et al., 2020). When widening the criterion for areas adversely affected by sea level rise to include coastal floodplains and low-elevation coastal zones, these numbers could grow up to 1.4 billion people as early as 2060 or in more conservative estimates between 493 million and 1.2 billion in 2100 (e.g. Jones and O'Neill, 2016; Neumann et al., 2015; Reimann et al., 2023).

Recent studies show that melting of ice shelves of West Antarctica will most probably increase in the future, accelerating the flow of upstream glaciers to the ocean (Gudmundsson et al., 2019; Naughten et al., 2023). The melting is governed by oceanic heat transport towards the ice shelves of the continent, causing basal melt of the ice shelves. However, the sparsity of observations makes accurate estimates about on-shore heat transport and the resulting ice shelf melt often difficult. This highlights the importance of understanding the processes involved in transporting warm water masses onto the continental shelves of Antarctica and the possible development of on-shore heat transport in the future. One region of particular vulnerability to climate change lies within the southern Weddell Sea. The Filchner Trough on the continental shelf is one of the most prominent regions of dense shelf water formation. At the same time studies have shown that the trough is an area for a possible tipping point that would strongly reduce dense shelf water formation and increase basal melt of the Filchner-Ronne Ice Shelf (Haid et al., 2023; Hellmer et al., 2012; Naughten et al., 2021; Teske et al., 2024b). Reduced dense shelf water export could lead to a slowdown of the global thermohaline circulation, affecting climate even in the northern hemisphere, while higher melt rates of the ice shelves accelerate the mass loss of the Antarctic Ice Sheet.

The possible tipping point in the Filchner Trough involves a switch from a cold water-dominated to a warm water dominated circulation on the shelf, leading to increased heat transport towards the Filchner Ice Shelf. The mechanisms driving the one-shore heat transport for present climate have been the topic of multiple studies. However, the development of heat transport towards the Filchner Ice Shelf front in the future is still an area of some uncertainty.

## 1.2 Structure & objectives of the thesis

In addition to the introduction, this thesis is divided into 6 chapters. Chapter 2 provides the scientific background about the climate system of Antarctica and the circulation and hydrography of the Southern Ocean. Chapter 3 contains information on the methodology, describing in brief the models and the diagnostic tools applied in this study. Based on this and the research objectives explained below, Chapter 4 to Chapter 6 present the main findings. The content of Chapter 3.1 and Chapter 4 are published in *Communications Earth & Environment* (Teske et al., 2024b). The original publication has been attached as Appendix D.1. The content of Chapter 3.2 and Chapter 6 have been submitted to *Ocean Science* (Teske et al., 2024a). The published preprint has been attached as Appendix D.2. Finally, Chapter 7 summarizes the main findings and gives an outlook.

The aim of this thesis is to study the impact of changes in the atmospheric conditions on the ocean circulation and sea-ice formation in the Weddell sea for the 21st century by addressing the following objectives:

1. Assessment of atmospheric conditions, oceanic processes and sea-ice production governing on-shore heat transport in climate runs of present climate

The processes governing heat transport in the form of modified Warm Deep Water onto the continental shelf of the southern Weddell Sea have been well defined from observations and idealized model simulations (Daae et al., 2020; Ryan et al., 2020). The aim is to analyze how well the processes governing the on-shore heat transport like ocean dynamics and sea-ice production are represented in a global climate simulation and in global ocean simulations of recent climate.

2. Assessment of changes in atmospheric conditions, oceanic processes and sea-ice production in climate model simulations for a suite of future emission scenarios

While a lot of studies analyze projections for the future development of the warm water intrusions onto the continental shelf in a warming climate, these are often done in idealized set-ups (e.g. Daae et al., 2020; Naughten et al., 2021). The processes of warm water intrusions and a possible regime shift in Filchner Trough will be explored within the hierarchy of four climate scenarios in global coupled climate simulations as well as two global ocean simulations. The ocean simulations are forced with atmospheric model output from (i) the high-emission scenario simulation with the coupled climate model (SSP3-7.0; coarse resolution), and (ii) with dynamically downscaled atmospheric data for the same scenario (high resolution).

3. Assessment of oceanic processes and sea-ice production in response to changes in atmospheric meso-scale processes

A previous study has shown the influence of resolution of the atmospheric forcing data on sea-ice formation and other processes (Haid and Timmermann, 2013). The two global ocean simulations listed above are analyzed to answer the question of how the polynya and ocean dynamics in the southern Weddell Sea change in response to scenario-based high-resolution atmospheric forcing above Antarctica in comparison to a coarse-scale atmospheric forcing.

CHAPTER

# TWO

# ANTARCTICA'S ROLE IN THE CLIMATE SYSTEM

## 2.1 Antarctica's climate

The climate system is composed of several spheres and their interactions: the atmosphere, the cryosphere, the hydrosphere, lithosphere and the biosphere (Stocker, 2011). All components react on different time scales to external or internal perturbations. While the atmosphere reacts within hours to weeks, the deep ocean or ice sheets react on the time scales of hundreds to thousands of years (Ruddiman, 2014). This thesis will concentrate on certain aspects of Antarctica's atmosphere, cryosphere, and hydrosphere, and skip the influences of lithosphere and biosphere.

### 2.1.1 Atmosphere

Antarctica is the coldest, windiest and driest continent on Earth. Its climate is shaped by the large ice sheet. Antarctica's atmosphere is cold and dry with strong horizontal and vertical temperature gradients (van den Broeke, 2000). The lowest measured air temperature on Earth was measured at the Vostok Station in July 1983 with -89.2°C (Turner et al., 2009). Satellite data collected during the Antarctic polar night shows that snow surface temperatures can reach -90°C or below. Winter mean surface air temperatures at the South Pole are $-59.2°C \pm 1.8°C$ (1981-2010), while coastal regions are warmer and reach mean temperatures between -5.6°C (Neumayer Station III on Ekström Ice Shelf) and 1.3°C (Bellinghausen Station at the Antarctic Peninsula) in summer (Turner et al., 2020).

The polar circulation cell above Antarctica is one of the three primary atmospheric circulations cells in each hemisphere, alongside the Hadley and Ferrel cells, and extends from approx. 60° latitude to the pole. The circulation is driven by cooling above the continent, creating high-pressure areas. The dense air then flows outward towards lower latitudes, where it meets warm air coming from the tropics. The warm air rises again and is returned to the pole. The northward flowing air current is deflected to the west by the Coriolis force, creating predominantly easterly winds above the continent. North of 60° latitude, the circulation is dominated by prevailing westerly winds, a result of Coriolis deflection of the southward trav-

eling air in mid-latitudes (Ruddiman, 2014). The atmospheric circulation variability over Antarctica and the Southern Ocean is dominated by the Southern Annular Mode (SAM), the El Niño-Southern Oscillation (ENSO), and the Pacific South American (PSA) mode. Theses modes are the dominating large-scale atmospheric drivers of Antarctica's surface climate variability (Thompson and Wallace, 2000; Thompson et al., 2000). The SAM, also called Antarctic Oscillation, describes variations in the pressure gradient between Antarctica and the lower latitudes, causing a north-south movement of the westerly wind belt that surrounds Antarctica. Its position determines the strength and location of fronts and storm systems in mid-latitudes, and influences the precipitation patterns over Australia. During a positive SAM event, the belt of westerly winds contracts towards the South Pole. This results in weaker westerly winds and high pressure over Australia, while stronger westerly winds at Antarctica's coast cause Circumpolar Deep Water upwelling onto the continental shelves, driving glacier and ice sheet regression (Rignot et al., 2019). The SAM also influences the temperature distribution in Antarctica. The strengthening of the circumpolar vortex during a positive SAM phase deepens the Amundsen Sea Low, warming the Peninsula and cooling most of the rest of the continent (Marshall, 2007). ENSO has the farthest reach of all climatic cycles on Earth on decadal time scales. During El Niño warm events, a large blocking high-pressure center often forms in the South Pacific, leading to exceptionally high temperatures at the Antarctic Peninsula and even East Antarctica (Turner et al., 2020). The Pacific South American mode primarily affects the climate variability of mid-to-high latitudes of the Southern Hemisphere. It consists of an east-ward propagating wave train extending from eastern Australia to Argentina and is the main connection by which the ENSO anomalies in the tropics reach the high southern latitudes (Mayewski et al., 2009).

### 2.1.2 Cryosphere

The cryosphere of Antarctica consists of the ice sheet covering the continent and the ice shelves and sea ice covering the ocean. Antarctic sea ice is an important component of the global ocean and climate system, and provides a habitat for seals, seabird and Antarctic krill (Turner et al., 2020). A consolidated sea-ice cover isolates the ocean from atmospheric influences including heat transfer and wind stress. In the process of sea-ice formation, brine is rejected and the density of the ocean surface layer increased. This mechanism produces Dense Shelf Water (DSW) on Antarctica's continental shelves, which is the basis for Antarctica Bottom Water (AABW) and thus a driver of the global thermohaline circulation (Foldvik et al., 1985; Jacobs, 2004). Areas of intense sea-ice formation can be found in polynyas along the coasts and ice shelf fronts. Coastal polynyas are areas of high radiative cooling of the ocean with enhanced sea-ice production (Tamura et al., 2016). Through the continuous export of freshly formed sea ice and renewed freezing, driven by prevailing winds and ocean currents, these areas are sources of High Salinity Shelf Water and DSW.

Antarctica's ice sheet contains 90 % of the global ice mass. This ice volume translates to a sea level rise equivalent of 57.9 m (Morlighem et al., 2020). The ice sheet covers 89 % of Antarctica and reaches elevations larger than 4000 m. Ice shelves, floating extensions of the ice sheet, surround the continent. They develop when the glaciers flowing down from the

ice sheet meet the ocean and lift off from the sea floor. Ice shelves provide buttressing that impedes the advance of the glaciers and stabilizes marine grounding zones (DeConto and Pollard, 2016). The Ross Ice Shelf and the Filchner-Ronne Ice Shelf cover two thirds of the total ice-shelf area, but account for only 15 % of net melting. Half of the meltwater comes from the so called warm-water ice shelves in the Southeast Pacific sector (Rignot et al., 2013), mainly in the Amundsen Sea.

### 2.1.3 Hydrosphere

The oceans play a central role in regulating the global climate. They transport large amounts of heat from the tropics to the poles. Oceans are able to store greenhouse gases and heat, working as a buffer for rapid changes in the climate system by storing and releasing said heat and gases, keeping Earth habitable. The currents of the oceans are driven by the Meridional Overturning Circulation (MOC). In areas of deep-water formation, near-surface water is cooled and brought down by convective mixing. The dense water mass is replaced by new warmer water coming from lower latitudes. Dense, cold water created in the northern polar region is transported at depths of 2000–4000 m into the south polar area where it is joined by dense water spilling over the continental shelves of Antarctica. The dense deep water is then brought to the tropics of the Indian Ocean, where upwelling brings it to the surface and it heats up again. The warm water, joining with a shallow warm current from the Pacific Ocean, flows around the southern tip of Africa and is returned towards the North Atlantic Ocean via the Gulf Stream (Ganachaud and Wunsch, 2003). The best known aspect of MOC is the thermohaline circulation, driven by meridional density gradients. Cooling and densification of surface waters in the polar regions lead to downwelling. In areas of wind-driven upwelling turbulent mixing with shallower water adapt the density to the overlying layers of the ocean (van Aken, 2007). Winds and tides generate internal waves that cause turbulent mixing and drive poleward advection of intermediate waters, closing the circulation loop (Kuhlbrodt et al., 2007; Munk and Wunsch, 1998).

The Southern Ocean is dominated by the Antarctic Circumpolar Current (ACC) and is structured by multiple circumpolar fronts, corresponding to water mass boundaries (Orsi et al., 1995). The southernmost front is the Antarctic Slope Front (ASF), separating coastal waters from the open ocean (Nicholls et al., 2009; Rintoul et al., 2001). The ASF, driven by prevailing easterly winds and Ekman downwelling, protects the continental shelf from inflow of Warm Deep Water (WDW) (Daae et al., 2020). Associated with the ASF, an eastward flowing current, the Antarctic Slope Current (ASC) follows the continental slope of Antarctica westward from Bellinghausen and Amundsen Seas, around East Antarctica and into the Weddell Sea. The ASC is a geostrophic current, created by the increased sea surface elevation towards the coast of Antarctica by Ekman transport and the density gradient across the shelf break (Foster and Carmack, 1976; Gill, 1973; Heywood et al., 2014). Armitage et al. (2018) found that the southward contraction of Westerlies during positive SAM enhances northward Ekman transport, dropping coastal sea level and weakening the ASF and the ASC. In negative SAM phases the opposite happens. While the impact of long-term positive SAM trends on the ASF is uncertain, modeling studies suggest that a

drop in Antarctic coastal sea level could weaken the ASF, leading to shoaling of the isopycnal on the continental slope (Spence et al., 2014, 2017). Similar events take place during El Niño events, where an anticyclonic atmospheric pressure anomaly over the Amundsen and Bellinghausen Seas lead to a weakening of the Antarctic Slope Front in the Pacific Sector of the Southern Ocean (Armitage et al., 2018; Spence et al., 2014).

An important region of DSW formation in the Southern Ocean lies in the Weddell Sea and is the area I will concentrate on in this study. The Southern Ocean connects all major ocean basins and has no meridional boundaries. The ACC in the Southern Ocean is estimated to have a transport of 107-161 Sv in Drake Passage and is thus the strongest current on Earth (Koenig et al., 2014; Renault et al., 2011). The interaction of the ACC and the continental shelf create two large gyres in the Southern Ocean: the Weddell Gyre in the Atlantic sector of the Southern Ocean, and the Ross Sea Gyre in the Pacific sector of the Southern Ocean. The Weddell Gyre is a cyclonic circulation, driven by wind forcing and steered by topography. It transports water from the ACC into the Weddell Sea, forming WDW, the local derivative of Circumpolar Deep Water transported by the ACC.

The ASC transports WDW westward along the continental slope. The WDW current splits at approx. 27°W into two branches, one continuing along the continental slope towards the Antarctica Peninsula, while the other follows the coast along the Brunt Ice Shelf Front and towards the Filchner Ice Shelf (Årthun et al., 2012). The ASC is estimated to transport between 7 Sv and 14 Sv in the Weddell Sea (Graham et al., 2013; Heywood et al., 1998). When crossing the Filchner Trough opening, modified WDW (mWDW) is regularly transported into Filchner Trough. These seasonal pulses were observed in several surveys (Årthun et al., 2012; Darelius et al., 2016; Foldvik et al., 1985; Ryan et al., 2017). The mWDW follows the eastern slope of the Filchner Trough southward, occasionally even reaching as far south as the Filchner Ice Shelf (Darelius et al., 2016). The on-shore transport is driven by DSW export from the shelf (Darelius et al., 2023; Morrison et al., 2020). Other conditions include a shoaling of the thermocline associated with the ASF and freshening of the shelf waters (Daae et al., 2020).

## 2.2 Recent signs of climate change in Antarctica

Antarctica is also affected by climate change, however the large internal multi-decadal variability exceeds the anthropogenic signal by a factor of three, masking anthropogenic warming across the interior of Antarctica during the twenty-first century (Clem et al., 2020). The effects of climate change can be found in, e.g., the increasing melt rates of ice shelves of West Antarctica, rising ocean temperatures, and the changing sea-ice distribution over the last few decades. In contrast to the Arctic, where polar amplification – amplified warming in the polar regions compared to the rest of the globe, caused by ice-albedo feedback effects – has already led to a distinct reduction in sea-ice area and volume since the beginning of satellite observations in the 1970s, sea-ice extent across the Southern Ocean has increased since the late 1970s, only suddenly dropping in 2016 after which sea-ice extent and concentration remained significantly lower than before, probably driven by subsurface ocean warming (Eayrs et al., 2021; Purich and Doddridge, 2023). Since the 1950s, sea surface temperatures

poleward of the ACC have risen by approx. 0.02°C per decade (Armour et al., 2016). Temperatures of the CDW have risen by 0.05°C in the Weddell Sea between 1980 and 2010 (Schmidtko et al., 2014).

The largest atmospheric warming trends were found at the Antarctic Peninsula, while some coastal regions in East Antarctica registered cooling trends (Turner et al., 2020). But also within the continent's interior rising temperatures were observed. According to Clem et al. (2020), the South Pole has experienced a record-high warming of 0.61±0.34°C per decade over the 30-year period of 1989-2018. This warming trend lies within the simulated multi-decadal variability of the combined results of the Coupled Model Intercomparison Project Phase 5 (CMIP5), however within the upper 0.1 % of all simulated trends (Clem et al., 2020). Turner et al. (2020) estimated a warming trend of only 0.29±0.23°C over the period of 1979-2018 at the South Pole, indicating an accelerating warming trend over the last 40 years that might eventually exceed the internal variability. The temperature trends in Antarctica are primarily associated with the variability of SAM (Marshall, 2007), although surface temperatures in the tropical Pacific are also known to play a role, connected through propagating Rossby wave trains from the tropical central Pacific to the West Antarctic (Zhang and Duan, 2023).

Over the last decades ocean surface winds above the Southern Ocean have shown an increase in zonal strength and a poleward shift due to ozone depletion and increased greenhouse gas forcing (Mahlstein et al., 2013; Thompson et al., 2011). Due to the complex feedback mechanisms, the change in atmospheric processes has a strong impact on the ocean and ice systems of Antarctica. Strong westerly winds increase northward advection of cold surface waters in the Southern Ocean through enhanced Ekman transport, but also enhanced upwelling of CDW, which may contribute to enhanced ice shelf melt and reduced sea-ice formation (Eayrs et al., 2021).

Continuous gravity measurements from the GRACE satellites during 2002-2015 have shown that the grounded ice mass of Antarctica is decreasing (Harig and Simons, 2015). Increasing basal melt rates of ice shelves in West Antarctica mainly in the Amundsen and Bellinghausen Seas in recent years have led to thinning of the ice shelves and enhanced seaward ice flow, grounding-zone thinning and retreat (DeConto and Pollard, 2016; Joughin et al., 2014; Pritchard et al., 2012). Other areas in the East Antarctic show small amounts of ice sheet growth, associated with reduced ice stream flow velocities and thickening (Joughin and Tulaczyk, 2002; Pritchard et al., 2012; Shepherd et al., 2012, 2018). However, Antarctica has lost increasing amounts of ice mass over the last decades ranging from approx. $40\,\mathrm{Gt\,y^{-1}}$ in 1979-1990 to $252\,\mathrm{Gt\,y^{-1}}$ in 2009-2017 (Rignot et al., 2019). The mass loss concentrates in areas where warm CDW flows onto the continental shelf and into the ice shelf cavities, increasing basal melting and destabilizing the grounding lines (Jacobs et al., 2012).

Most of the net mass loss is occurring in the Amundsen Sea sector, but observations and modeling studies have shown that in the Weddell Sea especially the Filchner Ice Shelf is susceptible to climate change. The Filchner Trough is a location for a possible tipping point with a regime shift from a cold, DSW-dominated trough to a warm, mWDW-dominated trough within this century (Darelius et al., 2016; Haid et al., 2023; Hellmer et al.,

2012; Nissen et al., 2022). Consequences would include a substantial increase in basal melt rates of the Filchner-Ronne Ice Shelf, caused by the intrusion of mWDW into the cavity (Naughten et al., 2021; Timmermann and Hellmer, 2013). The Filchner-Ronne Ice Shelf is the largest ice shelf of Antarctica, covering an area of approx. 430,000 $km^2$, about 30 % of Antarctica's ice shelves (Rignot et al., 2013). Increasing oceanic heat fluxes and resulting basal melt rates will have consequences for the stability of the Antarctic ice sheet as well as global sea level rise (Timmermann and Goeller, 2017). Projections for the future have shown a possibility of partial loss of the West Antarctic ice sheet by 2050 and complete loss by 2500 if emissions continue unabated, contributing more than a meter of sea-level rise by 2100 (DeConto and Pollard, 2016).

CHAPTER

# THREE

# METHODOLOGY

The following chapter provides a compilation of the methods used in this study. The content of Chapter 3.1 is unchanged from Teske et al. (2024b), the content of Chapter 3.2 is unchanged from Teske et al. (2024a).

## 3.1 The climate model AWI-CM

The simulations were performed with the AWI Climate Model (AWI-CM). It is a coupled model consisting of the Finite Element Sea ice-Ocean Model (FESOM v.1.4) and the atmospheric model ECHAM6, developed by the Max Planck Institute for Meteorology in Hamburg. The components are coupled via the OASIS3-MCT coupler. The ocean-sea ice model FESOM uses unstructured meshes which allow for a variable grid resolution in highly dynamic regions. More information on FESOM is provided by Wang et al. (2014). ECHAM6 is a spectral atmospheric model (Stevens et al., 2013), which was used without any additional modifications or tuning. For more information on the performance of AWI-CM see Rackow et al. (2018a); Semmler et al. (2020); Sidorenko et al. (2015).

The ocean grid 'MR' used in the coupled climate simulations in Chapter 4 has a medium resolution with a resolution distribution following the strategy proposed by Sein et al. (2016, 2017). The resolution is locally increased in areas of high sea surface height variability derived from satellite data and ranges between 8 km and 80 km (de la Vara et al., 2020; Rackow et al., 2018b; Sein et al., 2018). The horizontal resolution in the Weddell Sea varies between 12 km and 40 km. While eddy transport is not resolved, the eddy parameterization has been proven to work well with the mesh resolution used here, producing isopycnals very similar to atlas data (Rackow et al., 2019). The grid has 46 unevenly spaced layers with a minimum layer thickness of 10 m near the surface and a maximum spacing of 250 m at the bottom. The mesh does not include ice shelf cavities. Tides are not explicitly calculated, but the effect of barotropic tides is included in the calculation of the Richardson number as proposed by Lee et al. (2006) and Wang et al. (2014).

The atmosphere component uses the resolution of T127L95. T127 stands for the spectral truncation of wave number 127, which corresponds to approximately 100 km horizontal resolution in the tropics and higher resolution towards the poles. The atmosphere has 95 unevenly spaced layers with lower spacing of the levels near the surface and wider spacing towards the top of the atmosphere.

AWI-CM participated in the sixth round of the Coupled Model Intercomparison Project (CMIP6). The simulations include a historical forcing simulation and four subsequent climate simulations with forcing derived from Shared Socioeconomic Pathways (SSP Eyring et al., 2016; Meinshausen et al., 2020). For the historical time span, five ensemble members were simulated. Preceding the start of the historical simulations a spin-up period was computed. This includes 10 years ocean-only simulation, 500 years of pre-industrial control spin-up with constant pre-industrial forcing and 500 years of piControl from which the historical simulations were branched off in the years 150 (*hist1*), 175 (*hist2*), 200 (*hist3*), 225 (*hist4*) and 250 (*hist5*). The future climate simulations were performed for the scenarios SSP1-2.6, SSP2-4.5, SSP3-7.0 and SSP5-8.5. Only SSP3-7.0 has 5 ensemble members (Semmler et al., 2020). The scenarios SSP1-2.6, SSP2-4.5, SSP5-8.5 and the first member of SSP3-7.0 started from 2014 of *hist1*. The other ensemble members 2 to 5 of SSP3-7.0 were branched off the corresponding historical ensemble members.

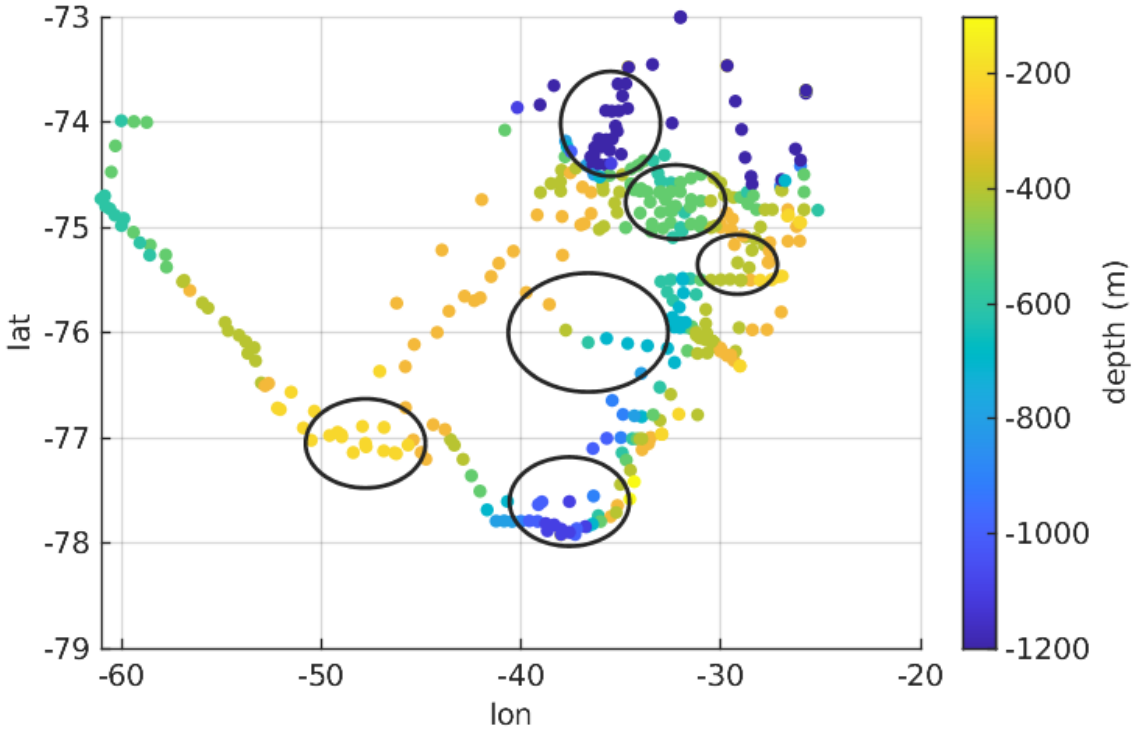


**Figure 3.1: Coordinates and depth of temperature data used for validation.** Key areas: central Filchner Trough (FT), Filchner Sill (FS), Filchner Trough at the Filchner ice shelf edge (FIS), Eastern Continental Shelf east of the Filchner Trough (ECS), Western Continental Shelf west of the Filchner Trough (WCS), and Off-Shore north of the continental shelf (OS). Data points over which the average value difference between observational data and model data has been calculated per area have been outlined in red.

### 3.1.1 Validation

To validate the climate model results we use a data set that has been compiled from in-situ observations by Mathias v. Caspel (pers. comm. 2022). The data set includes salinity and potential temperature from the years 1995 (Schröder, 2010), 2013 (Darelius et al., 2015; Schröder et al., 2014), 2016 (Schröder et al., 2016, 2019) and 2018 (Janout et al., 2019) at depths between 100 m and 1200 m in different areas of the southern Weddell Sea. We choose six key areas as shown in Fig. A.9 for validation: central Filchner Trough (FT), Filchner Sill (FS), the Filchner Trough at the Filchner ice shelf edge (FIS), the continental shelf east of the Filchner Trough (ECS), the continental shelf west of the Filchner Trough (WCS), and at 74°S off-shore of the continental shelf (OS). The locations were chosen to be representative for specific water masses.

We interpolated the model results vertically for temperature and salinity onto the greatest depth at each observation location, and interpolated between the three nearest horizontal grid points. The resulting temperature and salinity values were then compared to the observational data. From these differences we calculated the average difference and standard deviation in each key area, displayed in the flags of Fig. 4.5a and Fig. A.4a.

### 3.1.2 Calculation of diagnostic properties

The Antarctic Slope Front (ASF) is defined as the boundary between the continental shelf water masses and the denser and warmer (m)WDW of the slope current. To identify this boundary, we use the thermocline and pycnocline between the two water masses. The model data was selected for the area around 70°S as depicted in Fig. 4.8b. For each mesh layer, the data was then averaged in twelve equidistant bins approximately parallel to the coastline. The temperature and density gradients were calculated between the mesh layers, and the depth with the highest gradient between bins selected as the depth of the ASF. The temperature at the slope was calculated by averaging the temperature of the bottom bins. As this includes the surface layer and the bottom temperature at greater depth, the result underestimates the real slope current temperature.

To calculate a measure for the seasonal variability of the mWDW influx into the Filchner Trough, we choose section A approximately perpendicular to the main axis of the Filchner Trough, ranging from 75.95°S 37.31°W to 76.54°S 30.66°W (Fig. 4.2). Along this profile, the spatial maximum of the monthly mean temperature was selected. The seasonal variability was then computed as the difference between the temporal maximum and temporal minimum of the spatial maximum temperature per year.

## 3.2 The ocean model FESOM

For Chapters 5 and 6, ocean model simulations with the Finite Element Sea-ice Ocean Model FESOM-1.4 were performed (Wang et al., 2014). FESOM is a global ocean general circulation model based on unstructured-mesh methods coupled with a dynamic-thermodynamic sea-ice component, also including a representation of ice-shelf cavities (Danilov et al., 2015; Timmermann et al., 2012; Wang et al., 2014). The interaction between the ocean

and ice shelves is governed by the three-equation system that describes the flux of heat and fresh water through an exchange-controlling boundary layer (Hellmer and Olbers, 1989; Holland and Jenkins, 1999). The variable horizontal resolution of the ocean mesh ranges from (minimum) 4 km around Antarctica and its adjacent ice shelf cavities, via 25 km at 75°S in the Weddell Sea, to 250 km at the equator. In the vertical, the mesh has 99 depth levels (z-levels) of varying thickness (Gurses et al., 2019; Nissen et al., 2023). Here, we perform two ocean model simulations forced with atmospheric data from either a global climate model ("REF" simulation throughout the paper) or a higher-resolved regional atmospheric model (referred to as the "FECO" simulation) which will be described in more detail in the following section.

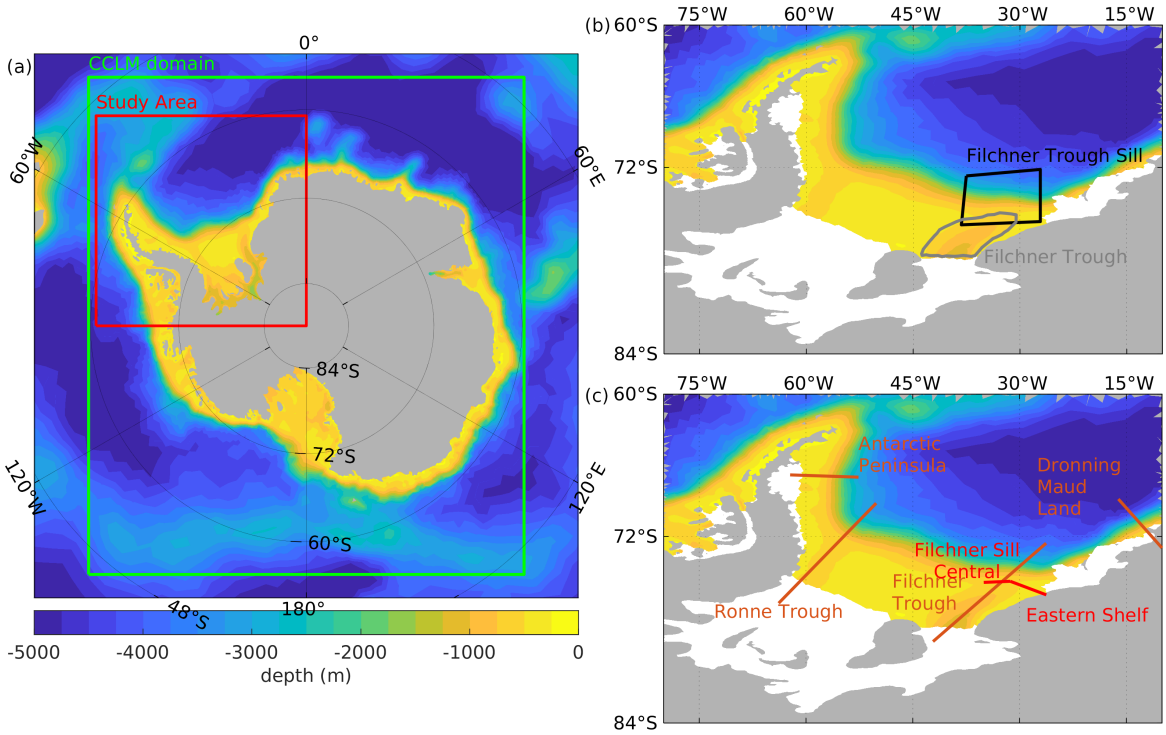


**Figure 3.2:** (a) FESOM bottom topography in the Southern Ocean, study area in the Weddell Sea (red line) and perimeter of the COSMO-Climate Model (CCLM) domain (green line). b) Location of areas and c) sections used in the analysis of Chapters 5 and 6. Areas shaded in white are ice shelves.

### 3.2.1 The atmospheric forcing data

The FESOM reference simulation (REF) is forced with global atmospheric data created with the AWI Climate Model (AWI-CM), a coupled global climate model using FESOM1.4 as the ocean model and ECHAM6.3.04p1 as the atmospheric model component, as a contribution to phase 6 of the Coupled Model Intercomparison Project (CMIP6, see above; Semmler et al., 2020). The atmospheric data resolution ranges from approx. 27 km to 52 km in zonal direction and corresponds to approx. 100 km in meridional direction. Our ocean model simulation is initialized in the year 2000 with FESOM output from Nissen et al. (2023) and is driven by 3-hourly atmospheric output of the historical AWI-CM simulation for the

period 2000 to 2014 and of the future Shared Socio-economic Pathways (SSP) 3-7.0 emission scenario (Meinshausen et al., 2020) projection for 2015 to 2100, identical to Nissen et al. (2023).

The FESOM FECO simulation is forced with a regional atmospheric forcing data set which was created with the COnsortium for Small-scale MOdeling - CLimate Mode model (COSMO-CLM or CCLM; Steger and Bucchignani, 2020; Zentek and Heinemann, 2020), a regional non-hydrostatic atmospheric model with terrain-following vertical coordinates at a horizontal resolution of 15 km. The used CCLM is a polar-adapted version including improved parameterizations for sea ice and the stable boundary layer (see Heinemann et al., 2022, for more details). The model is used in a forecast mode with daily re-initialization and a spin-up of 12 hours. The CCLM domain reaches the northernmost corners at approx. 50°S (Fig. 3.2a). At its lateral boundaries, it is driven by the global AWI-CM data sets described above. Sea-ice concentration and thickness are initially taken from FESOM data of the AWI-CM simulation, but are modified by the parameterizations of grid-scale and sub-grid-scale ice in leads and polynyas. For use as forcing for the global ocean model FESOM, the CCLM output is merged with the global AWI-CM atmospheric output. The merging follows the procedure from Haid et al. (2015) and uses a transition zone of 2° to linearly interpolate between the global AWI-CM data and the regional CCLM data. South of this 2° boundary only CCLM data is applied as forcing, while only AWI-CM data is used outside the CCLM domain. Inside the transition zone, the weighted average depending on the distance to the CCLM domain boundary is used. CCLM data are available for the three timeslices 2000-2014, 2036-2050, and 2086-2100. The following quantities are used from the downscaled CCLM simulations: 2m-temperature, 10m-wind, downward longwave and shortwave radiation at the ocean surface, mean sea level pressure, 2m specific humidity and total precipitation. We ran FESOM simulations forced with CCLM (henceforth called FECO) for each of the three time slices, each preceded by 10 years of spin-up, already driven by the CCLM data (2000-2009, 2036-2045, and 2086-2095, respectively). The spin-ups were branched off the REF simulation in 2000, 2036, and 2086, respectively.

### 3.2.2 The grade of connectivity

For the analysis in Chapter 6, we define the grade of connectivity (GOC) as a metric describing the coherency of the V-shape along the continental slope in a selected sector (here the Filchner Trough Sill, see Fig 3.2b). Motivated by the link between the V-shape and DSW export from the Weddell Sea continental shelf (Baines, 2009; Gill, 1973; Nissen et al., 2022) and on-shelf mWDW transport (Nøst et al., 2011; Stewart and Thompson, 2015a; Thompson et al., 2018), this metric quantifies the modification (or erosion) of the V-shape structure in response to cross-slope currents. The GOC is defined as the normalized zonal mean of the north-south variations of the deepest point of the V-shape in a horizontal plane. To calculate the GOC, we first interpolate the model data from the unstructured grid to a regular grid with a resolution of 0.1° through linear interpolation between FESOM grid points. As a second step, to find the meridional position $y_n$ of the deepest point of the V-shape for each longitude coordinate, we find the horizontal density minimum at the chosen depth by searching for the

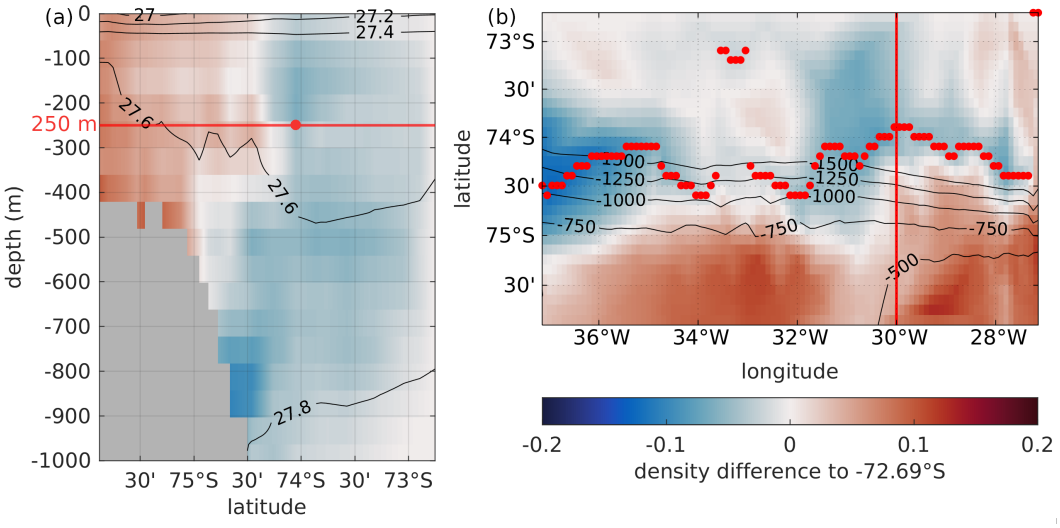


**Figure 3.3:** Section across Filchner Trough sill of the horizontal potential density distribution relative to the level-wise horizontal minimum density in December 2000 to illustrate the connection between the V-shaped density distribution and the grade of connectivity as defined in section 3.2.2. Isolines depict the potential density in $\mathrm{kg\,m^{-3}}$ relative to $1000\,\mathrm{kg\,m^{-3}}$. The red dot marks the location of the minimum density difference at 250 m depth, the horizontal line the position of the level presented in (b). (b) Horizontal projection of the density difference at 250 m depth with bottom isobaths. Red dots mark the location of the meridional minimum in longitudinal increments of 0.1°. The red line marks the location of the section shown in panel (a).

maximum density difference at 250 m depth compared to the northern border of the selected area (here 72.69°S; Fig. 3.3). $\Delta y_n$ then denotes the absolute meridional distance from the neighboring $y_n$. The average GOC is then calculated from monthly mean model output as

$$GOC = \frac{1}{n} \sum_{n} \begin{cases} 1, & if\ \Delta y_n \leq d_L \\ \frac{d_L}{\Delta y_n}, & if\ \Delta y_n > d_L \end{cases} \tag{3.1}$$

where $n$ is the number of grid cells in zonal direction, and the distance threshold $d_L = 0.2°$ is the maximum distance that counts two neighboring density minima as connected. In summary, the GOC is defined as the normalized zonal mean of the north-south variations of the deepest point of the V-shape in a horizontal plane. We normalize by $n$ so that it gives a number between 0 and 1, with lower values indicating a less coherent V-shape along the continental slope and a value of 1 indicating a V-shape without disruptions in longitudinal direction. As such, the GOC allows for a quantitative description of the slope front stability and a quantitative assessment of how this relates to, e.g., on-shelf transport of mWDW.

CHAPTER

# FOUR

## SUBSURFACE WARMING IN THE ANTARCTICA'S WEDDELL SEA CAN BE AVOIDED BY REACHING THE 2°C WARMING TARGET

This chapter is a reformatted copy of the published article of the same title:
Vanessa Teske, Ralph Timmermann, and Tido Semmler, Communications Earth & Environment, 5, 93 (2024). https://doi.org/10.1038/s43247-024-01238-5

The article in its published form is attached as Appendix D.1

V. Teske conducted the analyses and prepared the figures. T. Semmler ran the AWI-CM simulations. All authors contributed to the interpretation of the results and writing of the manuscript.

Recently, seasonal pulses of modified Warm Deep Water have been observed near the Filchner Ice Shelf front in the Weddell Sea, Antarctica. Here, we investigate the temperature evolution of subsurface waters in the Filchner Trough under four future scenarios of carbon dioxide emissions using the climate model AWI-CM. Our model simulates these warm intrusions, suggests more frequent pulses in a warmer climate, and supports the potential or a regime shift from cold to warm Filchner Trough in two high-emission scenarios. The regime shift is governed in particular by decreasing local sea-ice formation and a shoaling thermocline. Cavity circulation is not critical in triggering the change. Consequences would include increased ice shelf basal melting, reduced buttressing of fast-flowing ice streams, loss of grounded ice and an acceleration of global sea level rise. According to our simulations, the regime shift can be avoided and the Filchner Trough warming can be restricted to 0.5°C by reaching the 2°C climate goal

## 4.1 Warm water influx into Filchner Trough

Sea-level rise is one of the pressing topics of future climate change. The Antarctic ice sheet holds an ice volume equivalent to 58 m of sea level rise (Fretwell et al., 2013), but loses mass at an accelerating rate (Shepherd et al., 2018). Melting of the Antarctic ice sheet is dominated by melting at the base of the ice shelves, bodies of ice fringing the ice sheet and floating on the Southern Ocean (DeConto and Pollard, 2016). While most of the ice sheet mass loss currently occurs in the Amundsen Sea (Mouginot et al., 2014; Shepherd et al., 2012), where the cavities are filled with relatively warm water of deep-ocean origin (Arneborg et al., 2012; Jacobs et al., 2012), it has been suggested that a tipping point with a regime shift from cold to warm waters in the cavity and a dramatic increase of melt rates may exist for Filchner Ronne Ice Shelf in the Weddell Sea (Hellmer et al., 2012).

The continental shelf of the Weddell Sea is one of the main areas of dense shelf water production which is a precursor of Antarctic Bottom Water (AABW) and an important part of the global ocean circulation (Foldvik et al., 1985). Any changes to the water masses on the continental shelf can therefore have far-reaching consequences not only for the global sea level, but also for the global overturning circulation.

If such a regime shift occurs, basal melting is bound to increase substantially, causing a reduction of buttressing to the flow of grounded ice (Timmermann and Goeller, 2017) and an additional contribution to global sea-level rise. Model simulations with ocean/ice shelf models and prescribed atmospheric boundary conditions suggest that the occurrence of this regime shift and the magnitude of the anomaly are sensitive to the evolution of the future atmosphere (Naughten et al., 2021; Timmermann and Hellmer, 2013). Pulses of warm water (Hellmer et al., 2012; Timmermann and Hellmer, 2013) and a freshening of the continental shelf and Filchner-Ronne ice shelf cavity have been suggested to be precursors of the eventual tipping.

The circulation in the southern Weddell Sea is dominated by the Antarctic Coastal Current transporting Warm Deep Water (WDW; 0°C to 0.8°C) westwards along the continental shelf break. Mixing with overlying Winter Water (WW) forms modified Warm Deep Water (mWDW; $\Theta$<0°C). At 74.5°S, the current branches, one arm following the shelf break and

the other flowing onto the continental shelf, for example at 28°W (Årthun et al., 2012), 32°W (Foldvik et al., 1985; Nicholls et al., 2009), and 44°W (Nicholls et al., 2008), thereby entering the Filchner Trough. At the Filchner Sill, Dense Shelf Water (DSW), formed by brine rejection through sea-ice formation above the continental shelf, and Ice Shelf Water (ISW) originating from the Filchner ice shelf cavity, leave the continental shelf (Foldvik et al., 1985). They mix with overlying WW and mWDW while sinking along the continental slope. The water masses formed on the way down are Weddell Sea Deep Water (WDSW) and Weddell Sea Bottom Water (WSBS; Foldvik et al., 2004, Fig. 4.1). WSBW remains in the Weddell Sea, confined by the ocean ridges fringing the Weddell Basin. WSDW, in contrast, leaves the Weddell Sea towards the north, feeding the Antarctic Bottom Water in the process (Naveira Garabato et al., 2002).

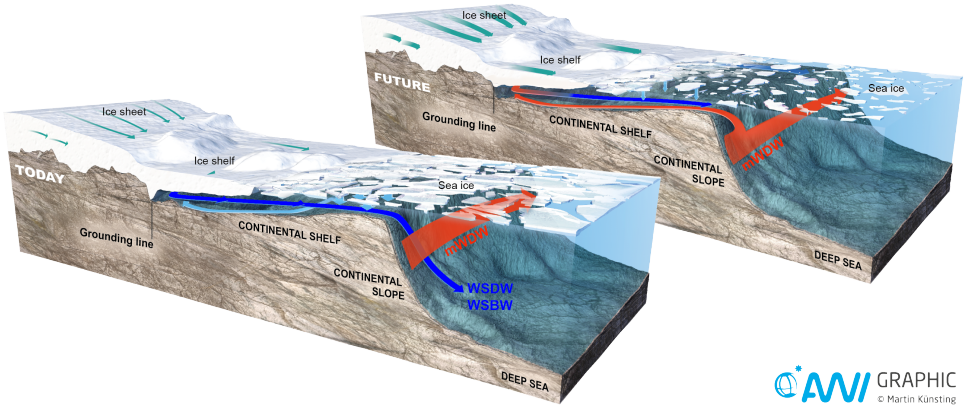


**Figure 4.1: Present and potential future circulation on the continental shelf.** Schematic representation of circulation patterns in the Filchner Trough and the Filchner Ronne Ice Shelf cavity illustrating the regime shift assessed in this study. Today: Trough and cavity are filled with cold shelf water masses. Future: mWDW branches of the slope current, warming the trough and cavity. Graphic created by Alfred Wegener Institute and Martin Künsting. The Alfred Wegener Institute provides permission to reuse it (source: Alfred-Wegener-Institut / Martin Künsting (CC-BY 4.0)).

The mWDW flux onto the continental shelf experiences seasonal variability. It is strongest at the shelf break in summer and autumn (February - April) and weakens in winter (Årthun et al., 2012). The mWDW current then follows the eastern slope of the Filchner Trough southward. March to June, it reaches 76°S (Ryan et al., 2017), and only a short time later 77°S and 78°S (Darelius et al., 2016). By that time its temperature has been reduced to -1.6°C. Observations, limited as they are, have until now only shown mWDW to be present on the continental shelf seasonally (Årthun et al., 2012; Foldvik et al., 1985; Nicholls et al., 2009), however increased shoaling of the WDW in the southern Weddell Sea (Schmidtko et al., 2014), and unprecedented variations in the Weddell Sea sea ice (Turner et al., 2020) might cause changes in the future.

In 2013, mWDW was observed at 78°S near the calving front of the Filchner Ice Shelf

(Darelius et al., 2016), which was then attributed to an uplift of the thermocline at the continental shelf break and an unusually strong coastal current. During the period of extended inflow of mWDW from February to October in 2017, the maximum temperature of the mWDW current was higher by approximately 0.5°C compared to temperatures previously observed at the eastern flank of the Filchner Trough (Ryan et al., 2020).

In numerical model studies, pulses of warm water on the continental shelf and mWDW reaching the ice shelf front have been identified as precursors to a regime shift in the Weddell Sea. They become more frequent in a warming climate and may at some point irreversibly enter the continental shelf and fill the Filchner Ice Shelf cavern, drastically increasing basal melt rates (Hellmer et al., 2012, 2017; Naughten et al., 2021; Timmermann and Hellmer, 2013). This situation compared to the situation in the past is schematically shown in Fig. 4.1. Ice shelf mass loss reduces the buttressing effect of the ice shelf and enhances the flow of grounded ice towards the ocean (Timmermann and Goeller, 2017), thus contributing to global sea level rise. Another precursor that has recently been identified is freshening of the continental shelf due to reduced sea-ice production and increased local sea-ice melting (Naughten et al., 2021). This flips the density gradients between the DSW in the Ronne Depression and the Filchner Ronne Ice Shelf cavity, as well as between the mWDW at the continental shelf break and the ISW leaving the ice shelf cavity. The changes lead to a reverse of the flow direction in the cavity. In these previous studies, this phenomenon has been simulated in regional and/or uncoupled model configurations considering ice shelf cavities and/or with idealised forcing scenarios.

While the connection between the flow of mWDW in Filchner Trough and the increase of basal melt rates in the ice shelf cavity is well understood (Hellmer et al., 2012), if and when the mWDW actually enters the trough has so far been only weakly constrained. This is the gap that we aim to fill. In this study, we analyse a suite of simulations performed with the AWI Climate Model (AWI-CM) for the Coupled Model Intercomparison Project (CMIP6) of the 6th Assessment Report of the Intergovernmental Panel on Climate Change (IPCC) (Eyring et al., 2016; Semmler et al., 2020). AWI-CM is a global coupled climate model with an eddy-permitting ocean component. The simulations were specifically designed to make projections of possible future climate evolution (O'Neill et al., 2016) rather than for specific case studies. Like other CMIP6 models, AWI-CM does not include ice shelf cavities or tides, but it features a horizontal ocean resolution of around 10 km in parts of the Southern Ocean, which is one of the highest in the CMIP6 model suite. The simulations include an ensemble of five historical simulations (hist1 to hist5, 1850 - 2014), and four climate scenarios with forcing derived from Shared Socioeconomic Pathways (Meinshausen et al., 2020)(SSP1-2.6, SSP2-4.5, SSP3-7.0, SSP5-8.5) covering 2015 to 2100. SSP3-7.0 also has five ensemble members.

We evaluate the distribution of mWDW in the southern Weddell Sea (Fig. 4.2) between 2000 and 2014 in the historical simulations, and we examine seasonal and long-term changers in the transport patterns of mWDW in Filchner Trough and attribute their divergent evolution to the spread between the different climate scenarios. We also show that for high-emission scenarios the Filchner Trough experiences a regime shift where the mean temperature in the trough can rise by 2°C until 2100. However, the regime shift can be avoided by limiting global

warming to 2°C or below.

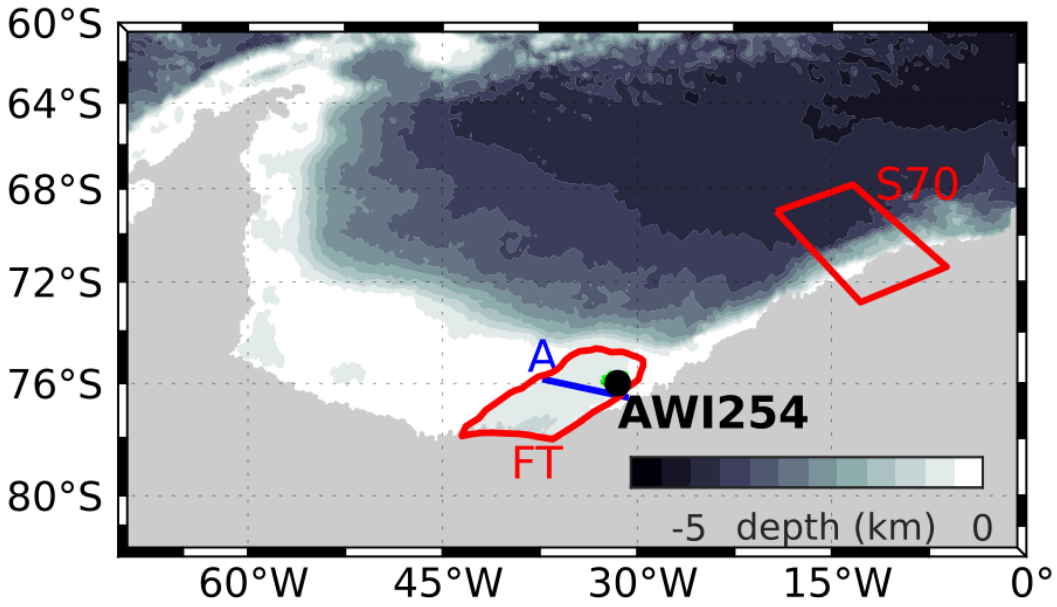


**Figure 4.2: Study area.** Model topography and the outlines of the Filchner Trough (FT) and the area around 70°S (S70) that have been used for mean calculations. The blue line represents section A. While the definition of S70 uses a simple latitude/longitude criterion, a polygon of surface grid nodes is used as a perimeter for the FT area. The bold black dot at 31.5°W 76°S indicates the location of the mooring AWI254 that is referred to in Fig. 4.6 (Schröder et al., 2019). The green area contours the grid nodes over which temperature was averaged for the comparison to AWI254 in Fig. 4.6.

## 4.2 Three phases of climate change

The analysis of the historical simulation and the four different climate scenarios shows the occurrence of pulses of warm mWDW similar to contemporary observations. The pulses have changing characteristics that allow for the definition of three phases. The beginning of each individual phase depends on the climate scenario (Table A.1).

I During the historical simulations (e.g. *hist1* in Fig. 4.3a), the Filchner Trough is filled with cold, dense shelf water with regular phases of weak warming during winter due to a seasonally enlarged (but still weak) inflow of mWDW.

II The beginning of the second phase is defined as the point in time when the mean temperature in Filchner Trough rises above the long-term mean of 1850-2014, i.e. when the annual mean temperature in the trough lies above the mean plus the standard deviation from phase I for longer than two consecutive years. Over the course of this phase, temperature in Filchner Trough is increasingly dominated by pulses of mWDW (Fig. 4.3a), while salinity in the trough slowly declines (Fig. 4.3b).

III The last phase begins when the mean temperature in the trough rises permanently above -1°C. In this state, the trough is mostly filled with mWDW and the seasonal signal has vanished. The mitigation scenario SSP1-2.6 is the only scenario that does not reach this state (Fig. 4.4, Fig. A.1).

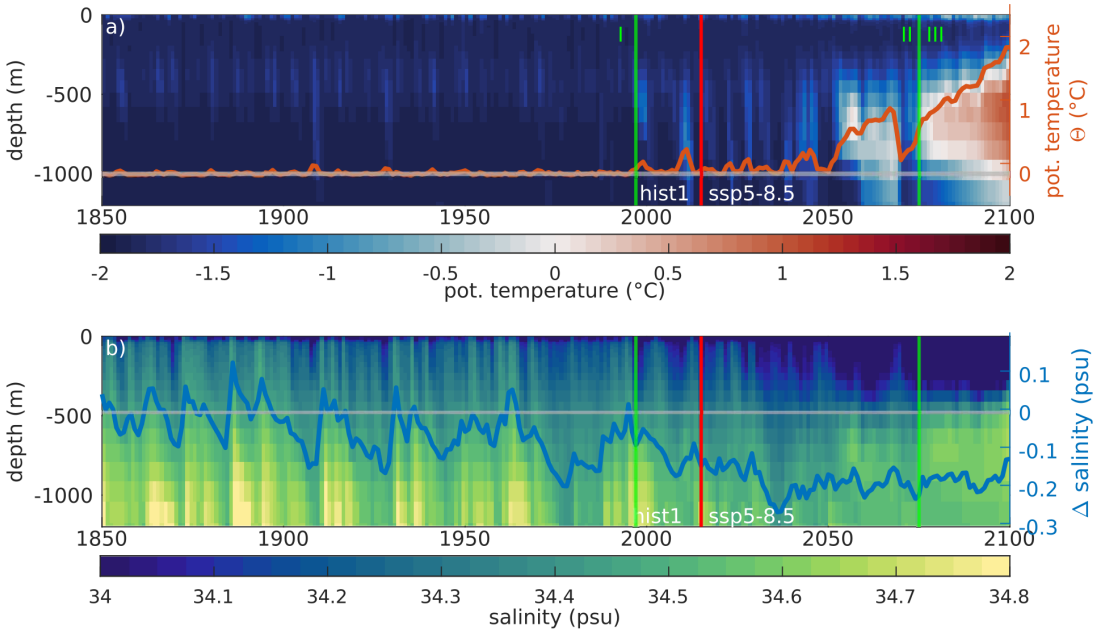


**Figure 4.3: Simulated temperature evolution in Filchner Trough in SSP5-8.5.** a) Hovmoeller plot of the yearly mean potential temperature in Filchner Trough for the historical simulation hist1 and the scenario SSP5-8.5, and the average temperature change (orange) relative to the 1850-1900 mean (gray). The red line marks the transition from historical to scenario simulation. The green lines mark the phase boundaries. b) same as a) but for salinity.

During Phase I, the average temperature in Filchner Trough stays low near -1.8°C and only shows seasonal warming by typically less than 0.25°C relative to the 1850-1900 mean, reaching no higher than -1.5°C (Fig. 4.4). During Phase II, the average maximum temperature of the current reaching the Filchner Trough over all scenarios is increased to -0.41°C ± 0.36°C (sampled at transect A, see Fig. 4.2). The longer the pulse lasts, the warmer the water that is registered in the trough, e.g the pulse in hist1 lasting from 2008 to 2012 reaches a peak temperature that is 0.68°C warmer (potential temperature of -0.19°C) compared to 2007 at its core along transect A. Most shorter warm water pulses show a lower temperature than this and remain below the temperature increase of 0.5°C described by Ryan et al. (2020). All our climate projections show increasing numbers of mWDW pulses entering the Filchner Trough during the second phase (Fig 4.4). The frequency of these pulses stays relatively constant until 2050.

In the second half of the 21st century, the multi-year intrusions of mWDW increase in length and frequency depending on the forcing scenario. While SSP1-2.6 remains in Phase II and returns to its DSW-filled state after each pulse (Fig. 4.4a), the SSP2-4.5 scenario transitions into Phase III during the last four years of the simulation with a warmer state than the SSP1-2.6 but colder than the temperatures reached in SSP3-7.0 or SSP5-8.5 (Fig. 4.4b).

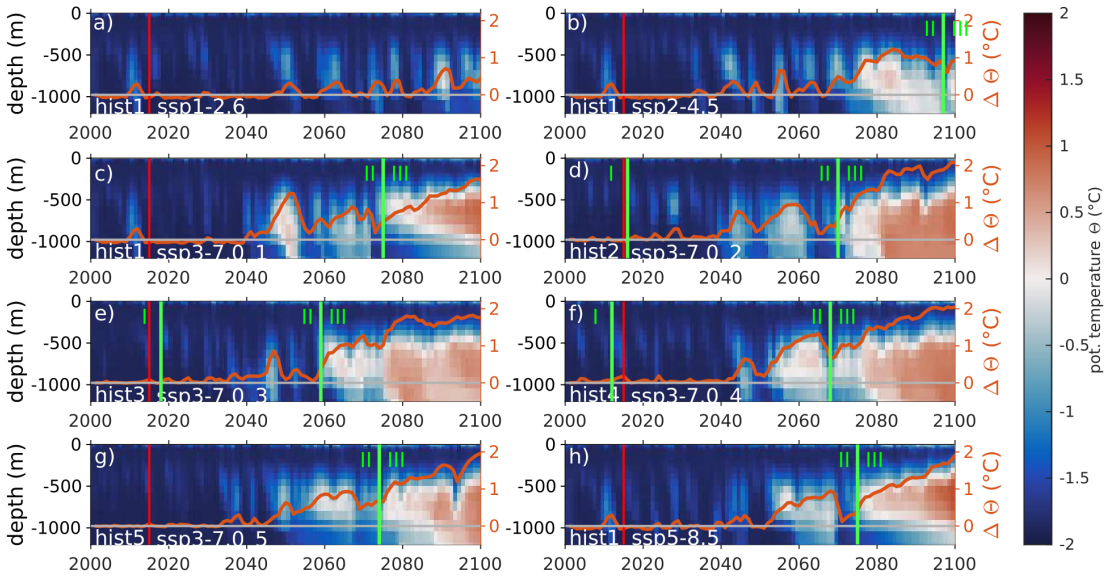


**Figure 4.4: Simulated potential temperature evolution in Filchner Trough for four climate scenarios.** Hovmoeller plots of the yearly mean potential temperature in Filchner Trough from the year 2000 to 2100, with the average temperature change in the Filchner Trough relative to 2000 shown in orange, for the climate scenarios: a) SSP1-2.6, b) SSP2-4.5, c)-g) SSP3-7.0 (five ensemble members) and h) SSP5-8.5. The vertical red lines divide the timeline into the historical simulations (before 2015) and the future climate scenarios (from 2015 onward). Green lines mark the phase boundaries.

It is unclear if the warm state would be maintained or the trough would return to a colder temperature if the scenario continued beyond the year 2100. In the SSP3-7.0 ensemble and in SSP5-8.5, the trough clearly shifts to a consistently warmer state (Fig. 4.4c-h). In these two higher-emission climate projections, the Filchner Trough in Phase III stays warm and is filled with mWDW. For this particular aspect, results from the SSP5-8.5 lie within the spread of the SSP3-7.0 ensemble.

The observation of an especially warm and prolonged mWDW presence on the continental shelf during 2017 (Ryan et al., 2020) suggests that the Filchner Trough in reality is either on the brink of transitioning or it has already transitioned into Phase II.

## 4.3 Evaluation of circulation characteristics

### 4.3.1 Present mean state

A particular feature of our climate model simulations is that for a global coupled climate model, many aspects of the results of the historical simulations for the period 2000-2014 are in remarkably good agreement with observations in key areas around the Filchner Trough (Fig. 4.5a, Fig. A.4a, for the definition of key areas see Methods and Fig. A.9). Due to the high variability of the water mass properties on the continental shelf and the fact that model years in a climate model do not reflect the actual year-to-year evolution, a direct comparison of the model results with hydrographic measurements taken as a snapshot or over a short

period of time is difficult. The position and strength of the modeled mWDW current shows a strong interannual variability (Fig. A.5) that can cover the true variations only with regard to their statistical properties. However, the temperature and salinity distributions in key areas show a similar pattern in the model results as in observations, indicating that the model can reproduce the main features and processes that define the circulation in the Weddell Sea, even without ice shelf cavities (Fig. 4.5, Fig. A.4a). The most important water masses and circulation features in the western Weddell Sea, except for Ice Shelf Water (ISW), can be clearly identified. The simulations do not produce ISW due to the absence of ice shelf cavities in the model grid. The coldest water mass in the Filchner Trough has in-situ surface freezing temperature (approx. -1.9°C). However, all other water mass properties compare well with observations even quantitatively (Fig. 4.5a, Fig. A.4a).

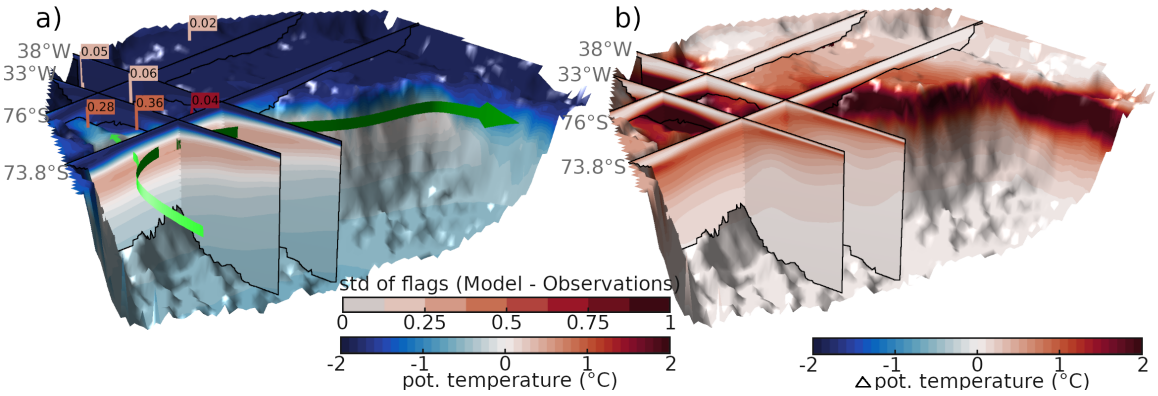


**Figure 4.5: Simulated potential temperature distribution and evolution in the southern Weddell Sea.** a) Potential temperature in a 15-year average of the ensemble mean of the historical scenario (2000 to 2014) at the sea floor and at sections along 33°W, 38°W, 73.8°S and 76°S with differences to observational data (flags Janout et al., 2019; Schröder, 2010; Schröder et al., 2014, 2016, 2019). Arrows indicate the slope current of WDW and mWDW flowing along the continental shelf break and onto the shelf. Upper colorbar: standard deviation of difference of model data to observational data in averaged key areas (flag color), lower colorbar: potential temperature along sections and sea floor. b) Change in potential temperature in the 15-year average 2086 to 2100 to compared to a) in the ensemble mean of SSP3-7.0.

Large-scale circulation features two cyclonic cells forming the Weddell Gyre (Fig. A.2a) as has been suggested by earlier model studies (Beckmann and Hellmer, 1999). The volume transport of the simulated Weddell Gyre is 46 Sv at the Prime Meridian and thus similar to observational data (Klatt et al., 2005; Reeve et al., 2019) (Fig. A.2b). Transport by the ACC across 60°W amounts to 170 Sv and is therefore on the high side of observation-based estimates (e.g., 107-161 Sv in Drake Passage (Koenig et al., 2014; Renault et al., 2011)). The Antarctic Slope Current transports mWDW with a potential temperature $\theta$>0°C along the continental slope southward (Fig. 4.5a). The main current turns west at about 74°S and follows the continental slope towards the Antarctic Peninsula (Fig. A.3). A side current branches off and cooler mWDW flows onto the continental shelf east of Filchner Trough and along the trough's eastern slope, indicated by a warm signature with temperatures between -0.5°C and 0°C on the eastern continental shelf, and approximately -1.5°C over the eastern slope of Filchner Trough (Fig. 4.5a), similar to the observations described by Foldvik et al.

(1985). In the 15-year mean, this southern branch can be traced south to 76°S (Fig. 4.5a). The simulation reproduces WSDW and WSBW in the Weddell Sea with temperatures between -0.8°C and 0°C, and Antarctic surface water with temperatures below -1.5°C and the lowest salinity values in the central Weddell Sea (S<34.3; Fig. 4.5a, Fig. A.4a).

The ensemble mean of the historical simulation is a close match for observational data in key areas in and around Filchner Trough (Darelius et al., 2015; Janout et al., 2019; Schröder, 2010; Schröder et al., 2014, 2016, 2019). In the central Filchner Trough (FT), at the Filchner ice shelf front (FIS), on the continental shelf west of the trough (WCS) and off-shore over the continental slope (OS), the mean ensemble temperature deviates by 0.06°C or less from observation data (flags in Fig. 4.5a). The standard deviation in each of the key region shows that the largest variations in the deviation between model and observations are found at the off-shore location, caused by a varying depth of the ASF. The largest positive temperature bias can be found on the eastern shelf and on the eastern slope of the Filchner Trough, areas that are subject to strong annual and interannual variability due to the varying mWDW flux. This area is 0.36±0.36°C warmer in the model average than in the observations. The bottom salinity of the ensemble mean ranges from 34.33 on the Berkner Shelf to 34.58 in the Filchner Trough and deviates by 0.12±0.06 psu from observations (Fig. A.4a). The model trough is filled with DSW with a minimum simulated temperature of 1.9°C. Generally, the model results are slightly warmer and fresher on the continental shelf than observational data suggest.

The circulation on the shelf agrees well with observed patterns in most areas outside of the ice shelf cavities (Foldvik et al., 1985; Nicholls et al., 2009). We identify three major areas of dense water overflow: the Filchner Sill, the center of the southern Weddell Sea continental shelf at approx. 47°W, and north of the Ronne Trough (Fig. A.3). Because of the lack of an ice shelf cavity, High Salinity Shelf Water/DSW produced in the Ronne Trough flows northward towards the Antarctic Peninsula and not through the cavity towards the Filchner Trough (Foldvik et al., 1988; Nicholls et al., 2001).

### 4.3.2 Seasonality

Phase I (as defined above) is characterized by a seasonal influx of varying length of mWDW into Filchner Trough, which increases the mean temperature in the trough during winter. The model results show the main transport of mWDW into the Filchner Trough taking place via the continental shelf east of the Filchner Trough (Fig. 4.5a, Fig. A.3), while occasionally smaller currents enter the trough over the central and western depression (Fig. A.5), reproducing observed patterns (Årthun et al., 2012; Janout et al., 2021; Nicholls et al., 2009). The warm water takes several months to travel from the slope southward before going west, down the slope into the trough.

The seasonal influx of mWDW onto the shelf east of Filchner Trough and along the eastern slope of the trough was reported to be the strongest during February to June and weaker during the spring and summer months (Årthun et al., 2012; Darelius et al., 2014, 2016; Ryan et al., 2017). Mooring data (AWI254) from 31.5°W 76°S shows the warming onset caused by mWDW during late March, early April (Fig. 4.6a, (Schröder et al., 2019)).

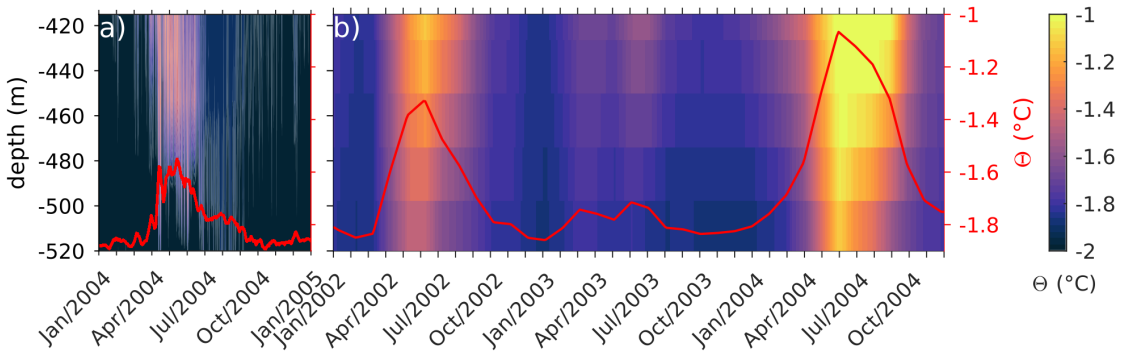


**Figure 4.6: Hovmoeller diagrams of potential temperature at mooring AWI254 (31.5°W 76°S).** a) mooring data from January 2016 to December 2016 (Schröder et al., 2019), b) Model output for the area outlined in green in Fig. 4.2 for 2002-2004. The red lines indicate the temperature averaged between 410 m and 520 m. In a) a a five-days running mean was applied to the vertically averaged temperature data. The temperature and depth scales are valid for both panels.

However, (Ryan et al., 2017) reported the presence of mWDW at 31°W already starting in January. To compare the model output to the mooring observations, we compute an area-weighted temperature average over the area outlined in Fig. 4.2. We see similar behaviour in the simulation as in the observations (Fig. 4.6b). MWDW generally starts to arrive at 76°S during March, however as the examples show, the onset can vary by several months and in strength. The timing of the maximum temperature varies between February and June (Ryan et al., 2017, 2020), and so does the timing in the simulations.

During April to August the model results show an intensification of the northbound transport of DSW along the western slope of the Filchner Trough (Fig. 4.7), caused by a higher sea-ice production over Berkner Shelf in autumn and winter. Morrison et al. (2020) proposed that northward DSW transport in a canyon or trough leads to a gradient in sea surface height due to the replacement of less dense water along the western canyon slope with DSW. This creates a barotropic pressure gradient which drives more lighter AASW and mWDW from the northeast into the trough (Morrison et al., 2020, their schematic in Fig. 5A). Given that our model results show similar characteristics in the density distribution across the Filchner Trough and a difference in sea surface height between eastern and western slope of the trough (Fig. 4.7), we conclude that the mechanism proposed by Morrison et al. (2020) offers a plausible explanation for the timing and structure of the seasonal mWDW inflow both in the model and in reality. The intensification of the north-bound transport and the simultaneously increased presence of denser water in autumn strengthen the pressure gradient across the trough and bring more mWDW into the trough, leading to the observed seasonal increase in temperature.

As an additional component, the depth of the thermocline at the continental slope also shows a weak seasonal oscillation. It rises during spring and summer, and deepens during autumn and winter. This facilitates the flow of mWDW onto the continental shelf during summer, when the thermocline is at its shallowest. The mWDW then takes two to three months to reach the Filchner Trough.

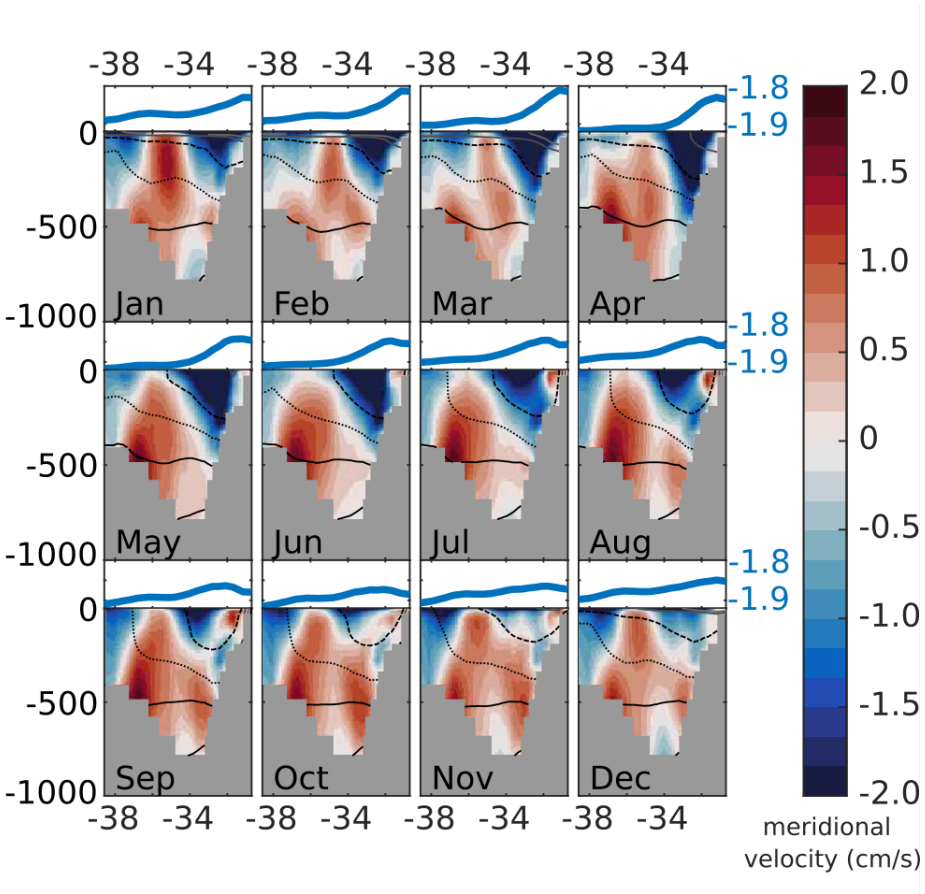


**Figure 4.7: Mean seasonal cycle across Transect A.** The line plot in blue shows the sea surface elevation (ssh in m). The panel below shows the meridional velocity component (m/s) as background color, with isopycnals (black: 27.7 kg/m³, dotted: 27.6 kg/m³, dashed: 27.5 kg/m³, gray: <27.5 kg/m³) for the simulated monthly means of 2000-2014. Positive numbers for the velocity (i.e. reddish colors) indicate northward flow.

## 4.4 Future evolution

During the climate projections for the 21st century, the characteristics of the water mass filling the Filchner Trough change significantly. Some of these changes can already be observed at the end of the historical simulations when the Filchner Trough reaches Phase II. Causes for these changes can be found in the local sea-ice formation as well as upstream, and in the position and temperature of the Antarctic Slope Current. The mechanism behind the increased presence of mWDW on the shelf is different from the one responsible for the seasonal variation. It will be described in the following.

### 4.4.1 Changes in Filchner Trough

In the emission scenario SSP3-7.0, the mean water temperature in Filchner Trough is warmer by approx. 2°C (Fig. 4.8a) and saltier by less than 0.2 psu (Fig. A.1c-g, Fig. A.4b) by the end of the century, showing the permanent presence of mWDW. Salinity of near-surface water on the continental shelf, however, has decreased by up to 0.8 psu, following a decrease in sea-ice formation (Fig. 4.8a). Further changes occur along the continental slope, where the

slope current warms by up to 1°C Fig. 4.5b, Fig. 4.8a). The high-emission scenario SSP5-8.5 shows similar warming patterns with an even further increase in bottom temperature on the continental shelf at the Berkner Bank and north of the Ronne Trough (temperature anomaly between 1.5°C and 1.8°C). The mitigation scenarios SSP1-2.6 and SSP2-4.5 show a similar distribution of warming water, but the temperature rise in Filchner Trough is limited to 1°C or less. The average salinity in Filchner Trough increases in SSP3-7.0 and SSP5-8.5 where mWDW, with a higher salinity than the fresher DSW, is registered permanently in the Filchner Trough (Fig. 4.3b, Fig. A.1c-h, Fig. A.4b).

In all scenarios, the increase of the average temperature in the Filchner Trough accelerates during Phase II. During the 2030s, the average temperature in the trough for the ensemble mean of SSP3-7.0 rises from -1.75°C to -1.6°C (thick red line in Fig. 4.8a), while temperature in SSP1-2.6 (thin red line in Fig. 4.8a) decreases slightly. Starting from 2040, the average temperature in the Filchner Trough in SSP3-7.0 rises quickly and reaches 0.3°C in 2100, 2°C warmer compared to 2000. This goes hand in hand with a strong decrease of sea-ice formation in the area of Filchner Trough beginning in the early 2030s (thick dark blue line in Fig. 4.8a). In 2000, the model produces on average approx. 2.4 m/yr of sea ice at the Filchner Trough. Towards the end of the century, this reduces to 1.6 m/yr. Changes in the mean temperature in Filchner Trough in the lowest-emission scenario SSP1-2.6 are comparably small. Compared to 2000, mean temperature in SSP1-2.6 increases by 0.15°C until 2050 similar to the higher-emission scenarios, but in contrast to those, temperature rises only by 0.5°C compared to 2000 until 2100. sea-ice formation in the Filchner Trough area does not decrease at all in SSP1-2.6 (thin dark blue line in Fig. 4.8a).

### 4.4.2 Changes upstream of Filchner Trough

While the temperature in Filchner Trough begins to rise in the 2030s and is scenario-sensitive with regard to magnitude and timing of the warming, the temperature of the slope current upstream of the Filchner Trough transporting mWDW towards the southern continental shelf increases over the whole simulation, independent of the climate scenario (orange lines in Fig. 4.8a). In all four scenarios, the average temperature at the bottom of the slope current at about 70°S increases from -0.45°C in 2000 to -0.1°C in 2100 (0.03°C per decade), which is a smaller trend than the CDW warming of approx. 0.05°C per decade that was observed in the Weddell Sea from 1980 to 2010 (Schmidtko et al., 2014). However, the shoaling of the thermocline is scenario-dependent with 10 m per decade in SSP3-7.0 and 7 m per decade in SSP1-2.6 (black lines in Fig. 4.8c).

The shoaling of the thermocline is consistent with observations, but the rate is lower than the 30 m per decade suggested from observations in the Weddell Sea (Schmidtko et al., 2014). The change in depth of the thermocline relates directly to the reduced down-welling at the continental slope (more negative average surface stress curl, gray line in Fig. 4.8c), caused by weakening Easterlies and a southward displacement of the transition zone between Westerlies and Easterlies above the Weddell Sea during January to March (Fig. A.6a). The wind field above the Weddell Sea gains strength during July to August (Fig. A.6b), while during January to March, the 15-year average wind speed above the continental shelf east of

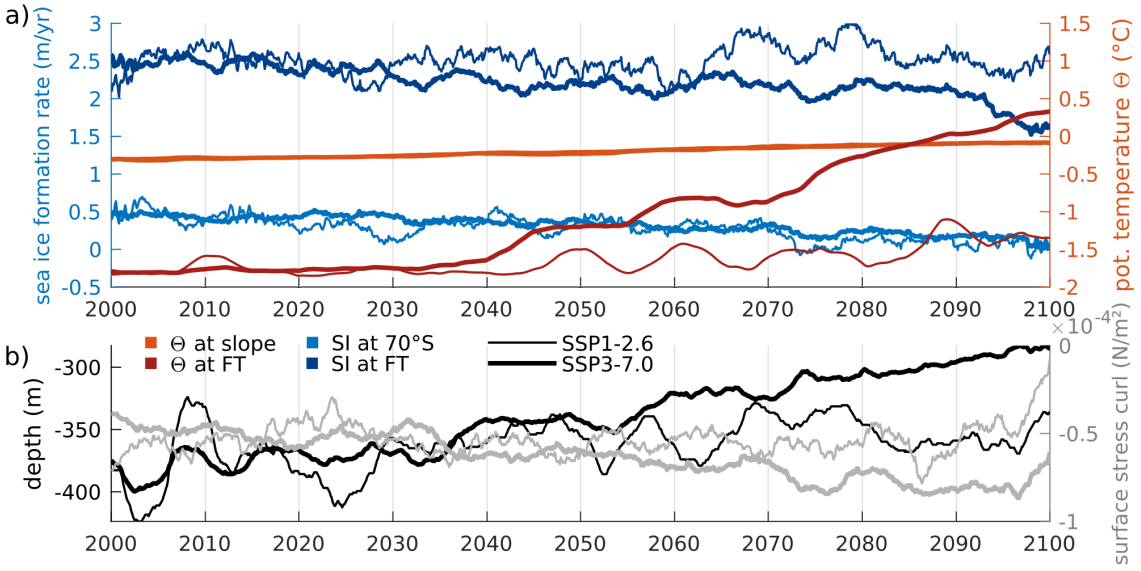


**Figure 4.8: Evolution of temperature, sea-ice formation, thermocline depth, and surface-stress curl in the Filchner Trough and upstream.** (a) 10-year running mean of yearly mean temperature and sea-ice formation rate at the slope at S70 (Fig. 4.2) and in the Filchner Trough for SSP1-2.6 and the ensemble mean of SSP3-7.0. Mean temperature (hues of red) was calculated for Filchner Trough and the bottom layer at the slope at S70. Mean sea-ice formation rate (hues of blue) was calculated for Filchner Trough and at S70. b) Depth of the thermocline at the shelf break (black) and area average of surface stress curl (gray) at S70 in SSP1-2.6 and the ensemble mean of SSP3-7.0.

15°W is reduced by 0.5 m/s between 2000-2014 and 2086-2100.

The decreasing sea-ice formation over the Filchner Sill and growing differences between the climate projections become visible in the sea-ice extent during the second half of the 21st century (Fig. 4.8 & 4.9). Until 2050, the spread between the different scenarios (Fig. 4.9a/b) is not larger than the spread between the different ensemble members for the SSP3-7.0 scenario (Fig. 4.9c/d).

In SSP5-8.5, summer sea ice shrinks until only a small area in the southwestern Weddell Sea remains ice-covered. Average summer sea-ice thickness reduces in the Weddell Sea by up to 1.3 m. In contrast to the other scenarios, SSP1-2.6 shows no further area loss in summer sea ice after 2050 (Fig. 4.9a). While the sea-ice extent in the southeastern Weddell Sea reaches 73°S for 2000 to 2014, ice coverage reduces with increasingly warmer climate until the sea-ice cover in the southern Weddell Sea is confined in summer to south of 74°S by 2050 (Fig. 4.9). Summer sea-ice extent reduces in SSP5-8.5 by $\approx 76\,\%$ in the Weddell Sea from $3.69 \times 10^6$ km$^2$ to $0.88 \times 10^6$ km$^2$. The sea ice opens first along the eastern coast of the Weddell Sea, clearing the Filchner Trough of summer sea ice. By the end of the projected time period, the Filchner Trough is only partly ice-covered (SSP1-2.6, SSP2-4.5) or completely ice-free in summer (SSP3-7.0, SSP5-8.5). The winter sea-ice extent by contrast shows far less variability. The largest changes in September sea ice occur in SSP5-8.5 towards the end of the century. But even though the sea ice extends as far north during the period of 2086 to 2100 as it did in the beginning of the simulation, sea-ice freezing rates during winter are much lower, causing a decrease in sea-ice thickness by up to 1 m in September compared to the historical period

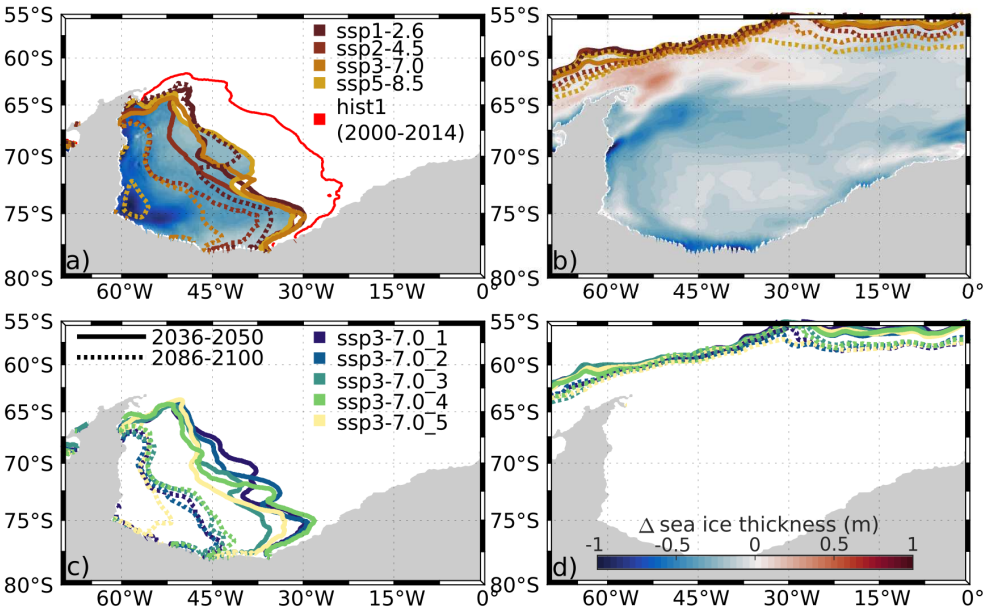


**Figure 4.9: sea-ice extent (threshold: 15 % sea-ice concentration per area) and thickness difference in the historical simulations and for the four different climate scenarios in two 15-year averages.** a) March and b) September sea-ice extent in the Weddell Sea, with results from the historical simulations and SSP3-7.0 being averaged over all five ensemble members (line plots). Shading in the background of a) and b) shows sea-ice thickness difference between the 15-year averages of hist1 (2000-2014) and SSP5-8.5 (2086-2100). c) and d) same as a) and b), but all ensemble members of SSP3-7.0 shown individually.

and reducing the amount of sea-ice melting in summer.

### 4.4.3 Changes of Seasonality

Over the course of Phase II after 2050, the seasonal variation in Filchner Trough temperature decreases more or less strongly, depending on the climate scenario (Fig. 4.10). The weaker seasonal signal is particularly pronounced in SSP3-7.0 and SSP5-8.5 (Fig. 4.10), but it can also be found during a brief period in 2089 and 2090 in SSP1-2.6 (Fig. 4.10a). The connection of the seasonality and the local sea-ice formation becomes only clear when the sea-ice formation is particularly low. In SSP5-8.5, this is the case 2050 onward Fig. 4.10b). Before that, a decrease in sea-ice formation rate does not coincide with lower seasonality. The permanent loss of the seasonal signal marks the transition from Phase II to Phase III as defined above.

## 4.5 Discussion

The present study shows that over the course of this century strong changes in the hydrography of the Filchner Trough are imminent. Already in the present climate, warm water pulses reach the Filchner ice shelf front both in the model simulations presented here and according to observations (Darelius et al., 2016; Janout et al., 2021; Ryan et al., 2020).

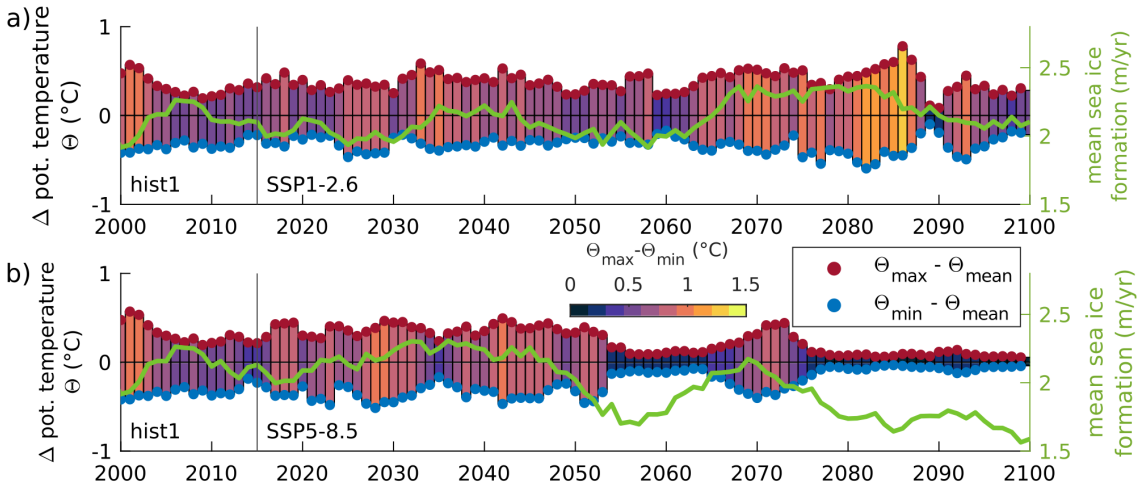


**Figure 4.10: Development of the seasonality of the spatial maximum temperature below 200 m depth along section A.** a) for SSP1-2.6 and b) for SSP5-8.5. Red (blue) dots depict the difference between the temporal and spatial maximum (minimum) of the area to the temporal mean of the spatial maximum along the transect in the Filchner Trough (Fig. 4.8). The bars illustrate the seasonal variation. The green line represents the sea-ice formation in the Filchner Trough.

The comparability between the historical simulations and observations gives confidence into our model projections for the future climate evolution.

It should be noted that in the current simulations ice shelf cavities are not considered. Previous specialized ocean model simulations with ice shelf cavities (e.g. Hellmer et al., 2012; Naughten et al., 2021) showed the same three modes as our CMIP6 simulations: seasonal warm water only in Phase I, intermittent warm water pulses in Phase II (and in present-day climate), and persistent warm water in Phase III, occurring in future climate scenarios with strong emission of greenhouse gases. This implies that cavity circulation is not a critical component in triggering the simulated changes in the Filchner Trough hydrography. Instead, reduced sea-ice formation and changing wind fields play a major role. This concurs with the results from Naughten et al. (2021), who showed that the intrusion of mWDW into the ice shelf cavity can only happen after the density on the continental shelf has reduced to a critical value, therefore sea-ice formation on the shelf has a larger direct impact on the mWDW flux than any processes below the ice shelves.

The amount of heat that reaches the Filchner Trough depends on two factors: The amount of southward transport of (m)WDW onto the continental shelf and the grade of modification of the WDW by vertical mixing through DSW formation (Fig. A.7). Of these two, the first factor depends on the density gradient between the continental shelf waters and the slope current, and on the depth of the ASF at the continental slope. The grade of modification depends on the depth and intensity of convection and thus primarily on the rate of sea-ice formation. However, DSW formation also influences the density gradient at the shelf edge and thus the on-shelf transport. A clear separation between the two processes is therefore not possible, but we conclude that sea-ice formation plays a dominant role in governing the mWDW transport into the trough.

As a caveat, we note that in reality density of the water masses on the continental shelf is clearly influenced by the ISW outflow from under the ice shelf, which may have an impact on the timing of the regime shift we find in the high-emission scenarios. Given that ice shelf melting is a source of freshwater, it could be argued that adding ice shelves to our simulation would reduce the density of water masses on the continental shelf, potentially accelerating the regime shift towards a warm continental shelf. But then, given the very low temperatures of ISW, the mixing product of ISW and (m)WDW is a very dense water mass known to contribute to WSBW formation. A denser watermass on the shelf would potentially delay the regime shift. Which of these effects dominates is not obvious to us, but we note that they counteract each other, which mitigates a potential bias caused by the missing ice shelves in our simulations. A similar case can be made for the fact that we neglect the freshwater input from the ice shelves in the eastern Weddell Sea, upstream of Filchner Trough. In the presence of these ice shelf cavities, we would expect a stronger stratification over the shelf break, strengthening the Antarctic Slope Front (ASF) and reducing the mWDW flux onto the shelf. However, increased freshening of the shelf water masses might also a) cause baroclinic instabilities and thus an uplift of the thermocline (Hatterman, 2018; Nøst et al., 2011) and b) reduce the density gradient between the continental shelf and the Filchner-Ronne ice shelf cavity. Whether the ice shelves in the eastern Weddell Sea rather facilitate or inhibit the flow of warm water into the Filchner Trough is therefore not clear and needs to be addressed in a follow-up study.

While sea ice is the main driver behind the variations of mWDW transport onto the shelf and into the Filchner Trough, the model underestimates summer sea-ice extent in the Antarctic, but slightly overestimates the winter sea-ice extent (Semmler et al., 2020). The smaller sea-ice area in summer might increase heat uptake during the warmest part of the year, creating a feedback loop of warmer sea surface temperatures decreasing and delaying sea-ice formation. This would decrease the modification of WDW so that water closer in temperature to WDW reaches the trough and might cause an overestimation of simulated warming in Filchner Trough in SSP3-7.0 and SSP5-8.5. On the other hand, a reduced summer sea-ice extent leads to additional sea-ice formation in fall and thus additional salt input (similarly to the processes in coastal polynyas), potentially compensating or even overcompensating for the effect of too strong heat uptake in summer.

Despite the caveats outlined above, and given that the sign of the bias each of them could create is not obvious in all cases, we are confident that our main findings are robust. We find a decrease of ASF depth over the course of the high-emission scenario simulations that might facilitate the warm water influx to the Filchner Trough, notably in combination with pronounced density changes on the shelf. The receding sea ice and reduced freezing rates on the continental shelf in a warming climate cause the DSW in the Filchner Trough to freshen, reducing the intensity of vertical mixing between DSW and the underlying mWDW. A decline in density on the shelf weakens the density gradient at the continental shelf break and allows mWDW to flow into the trough (Daae et al., 2020; Timmermann and Hellmer, 2013). This effect is especially large in the high-emission scenarios. Because the sea-ice formation mostly depends on atmospheric processes, the differences in forcing in the SSP scenarios heavily impact changes in sea-ice formation rates in the Weddell Sea.

The uplift of the ASF above the continental shelf in turn is caused by changing wind fields, reducing downwelling at the continental slope by lessening the coastward Ekman transport by easterly winds from January to March. Stronger westerly winds above the central Weddell Sea and a southward shift of the transition zone between Westerlies and Easterlies further decrease areas of downwelling along the coast. The wind above the continental shelf east and north of the Filchner Trough has a much higher westward component during the summer months of the high-emission scenarios SSP3-7.0 and SSP5-8.5 in 2086-2100 compared to 2000-2014. Even though the lower sea-ice concentration in the high emission scenarios should increase the wind stress on the ocean, the effect is balanced by weaker wind during summer, a northwest-going wind field during the following months promoting upwelling along the coast, and reduced erosion of mWDW on the continental shelf by sea-ice formation during the following autumn and winter.

There is a clear seasonality in the mWDW influx both in our model simulations and according to Darelius et al. (2016) as well as Ryan et al. (2017, 2020). While Ryan et al. (2020) attribute the seasonal inflow of mWDW to an inflow of freshened shelf waters from the coast of Dronning Maud Land, causing baroclinic instabilities and lifting the thermocline, we mainly attribute this seasonal inflow to the autumn maximum in local sea-ice production. According to Morrison et al. (2020), sea-ice formation causes increased DSW production and northbound transport in the Filchner Trough and establishes a pressure gradient across the trough that fosters the near-surface inflow of mWDW.

The sea-ice decrease towards the end of the century in the high-emission scenarios, especially in thickness, is caused by the increased heat flux from the atmosphere. Higher CO2-concentration in the atmosphere escalates the greenhouse gas effect and changes the heat flux in the western Weddell Sea from net heat loss to heat gain (Fig. A.8), warming the ocean and reducing sea-ice formation. The southward displacement of the wind belt, stronger variability of the wind fields and strengthening of the wind field increase the off-shore sea-ice transport and cause stronger sea-ice deformation, which could potentially increase sea-ice formation rates. However, weakening easterlies above the continental shelf in the eastern Weddell Sea during summer and a stronger heat flux towards the ocean counteract this effect, increase sea surface temperature and lead to thinning of the sea ice in the Weddell Sea. The driving factor behind the reduced sea-ice formation is therefore not the wind but the increased heat flux at the surface during the climate scenarios.

Towards the end of the century, the general decrease in sea-ice formation in the simulations leads to a decrease in the strength of the seasonal signal of the mWDW. The reduction of the density of the DSW outflow along the western slope of Filchner Trough causes a weakening of the across-trough pressure gradient during winter. The reduced sea-ice production weakens the convection in winter, when in the present state the flow of mWDW is eroded by deep vertical mixing triggered by sea-ice formation. Together with the uplift of the thermocline above the continental shelf break (Fig. 4.8b), the weaker winds during the following summer months prolong the time where mWDW intrusions are possible, leading to a year-round presence of mWDW on the shelf. A regime shift occurs when DSW production in the Filchner Trough and surrounding continental shelf is not sufficient anymore to erode the inflow of mWDW into the trough during winter and spring. This point is reached between

2070 and 2080 in the high-emission scenarios SSP3-7.0 and SSP5-8.5, confirming the timing suggested by previous numerical model simulations with different, prescribed atmospheric forcing (Daae et al., 2020; Hellmer et al., 2012, 2017; Timmermann and Goeller, 2017; Timmermann and Hellmer, 2013).

An important finding in our model results is that sea-ice formation and extent, temperature in Filchner Trough and depth of the ASF all really start to differentiate between the different SSP scenarios in the 2040s. The slope current temperature even does not vary between the scenarios at all until 2100. This indicates that any endeavors to change the course of the current and future climate development will only start to show results in 20 to 30 years or later. If we as humanity do not change our habit of emitting greenhouse gases soon, the pulses of warm water reaching the continental shelf could be replaced by a permanent warm water flow (according to the strong emission scenarios SSP3-7.0 and SSP5-8.5). The presence of this warm water is bound to increase ice shelf basal melt, leading to a thinning of the ice shelf, a reduced buttressing to the ice flow, and additional sea-level rise. If a marine ice sheet instability is triggered, this process is self-sustained and can accelerate even if the original perturbation (here: the warm water inflow) is removed. If we do make the effort to restrict greenhouse gas emissions substantially, we could preserve the state of intermittent pulses of warm water reaching the continental shelf and possibly restrict ice shelf melting. According to our findings, a regime shift towards a warm cavity under Filchner Ronne Ice Shelf with strongly increased basal melt rates and an increased contribution to global sea-level rise can only be sustainably avoided by reaching the 2°C (SSP1-2.6) climate goal. With the SSP2-4.5 scenario, restricting the global warming to 3°C, no regime shift to a permanent warm inflow occurs in our simulation until 2100, but the water in Filchner Trough still warms by 1°C in this scenario. Whether this may still trigger a marine ice sheet instability or leads to the crossing of any tipping point with a large impact on global sea-level rise is a topic of ongoing research.

CHAPTER

# FIVE

## COASTAL POLYNYA EVOLUTION IN THE WEDDELL SEA IN A WARMING CLIMATE

The density distribution on the southern Weddell Sea continental shelf is strongly influenced by the local sea-ice formation. One of the hot spot for sea-ice formation are coastal polynyas, and the development of coastal polynyas strongly depend on atmospheric conditions. The sensitivity of coastal polynyas in the south-western Weddell Sea to meso-scale atmospheric processes in a warming climate is investigated with the Finite-Element Sea ice-Ocean Model (FESOM) in two 21st-century ocean-only model simulations for a high-emission climate scenario, forced with atmospheric model output of a global climate simulation and a regional atmospheric simulation of different resolutions. A higher resolved atmosphere leads to stronger off-shore winds in regions with strong topographic gradients like Coats Land and the eastern Ronne Ice Shelf front and weakening at the Antarctic Peninsula where the higher resolution is able to resolve the mountain range, which reduces the westerly winds crossing the peninsula. In combination with lower air temperature especially during winter, this leads to higher sea-ice production rates in coastal polynyas, however the total polynya area is reduced compared to the reference simulation. At the end of the century, higher resolved atmospheric processes favor the growth of larger polynyas relative to the reference simulation, aided by lower air temperatures creating a larger sea-ice cover. The higher sea-ice melt rates in summer decrease the density on the shelf, creating the right conditions for a regime shift in the Filchner Trough. Despite higher air temperatures in summer, the regime shift is only produced with high-resolution forcing, aided by the low export of sea ice obstructing the formation of additional sea ice. We find that the better representation of orographic features in the high-resolution simulation shows the importance of the interplay between wind-driven sea-ice export and local sea-ice formation for the dense water mass formation on the continental shelf.

## 5.1 Coastal polynyas in the southern Ocean

Coastal polynyas on the continental shelves of Antarctica are important for the global climate because of their intense sea-ice production and associated brine rejection, forming one of the densest water masses on Earth (High Salinity Shelf Water; HSSW). HSSW is a base for Antarctic Bottom Water, which forms the lower arm of the global thermohaline circulation (Foldvik et al., 1985). Coastal polynyas are areas of open water or thin ice forced by strong offshore winds (Comiso and Gordon, 1996; Tamura et al., 2008), in contrast to open-ocean polynyas, where the openings in the sea-ice cover are forced by diverging ocean currents (Wei et al., 2021). Between 1992 and 1998, sea-ice production in the Ronne Polynya accounted for 6.08 % of total sea-ice production in the Weddell Sea (Renfrew et al., 2002) illustrating the importance of polynyas for sea-ice production.

Model results showe a close relationship between offshore winds and sea-ice production. Strong offshore wind events are typically associated with the passage of synoptic- or meso-scale cyclones. A 2-3 times higher wind speed can increase the sea-ice velocity 3-4 times, decrease sea-ice concentration by 20-40 % and can up to quadruple sea-ice production (Wang et al., 2021). Previous modeling studies have shown that increasing atmospheric resolution intensifies the off-shore component of coastal winds, especially at valleys channeling the katabatic flow (Haid et al., 2015; Huot et al., 2021), caused by better resolved topography

with stronger gradients. With stronger off-shore winds, polynya open wider and more frequently, and dense water production is enhanced. The lack of sea ice along the coast enhances the atmosphere-ocean interaction. Especially the heat flux depends strongly on atmospheric conditions such as air temperature and wind speed (Haid and Timmermann, 2013).

Over the last 44 years there has been a increase in area of Antarctic polynyas across all sectors except the Amundsen and Bellinghausen Seas. Duffy et al. (2024) cite the increasingly positive Southern Annular Mode and more negative Interdecadal Pacific Oscillation index as the cause. The analysis of sea-ice production derived from satellite data and reanalysis data (ERAinterim) showed that the interannual variability of sea-ice production around Antarctica correlates more strongly with the polynya extent than with atmospheric forcing itself (Tamura et al., 2016). This is important in relation to other factors increasing polynya area and occurrence like divergent ocean currents (Arbetter et al., 2004; Morales Maqueda et al., 2004), which a lot of studies, only concentrating on atmospheric causes, neglect.

Future response of coastal polynyas to climate change differ widely between the Arctic and Antarctic. Arctic systems are undergoing the largest, most rapid change and it is expected that polynyas within the Arctic will largely respond by a decrease in the duration each season. The response of Antarctic polynyas is expected to be much less uniform (Smith and Barber, 2007). Modeling studies of the 21st century have shown that a doubling of the atmospheric $CO_2$ concentration until 2100 leads to a decrease in sea-ice production by 6-8 %, however four times the $CO_2$ concentration reduces sea-ice production by 10-30 %. The effect on Dense Shelf Water (DSW) formation in the Weddell Sea is more extreme with an approx. 75 % decrease in a double $CO_2$ world and a complete shut down of DSW formation with four times $CO_2$ (Jeong et al., 2023). Other studies suggest a 40 % - 81 % reduced DSW export in a 2°C warmer world (Marsland et al., 2007).

The spread of existing studies shows the general consensus that the ongoing climate change will impact polynya formation around Antarctica. The scope however needs further analysis. The aim of this study is to investigate the consequences a warming climate of the future Shared Socioeconomic Pathways high-emission (SSP) scenario 3-7.0 has for polynya, sea ice and DSW formation in the southern Weddell Sea under the influence of two atmospheric data sets of different resolutions.

## 5.2 Differences in forcing fields

### 5.2.1 Ten-Meter wind fields

The wind patterns over the Weddell Sea in the AWI-CM dataset for 2000 to 2014 that is used to force the reference simulation, shows mean speeds between 4.5 $ms^{-1}$ at the Filchner Ice Shelf front and >8 $ms^{-1}$ north of the Antarctic Peninsula (shown as REF in Fig. 5.1a). While the northern half of the Weddell Sea is dominated by the strong westerly band that surrounds Antarctica, the southern Weddell Sea continental shelf is influenced by a seasonally changing north-south displacement of the boundary between easterlies above the continent and westerlies (Fig. B.2). Over the course of the year, we see a weakening of the wind field

during summer (Fig. 5.1i), especially at the coast between Brunt and Filchner Ice Shelves and north of the Antarctic Peninsula, but also along the Filchner-Ronne Ice Shelf Front. Towards the end of the century, we find a general strengthening of the wind field (Fig. 5.1c), accompanied by a stronger seasonality in the wind strength. AWI-CM produced stronger wind speeds during the winter seasons between 2086 and 2100 than at the beginning of the century (Fig. 5.1e & g). In the shelf regions of the southern Weddell Sea summer wind speed strongly decreases in comparison to winter wind speeds, but also in comparison to 2000-2014 (Fig. 5.1i & k).

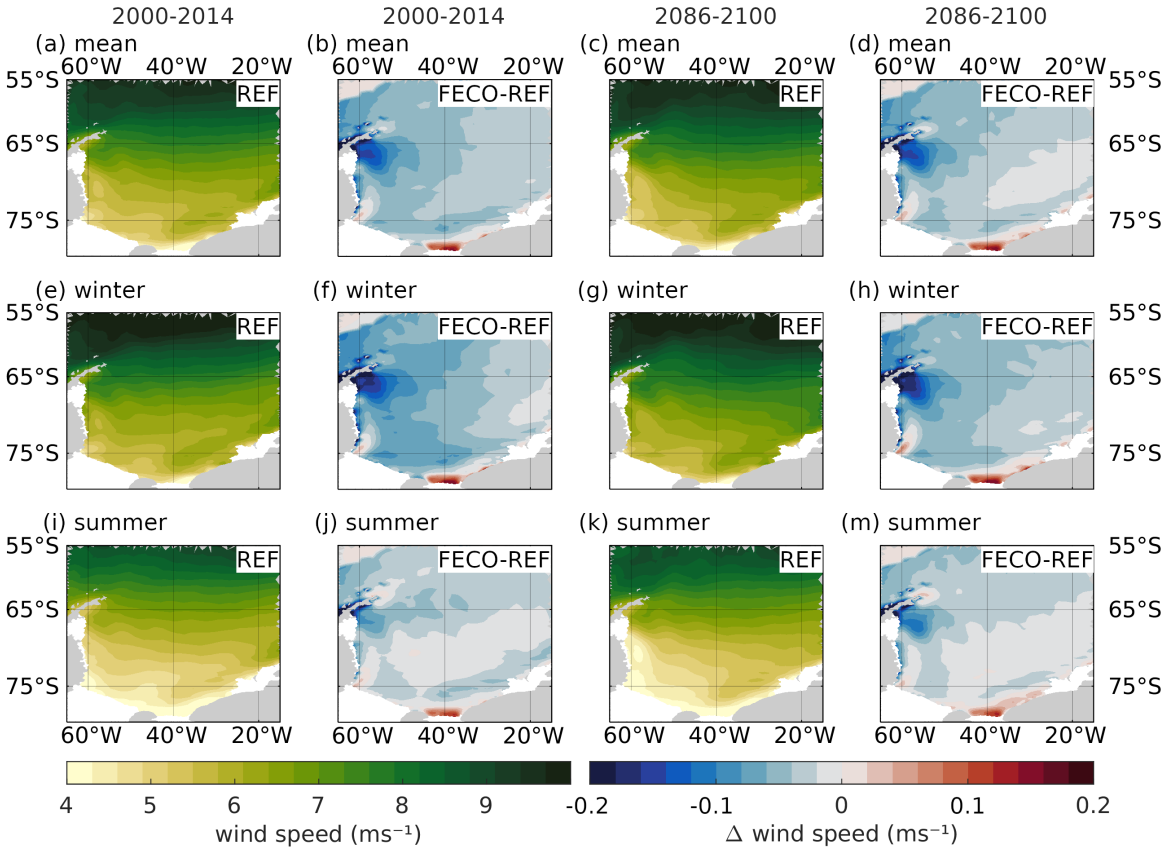


**Figure 5.1:** (a) Mean 10m wind speed (2000-2014) in REF. (b) Mean wind speed difference between FECO and REF (2000-2014). (c) Mean wind speed (2086-2100) in REF. (d) Mean wind speed difference between FECO and REF (2086-2100). (e)-(h) same as (a)-(d) but only for summer means (December-February), and (i)-(l) for winter means (June-August).

The dynamic downscaling of the wind field in the CCLM simulation produces strong differences to the AWI-CM wind fields (named FECO in Fig. 5.1). The yearly mean wind speeds over most of the area are significantly lower in CCLM than in AWI-CM for both, the beginning and the end of the 21st century. Only exceptions are small areas at the western Ronne Ice Shelf front, the Filchner Ice Shelf front and small areas in front of the Riiser-Larsen and Brunt Ice Shelves. The largest decrease is found at the eastern coast of the Antarctic Peninsula. Especially in winter, wind speeds are up to $0.16\,\mathrm{ms}^{-1}$ in 2000-2014 and up to $2\,\mathrm{ms}^{-1}$ in 2086-2100 lower compared to the low-resolution data. This decrease in wind speed between CCLM and AWI-CM can be attributed to the better resolved topography of the peninsula. The lower resolution of AWI-CM leads to smoothing of the topography of the

Antarctic Peninsula and the mountains there are not well represented. Thus, westerly winds are too strong in the AWI-CM forcing data (Stössel et al., 2011).

### 5.2.2 Two-Meter air temperature

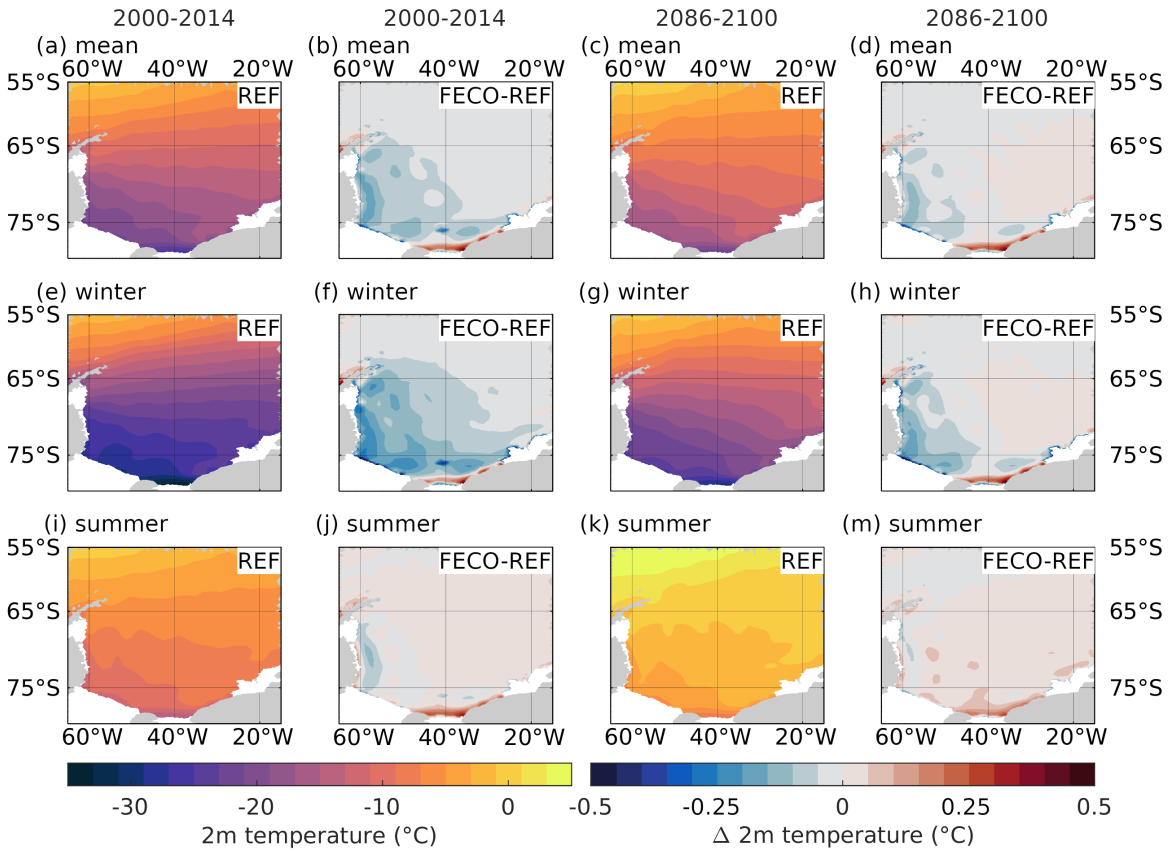


**Figure 5.2:** Same as Fig. 5.1 but for 2m air temperature.

The 2m-temperature in AWI-CM decreases southward toward a minimum at the Filchner Ice Shelf front. During winter, average air temperatures in this southern most area sink below -32°C (Fig. 5.2e), while average summer temperatures rise to approx. -10°C (Fig. 5.2i). The rise in greenhouse gas concentration in the SSP3-7.0 scenario causes an increase in the global 2m air temperature from 16.9°C to 19.4°C. A global warming of 2.48°C between the 15-year means of 2000-2014 and 2086-2100 lies at the lower end of projected climate development for the SSP3-7.0 climate scenario (best estimate 3.6°C, very likely range 2.8°C-4.6°C (IPCC, 2023)). In the Weddell Sea, mean air temperature rises by 3.22°C, stronger than in the global average, which might be an effect of polar amplification. The average temperature patterns in AWI-CM do not change much towards the end of the century, however winter temperatures rise more than summer temperatures. The average winter temperatures in the Weddell Sea increases by approx. 4.88°C, while summer temperatures only increase by approx. 1.89°C.

The CCLM data shows similar air temperature patterns as AWI-CM, however in both time periods strong local differences can be found that show a similar distribution at all times (Fig. 5.2b & d). CCLM produces lower air temperatures mostly along the Antarctic Peninsula and above the continental shelf except for a prominent warmer band reaching from

Berkner Island eastward towards Brunt Ice Shelf. Cold halos around the ice shelf fronts are caused by a mismatch of the ice shelf masks used in AWI-CM and CCLM (Fig B.1). The area with a strong negative anomaly at approx. 76°S 42°W is the signature of the iceberg A23a, which was included in the CCLM land mask but disregarded in the AWI-CM simulations (Fig. B.1b).

Temperature differences between AWI-CM and CCLM are stronger in winter than in summer. While large areas of the Weddell Sea are warmer in summer in CCLM than in AWI-CM, the average of the 15 years between 2000 and 2014 shows colder air temperatures. In contrast to the wind speed differences between the simulations that increase towards the end of the 21st century, air temperatures become more similar.

## 5.3 The development of coastal polynyas in a warming climate

### 5.3.1 Sea-ice production in the southern Weddell Sea

The sea-ice distribution and production in the southern Weddell Sea has a clear northeast-southwest gradient in REF. The highest sea-ice concentration can be found in the southwestern Weddell Sea, where sea ice can be found year round in 2000-2014. Along the Larsen C Ice Shelf edge and at the central Filchner Ronne Ice Shelf front, sea ice is particularly thick (up to 3 m). Low sea-ice drift and the low but continuous freezing at the Ronne Polynya in summer forms a ridge of particularly thick sea ice extending from Berkner Island, north of the Ronne polynya, and along the Antarctic Peninsula during the warmest season.

The sea-ice production rates are highest in the polynyas along the coast (Fig. B.3a). During the time period at the end of the century, the sea ice does not extend as far north as it did at the beginning of the century. Areas of sea-ice production and melting move southward (Fig. B.3c & d). While the hot-spots of sea-ice formation remain at the coast, areas of sea-ice formation during the freezing season can be found south of 65°S. Areas of sea-ice melting are also displaced southward onto the continental shelf, where previously melt rates where low, affecting the density of DSW. Additionally, a narrow band of sea-ice formation that remains in summer in 2000-2014 at the Ronne Ice Shelf front vanishes in the 2086-2100 summer mean, removing one source for DSW formation in summer.

The addition of CCLM as forcing in FECO during the 2000-2014 period leads to a thickening of the sea ice on the continental shelf by 0.2-0.3 m and higher concentration. The differences are smaller in winter than in summer, where especially above Berkner Bank, sea-ice thickness increases by up to 0.5 m. Towards the end of the century, regional differences in sea-ice thickness are much more varied. The sea-ice thickness decreases mainly in areas of strong off-shore winds at the Ronne polynya and the Filchner Ice Shelf front, as well as along the fronts of Brunt and Riiser-Larsen Ice Shelves, while areas above the Berkner Bank and along the coast of the Antarctic Peninsula feature thicker sea-ice covers.

### 5.3.2 Spatial distribution of sea-ice production

Coastal polynyas are hot-spots for sea-ice production. In the following sections we will include open-ocean polynyas in calculations of areas and mean sea-ice productions for the Weddell

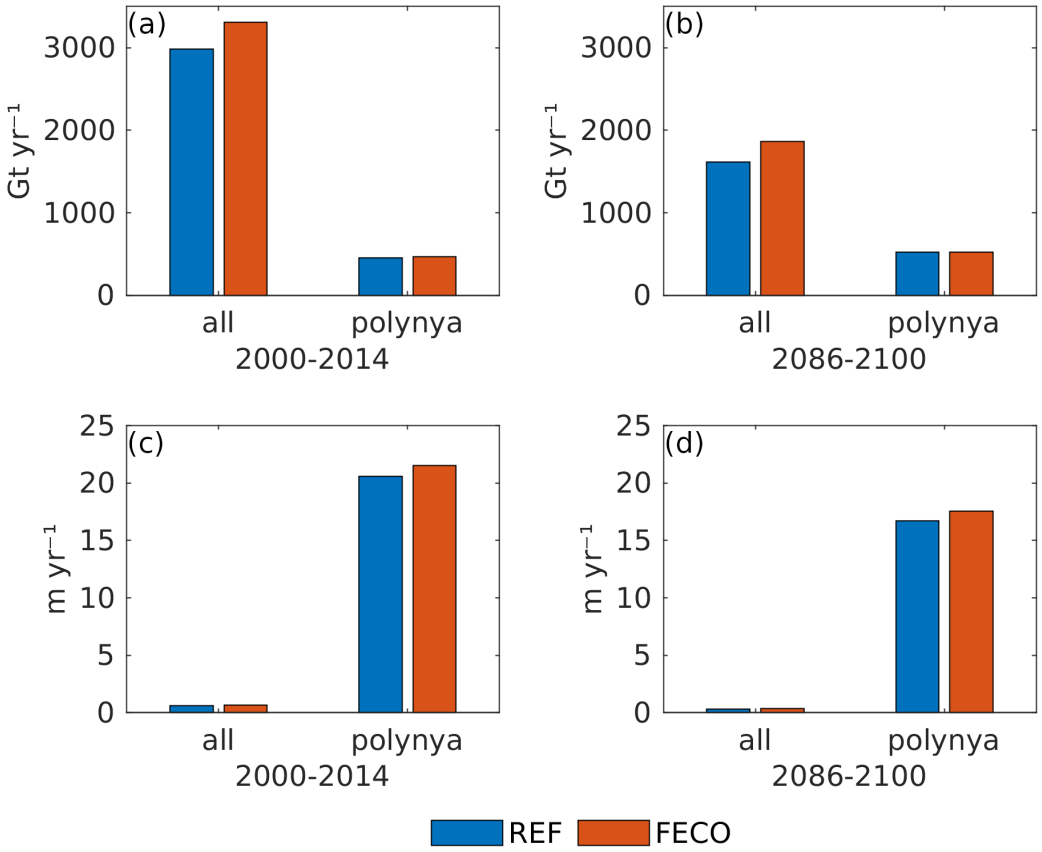


**Figure 5.3:** Total mean sea-ice production in Gt $yr^{-1}$ in the Weddell Sea and in the coastal polynyas of the Weddell Sea in (a) 2000-2014 and (b) 2086-2100 in REF (blue) and FECO (red). (c) and (d) same as (a) and (b) but for mean sea-ice production rates in m $yr^{-1}$.

Sea, but concentrate in greater detail on the coastal polynyas along the southern Antarctic Peninsula, the Ronne and Filchner Ice Shelf fronts, the coast of Coats Land, and the Brunt Ice Shelf (Fig. 3.2a). We excluded the northern half of the Antarctic Peninsula, because DSW production in this area does not affect the southern Weddell Sea continental shelf. The areas have been adapted from Paul et al. (2015). The polynyas include all grid nodes within the designated regions where sea-ice concentration C<70 % or sea-ice thickness h<20 cm.

The comparison of the mean sea-ice production in the western Weddell Sea and in the polynyas within this region for REF in 2000-2014 reveals that while only 15.13 % of sea-ice volume in the western Weddell Sea are formed in polynyas due to the small total area of the polynya (Fig. 5.3a), local sea-ice formation rates per area far exceed sea-ice formation rates in the rest of the Weddell Sea (Fig. 5.3c). In FECO, mean sea-ice production in the Weddell Sea is higher by 327.42 Gt $yr^{-1}$ than REF (Fig. 5.3a), however sea-ice production in the polynya is barely affected, despite increased freezing rates under the influence of higher off-shore wind speeds at the Filchner Ice Shelf front and the Ronne polynya (Fig. 5.3c).

Towards the end of the century, sea-ice formation in the Weddell Sea declines. The average sea-ice production is halved while sea-ice production in polynya increases in REF and in FECO. The decline in total production is caused by a reduced northward sea-ice extend and lower freezing rates, while production in coastal polynya increases (Fig. 5.3b). Similar to the mean production, sea-ice formation rates in REF and FECO for the whole

Weddell Sea are reduce by half (Fig. 5.3d). However, formation rates in the polynya areas remain high, although they are lower than at the beginning of the century.

### 5.3.3 Coastal polynya distribution in REF

For comparability to observations-based data produced by PAUL ET AL. (2015), we calculated the mean winter values for area and sea-ice production for May to September. The total polynya area in the western Weddell Sea in our calculation includes also possible open-ocean polynyas (Table 5.1). The distribution of sea ice in REF prominently shows the Ronne Polynya, as well as the sea-ice production area at the Brunt Ice Shelf (Fig. 5.5a, e, i). Another region of high polynya activity can be found at the northern tip of the Antarctic Peninsula, but processes there have no impact on the ocean conditions of the southern continental shelf. The region of the southern Peninsula and the Ronne Polynya produce winter means of 433 $km^2$ and 3239 $km^2$ respectively (Table 5.1) which agree well with observed polynyas between 2002 and 2014 described by PAUL ET AL. (2015). However, the polynya areas at the Filchner Ice Shelf front and at the coast of Coats Land are larger than observed values. Our definition of the Filchner region includes the area occupied by the grounded iceberg A23a in observations during the early 2000s, which is not included in our simulations. For comparison we combine the area of observed polynyas for Filchner Ice Shelf and iceberg A23a from Paul et al. to cover approximately the same region. This results in an area of approx. 2049±703 $km^2$ (PAUL ET AL., 2015). Our model produces an average polynya area for the Filchner region that lies within the standard deviation. However, further to the east the area of the modeled near-shore polynyas is much larger than suggested by observations. The polynya area off the Brunt ice shelf covers nearly triple the observed amount with 9995 $km^2$. Generally, polynyas along the south-western coast of the southern Weddell Sea agree better with observations than the eastern coast. As a result, the accumulated sea-ice production during winter generally exceeds observational values at the eastern coast, but also the western continental shelf produces more sea ice in the model, with the Antarctic Peninsula being the only exception.

The comparison of the mean winter sea-ice concentration (Fig. 5.5) with satellite ra-

**Table 5.1:** Mean polynya areas and accumulated sea-ice production in AWI-CM, REF and FECO for the different regions shown in Fig. 5.5a in a 15-year winter mean (May-September) in 2000-2014 and 2086-2100. The areas are provided in $km^2$, accumulated sea-ice production in $km^3$.

| | 2000-2014 | | | | | | 2086-2100 | | | | | |
|---|---|---|---|---|---|---|---|---|---|---|---|---|
| | AWI-CM | | REF | | FECO | | AWI-CM | | REF | | FECO | |
| | area $km^2$ | sea ice $km^3$ | area $km^2$ | sea ice $km^3$ | area $km^2$ | sea ice $km^3$ | area $km^2$ | sea ice $km^3$ | area $km^2$ | sea ice $km^3$ | area $km^2$ | sea ice $km^3$ |
| Peninsula | 1,100 | 4 | 433 | 5 | 518 | 6 | 8 | 0.01 | 1,626 | 15 | 1,597 | 16 |
| Ronne | 764 | 7 | 3,239 | 74 | 3,096 | 71 | 0 | 0 | 6,981 | 125 | 6,504 | 121 |
| Filchner | 167 | 2 | 2,749 | 34 | 2,604 | 33 | 0 | 0 | 2,987 | 32 | 2,618 | 27 |
| Coats Land | 271 | 2 | 2,168 | 23 | 2,107 | 22 | 0 | 0 | 3,258 | 23 | 2,821 | 21 |
| Brunt | 508 | 3 | 9,995 | 154 | 10,665 | 156 | 687 | 0.4 | 14,773 | 172 | 14,171 | 173 |
| Total (Weddell) | 5,140,373 | 2,067 | 5,397,820 | 4,924 | 5,397,820 | 5,097 | 5,140,373 | 2,067 | 5,397,820 | 4,433 | 5,397,820 | 4,560 |
| Total (Polynya) | 22,495 | 79 | 33,135 | 390 | 33,425 | 415 | 3,415 | 2 | 44,969 | 452 | 39,962 | 435 |

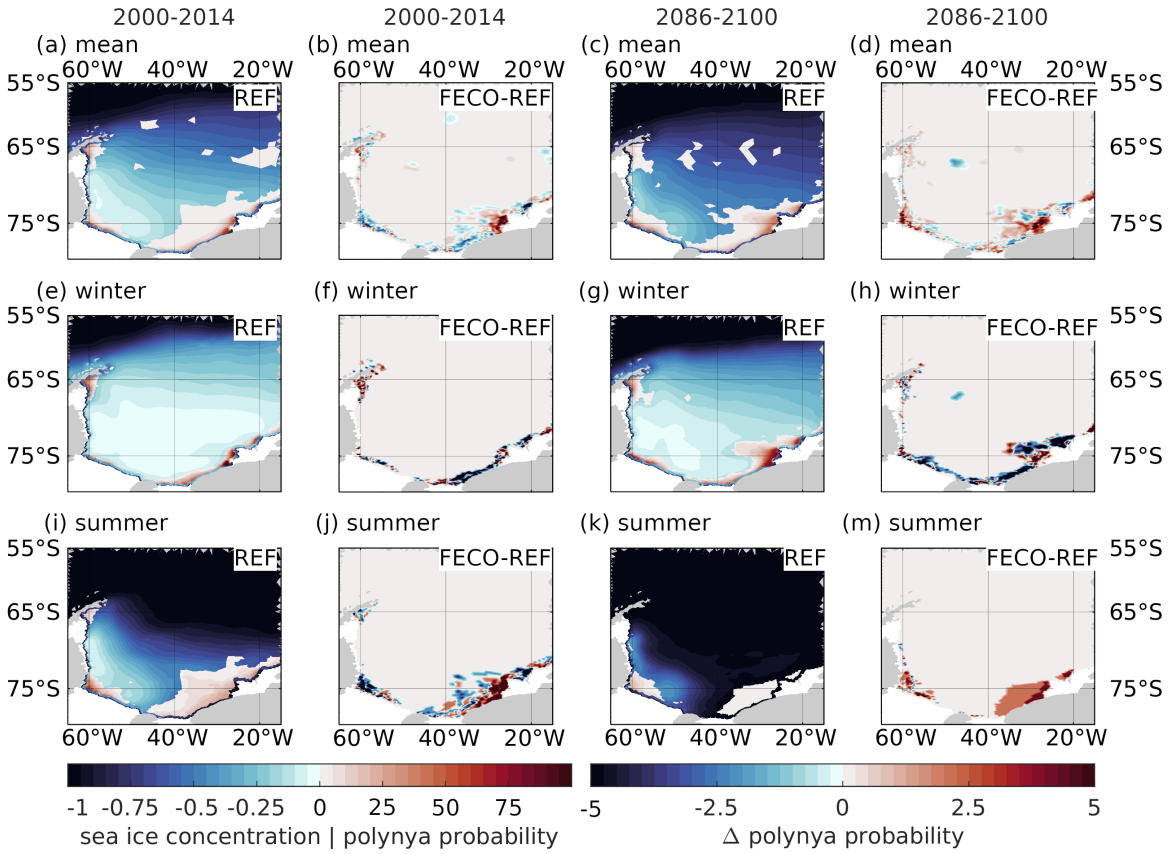


**Figure 5.4:** Mean sea-ice concentration and polynya probability in REF during 2000-2014 (a). Sea-ice concentration has a range between 0 and 1 (shaded of blue), the probability of a node to be part of a polynya is given in % (shades of red. (b) Difference in polynya probability between FECO and REF during 2000-2014. (c) and (d) same as (a) and (b) but for 2086-2100. (e)-(h) are the same as (a)-(d) but for winter means (June-August) and (e)-(m) for summer means (December-February).

diometer data shows the reason for the large polynya areas and productivity (Grosfeld et al., 2016; Spreen et al., 2008). The sea-ice concentration for winter in observations shows wide-spread values above 95 %, while the simulation reaches equally high sea-ice concentrations in a smaller area in the southwestern Weddell Sea above the continental shelf. The lower sea-ice concentration especially along the eastern coast in the regions off Filchner Ice Shelf, Coats Land and Brunt Ice Shelf leads to a higher detection rate and consequently areas of polynas that are much larger than the values extracted from satellite data by Paul et al. (2015).

Over the course of the 21st century, polynyas increase in size, continuing the positive trend observed over the last 44 years (Fig. B.4 Duffy et al., 2024), albeit with a smaller rate. The different polynyas change in size and productivity. Because of the decreasing sea-ice concentration and thickness over the course of the century, larger coastal polynyas develop during the later period of 2086-2100 than at the beginning of the century (Table 5.1). The average total area of polynyas during winter in the western Weddell Sea increases in size by approximately a third of its size in 2000-2014, and sea-ice production in the polynyas increases by a bit less than a third to 452 $km^3$. At the Peninsula, the model produces a polynya area nearly four times of the 2000-2014 mean, other regions remain closer to the original values.

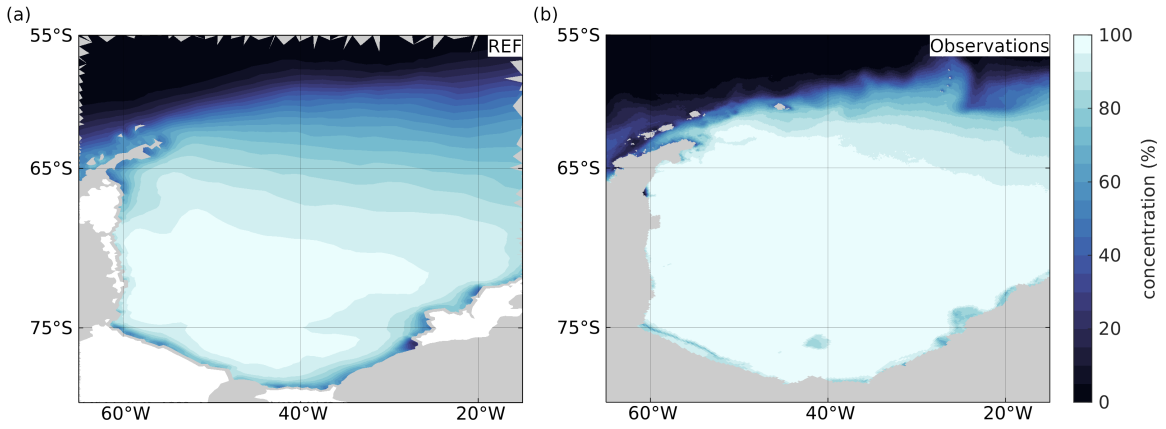


**Figure 5.5:** Mean sea-ice concentration in May-September for the years 2011 to 2014 in (a) REF and (b) from satellite radiometer AMSR-E and AMSR2 data (Grosfeld et al., 2016; Spreen et al., 2008).

The regions at the western continental shelf experience an increase in sea-ice production, and so does the Brunt region. In contrast to this, the Filchner region ad the coast of Coats Land remain at approx. the same level. Despite the increase in winter sea-ice production in most of the coastal polynyas, the total winter sea-ice production in the Weddell Sea decreases due to the rising air temperatures in the warming climate of the SSP3-7.0 scenario.

In summer, areas in REF that are recognized by our criteria as polynyas during the 2000-2014 period are larger than in winter, except for the Brunt region. However, only the Ronne Polynya retains sea-ice freezing during the summer months. All other areas show negative accumulated sea-ice production which means the polynyas are not areas of high sea-ice production anymore, but instead areas of intensified sea-ice melt surrounded by sea ice. The net sea-ice production of 274 $km^3$ in the Weddell Sea can be attributed to the export of sea ice from the Weddell Sea and the continuing ice melt in March which is not included in the calculation for summer polynyas.

During the later period at the end of the 21st century summer polynya areas decrease in contrast to winter, where the polynya sizes increase. This is also a result of the decreasing sea-ice thickness and concentration. While in winter, less sea ice increases the possibility of polynyas to occur in the ice, the lack of sea ice itself in summer at the end of the century removes the conditions for polynyas to form as holes surrounded by sea ice.

### 5.3.4 Coastal polynya distribution in FECO

Through the use of the down-scaled data set as forcing, the total winter polynya area in the Weddell Sea increases at the beginning of the century, however some areas also show decreased polynya activity (Table 5.1; Fig. 5.4), such as the Ronne and the Filchner regions as well as at the Coats Land coast (Table 5.1). An other area where FECO produces more polynyas in winter is the tip of the Antarctic Peninsula, which was not included in the table. The differences to REF can be attributed to colder winter air temperatures above large parts of the Weddell Sea (Fig. 5.2), which produces a more continuous ice cover above the continental shelf. The decrease in the winter wind speed in large parts of the Weddell Sea

also plays a major role, reducing sea-ice export. Frozen sea ice remains in place, blocking the way for the formation of additional sea ice, shrinking the ice free area. Corresponding to the changes in area, accumulated sea-ice production in winter increases slightly at the southern Antarctic Peninsula and Brunt Ice Shelf, while decreasing above the southern continental shelf. In summer, FECO shows a west-east separation of areas where the polynya sizes decrease (Antarctic Peninsula, Ronne Ice Shelf, Filchner Ice Shelf) or increase (Coats Land, Brunt Ice Shelf), caused by higher air temperatures along the eastern coast of the southern Weddell Sea. Especially the Ronne Polynya decreases in size and probability in summer, shrinking by approx. 811 $km^2$ compared to REF. While the size of coastal polynyas in summer increases along the eastern coast, sea-ice production/melting barely changes in these regions. The Ronne Polynya produces less ice because of the reduced´ area. The Filchner region shows a different behavious, as here, we find mainly melting in REF, but very low net freezing rates in FECO during 2000-2014 despite showing higher 2m-temperatures above the ocean.

The FECO simulations produce in total more polynyas in winter then REF (Fig. 5.4h), but at the end of the century, the trend for total polynya area in the Weddell Sea reverses. In 2086-2100 in FECO, total polynya area is approx. 5007 $km^2$ smaller than in REF. Locally however, all four regions on the southern continental shelf increase in size and productivity in winter. The only exception is Coats Land, where mean polynya size increases, sea-ice production however reduces slightly. In summer the picture looks different. Here we find an increase of the polynya areas in FECO compared to REF, except for the Filchner polynya, which nearly vanishes compared to REF. While the summer polynya probability still decreases strongly between 2000-2014 and 2086-2100, the mean total polynya area in the western Weddell Sea in FECO is nearly double the size of REF during the same time span. The sectors with the largest growth include the Coats Land and Brunt regions (Fig. 5.4m). The increase in polynya areas in summer is also a result of higher summer temperatures.

## 5.4 Dense Shelf Water formation

It has been already shown above that under the high-emission scenario, water mass properties are projected to change (De Lavergne et al., 2014; Nissen et al., 2022). The change in density on the southern Weddell Sea continental shelf can be assessed within the water mass transformation framework, which relates buoyancy fluxes to surface density and water mass distribution. Total water mass transformation rates are largely positive in the southern Weddell Sea (black line in Fig. 5.6a/c), showing the densification across large areas in this region in REF and FECO. The peak densification causes a total flux of 7.39 Sv in 2000-2014, which is nearly double the estimates from recent observations of DSW export from the continental shelf in the Weddell Sea towards the abyss (4.5 Sv±0.3; Akhoudas et al., 2021). Sea-ice formation has the largest impact on the densification (dark blue dashed line Fig. 5.6b), which is counteracted in part through freshwater input due to ice shelf basal melting (dotted dark blue line in Fig. 5.6d). Evaporation and precipitation (E-P) only play a secondary role in reducing the density (approx. 0.16 Sv).

Under the influence of the warming climate the reduced sea-ice formation causes a shift in the density classes produced by sea-ice formation, decreasing the dense water formation by

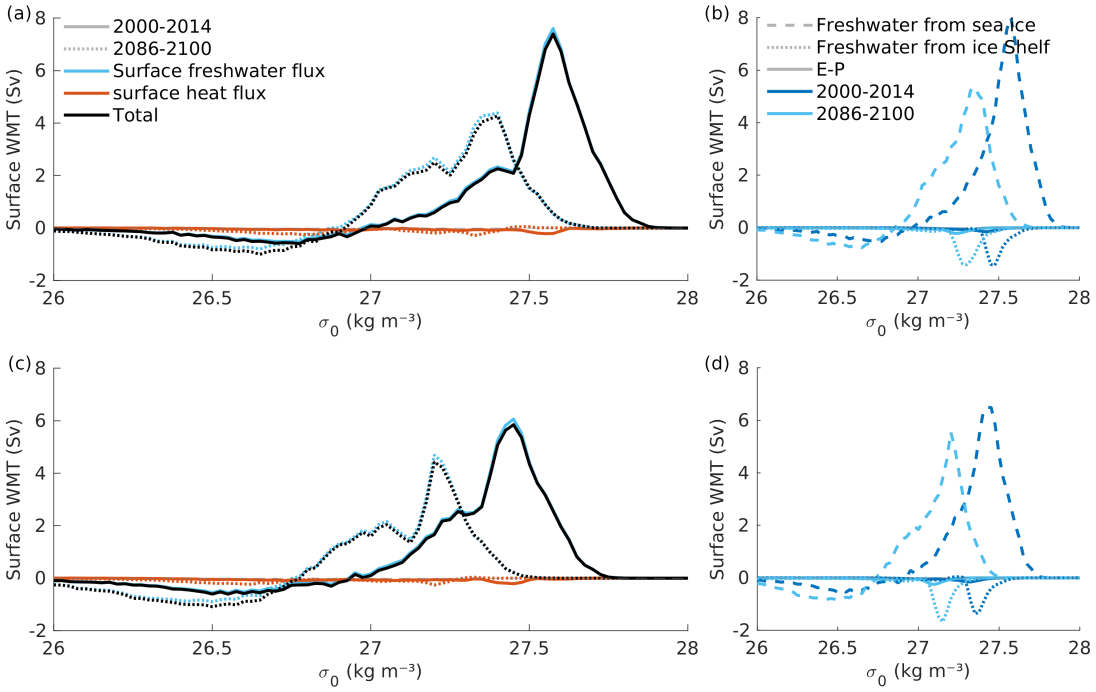


**Figure 5.6:** Surface water mass transformation rates (WMT) in Sverdrup (Sv) on the southern Weddell Sea continental shelf (see area in map) in (a) REF in the time periods 2000-2014 (straight lines) and 2086-2100 (dotted lines). (b) Freshwater fluxes split into sea ice, ice shelf and E-P (evaporation - precipitation) for the same time spans. (c) and (d) are the same as (a) and (b) but for the FECO simulation.

approx. 3.12 Sv (dotted black line in Fig. 5.6a). Densification through sea-ice flux decreases by 30 % between 2000-2014, but freshwater flux by basal ice shelf melt remains stable. However, reducing density through E-P increases from 0.16 Sv to 0.22 Sv, caused by rising air temperatures.

The higher resolved atmosphere in the FECO simulations reduces the peak total DSW formation in 2000-2014 to 5.85 Sv, which is closer to the observations. The produced density (class) decreases from 1027.575 to 1027.45 kg m$^{-3}$ s$^{-1}$ (Fig. 5.6c). These changes are caused by higher melt rates on the continental shelf in summer compared to REF. The DSW formation at the end of the century reduces in FECO to 4.43 Sv, which corresponds to a reduction of 24 %, which is far less than in REF, where the climate change over the 21st century causes a reduction of DSW formation by 44 %. Reasons can again be found in the sea-ice formation, the main driver for dense water formation on the southern Weddell Sea continental shelf (Fig. 5.6d). Additionally, in FECO the increase of basal melt has a bigger influence on the water mass transformation than in REF (dotted light blue line in Fig. 5.6d). Due to a sudden increase in mWDW transport into Filchner Trough in 2093, larger amounts of warm water are able to intrude into the Filchner Ice Shelf cavity, increasing basal melting. Such a scenario does not occur in REF, where instead the melt water component decreases.

## 5.5 Discussion

Using an ocean model forced with results from atmospheric simulations at two different resolutions, we investigate the impact of atmospheric resolution on coastal polynyas in a warming climate scenario. We find that the lower air temperatures in the high-resolution experiment increase the overall sea-ice formation in the Weddell Sea but reduce polynya areas in recent climate. At the end of the century, the higher sea-ice concentration in the high-resolution experiment leads to a larger possibility for polynya formation than in the low-resolution reference experiment.

The areas of the polynyas detected in the reference simulation during recent climate agree largely with satellite-based polynya data (Paul et al., 2015), sea-ice production in the polynyas, however, is much higher in our model results than the observation-based estimates suggest. In FECO, the smaller polynya areas also slightly reduce freezing rates of sea ice but the change is insufficient to compensate for the apparent overestimation of sea-ice production at Coats Land and the Brunt Ice Shelf front. The satellite-based polynya detection scheme by Paul et al. (2015). is based on ERA-Interim reanalysis data to calculate the surface energy balance. Stulic et al. (2023) suggested that the warm bias in the ERA-Interim data might cause a reduction of polynya area and sea-ice production, leading to low values in Paul et al. (2015). Another reason for the differing values in sea-ice production between observations and our model results lies in the presence of A23a. This iceberg calved from the Filchner-Ronne Ice Shelf in the 1986 and was stuck on the continental shelf for the following 34 years until in 2020 it started moving again. According to Markus (1996), the grounded iceberg increases sea-ice concentration at the Filchner Ice Shelf. Our model does not include A23a, leading to lower sea-ice concentration and higher sea-ice production at the Filchner Ice Shelf front. At the same time, polynyas develop on the lee side of the grounded iceberg (Morales Maqueda et al., 2004; Paul et al., 2015), increasing sea-ice production north of Berkner Island. Stulic et al. (2023) investigated the influence of the iceberg on the polynya sea-ice formation in the region and showed that without the iceberg sea-ice production at the Filchner Ice Shelf front is nearly three times as large as with the iceberg, while sea-ice formation north of Berkner Island reduces significantly. The effect on the polynya areas east of the Filchner Ice Shelf seems to be smaller and does not explain the overestimation of sea-ice production in our model at Coats Land and the Brunt Ice Shelf front. This overestimation of sea-ice production also needs to be taken into account when evaluating the changes in polynya areas and sea-ice production at the end of the century.

At the end of the 21st century, the differences between the forcing data sets used in REF and FECO are of similar magnitude and distribution as at the beginning of the century. As an effect, polynyas in FECO are again slightly smaller than in REF, similar to the time period 2000-2014. In contrast to the first period, Brunt area also produces smaller polynyas in FECO than in REF. The generally lower sea-ice production, caused by the warmer climate at the end of the century, causes density loss in the DSW on the continental shelf. In 2093, the conditions for a regime shift in Filchner Trough are met in FECO, where mWDW enters the trough as a near-bottom current, increasing temperatures in the Filchner Trough and, when reaching the Filchner Ice Shelf, raising melt rates in the cavity. The overestimation of

sea-ice production implies that in a simulation with a more realistic sea-ice representation, the density loss on the continental shelf and particularly in Filchner Trough would progress even faster, moving the regime shift forward in time. In Teske et al. (2024b), the regime shift in Filchner trough was projected to happen around 2075. The very-high emission scenario SSP5-8.5 simulation by Nissen et al. (2023) projected a possible regime shift to begin in the 2080s.

The main drivers behind the differing polynya formation behaviour in REF and FECO are the lower air temperatures and weaker wind fields in large areas of the Weddell Sea in the CCLM forcing data. Haid et al. (2015) showed that large-scale wind patterns have a stronger impact on polynya formation than local wind patterns in the Weddell Sea. Our results agree with this. While CCLM produces stronger off-shore wind speeds at the eastern Ronne Ice Shelf front, the Filchner Ice Shelf front and along the coast of Coats Land, the additional local sea-ice formation is compensated by lower export of sea ice from the continental shelf and higher sea-ice thickness and sea-ice concentration on the continental shelf.

One area that stands out in the wind and temperature patterns in CCLM that differ strongly from the AWI-CM data is the Filchner Ice Shelf front and the coast of Coats Land. Here, stronger off-shore winds prevail in CCLM while air temperatures are higher by up to 0.3°C. The higher resolution above Coats Land increases the roughness in the model. The lower atmosphere in Antarctica has a more or less stable layering with a cold bottom layer. Increased roughness of the terrain leads to stronger turbulent mixing of the lower layer, increasing the 2m temperature used to force the ocean simulation. A secondary role might by played by the representation of katabatic winds in the high-resolution CCLM. The better representation of gradients focuses down-hill katabatic winds into smaller regions, displaying them more precisely than AWI-CM. In AWI-CM, katabatic winds are broadened and smoothed by the lower horizontal resolution, leading to cooling over larger areas above the coastal waters. Thus AWI-CM has a cold bias, which is corrected in CCLM by the more precise representation of local cold winds.

Our results confirm that the development of polynyas in the Weddell Sea depends on the representation of the local orography in the atmospheric component of the model system. Dynamic downscaling of atmospheric model results to a higher resolution improves the representation of gradients in mountainous areas, influencing wind and temperature distributions above the ocean. For the future projections, lower air temperatures and weaker winds in the high-resolution atmosphere simulation increase the sea-ice formation compared to the low-resolution reference simulation. But despite higher sea-ice formation rates in polynyas, a shift in the sea-ice melt regions onto the continental shelf in the high-resolution simulation leads to the formation of lower-density water masses, creating conditions favourable for a regime shift in Filchner Trough.

CHAPTER

# SIX

# ACCELERATED FUTURE DENSITY REORGANIZATION ON THE WEDDELL SEA CONTINENTAL SHELF WITH HIGH-RESOLUTION ATMOSPHERIC FORCING

This chapter is a reformatted copy of the published article of the same title:
Teske, V., Timmermann, R., Nissen, C., Zentek, R., Semmler, T., and Heinemann, G., EGUsphere [preprint],(2024). https://doi.org/10.5194/egusphere-2024-2873.

The article in its published form is attached as Appendix D.2

V. Teske ran the FESOM simulations, conducted the analyses, and prepared the figures. C. Nissen and V. Teske prepared the FESOM model code. G. Heinemann and R. Zentek prepared the CCLM model code and ran the simulations. V. Teske, R. Timmermann and T. Semmler contributed to the interpretation of the results. All authors contributed to the writing and editing of the manuscript.

The strong Antarctic Slope Front in the southern Weddell Sea limits the present-day transport of modified Warm Deep Water onto the continental shelf and is associated with a characteristic V-shape in the density structure all along the continental slope. The mechanisms controlling today's V-shape are well studied, but its future development is not yet well constrained. In this study, we run ocean model simulations for a 21st-century Shared Socio-economic Pathways (SSP) 3-7.0 emission scenario forced with atmospheric model output from simulations with a global climate model and from a higher-resolved regional atmospheric model, respectively. We find that the resolution of the atmospheric model component influences the simulated future transport of modified Warm Deep Water onto the continental shelf through differences in the evolution of the depth and symmetry of the V-shape over the 21st century. In both simulations, reduced sea-ice formation and weakened Ekman downwelling reduce the depth of the V-shape and increase the sensitivity of its position above the slope to seasonal variations in sea-ice production and in the wind field. Using data from an atmosphere model with higher resolution leads to an acceleration of the density redistribution on the continental shelf, provoking a regime shift from cold to warm Filchner Trough through a cross-slope current before the end of the 21st century. As cross-slope currents disturb the continuity of the V-shape, we define a grade of connectivity to quantify the lateral integrity of the V-shape along the continental slope. We find that the integrity of the V-shape reduces with a delay of 3 months after a strong cross-slope current of modified Warm Deep Water enters Filchner Trough. Our results also indicate that the SSP3-7.0 climate scenario may have a higher potential for a regime shift than other ocean simulations for the same scenario but with lower atmospheric resolution suggest. Atmospheric downscaling increases the potential for a regime shift, dominated by warmer summer air temperatures. The Antarctic Slope Front is temporarily disturbed by cross-slope currents but the primary reason for the regime shift is the cross-slope density gradient.

## 6.1 The density distribution at the Filchner Trough sill

The Filchner Trough on the continental shelf in the southern Weddell Sea, Antarctica (Fig. 3.2), is one of the key regions of Dense Shelf Water (DSW) export and therefore plays an important role in the global ocean circulation (Heywood et al., 2014). However, the Filchner Trough is also a region where a southward current of modified Warm Deep Water (mWDW), the local cooler derivative of Circumpolar Deep Water, may reach the Filchner ice shelf cavity and significantly increase melt rates (Darelius et al., 2016; Ryan et al., 2020). Future climate projections for different warming scenarios have shown that a regime shift from a cold DSW-dominated to a warm mWDW-dominated Filchner Trough is possible during the 21st century (Daae et al., 2020; Haid et al., 2023; Nissen et al., 2023; Teske et al., 2024b; Timmermann and Hellmer, 2013). Numerous studies have demonstrated that the density ratio between the continental shelf and the open ocean is critical in controlling the on-shelf transport of relatively warm off-shore water (Daae et al., 2020; Haid et al., 2023; Nissen et al., 2023). While a higher density of shelf waters prevents a warm inflow onto the shelf, projections have shown the potential for a reversal of the density ratio (Haid et al., 2023; Nissen et al., 2023), allowing for mWDW transport onto the continental shelf.

North of Filchner Trough above or near the continental shelf break sits the Antarctic Slope Front (ASF), the frontal zone between coastal and open-ocean waters which is associated with strong subsurface temperature and salinity gradients. Around Antarctica, the structure of the ASF varies depending on hydrographic properties over the continental shelf and shelf break, and can be classified into three groups: fresh shelf, warm shelf, and dense shelf (Thompson et al., 2018). With its DSW production and export, the continental shelf of the southern Weddell Sea is an example for a dense shelf. For dense shelves, density surfaces tilt down southward towards the continental slope, but shoal again above the DSW layer. This creates a characteristic V-shape running perpendicular to the continental slope (see also Fig. 3.3a) which has been described in many studies (e.g., Baines, 2009; Gill, 1973; Ou, 2007; Thompson et al., 2018). Variability in the V-shape has been linked to variability in both DSW export and on-shelf transport of mWDW. While the northern arm of the V-shape is formed by Ekman downwelling (Sverdrup, 1954), the southern arm of the V-shape is formed by entrainment of overlying surface water to the descending flow of DSW (Baines, 2009; Gill, 1973). The V-shape shows seasonal variability in depth that has been associated with variations in the along-shore wind strength (Graham et al., 2013). For example, a peak in wind strength in the southeastern Indian Ocean in April 2009 led to increased mixing, on-shore Ekman transport and convergent downwelling on the continental shelf near 113°E. Similar behaviour was observed in 2010 and 2011 (Peña-Molino et al., 2016). Kida (2011) showed in a numerical model experiment with an idealized set-up of the Filchner Trough and the southern Weddell Sea that enhanced winds lead to a deepening of the V-shape and a decrease of the ocean stratification near the continental shelf break. The larger amount of lighter surface water at greater depth increases the density gradient across the shelf break and enhances the overflow transport. In contrast, three-dimensional eddy-resolving simulations by Stewart and Thompson (2015a,b) showed nearly no sensitivity of the DSW export to wind strength. Reanalysis of ship-based observations, argo floats and data from marine mammals showed a steepening of the angle of the northern arm of the V-shape in the southern Weddell Sea in winter and a flattening in summer (Le Paih et al., 2020; Pauthenet et al., 2021). The seasonal variability of the V-shape and the associated thermocline at the continental slope leads to seasonal pulses of mWDW flowing into the Filchner Trough (Årthun et al., 2012; Hellmer et al., 2017). Several studies have shown that an intensification of these seasonal pulses is a precursor for an impending regime shift in the Filchner Trough (Hellmer et al., 2017; Naughten et al., 2021; Teske et al., 2024b).

Despite its importance for the on-shelf supply of heat governing Antarctic ice shelf melting, only comparatively few studies with global ocean or climate models have focused on the Antarctic Slope Current or the ASF due to the high resolution requirements to adequately resolve coastal ocean dynamics (Beadling et al., 2022; Huneke et al., 2022; Mathiot et al., 2011; Stewart et al., 2019). While only Beadling et al. (2022) concentrated on possible responses of the ocean to changes in the wind field and meltwater input in a future climate, their model resolution of 100 km to 200 km is relatively coarse. Mathiot et al. (2011) showed that a downscaling of the atmospheric forcing to 40 km in a hindcast scenario increases katabatic winds and increases the strength of the seasonal cycle in the wind and

temperature fields. While modeling studies on different aspects that affect the Antarctic Slope Current, like freshwater input or changes in the wind strength and direction are more abundant, they often use idealized set-ups, regional models, or are only coarsely resolved (Dinniman et al., 2012; Hattermann et al., 2014; Kida, 2011; Lockwood et al., 2021; Nøst et al., 2011; Ong et al., 2023; St-Laurent et al., 2013). Previous studies have described a possible regime shift in the Filchner Trough, but less attention has been paid to the consequences that a shift in the current regime might have for the density structure at the continental slope which is controlling the mWDW inflow into Filchner Trough (Hellmer et al., 2012; Naughten et al., 2021; Nissen et al., 2022, 2023, 2024; Timmermann and Hellmer, 2013). The sensitivity of the ocean processes in response to the atmospheric forcing was demonstrated by Hattermann et al. (2014), Haid et al. (2015) and Dinniman et al. (2015). This leads us to the hypothesis that resolved mesoscale atmospheric processes may intensify the seasonality of the V-shape, the on-shore mWDW transport and the export of DSW in the Weddell Sea. Additionally, a finer atmospheric resolution produces more detailed and more pronounced temperature and wind speed gradients mostly related to katabatic winds and foehn wind (Cape et al., 2015; Elvidge et al., 2014; Mathiot et al., 2011; Van Lipzig et al., 2004; Van Wessem et al., 2015).

The aim of this study is to explore the evolution of the V-shaped ASF in the southwestern Weddell Sea in a warming climate (for study area see Fig. 3.2). By using ocean model simulations forced with data from two atmosphere models with different grid resolutions, we assess the processes governing the structure of the ASF and the transport of mWDW onto the continental shelf. To reach that goal, we analyse (i) how the cross-slope structure of the V-shape at the Filchner Trough sill develops in a high-emission climate scenario for the 21st century in Chapters 6.2.2 and 6.3.1, (ii) the change in seasonal atmospheric variability and its influence on the symmetry and structure of the V-shape (Chapters 6.3.2 and 6.3.3), and (iii) the longitudinal integrity of the V-shape as an indicator for the stability of the ASF and a possible regime shift in the Filchner Trough in a warming climate (Chapter 6.4).

## 6.2 The shelf regions of the southern Weddell Sea

### 6.2.1 Present-day V-shape in the Weddell Sea (REF simulation)

The reference simulation REF shows a distinct wedge structure of the isopycnals above the continental slope for the period 2010-2014, but details vary substantially across different sectors of the Weddell Sea (Fig. 6.1). In the following, the potential density is always given relative to 1000 kg $m^{-3}$. At the coast of Dronning Maud Land (DML) in the eastern Weddell Sea, a fresh-shelf region, the narrow continental shelf prevents the accumulation of large amounts of DSW. Cold, fresh surface water is pushed towards the coast and subducted, pressing down on the isopycnals of greater density (Fig. 6.1a). The planes of equal density dip towards the continental shelf and the coast, forming only the northern arm of a V-shape. The section at Filchner Trough (Fig. 6.1b), a dense-shelf region, shows a strongly pronounced V-shape in which the 27.7 kg $m^{-3}$ isopycnal is found at approx. 500 m greater depth above the continental slope than on the continental shelf. The southern arm of the V-shape is

pronounced in the Filchner Trough, as this is an area of DSW overflow (Fig. C.1). Further to the west at the Ronne Trough (Fig. 6.1c), water of colder temperature reaches deeper than at the Filchner Trough. However, the V-shape is less pronounced in the upper open ocean, i.e., the region displays a less pronounced northern arm, due to the deepening of the slope current along its path following the continental slope. At the Antarctic Peninsula in the western Weddell Sea (Fig. 6.1d), a V-shape in the isolines is clearly visible only in the temperature field and for the 27.7 kg $m^{-3}$ isopycnal and higher-density but not for lower-density isopycnals. In addition, mWDW at temperatures around -1°C can be found on the continental Shelf and in the Larsen Ice Shelf cavity originating from Ronne Trough and following the coast northward (Fig. C.1a). The Filchner Trough has previously been shown to be an entrance point for mWDW to reach the Filchner Ronne ice shelf (e.g. Foldvik et al., 1985; Ryan et al., 2017). Because of its particular relevance, we will focus on the Filchner Trough in our further analysis.

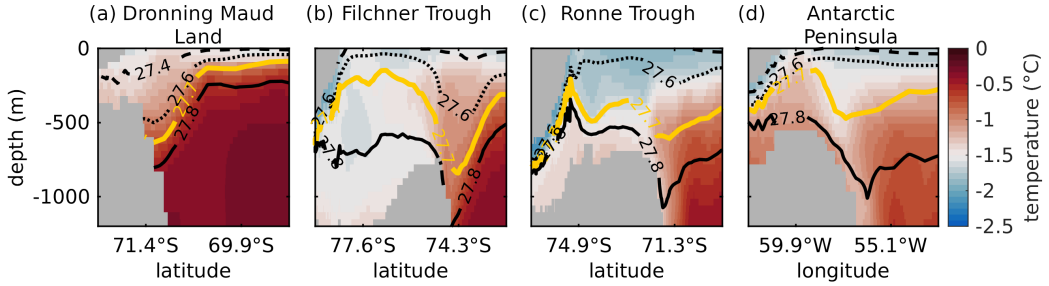


**Figure 6.1:** Potential temperature sections across the continental slope in the southern Weddell Sea with isopycnals shown relative to 1000 kg $m^{-3}$ for 27.4, 27.6 27.7 (orange) and 27.8 kg $m^{-3}$ for the average over 2010-2014 in REF. a) Dronning Maud Land, b) Filchner Trough, c) Ronne Trough, and d) Antarctic Peninsula. The continent and ice shelves (marked in grey) are on the left-hand side for all panels. See Figure 3.2 for the exact locations of the transects.

### 6.2.2 Present-day seasonality of the V-shape at Filchner Trough (REF simulation)

Previous studies have shown that seasonal variations in the density distribution at the continental shelf break control the on-shore flow of mWDW (e.g. Teske et al., 2024b). During the historical 2010-2014 time period in REF, the depth and steepness of the V-shape shows seasonal variations (Fig. 6.2). More intense sea-ice formation on the continental shelf leads to thicker sea-ice above the continental shelf (Fig. C.3) and stronger DSW export in winter and spring than in summer and autumn, which pushes down the isopycnals at the continental slope by approx. 50 m (Fig. 6.2 a, b). This is consistent with observed variations in the thermocline depth at the Filchner Trough sill (Hattermann, 2018), though with a smaller amplitude than in the observations. Sea-ice melting during summer reduces the steepness of the arm of the V-shape above the continental shelf (Fig. 6.2c). Subsequently, stronger densification over the continental shelf through sea-ice formation in autumn strengthens the southern arm again (Fig. 6.2d). Sea-ice formation in winter is particularly pronounced along the coasts of the Weddell Sea (Fig. C.2e), while in summer most of the Weddell Sea is dom-

inated by sea-ice melting (Fig. C.2i). Only a small band along the Filchner-Ronne Ice Shelf edge produces sea ice year round, which - together with sea-ice deformation by tides and variable winds - leads to a band of exceptionally thick sea ice north of Ronne Ice Shelf in summer (Fig. C.3i).

The rise of the thermocline in summer also enables seasonal pulses of mWDW to flow onto the continental shelf (see also Ryan et al., 2020; Teske et al., 2024b). The horizontal temperature gradient in 300 m depth is strongest during winter - which is consistent with observations (Fig. C.4; Pauthenet et al., 2021) - however the northern arm of the V-shape has its steepest angle during summer (blue line in Fig. C.5). During summer, reduced DSW export (Fig. C.6) and weakened Ekman downwelling (see also Fig. 6.5) reduce the depth of the V-shape compared to winter (Fig. 6.2c). The main mechanisms behind the seasonal variations are thus the seasonal production of DSW and seasonally varying Ekman downwelling. These mechanisms as found in the simulation agree with observations and previous modelling studies (Le Paih et al., 2020; Pauthenet et al., 2021; Peña-Molino et al., 2016; Ryan et al., 2020).

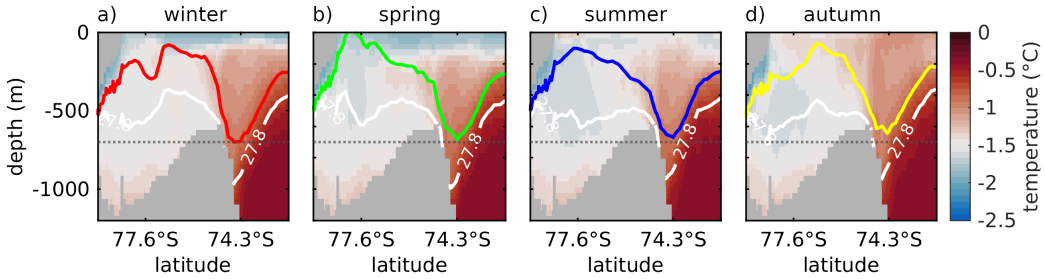


**Figure 6.2:** Potential temperature in the 2010-2014 mean of the Filchner Trough section in REF for winter (June-August), spring (September-November), summer (December-February), and autumn (March-May). The colored (white) lines show the position of the 27.7 kg m$^{-3}$ (27.8 kg m$^{-3}$) isopycnal in the respective season. Horizontal dotted line shows the maximum depth of the 27.7 kg m$^{-3}$ isopycnal in winter. The continent and ice shelves (marked in grey) are on the left-hand side for all panels. See Figure 3.2 for the exact locations of the transects.

## 6.3 Effects of the atmosphere

### 6.3.1 Effect of a warming climate on the seasonally varying V-shape geometry (REF simulation)

Over the 21st century, increased summer sea-ice melting and reduced freezing rates in winter above the continental shelf (Fig. C.2) lead to freshening of the continental shelf and to a density redistribution in the Filchner Trough and across the continental slope. While the geometry of the V-shaped density distribution is mostly symmetrical in 2010-2014 (Fig. 6.2), it becomes lopsided towards the end of the century in the REF simulation (Fig. 6.3). A reduction of the density over large parts of the water column in Filchner Trough by up to 0.2 kg m$^{-3}$ between 2000 and 2100 reduces the vertical extent of the southern arm of the V-shape. In addition, a shoaling of the slope current over the course of the century reduces the

depth of the V-shape so that the yearly mean depth of the 27.8 kg m$^{-3}$ isopycnal lifts from approx. 992 m to 791 m between 2010-2014 and 2096-2100 (dotted and dashed horizontal lines in Fig. 6.3, respectively). Of all seasons, the V-shape reaches its deepest position in summer by the end of the century (Fig. 6.3c), as opposed to in winter for the 2010-2014 period (Fig. 6.2).

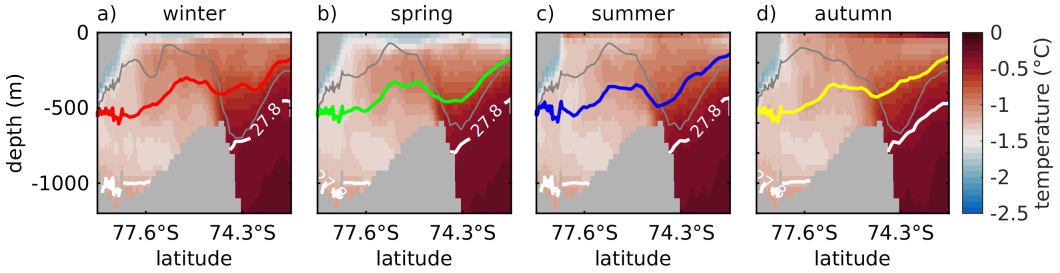


**Figure 6.3:** Potential temperature in the 2096-2100 mean of the Filchner Trough section in REF for a) winter (June-August), b) spring (September-November), c) summer (December-February), and d) autumn (March-May). The colored lines show the position of the 27.55 kg m$^{-3}$ isopycnal in the respective season, the white line the 27.8 kg m$^{-3}$ isopycnal. The gray line shows the position of the 27.7 kg m$^{-3}$ from Fig. 6.2. The dotted (dashed) horizontal gray line shows the mean depth of the 27.8 kg m$^{-3}$ isopycnal in the multi-year mean of 2010-2014 (2096-2100).

The change in sea-ice thickness and concentration (Fig. C.7a & b) during the 21st century does not only lead to freshening of shelf waters, but also influences how the wind field impacts the ocean surface. To isolate the relative effects of wind speed changes and changes in sea-ice properties, we compute the wind stress curl from the 2m wind field assuming a constant drag coefficient over ocean ($C_{AO}$=1.00e-3) and sea ice ($C_{AI}$=1.32e-3), weighted by sea-ice concentration per grid cell. We find that an intensification of the wind field towards the end of the century enhances existing wind stress curl patterns in winter (Fig. 6.4a-d), while qualitatively the patterns remain largely unchanged. In contrast, considering the ocean surface stress, i.e. taking the effect of the sea-ice cover into account, we find an alternating pattern of negative and positive surface stress curl, corresponding to alternating areas of up- and downwelling, respectively (Fig. 6.4e). With a reduction of winter sea-ice thickness by up to 80 % compared to at the beginning of the century, some of the up- and downwelling areas are redistributed. Regional variability is slightly reduced so that the surface stress curl resembles the wind stress curl more closely at the end of the century. Similar changes in the wind stress curl can be seen in spring and autumn (Fig. 6.4 b/d vs. f/h). In summer, when the sea-ice thickness (Fig. C.2) and concentration (not shown) in the Filchner Trough is already low between 2010 and 2014, a southward shift of the wind field increases areas of downwelling above the continental slope. The impact of sea ice on the surface stress curl is especially visible in autumn where in the 5-year average for March to May, the Filchner Trough is covered approximately halfway by sea ice. South of approx. 76°S, sea ice creates alternating patterns of positive and negative surface stress curl, while north of this, surface stress curl closely resembles the wind stress curl (Fig. 6.4 d, h).

From the fact that in the comparison between 2096-2100 and 2010-2014 we find modified patterns of spatial variability in the ocean surface stress curl (lower panels in Fig. 6.4) much

more pronounced than in the wind stress curl (upper panels in Fig. 6.4), we conclude that the long-term trend in up- and downwelling patterns is created by trends in the sea-ice cover rather than in the wind field. The combination of reduced DSW export in winter and spring and the enhanced wind stress impact on the ocean is then responsible for the change in the seasonal variations of the V-shape.

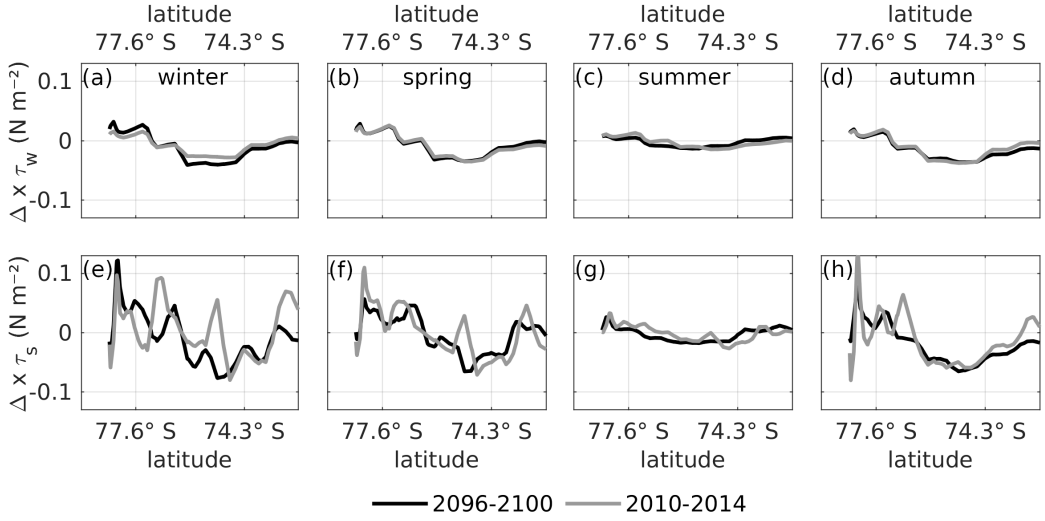


**Figure 6.4:** Wind stress curl ($\mathrm{N\,m^{-3}}$), estimated from the 2m-wind field, in the 5-year means of 2096-2100 (black line) and 2010-2014 (gray line) in REF above the Filcher Trough section (see Fig. 1) for (a) winter (June-August), (b) spring (September-November), (c) summer (December-February), and (d) autumn (March-May). (e)-(h) Same as (a)-(d) but for surface stress curl on the liquid ocean from overlying atmosphere and sea ice. Positive curl corresponds to downwelling.

### 6.3.2 Sensitivity of the Filchner Trough circulation to atmospheric forcing

The application of the regional higher-resolved CCLM forcing in FECO affects the transport of mWDW onto the continental shelf. Reduced freezing rates along the coasts in winter and higher melt rates in summer (Fig. C.2) due to higher air temperatures (not shown) compared to REF lead to an additional decrease of the Filchner Trough mean salinity by up to 0.2 psu over the course of 10 years of transition time, converging to a new mean state for all three time slices (Fig. 6.5d). Additionally, lower wind speeds in most of the southern Weddell Sea reduce the wind stress on sea ice and ocean, except for some areas at the eastern Ronne Ice Shelf Front and the Filchner Ice Shelf, where stronger off-shore winds dominate. In contrast to the salinity, the mean potential temperature does not appear to be sensitive to the forcing change (Fig. 6.5c) in the transition time. In the FECO experiment, the circulation across the Filchner Trough sill and in the trough experiences a regime shift that REF does not. In 2093, mWDW enters the Filchner Trough as a near-bottom current across the sill, strongly increasing the temperature in the trough (Fig. 6.5c). This is not the first occasion for mWDW to influence the temperature of the Filchner Trough. Over the course of the 21st century, REF shows increasingly stronger seasonal pulses of mWDW crossing into the Filchner Trough across the shelf east of Filchner Trough and along the eastern slope of the trough (Fig. C.8). Over the course of the reference simulation, we find an increase in the temperature of the mWDW

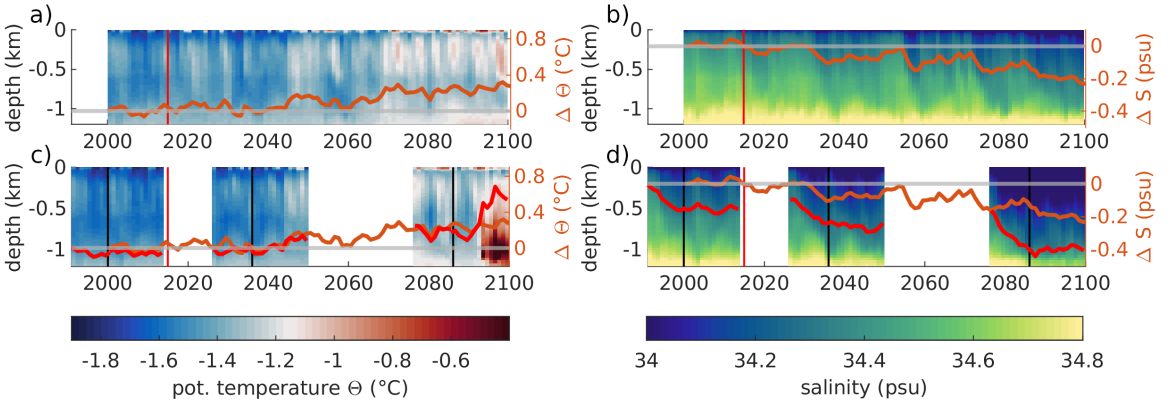


**Figure 6.5:** Hovmöller diagram of the yearly mean temperature in Filchner Trough (see Fig. 3.2) for (a) REF and (c) FECO. Colored lines show the relative temperature change of the horizontally and vertically averaged temperature of the whole water column compared to 2000. (b) & (d) Same as (a) & (c) but for salinity. Orange lines in (c) and (d) are the same as the orange lines in (a) and (b), respectively. Red line marks the relative change of the average temperature/salinity in FECO. Red vertical line: boundary between historical and future climate scenario. Black vertical lines: boundary between transition time and experiment in FECO.

pulses, originating in a warming of the slope current. The slope current shows a warming trend of approx. 0.053°C per decade between 2000 and 2100. This agrees well with the 0.05°C per decade that were observed between 1980 and 2010 (Schmidtko et al., 2014). Previous studies have suggested that warmer and longer-lasting pulses can be a precursor for a regime shift in the Filchner Trough from a DSW-dominated to a mWDW dominated state (Nissen et al., 2023; Ryan et al., 2020; Teske et al., 2024b; Timmermann and Goeller, 2017; Timmermann and Hellmer, 2013), but despite the increase in the mean temperature and the visible mWDW pulses, no sudden warming of the trough occurs in REF.

Before the regime shift in FECO, the reduced density of the upper 1000 m in the open ocean leads to changes in the position and symmetry of the V-shape above the continental slope (Fig. 6.6). The comparison of the seasonal positions of the deepest point of the 27.4 $kg\,m^{-3}$ isopycnal in FECO for 2088-2092 (Fig. 6.6b) - chosen for its position at depth above the continental slope at all times, but nearly no intersection with the surface in REF - yields an additional horizontal component to the seasonal depth variation seen in REF (Fig. 6.6a). This horizontal movement displaces the V-shape by approx. 50 km between summer, when the deepest point of the V-shape is at its southernmost point, and winter. The deepest point of the V-shape is closest to the sill in summer and furthest away in winter (Fig. 6.6b). In addition, the V-shape reaches its deepest position in spring and summer, while REF reaches the deepest point in winter and spring. The fresher water masses on the continental shelf in FECO cause the southern arm of the V-shape to be very flat and to vanish during autumn (Fig. 6.6b, yellow curve). Stronger Ekman downwelling in autumn, but a late onset of the freezing season lead to a situation that temporarily resembles fresh-shelf regions like the Dronning Maud Land section (Fig. 6.1d), though sea-ice formation in winter regularly restores the V-shape.

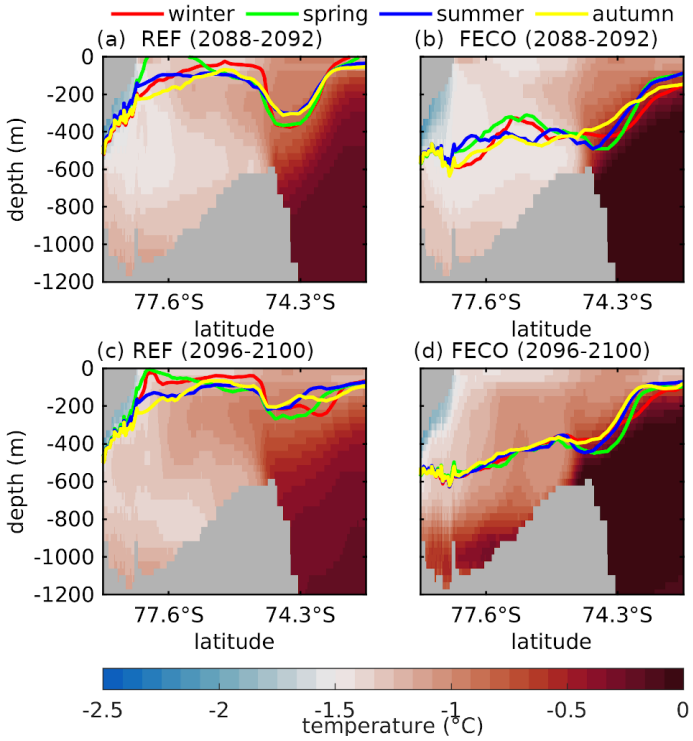


**Figure 6.6:** Potential temperature in the 2088-2092 mean (5 years before regime shift in FECO) in a) REF and b) FECO. Colored lines show the position of the 27.4 kg m$^{-3}$ isopycnal. c) and d) same as a) and b) but for 2096-2100.

### 6.3.3 Accelerated density redistribution with high-resolution atmospheric forcing

The high-resolution atmospheric forcing does not only affect the slope front symmetry and seasonality, but also accelerates the reduction of density over the 21st century compared to REF (Fig. 6.7). The differences in the density evolution between REF and FECO are particularly large in Filchner Trough (Fig 6.7a). Here, the application of CCLM forcing leads to a negative density trend between 2000 and 2092 that is 1.47 times larger than in REF. Values after 2092 were excluded from the calculation due to the impact the regime shift has on the density of the Filchner Trough. In contrast, above the continental slope north of the Filchner Trough sill, the trend is slightly smaller in FECO than in REF (-1.5 kg m$^{-3}$ century$^{-1}$ as compared to -1.6 kg m$^{-3}$ century$^{-1}$; Fig. 6.7b). Separately assessing the trends in temperature and salinity reveals that the density trend on the continental shelf is driven by freshening, while the trend in the slope current is driven by a combination of warming and freshening (Fig. C.9). From this we conclude that reduced sea-ice formation is not the only factor influencing the density distribution across the continental slope, but the dominating one for the existence of the V-shape.

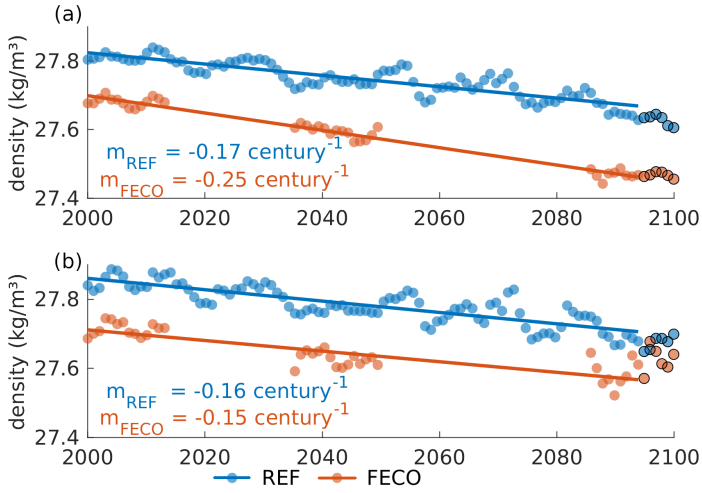


**Figure 6.7:** Linear regression of the annual mean potential density relative to 1000 kg $m^{-3}$ over time in a) the Filchner Trough and b) at the Filchner Trough Sill at 636 m depth for REF in blue and FECO in red. The slope of each linear fit is given in the figure. Data points outlined in black were excluded from the calculation due to the regime shift in 2093. The areas over which properties are averaged for the time series are indicated in Fig. 3.2.

## 6.4 Influence of cross-slope currents on the V-shaped density distribution

With the onset of the near-bottom current of mWDW entering the Filchner Trough in FECO in 2093, the V-shaped density distribution at the continental slope experiences pronounced structural changes that lead to the loss of the southern arm of the V-shape. Visible as a sudden increase in the average temperature in the Filchner Trough (Fig. 6.5c), the inflow of mWDW in FECO in 2093 brings the bottom density in the Filchner Trough closer to that of the slope current. This has the effect of increasing the stratification of the water column. In combination with low sea-ice formation rates and reduced mixing (not shown) during the freezing season, the seasonal variations in the southern arm of the V-shape vanish at depths below approx. 450 m (Fig. 6.6d), in contrast to REF, where the V-shape is formed also at greater depths (Fig. 6.6c). Seasonal variations of the depth of the V-shape and the position of the northern arm remain, however, the southern arm of the V-shape decreases strongly in vertical extent. From a height difference in spring of approx. 200 m between the deepest point of the V-shape and the shallowest point above the continental shelf, the 27.4 kg $m^{-3}$ isopycnal position reduces to a vertical range of approx. 80 m after the bottom current onset. With the near-bottom inflow of mWDW into the trough, the sensitivity of the southern arm of the V-shape to sea-ice formation is reduced, while the northern arm, which is created by the wind, remains.

The timing of the intensified mWDW flux in FECO can be related directly to the density gradient across the Filchner Sill and the depth of the thermocline at the sill. In FECO, the thermocline remains above the Filchner Trough sill depth throughout the 15-year FECO simulation and stays between 400 m to 600 m depths, while the thermocline in REF rises from approx. 1000 m in 2000 to 600 m depth over the course of the 21st century (last 15 years

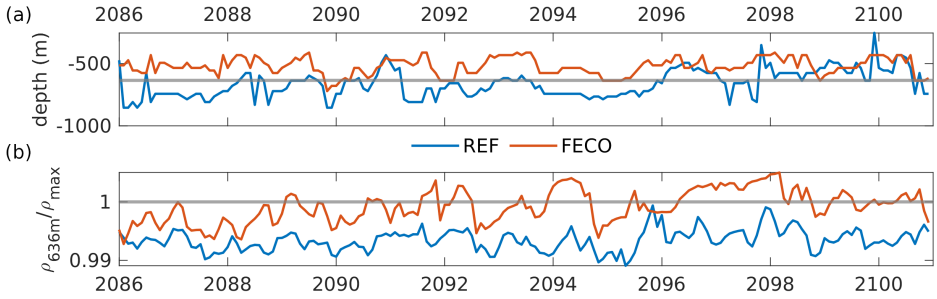


**Figure 6.8:** a) Depth of the thermocline at the Filchner Sill (horizontal line: sill depth at 636 m) and b) density ratio between the maximum density in Filchner Trough ($\rho_{max}$) and the mean density at the Filchner Trough sill (see Fig. 3.2) at 636 m depth ($\rho_{636m}$).

shown in Fig. 6.8a). The sill depth of approx. 600 m (horizontal gray line in Fig. 6.8a) is only crossed occasionally and never for an extended period of time. Despite the thermocline in FECO already reaching above the sill from the beginning of the time slice 2086-2100, the warm near-bottom current is still only developing at a later date. This agrees with the conclusions presented by Haid et al. (2023) suggesting that another key factor for or against an inflow of mWDW onto the continental shelf in addition to the depth of the mWDW at the slope is the density ratio between the dense water on the shelf and the slope current (see also Nissen et al., 2023).

The inflow of mWDW onto the continental shelf is not only visible in the cross-slope density structure, but also as a disruption of the V-shape in along-slope direction. In both simulations, the GOC at the Filchner Sill shows multiple minima between 2086 and 2100, demonstrating phases of instability of the Antarctic Slope Front where the barrier across the sill is weakened (Fig. 6.9). However, not all of the recognised events of a minimum GOC are related to an increased flow of mWDW into the Filchner Trough. The comparison of the southward mWDW ($\Theta$ >-0.8°C) transport in the Filchner trough across the central Filchner Trough sill with the GOC in FECO shows a significant correlation with a lag of 3 months (p=0.0005, r=0.35) between the maximum mWDW transport and a minimum of the GOC after 2093 (Fig. 6.9). In REF, there is not only a lagged correlation between the inflow of mWDW with the GOC (p=7e-7, r=0.36) but also weakly between the outflowing DSW ($\Theta$ <-0.8°C) and the GOC (p=0.0001, r=0.29), while FECO does not show this correlation (p=0.27, r=0.08). The calculation of the GOC was performed for 250 m depth, where the V-shape is present at all times, even when it is less pronounced. The changing circulation patterns associated with the density reorganization on the shelf in FECO decouple the weak correlation between the water export and GOC that can be found in REF.

## 6.5 Discussion

### 6.5.1 Drivers of the accelerated density redistribution: wind speed and sea ice

Our results show that for the high-emission scenario SSP3-7.0, lower sea-ice production in a simulation with high-resolution atmospheric forcing data accelerate the density redistribution

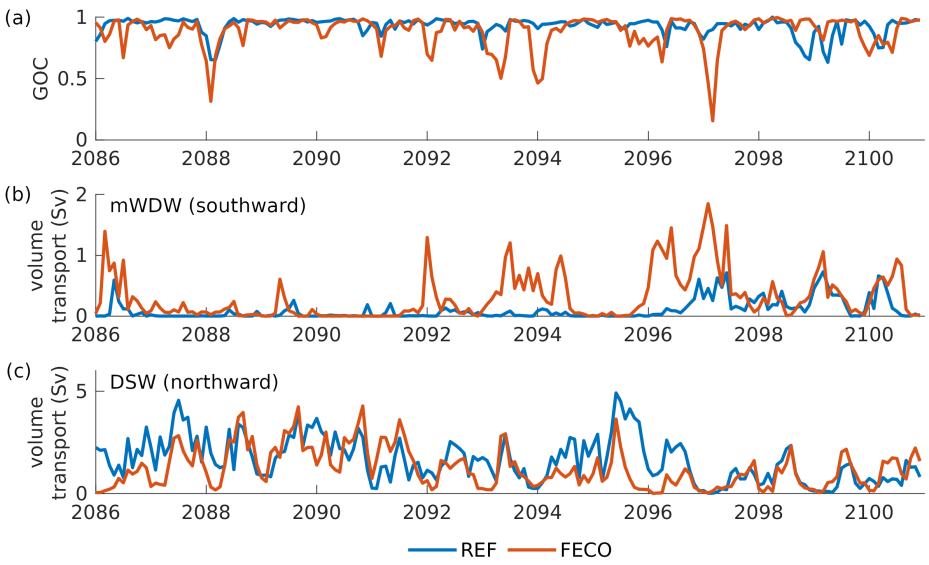


**Figure 6.9:** a) Time series of the grade of connectivity (GOC) of the V-shaped density structure above the continental slope at the Filchner Trough sill for REF (in blue) and FECO (in red; for area outline see Fig. 3.2; for calculation see section 3.2.2). b) Southward volume transport in Sv across Filchner Sill Central (see Fig. 3.2) of water masses mWDW with a potential temperature of $\Theta$>-0.8°C and c) northward volume transport of DSW ($\Theta$<-0.8°C).

on the continental shelf of the southern Weddell Sea relative to a simulation with lower-resolution atmospheric forcing. Subsequently, the accelerated density redistribution induces a regime shift in the Filchner Trough area before the end of the 21st century. The regime shift from a DSW-dominated to a mWDW-dominated state is accompanied by the near-loss of the southern arm of the V-shaped density distribution at the continental slope that prominently separates the shelf from the open ocean in today's climate.

The main factors controlling the circulation regime in Filchner Trough are the wind field and sea-ice production (Teske et al., 2024b), which directly influence the density distribution on the shelf. The on-shore transport of mWDW, which intensifies in the case of a regime shift, strongly depends on the density ratio across the continental slope at the Filchner Trough sill. This ratio changes faster in FECO than in REF, driven by an accelerated freshening of the continental shelf in response to higher summer temperatures and weaker wind speeds in CCLM. Higher summer air temperatures in FECO compared to REF lead to a stronger decline and local melting of summer sea-ice. Since multi-year mean air temperatures are actually lower in FECO than in REF, this emphasizes the importance of the seasonal cycle.

Weaker wind speeds may have two effects: (i) smaller heat loss to the atmosphere, and (ii) less wind-driven sea-ice transport. Both effects tend to reduce sea-ice production and thus winter brine release in regions that are dominated by freezing and export of sea ice. In contrast, stronger off-shore winds at the Filchner Ice Shelf front in FECO increase the occurrence and width of coastal polynyas that locally cause higher sea-ice production rates. While this could counteract some of the freshening of the Filchner Trough, the net effect appears to be dominated by the weaker off-shore winds in the high-resolution atmosphere

model.

In the historical time period between 2010 and 2014, REF produces a steeper, narrower temperature and density gradient across the ASF at 300 m depth during winter than during summer, which agrees with the assessment of the ASF by Pauthenet et al. (2021). According to their study, the ASF forming the northern arm of the V-shape has the smallest meridional extent during winter months, which translates to a strong temperature gradient. The steepening is a result of stronger DSW export in winter. The entrainment of colder, fresher surface water suppresses the isopycnal and forces the isopycnal and thermocline into a steeper position. However, observational data for winter in the ice-covered southern Weddell Sea are scarce, leading to high uncertainties in the assessment of the position and extent of the ASF in the southern Weddell Sea. Additionally, Pauthenet et al. applied their analysis at 300 m at relatively shallow depths for the Weddell Sea, where the pycnocline extends deeper than 380 m (Thompson et al., 2018). As Fig. 6.2 has shown, the isopycnals are steeper in greater depth. It is therefore unclear if the shift in the minimum extent of 1.53° of the distance between the -0.7°C and -0.3°C isotherms at 300 m depth in winter during 2010-2014 of REF to a minimum extent of 5.41° in summer in 2096-2100 (Fig. C.4b) is an effect of climate change and the shift in the front dynamics.

The decreasing wind strength over the 21st century in REF reduces the Ekman transport and downwelling above the continental shelf. Multiple studies have shown that a strengthening and poleward shift of the westerlies and a weakening of the easterly winds above the continental shelf will weaken the Ekman downwelling along the coast of the Weddell Sea (Naughten et al., 2021; Spence et al., 2017; Teske et al., 2024b). The indirect influence of the wind strength on the flow of Antarctic Surface Water and mWDW onto the continental shelf has also been shown in previous studies (Dinniman et al., 2015; Haid et al., 2015; Hatterman, 2018; Hattermann et al., 2014). In particular, Hattermann et al. (2014) described the weakening of shallow and the strengthening of deep inflow towards the Fimbul ice shelf cavity in response to weaker easterly winds based on observations and modelling results. The projected reduced wind speed of the easterlies in our model towards the end of the 21st century and the southward shift of the mid-latitude westerlies, consistent with Spence et al. (2014) and Goyal et al. (2021), broaden the V-shaped density structure at the continental slope and reduce its depth in REF, as seen in Fig. 6.1. The uplift of the thermocline due to weakened downwelling lifts mWDW closer to the sill depth and slowly increases the amount of mWDW flowing into the Filchner Trough. A similar signature is found when comparing results from FECO with those from REF: The generally weaker wind speeds in the southern Weddell Sea in FECO than in REF weaken the Ekman downwelling further, reducing the V-shape depth in comparison to REF. The reduced density gradient weakens the barrier effect of the cross-slope gradient further and allows the strong cross-slope current to develop towards the end of the century that does not develop in REF.

### 6.5.2 Drivers of the accelerated density redistribution: cross-slope density gradient

One of the main criteria for the potential of the current system in the Filchner Trough to switch from a DSW-dominated state to the mWDW-dominated state is the density gradient across the Filchner Trough sill as has been previously shown (Haid et al., 2023; Nissen et al., 2023; Ryan et al., 2017). A near-bottom current of mWDW onto the continental shelf only develops once this gradient flattens out or reverses. Our results show that this on-shelf current disrupts the V-structure at the slope, reducing the V-shape to the upper 450 m of the water column and warming the Filchner Trough. The horizontal distance of the ASF (northern arm of the V-shape) to the continental slope varies over the year as shown in an analysis of observational data by Pauthenet et al. (2021). The introduction of the GOC provides a metric for the stability of the ASF in areas of cross-slope transport in dense-shelf areas. However, not all features of the V-shape of the ASF are included. The GOC is useful to detect strong changes in the cross-slope density distribution that remove the dip in the isopycnals or lead to a very large meridional displacement within the V-shape. What the GOC is not able to do, is to differentiate between a lot of small displacements that just exceed the distance threshold $d_L$ and few very large meridional distances. Also, the selection of $d_L$ as a maximum displacement before it reduces the GOC influences the result. A distance larger than ten times the grid size reduces the number of recognised events by 12.5 % compared to a $d_L$ of two times the grid size; with $d_L$ 100 times the grid size, the number of recognised events decreases by 29.1 %. The three-month delay between intensified cross-slope currents and a minimum event of the GOC at 250 m depth indicates a connection based on seasonal cross-slope water transport. Ryan et al. (2017) showed that during winter intensified DSW production and export suppress the isopycnals at the continental slope, reducing or stopping on-shore transport of mWDW. This conclusion is back up by the lack of correlation in FECO where DSW production is reduced compared to REF. The lack of non-delayed correlation between cross-slope currents and the GOC indicates that an intensified bottom current does not destabilize the ASF in shallower than sill depth. This also implies that a (hypothetical) decreasing trend in the GOC cannot be regarded as an indicator that a cold-to-warm regime shift in Filchner Trough is about to occur in the near future.

#### Comparison to other studies

Considering our results in the context of other scenario simulations for the 21st century, it becomes clear that the choice of atmospheric forcing data has a strong impact on the susceptibility of Filchner Trough to undergo a regime shift before 2100. Previous future projections produced a tipping of the Filchner Trough circulation in very high-emission scenarios (e.g., SSP5-8.5 or similar; Nissen et al., 2023; Timmermann and Hellmer, 2013) or idealized scenarios (e.g., 1pctCO2 scenario; Naughten et al., 2021). Ocean simulations with lower emission scenarios generally did not produce a regime shift (Nissen et al., 2023; Timmermann and Hellmer, 2013), except in case of a coupled atmospheric component (Teske et al., 2024b, regime shift in SSP3-7.0 and SSP5-8.5 scenarios). While our reference simulation for the emission scenario SSP3-7.0 does not produce a regime shift during the 21st

century, downscaling of the atmosphere in FECO induces a strong mWDW inflow before the end of the 21st century. We therefore conclude that the potential for a regime shift in a warming climate in the SSP3-7.0 scenario might be higher than suggested by previous studies using relatively low-resolution atmospheric forcing (Nissen et al., 2023). With the currently implemented policies, global warming is projected to be between 2.2°C and 3.5°C by 2100, which corresponds to the warming projected for the SSP2-4.5 (2.1°C-3.5°C) and SSP3-7.0 (2.8°C-4.6°C) scenarios (IPCC, 2023). Our results thus highlight the importance of developing a better understanding of the potential implications for vulnerable climate components like the Antarctic Slope Front and the Filchner Trough in the current climate development.

### 6.5.3 Limitations and caveats

Several studies have suggested that eddies play an important role in the transport of Circumpolar Deep Water across the continental shelf break (Nøst et al., 2011; Stewart and Thompson, 2015a). Our model is not eddy-resolving, but it has an eddy-permitting grid resolution on the Weddell Sea continental shelf (∼3-12 km). It has been proposed by Nøst et al. (2011) that freshening of the shelf can lead to increased eddy kinetic energy which drives onshore cross-ASF eddy transport. The resolution of approx. 12 km at the continental slope in our model grid might lead to an underrepresentation of eddies, the Rossby radius in the southern Weddell Sea being 2-5 km. With reduced eddy presence, the model might underestimate cross-slope volume transport. An underrepresentation of eddy-driven on-shore transport of mWDW would mean a greater depth of the V-shape as the lack of mesoscale eddies reduces the relaxation of the isopycnals above the continental slope (Dettling et al., 2024). As a result, the temperatures on the continental shelf would be underestimated. A shallower V-shape at the continental slope in a simulation with an adequate eddy representation might lead to an earlier regime shift of the Filchner Trough due to the lower density gradient into the shelf and the higher connectivity between the slope current and the Filchner Trough through the sloping isopycnals.

We have presented model results indicating the future evolution of the density distribution across the Filchner Trough sill, a key property of the Antarctic Slope Front in the Southern Weddell Sea. The reference simulation REF and the experiment simulation FECO with downscaled atmospheric forcing both reproduce the typical V-shaped density distribution that is formed by interplay of Ekman downwelling and Dense Shelf Water export in the southern Weddell Sea. Sea ice loss in the warming climate of the SSP3-7.0 emission scenario decreases the density on the continental shelf and flattens the southern arm of the V-shape in REF and FECO. This causes an increased sensitivity of the density distribution on the continental shelf to seasonal wind speed variations. Using results from a regional, high-resolution atmosphere model as forcing, we find an acceleration of the density redistribution on the continental shelf, which leads to a regime shift with modified Warm Deep Water entering Filchner Trough before the end of the 21st century for the high emission scenario SSP3-7.0. Colder air temperatures in the multi-year mean are more than outweighed by the warmer summer air temperatures of the regionally down-scaled atmosphere, accelerating density loss on the continental shelf,

which ultimately leads to a regime shift from a cold Dense Shelf Water dominated Filchner Trough to a warm, modified Warm Deep Water dominated trough in 2093. The criterion of spatial coherency of the V-shape along the continental slope, quantified by the grade of connectivity, is not usable as a tool to predict an imminent regime shift because the southward transport of modified Warm Deep Water is, contrary to our expectations, not a result of a weakening of the slope front, but instead leads to a temporary disturbance of the ASF and the associated V-shape. While the density minimum is completely restored after disruption in present-day climate, in a warming climate the distinct V-shape remains confined to the upper ocean. Due to the geostrophic nature of the Antarctic Slope Current, the flattening of the northern arm of the V-shape and stronger seasonality will affect the transport of the slope current and the transport of heat towards the peninsula and onto the continental shelf in the future.

The accelerated density redistribution by the high-resolution atmospheric data and the resulting regime shift show that the potential for a regime shift in the Filchner Trough in the SSP3-7.0 scenarios is higher than previously published ocean simulations of the same scenario suggest. With the current climate policies, the projected 21st-century global warming lies within the potential range of the SSP3-7.0 scenario, increasing the urgency to better understand and represent vulnerable climate components.

CHAPTER

# SEVEN

## FINAL CONSIDERATIONS

### 7.1 Summary

In this thesis, the impact of changing atmospheric conditions on the sea-ice formation in the southern Weddell Sea and on the ocean circulation in Filchner Trough was analyzed. For this purpose, in addition to a historical coupled climate simulation for the years 2000 to 2014, one low (SSP1-2.6), medium (SSP2-4.5), high (SSP3-7.0) and very high (SSP5-8.5) emission scenario were analyzed with regard to changing characteristics of the southward transport of mWDW into Filchner Trough, and its drivers. To further look into the influence of atmospheric conditions on sea ice and the underlying ocean, global ocean simulations forced with atmospheric data from the coupled climate simulation (high emission scenario SSP3-7.0, low resolution) and with a dynamically downscaled data set with higher model resolution for the same scenario were performed. In the following, I will summarize the results of the previous chapters in light of the research objectives stated in Chapter 1:

1. Assessment of atmospheric conditions, oceanic processes and sea-ice production governing on-shore heat transport in climate runs of present climate

The previous chapters have presented three simulations that cover the historical period of recent climate from 2000 to 2014: the coupled climate simulation for CMIP6, the ocean simulation REF (forced with atmospheric output from the coupled climate model) and the ocean simulation FECO (forced with data from the high-resolution atmosphere model CCLM). Of these three, the coupled climate simulation reproduces the seasonal pulsing character of seasonal southward mWDW transport seen in observations the best. While REF and FECO also produce on-shore transport of mWDW of similar volume, the seasonal signal is very weak compared to the coupled climate simulation. In Chapter 4, the main drivers for mWDW transport have been found to be local sea-ice formation and a shoaling thermocline at the continental slope, agreeing well with other modeling studies and observations (Daae et al., 2020; Darelius et al., 2016; Morrison et al., 2020; Ryan et al., 2020). The variability is less pronounced in the standalone ocean simulations, the higher density on the shelf preventing strong mWDW pulses. It has also been shown that the thermocline depth at

the continental slope is suppressed by local downwelling related to the surface stress curl (Chapters 4 & 6). With atmospheric data with lower wind speeds (FECO), this leads to a relaxation of the thermocline. Generally, it was found that the processes governing the southward heat transport into Filchner Trough could be produced in coupled climate as well as standalone ocean simulations.

2. Assessment of changes in atmospheric conditions, oceanic processes and sea-ice production in climate model simulations for a suite of future emission scenarios

It has been shown in Chapter 4 that the development of the Filchner Trough hydrography and dynamics strongly depend on the forcing scenario. The process of warm water intrusions in Filchner Trough has been assessed in coupled climate simulations within the hierarchy of four climate scenarios. Of the four scenarios, the high and very high emission scenarios SSP3-7.0 and SSP5-8.5 produce a regime shift in the Filchner Trough that will lead to increasing melt rates at the ice shelves and accelerated ice sheet mass loss. The regime shift is driven by density loss on the continental shelf and a strong shoaling of the thermocline at the continental slope, lifting mWDW above the Filchner Trough sill. In Chapter 6, is has also been demonstrated that the ocean simulation REF, which is forced with data from the SSP3-7.0 scenario, does not produce the regime shift. Instead, the temperature development showed a gradual increase over the whole 21st century.

In Chapter 4, three phases of ocean climate change in Filchner Trough were defined: I. The Filchner Trough is filled with cold, dense shelf water with seasonal phases of weak inflow of mWDW. II. The Filchner Trough is increasingly dominated by pulses of mWDW while salinity in the trough slowly declines. III. The mean temperature in the trough rises permanently above -1°C and the trough is mostly filled with mWDW. These phases can also be identified in the REF simulation, which shows an increase in the duration and warmth of mWDW pulses but does not reach Phase III. The warmer and longer pulses are caused by the decrease in density especially in the upper part of the water column through reduced sea-ice formation and increased melting on the continental shelf, the uplift of the thermocline above sill depth allowing southward mWDW transport. However, the density loss on the shelf is not large enough to tip the density scale as defined by Haid et al. (2023) in favor of the off-shore mWDW. The density on the continental shelf is mainly influenced by salinity. The comparison of the shelf water salinity in the Filchner Trough between the coupled climate simulation (Fig. A.1) and REF (Fig. 6.7) shows that the salinity in REF is generally higher over the whole simulation than in the coupled climate simulation. The main mechanism behind the density and salinity changes on the continental shelves can be found in the differences in sea-ice formation. Comparison of polynya size and productivity in Chapter 5 have shown much higher sea-ice production rates in REF compared to the coupled climate simulation for the same scenario, resulting in higher brine rejection rates and a denser DSW on the continental shelf. Due to increased radiative forcing in the SSP3-7.0, lower amounts of sea ice are formed in the Weddell Sea towards the end of the century. In contrast to REF, the ocean simulation with downscaled atmospheric forcing (FECO) has been found to produce a regime shift in the Filchner Trough (Chapter 6). While the three time slices that were performed for this simulation do not produce a continuous temperature record for Filchner Trough for the 21st

century, Fig. 6.3 shows the increase in the duration and temperature of the mWDW pulses shallower than 500 m. The simulation reaches Phase III in 2093, when a near-bottom current develops and transports large amounts of heat/mWDW into the trough, caused by a stronger density loss than in REF.

The regime shift is associated with a strong near-bottom current of mWDW crossing the continental slope into the trough. In an attempt to find an early indicator for an imminent regime shift, in Chapter 6 we established the grade of connectivity (GOC) as a spatial indicator for the coherence of the Antarctica Slope Front. However, a weakening of the slope front in the upper 300 m of the water column is not a cause for a cross slope current, but instead only for a temporary disturbance following the current crossing the slope. The GOC as defined in this study is thus not applicable as an early warning system for a regime shift.

3. Assessment of oceanic processes and sea-ice production in response to changes in atmospheric meso-scale processes

To assess the influence of meso-scale atmospheric processes on sea-ice production in polynyas on the continental shelf of the southern Weddell Sea and on the southward heat transport into Filchner Trough, Chapter 5 & 6 analyzed the ocean simulations REF and FECO. It has been shown that the application of data from a high-resolution atmosphere model in FECO provokes a regime shift at the end of the century. Chapter 5 also demonstrated the changes to the atmosphere caused by the dynamic downscaling, the more detailed representation of local orography leading to lower 2-m temperatures and lower wind speeds over large regions of the Weddell Sea. This has the effect of generally increasing sea-ice formation north of the continental shelf, but decreasing sea-ice formation rates in the polynyas on the continental shelf. Towards the end of the century, the changes in the forcing even lead to a redistribution of melting and freezing regions, leading to an even stronger freshening of the continental shelf. Comparison of the shelf salinity between FECO and the coupled climate simulation of SSP3-7.0 shows that the freshening on the shelf places FECO closer to the coupled climate simulation relative to REF, creating the necessary conditions for a regime shift in FECO.

We conclude that the future evolution of hydrography in and around Filchner Trough, i.e. in a key region of ocean-ice sheet interaction that - despite its regional character - is relevant literally on a global scale, is determined by the trajectory of future climate change, with the atmosphere being the dominant component. A tipping point in the ocean and the Antarctic ice sheet can only be avoided if ambitious climate change mitigation steps are taken. With the current climate policies, the projected 21st-century global warming lies within the potential range of the SSP3-7.0 scenario. In the SSP3-7.0 scenario the applied atmospheric data plays a deciding role in the tipping behaviour of the Filchner Trough. The propensity for a regime shift is larger with highly resolved atmospheric data than with the coarser data set. Given that most previous projections are based on coarse-scale atmosphere models, our results also indicate that the potential for a regime shift or tipping point in the Filchner Trough may be higher than previously suggested.

## 7.2 Outlook

To accurately project or predict the fate of the Antarctic Ice Sheet, we need to understand all mechanisms involved in the heat transport towards its vulnerable ice shelves. The primary reason for a regime shift or tipping point is the reversal of the cross-slope density gradient, but its development depends on the climate scenario and the representation of atmospheric processes. In this thesis, only the influences of atmospheric processes on the on-shore heat transport and the structural changes at the Antarctic Slope Front at the Filchner Trough sill were covered. To improve the process representation in the ocean, additional dynamical components need to be considered. It has been established that tides have a large influence on heat transport onto the shelf and specifically into the ice shelf cavities of the southern Weddell Sea (Hausmann et al., 2020; Stewart et al., 2019). The influence of eddy overturning of the Antarctic Slope Front has also been recognised as an important component of on-shore heat transport (Huneke et al., 2022; Nøst et al., 2011). The model grids used in our simulations permit the development of eddies, but they do not reach a resolution that is sufficient to fully resolve them. In order to improve the current results and obtain realistic predictions or robust projections for ocean dynamics and hydrography on the continental shelves of the southern Weddell Sea in a warming climate, these components need to be integrated into the model. Lastly, the available long-term observations of the Filchner Trough are limited, hampering our knowledge of the actual pathways onto and on the continental shelf of the southern Weddell Sea. The results of this thesis show that a substantial part of the seasonal heat transport crosses onto the continental shelf via the eastern slope of the Filchner Trough, and even via the eastern shelf directly. However, long-term observations do only cover a very small section of this area. Additionally, the western slope of the Filchner Trough is not covered by long-term observations at all, which are needed to cover all branches of the local ocean circulation in and around the Filchner Trough.

# BIBLIOGRAPHY


Akhoudas, C.H., Sallée, J.B., Haumann, F.A., Meredith, M.P., Garabato, A.N., Reverdin, G., Jullion, L., Aloisi, G., Benetti, M., Leng, M.J., Arrowsmith, C., Ventilation of the abyss in the Atlantic sector of the Southern Ocean. Scientific reports, Vol. 11 (2021):6760, doi:10.1038/s41598-021-86043-2

Arbetter, T.E., Lynch, A.H., Bailey, D.A., Relationship between synoptic forcing and polynya formation in the Cosmonaut Sea: 1. Polynya climatology. Journal of Geophysical Research: Oceans, Vol. 109 (2004):1–12, doi:10.1029/2003JC001837

Armitage, T.W.K., Kwok, R., Thompson, A.F., Cunningham, G., Dynamic Topography and Sea Level Anomalies of the Southern Ocean: Variability and Teleconnections. Journal of Geophysical Research: Oceans, Vol. 123 (2018):613–630, doi:10.1002/2017JC013534

Armour, K.C., Marshall, J., Scott, J.R., Donohoe, A., Newsom, E.R., Southern Ocean warming delayed by circumpolar upwelling and equatorward transport. Nature Geoscience, Vol. 9 (2016)(7):549–554, doi:10.1038/ngeo2731

Arneborg, L., Wåhlin, A.K., Björk, G., Liljebladh, B., Orsi, A.H., Persistent inflow of warm wate ronto the central Amundsen shelf. Nature Geoscience, Vol. 5(12) (2012):876–880, doi:10.1038/ngeo1644

Årthun, M., Nicholls, K.W., Makinson, K., Fedak, M.A., Boehme, L., Seasonal inflow of warm water onto the southern Weddell Sea continental shelf, Antarctica. Geophysical Research Letters, Vol. 39(17) (2012):2–7, doi:10.1029/2012GL052856

Baines, P., A model for the structure of the Antarctic Slope Front. Deep Sea Research Part II: Topcial Studies in Oceanography, Vol. 56 (2009):859–873, doi:10.1016/j.dsr2.2008.10.030

Beadling, R.L., Krasting, J.P., Griffies, S.M., Hurlin, W.J., Bronselaer, B., Russell, J.L., MacGilchrist, G.A., Tesdal, J., Winton, M., Importance of the Antarctic Slope Current in the Southern Ocean Response to Ice Sheet Melt and Wind Stress Change. Journal of Geophysical Research: Oceans, Vol. 127 (2022):e2021JC017608, doi:10.1029/2021JC017608

Beckmann, A., Hellmer, H. H. andand Timmermann, R., A numerical model of the Weddell Sea: Large-scale circulation and water mass distribution. Journal of Geophysical Research, Vol. 10(C10) (1999):375–391, doi:10.1029/1999jc900194

Blanchard-Wrigglesworth, E., Cox, T., Espinosa, Z.I., Donohoe, A., The Largest Ever Recorded Heatwave—Characteristics and Attribution of the Antarctic Heatwave of March 2022. Geophysical Research Letters, Vol. 50 (2023)(17):1–11, doi:10.1029/2023GL104910

Boisvert, L., Vihma, T., Shie, C., Evaporation From the Southern Ocean Estimated on the Basis of AIRS Satellite Data. Journal of Geophysical Research: Atmospheres, Vol. 125 (2020)(1):1–26, doi:10.1029/2019JD030845

Cape, M.R., Vernet, M., Skvarca, P., Marinsek, S., Scambos, T., Domack, E., Foehn winds link climate-driven warming to ice shelf evolution in Antarctica. Journal of Geophysical Research: Atmosphere, Vol. 120 (2015), doi:10.1002/2015JD023465

Church, J.A., White, N.J., Sea-Level Rise from the Late 19th to the Early 21st Century. Surveys in Geophysics, Vol. 32 (2011)(4-5):585–602, doi:10.1007/s10712-011-9119-1

Clem, K.R., Fogt, R.L., Turner, J., Lintner, B.R., Marshall, G.J., Miller, J.R., Renwick, J.A., Record warming at the South Pole during the past three decades. Nature Climate Change, (2020):762–770, doi:10.1038/s41558-020-0815-z

Comiso, J.C., Gordon, A.L., Cosmonaut polynya in the Southern Ocean: Structure and variability. Journal of Geophysical Research: Oceans, Vol. 101 (1996):18297–18313, doi:10.1029/96JC01500

Daae, K., Hattermann, T., Darelius, E., Mueller, R., Naughten, K.A., Timmermann, R.e.a., Necessary Conditions for Warm Inflow Toward the Filchner Ice Shelf, Weddell Sea. Geophysical Research Letters, Vol. 47(22) (2020):e2020GL089237, doi:10.1029/2020GL089237

Danilov, S., Wang, Q., Timmermann, R., Iakovlev, N., Sidorenko, D., Kimmritz, M., Jung, T., Schröter, J., Finite-Element Sea Ice Model (FESIM), version 2. Geoscientific Model Development, (2015):1747–1761, doi:10.5194/gmd-8-1747-2015

Darelius, E., Strand, K.O., Østerhus, S., Gammeslrød, T., Årthun, M., Fer, I., On the seasonal signal of the Filchner overflow, Weddell Sea, Antarctica. Journal of Physical Oceanography, Vol. 44(4) (2014):1230–1243, doi:10.1175/JPO-D-13-0180.1

Darelius, E., , Fer, I. (2015): Physical oceanography from CTD in the Filchner Depression (Weddell Sea, Antarctica) during Ernest Shackleton cruise ES060. doi:10.1594/PANGAEA.846962

Darelius, E., Fer, I., Nicholls, K.W., Observed vulnerability of Filchner-Ronne Ice Shelf to wind-driven inflow of warm deep water. Nature Communications, Vol. 7 (2016):1–7, doi:10.1038/ncomms12300

Darelius, E., Daae, K., Dundas, V., Fer, I., Hellmer, H.H., Janout, M., Nicholls, K.W., Sallée, J.B., Østerhus, S., Observational evidence for on-shelf heat transport driven by dense water export in the Weddell Sea. Nature Communications, Vol. 14 (2023)(1), doi:10.1038/s41467-023-36580-3

de la Vara, A., Cabos, W., Sein, D.V., Sidorenko, D., Koldunov, N.V., Koseki, S.e.a., On the impact of atmospheric vs oceanic resolutions on the representation of the sea surface temperature in the South Eastern Tropical Atlantic. Climate Dynamics, Vol. 54(11-12) (2020):4733–4757, doi:10.1007/s00382-020-05256-9

De Lavergne, C., Palter, J.B., Galbraith, E.D., Bernardello, R., Marinov, I., Cessation of deep convection in the open Southern Ocean under anthropogenic climate change. Nature Climate Change, Vol. 4 (2014)(4):278–282, doi:10.1038/nclimate2132

DeConto, R., Pollard, D., Contribution of Antarctica to past and future sea-level rise. Nature, Vol. 531 (2016):591–597, doi:10.1038/nature17145

Dettling, N., Losch, M., Pollmann, F., Kanzow, T., Toward Parameterizing Eddy-Mediated Transport of Warm Deep Water across the Weddell Sea Continental Slope. Journal of Physical Oceanography, Vol. 54 (2024), doi:10.1175/JPO-D-23-0215.1

Dinniman, M., Klinck, J., Bai, L.S., Bromwich, D., Hines, K.M., Holland, D., The effect of atmospheric forcing resolution on the delivery of ocean heat to the Antarctic floating ice shelves. Journal of Climate, (2015):6067–6085, doi:10.1175/JCLI-D-14-00374.1

Dinniman, M.S., Klinck, J.M., Hofmann, E.E., Sensitivity of Circumpolar Deep Water Transport and Ice Shelf Basal Melt along the West Antarctic Peninsula to Changes in the Winds. Journal of Climate, Vol. 2012 (2012):4799–4816, doi:10.1175/JCLI-D-11-00307.1

Duffy, G.A., Montiel, F., Purich, A., Fraser, C.I., Emerging long-term trends and interdecadal cycles in Antarctic polynyas. Proceedings of the National Academy of Sciences, Vol. 121 (2024):2017, doi:10.1073/pnas.2321595121

Eayrs, C., Li, X., Raphael, M.N., Holland, D.M., Rapid decline in Antarctic sea ice in recent years hints at future change. Nature Geoscience, Vol. 14 (2021)(7):460–464, doi:10.1038/s41561-021-00768-3

Elvidge, A., Renfrew, I., King, J., Orr, A., Lachlan-Cope, T., Foehn warming distributions in non-linear and linear flow regimes: A focus on the Antarctic Peninsula. Quarterly Journal of the Royal Meteorological Society, Vol. 142 (2014), doi:10.1002/qj.2489

Eyring, V., Bony, S., Meehl, G.A., Senior, C.A., Stevens, B., Stouffer, R.J., Taylor, K.E., Overview of the Coupled Model Intercomparison Project Phase 6 (CMIP6) experimental design and organization. Geoscientific Model Development, Vol. 9(5) (2016):1937–1958, doi:10.5194/gmd-9-1937-2016

Foldvik, A., Gammelsrø d, T., Torresen, T., Circulation and Water Masses on the Southern Weddell Sea Shelf. Oceanology of the Antarctic Continental Shelf, Vol. 43 (1985):5–20, doi:10.1029/AR043p0005

Foldvik, A., , Gammelsrød, T., Notes on Southern Ocean Hydrography, Sea-Ice and Bottom Water Formation. Palaeography, Palaeoclimatology, Palaeoecology, Vol. 67 (1988):3–17, doi:10.1016/0031-0182(88)90119-8

Foldvik, A., Gammelsrød, T., Østerhus, S., Fahrbach, E., Rohardt, G., Schröder, M.e.a., Ice shelf water overflow and bottom water formation in the southern Weddell Sea. Journal of Geophysical Research, Vol. 109(2) (2004):C02015, doi:10.1029/2003JC002008

Foster, T.D., Carmack, E.C., Frontal zone mixing and Antarctic Bottom water formation in the southern Weddell Sea. Deep-Sea Research and Oceanographic Abstracts, Vol. 23 (1976)(4):301–317, doi:10.1016/0011-7471(76)90872-X

Fretwell, P., Pritchard, H.D., Vaughan, D.G., Bamber, J.L., Barrand, N.E., Bell, R., et al., Bedmap2: improved ice bed, surface and thickness datasets for Antarctica. The Cryosphere, Vol. 7 (2013):375–393, doi:10.5194/tc-7-375-2013

Ganachaud, A., Wunsch, C., Large-Scale Ocean Heat and Freshwater Transports during the World Ocean Circulation Experiment. Journal of Climate, Vol. 16 (2003)(4):696–705, doi:10.1175/1520-0442(2003)016<0696:LSOHAF>2.0.CO;2

Gill, A., Circulation and bottom water production in the Weddell Sea. Deep-Sea Research and Oceanographic Abstracts, Vol. 20 (1973):111–140, doi:10.1016/0011-7471(73)90048-X

González-Herrero, S., Vasallo, F., Bech, J., Gorodetskaya, I., Elvira, B., Justel, A., Extreme precipitation records in Antarctica. International Journal of Climatology, Vol. 43 (2023)(7):3125–3138, doi:10.1002/joc.8020

Gorodetskaya, I.V., Durán-Alarcón, C., González-Herrero, S., Clem, K.R., Zou, X., Rowe, P., Rodriguez Imazio, P., Campos, D., Leroy-Dos Santos, C., Dutrievoz, N., Wille, J.D., Chyhareva, A., Favier, V., Blanchet, J., Pohl, B., Cordero, R.R., Park, S.J., Colwell, S., Lazzara, M.A., Carrasco, J., Gulisano, A.M., Krakovska, S., Ralph, F.M., Dethinne, T., Picard, G., Record-high Antarctic Peninsula temperatures and surface melt in February 2022: a compound event with an intense atmospheric river. npj Climate and Atmospheric Science, Vol. 6 (2023)(1):202, doi:10.1038/s41612-023-00529-6

Goyal, R., Sen Gupta, A., Jucker, M., England, M.H., Historical and Projected Changes in the Southern Hemisphere Surface Westerlies. Geophysical Research Letters, Vol. 48 (2021):1–13, doi:10.1029/2020GL090849

Graham, J., Heywood, C., Chavanne, C.P., Holland, P.R., Seasonal variability of water masses and transport on the Antarctic continental shelf and slope in the southeastern Weddell Sea. Journal of Geophysical Research: Oceans, Vol. 118 (2013):2201–2214, doi:10.1002/jgrc.20174

Grosfeld, K., Treffeisen, R., Asseng, J., Bartsch, A., Bräuer, B., Fritzsch, B., Gerdes, R., Hendricks, S., Hiller, W., Heygster, G., Krumpen, T., Lemke,

P., Melsheimer, C., Nicolaus, M., Ricker, R., Weigelt, M., Online sea-ice knowledge and data platform <www.meereisportal.de>. Polarforschung, Bremerhaven, Alfred Wegener Institute for Polar and Marine Research & German Society of Polar Research, Vol. 85 (2016):143–155, doi:10.2312/polfor.2016.011

Gudmundsson, G.H., Paolo, F.S., Adusumilli, S., Fricker, H.A., Instantaneous Antarctic ice sheet mass loss driven by thinning ice shelves. Geophysical Research Letters, Vol. 46 (2019)(23):13903–13909, doi:10.1029/2019GL085027

Gurses, O., Kolatschek, V., Wang, Q., Rodehacke, C.B., Brief communication: A submarine wall protecting the Amundsen Sea intensifies melting of neighboring ice shelves. The Cryosphere, Vol. 13 (2019):2317–2324, doi:10.5194/tc-13-2317-2019

Haid, V., Timmermann, R., Simulated heat flux and sea ice production at coastal polynyas in the southwestern Weddell Sea. Journal of Geophysical Research: Oceans, Vol. 118 (2013):2640–2652, doi:10.1002/jgrc.20133

Haid, V., Timmermann, R., Ebner, L., Heinemann, G., Atmospheric forcing of coastal polynyas in the southwestern Weddell Sea. Antarctic Science, Vol. 27 (2015):388–402, doi:10.1017/S0954102014000893

Haid, V., Timmermann, R., Gurses, O., Hellmer, H.H., On the drivers of regime shifts in the Antarctic marginal seas, exemplified by the Weddell Sea. Ocean Science, Vol. 19 (2023):1529–1544, doi:10.5194/os-19-1529-2023

Harig, C., Simons, F.J., Accelerated West Antarctic ice mass loss continues to outpace East Antarctic gains. Earth and Planetary Science Letters, Vol. 415 (2015):134–141, doi:10.1016/j.epsl.2015.01.029

Hatterman, T., Antarctic thermocline dynamics along a narrow shelf with easterly winds. Journal of Physical Oceanography, Vol. 48(10) (2018):2419–2443, doi:10.1175/JPO-D-18-0064.1

Hattermann, T., Antarctic thermocline dynamics along a narrow shelf with easterly winds. Journal of Physical Oceanography, Vol. 48 (2018):2419–2443, doi:10.1175/JPO-D-18-0064.1

Hattermann, T., Smedsrud, L.H., Nøst, O.A., Lilly, J.M., Galton-Fenzi, B.K., Eddy-resolving simulations of the Fimbul Ice Shelf cavity circulation: Basal melting and exchange with open ocean. Ocean Modelling, Vol. 82 (2014):28–44

Hausmann, U., Sallée, J.B., Jourdain, N.C., Mathiot, P., Rousset, C., Madec, G., Deshayes, J., Hattermann, T., The Role of Tides in Ocean-Ice Shelf Interactions in the Southwestern Weddell Sea. Journal of Geophysical Research: Oceans, Vol. 125 (2020)(6):1–29, doi:10.1029/2019JC015847

Heinemann, G., Schefczyk, L., Willmes, S., Shupe, M.D., Evaluation of simulations of near-surface variables using the regional climate model CCLM for the MOSAiC winter

period. Elementa: Science of the Anthropocene, Vol. 10 (2022):1–22, doi:10.1525/elementa.2022.00033

Hellmer, H.H., Olbers, D.J., A two-dimensional model for the thermohaline circulation under an ice shelf. Antarctic Science, Vol. 1 (1989):325–336, doi:10.1017/S0954102089000490

Hellmer, H.H., Kauker, F., Timmermann, R., Determann, J., Rae, J., Twenty-first-century warming of a large Antarctic ice-shelf cavity by a redirected coastal current. Nature, Vol. 485(7397) (2012):225–228, doi:10.1038/nature11064

Hellmer, H.H., Kauker, F., Timmermann, R., , Hattermann, T., The fate of the Southern Weddell sea continental shelf in a warming climate. Journal of Climate, Vol. 30(12) (2017):4337–4350, doi:10.1175/JCLI-D-16-0420.1

Heywood, K.J., Locarnini, R.A., Frew, R.D., Dennis, P.F., King, B.A. (1998): Transport and Water Masses of the Antarctic Slope Front System in The Eastern Weddell Sea. In: S.S. Jacobs, R.F. Weiss (Hg.), Antarctic Research Series, Vol. 75, Chap. Ocean, Ice, and atmsophere: Interactions at the Antarctic Continental Margin, 203–214, American Geophysical Union, doi:10.1029/AR075p0203

Heywood, K.J., Schmidtko, S., Heuzé, C., Kaiser, J., Jickells, T.D., Queste, B.Y., Stevens, D.P., Wadley, M., Thompson, A.F., Fielding, S., Guihen, D., Creed, E., Ridley, J.K., Smith, W., Ocean processes at the Antarctic continental slope. Philosophical Transactions of the Royal Society A, Vol. 372 (2014):20130047, doi:10.1098/rsta.2013.0047

Hinkel, J., Lincke, D., Vafeidis, A.T., Perrette, M., Nicholls, R.J., Tol, R.S., Marzeion, B., Fettweis, X., Ionescu, C., Levermann, A., Coastal flood damage and adaptation costs under 21st century sea-level rise. Proceedings of the National Academy of Sciences of the United States of America, Vol. 111 (2014)(9):3292–3297, doi:10.1073/pnas.1222469111

Holland, D.M., Jenkins, A., Modeling Thermodynamic Ice–Ocean Interactions at the Base of an Ice Shelf. Journal of Physical Oceanography, Vol. 29 (1999):1787–1800, doi:10.1175/1520-0485(1999)029<1787:MTIOIA>2.0.CO;2

Huneke, W.G.C., Morrison, A.K., Hogg, A.M., Spatial and Subannual Variability of the Antarctic Slope Current in an Eddying Ocean–Sea Ice Model. Journal of Physical Oceanography, Vol. 52 (2022):347–361, doi:10.1175/JPO-D-21-0143.1

Huot, P.V., Kittel, C., Fichefet, T., Jourdain, N.C., Sterlin, J., Fettweis, X., Effects of the atmospheric forcing resolution on simulated sea ice and polynyas off Adélie Land, East Antarctica. Ocean Modelling, Vol. 168 (2021), doi:10.1016/j.ocemod.2021.101901

IPCC (2019): IPCC Special Report on the Ocean and Cryosphere in a Changing Climate. Cambridge University Press, Cambridge, UK and New York, NY, USA, doi: 10.1017/9781009157964

IPCC (2023): Climate Change 2023: Synthesis Report. Contribution of Working Groups I, II and III to the Sixth Assessment Report of the Intergovernmental Panel on Climate Change. IPCC, Geneva, Switzerland, doi:doi:10.59327/IPCC/AR6-9789291691647

Jacobs, S., Jenkins, A., Hellmer, H., Giulivi, C., Nitsche, F., Huber, B., Guerrero, R., The Amundsen Sea and the Antarctic Ice Sheet. Oceanography, Vol. 25(3) (2012):154–163, doi:10.5670/oceanog.2012.90

Jacobs, S.S., Bottom water production and its links with the thermohaline circulation. Antarctic Science, Vol. 16 (2004)(4):427–437, doi:10.1017/S095410200400224X

Janout, M., Hellmer, H.H., Hattermann, T., Huhn, O., Sültenfuss, J., Østerhus, S., Stulic, L., Ryan, S., Schöder, M., Kanzow, T., FRIS Revisited in 2018: On the Circulation and Water Masses at the Filchner and Ronne Ice Shelves in the Southern Weddell Sea. Journal of Geophysical Research: Oceans, Vol. 126 (2021):e2021JC017269, doi:10.1029/2021JC017269

Janout, M.A., Hellmer, H.H., Schröder, M., Wisotzki, A. (2019): Physical oceanography during POLARSTERN cruise PS111 (ANT-XXXIII/2). doi:10.1594/PANGAEA.897280

Jeong, H., Lee, S.S., Park, H.S., Stewart, A.L., Future changes in Antarctic coastal polynyas and bottom water formation simulated by a high-resolution coupled model. Communications Earth and Environment, Vol. 4 (2023):490, doi:10.1038/s43247-023-01156-y

Jones, B., O'Neill, B.C., Spatially explicit global population scenarios consistent with the Shared Socioeconomic Pathways. Environmental Research Letters, Vol. 11 (2016)(8):084003, doi:10.1088/1748-9326/11/8/084003

Jones, M.E., Bromwich, D.H., Nicolas, J.P., Carrasco, J., Plavcová, E., Zou, X., Wang, S.H., Sixty Years of Widespread Warming in the Southern Middle and High Latitudes (1957–2016). Journal of Climate, Vol. 32 (2019)(20):6875–6898, doi:10.1175/JCLI-D-18-0565.1

Joughin, I., Tulaczyk, S., Positive mass balance of the Ross ice streams, West Antarctica. Science, Vol. 295 (2002)(5554):476–480, doi:10.1126/science.1066875

Joughin, I., Smith, B.E., Medley, B., Marine Ice Sheet Collapse Potentially Under Way for the Thwaites Glacier Basin, West Antarctica. Science, Vol. 344 (2014)(61852):735–738, doi:10.1126/science.1249055

Kida, S., The impact of open oceanic processes on the Antarctic Bottom Water outflows. Journal of Physical Oceanography, Vol. 41 (2011):1941–1957, doi:10.1175/2011JPO4571.1

Klatt, O., Fahrbach, E., Hoppema, M., , Rohardt, G., The transport of the Weddell Gyre across the Prime Meridian. Deep-Sea Research Part II, Vol. 52(3-4) (2005):513–528, doi:10.1016/j.dsr2.2004.12.015

Koenig, Z., Provost, C., Ferrari, R., Sennéchael, N., , Rio, M.H., Volume transport of the Antarctic Circumpolar Current: Production and validation of a 20 year long time series obtained from in situ and satellite observations. Journal of Geophysical Research: Oceans, Vol. 119 (2014):5407–5433, doi:10.1002/2014JC009966

Kuhlbrodt, T., Griesel, A., Montoya, M., Levermann, A., Hofmann, M., Rahmstorf, S., On the driving processes of the Atlantic meridional overturning circulation. Reviews of Geophysics, Vol. 45 (2007)(2), doi:10.1029/2004RG000166

Le Paih, N., Hattermann, T., Boebel, O., Kanzow, T., Lüpkes, C., Rohardt, G., Strass, V., Herbette, S., Coherent Seasonal Acceleration of the Weddell Sea Boundary Current System Driven by Upstream Winds. Journal of Geophysical Research: Oceans, Vol. 125 (2020):1–20, doi:10.1029/2020JC016316

Lee, H.C., Rosati, A., , Spelman, M.J., Barotropic tidal mixing effects in a coupled climate model: oceanic conditions in the Northern Atlantic. Ocean Model, Vol. 11 (2006):464–477, doi:10.1016/j.ocemode.2005.03.003

Lockwood, J.W., Dufour, C.O., Griffies, S.M., Winton, M., On the Role of the Antarctic Slope Front on the Occurrence of the Weddell Sea Polynya under Climate Change. Journal of Climate, Vol. 34 (2021):2529–2548, doi:10.1175/JCLI-D-20-0069.1

Mahlstein, I., Gent, P.R., Solomon, S., Historical Antarctic mean sea ice area, sea ice trends, and winds in CMIP5 simulations. Journal of Geophysical Research: Atmospheres, Vol. 118 (2013)(11):5105–5110, doi:10.1002/jgrd.50443

Manton, M.J., Huang, Y., Siems, S.T., Variations in precipitation across the Southern Ocean. Journal of Climate, Vol. 33 (2020)(24):10653–10670, doi:10.1175/JCLI-D-20-0120.1

Markus, T. (1996): The effect of the grounded tabular icebergs in front of Berkner Island on the Weddell Sea ice drift as seen from satellite passive microwave sensors. In: IGARSS '96. 1996 International Geoscience and Remote Sensing Symposium, Vol. 3, 1791–1793, IEEE, ISBN 0-7803-3068-4, doi:10.1109/IGARSS.1996.516802

Marshall, G.J., Half-century seasonal relationships between the Southern Annular Mode and Antarctic temperatures. International Journal of Climatology, Vol. 27 (2007):373–383, doi:10.1002/joc.1407

Marsland, S.J., Church, J.A., Bindoff, N.L., Williams, G.D., Antarctic coastal polynya response to climate change. Journal of Geophysical Research: Oceans, Vol. 112 (2007):1–12, doi:10.1029/2005JC003291

Mathiot, P., Goosse, H., Fichefet, T., Barnier, B., Gallée, H., Modelling the seasonal variability of the Antarctic Slope Current. Ocean Science, Vol. 7 (2011):455–470, doi:10.5194/os-7-455-2011

Mayewski, P.A., Meredith, M.P., Summerhayes, C.P., Turner, J., Worby, A., Barrett, P.J., Casassa, G., Bertler, N.A., Bracegirdle, T., Naveira Garabato, A.C., Bromwich, D., Campbell, H., Hamilton, G.S., Lyons, W.B., Maasch, K.A., Aoki, S., Xiao, C., Van Ommen, T., State of the Antarctic and Southern Ocean climate system. Reviews of Geophysics, Vol. 47 (2009):1–38, doi:10.1029/2007RG000231

McMichael, C., Dasgupta, S., Ayeb-Karlsson, S., Kelman, I., A review of estimating population exposure to sea-level rise and the relevance for migration. Environmental Research Letters, Vol. 15 (2020)(12):123005, doi:10.1088/1748-9326/abb398

Meinshausen, M., Nicholls, Z.R., Lewis, J., Gidden, M.J., Vogel, E., Freund, M.e.a., The shared socio-economic pathway (SSP) greenhouse gas concentrations and their extensions to 2500. Geoscientific Model Development, Vol. 13(8) (2020):3571–3605, doi:10.5194/gmd-13-3571-2020

Morales Maqueda, M.A., Willmott, A.J., Biggs, N.R., Polynya dynamics: A review of observations and modeling. Reviews of Geophysics, Vol. 42 (2004), doi:10.1029/2002RG000116

Morlighem, M., Rignot, E., Binder, T., Blankenship, D., Drews, R., Eagles, G., Eisen, O., Ferraccioli, F., Forsberg, R., Fretwell, P., Goel, V., Greenbaum, J.S., Gudmundsson, H., Guo, J., Helm, V., Hofstede, C., Howat, I., Humbert, A., Jokat, W., Karlsson, N.B., Lee, W.S., Matsuoka, K., Millan, R., Mouginot, J., Paden, J., Pattyn, F., Roberts, J., Rosier, S., Ruppel, A., Seroussi, H., Smith, E.C., Steinhage, D., Sun, B., Broeke, M.R.v.d., Ommen, T.D.v., Wessem, M.v., Young, D.A., Deep glacial troughs and stabilizing ridges unveiled beneath the margins of the Antarctic ice sheet. Nature Geoscience, Vol. 13 (2020):132–137, doi:10.1038/s41561-019-0510-8

Morrison, A.K., Hogg, A.M., England, M.H., , Spence, P., Warm Circumpolar Deep Water transport toward Antarctica driven by local dense water export in canyons. Science Advances, Vol. 6 (2020):eaav2516, doi:10.1126/sciadv.aav2516

Mouginot, J., Rginot, E., Scheuchl, B., Sustained increase in ice discharge form the Amundsen Sea Embayment, West Antarctica, from 1973 to 2013. Geophysical Research Letters, Vol. 41 (2014):1576–1584, doi:10.1002/2013GL059069

Munk, W., Wunsch, C., Abyssal recipes II: energetics of tidal and wind mixing. Deep Sea Research Part I: Oceanographic Research Papers, Vol. 45 (1998)(12):1977–2010, doi:10.1016/S0967-0637(98)00070-3

Naughten, K.A., De Rydt, J., Rosier, S.H.R., Jenkins, A., Holland, P.R., Ridley, J.K., Two-timescale response of a large Antarctic ice shelf to climate change. Nature Communications, Vol. 12(1) (2021):1–10, doi:10.1038/s41467-021-22259-0

Naughten, K.A., Holland, P.R., De Rydt, J., Unavoidable future increase in West Antarctic ice-shelf melting over the twenty-first century. Nature Climate Change, Vol. 13 (2023)(11):1222–1228, doi:10.1038/s41558-023-01818-x

Naveira Garabato, A.C., McDonagh, E.L., Stevens, D.P., Heywood, K.J., , Sanders, R.J., On the export of Antarctic Bottom Water from the Weddell Sea. Deep-Sea Research Part II: Topical Studies in Oceanography, Vol. 49(21) (2002):4715–4742, doi:10.1016/S0967-0645(02)00156-X

Neumann, B., Vafeidis, A.T., Zimmermann, J., Nicholls, R.J., Future coastal population growth and exposure to sea-level rise and coastal flooding - A global assessment. PLoS ONE, Vol. 10 (2015)(3), doi:10.1371/journal.pone.0118571

Nicholls, K., Østerhus, S., Makinson, K., Gammelsrød, T., , Fahrbach, E., Ice-ocean processes over the continental shelf of the Southern Weddell Sea, Antarctica: A review. Reviews of Geophysics, Vol. 47(3) (2009):1–23, doi:10.1029/2007RG000250

Nicholls, K.W., Østerhus, S., Makinson, K., , Johnson, M.R., Oceanographic conditions south of Berkner Island, beneath Filchner-Ronne ice Shelf, Antarctica. Journal of Geophysical Researth, Vol. 106(C6) (2001):11481–11492, doi:10.1029/2000jc000350

Nicholls, K.W., Boehme, L., Biuw, M., , Fedak, M.A., Wintertime ocean conditions over the southern Weddell Sea continental shelf, Antarctica. Geophys. Res. Lett., Vol. 35 (2008):L21605, doi:10.1029/2008GL035742

Nicholls, R.J., Marinova, N., Lowe, J.A., Brown, S., Vellinga, P., de Gusmão, D., Hinkel, J., Tol, R.S.J., Sea-level rise and its possible impacts given a 'beyond 4 C° world' in the twenty-first century. Philosophical Transactions of the Royal Society, Vol. 369 (2011):161–81, doi:10.1098/rsta.2010.0291

Nissen, C., Timmermann, R., Hoppema, M., Gürses, Ö., Hauck, J., Abruptly attenuated carbon sequestration with Weddell Sea dense waters by 2100. Nature Communications, Vol. 13 (2022), doi:10.1038/s41467-022-30671-3

Nissen, C., Timmermann, R., Hoppema, M., Hauck, J., A regime shift on Weddell Sea Continental Shelves with Local and Remove Physical and Biogeochemical Implications is Avoidable in a 2°C Scenario. Journal of Climate, Vol. 36 (2023):6613–6630, doi:10.1175/JCLI-D-22-0926.1

Nissen, C., Timmermann, R., van Caspel, M., Wekerle, C., Altered Weddell Sea warm- and dense-water pathways in response to 21st-century climate change. Ocean Science, Vol. 20 (2024)(1):85–101, ISSN 1812-0792, doi:10.5194/os-20-85-2024, URL https://os.copernicus.org/articles/20/85/2024/

Nøst, O., Biuw, M., Tverberg, V., Lydersen, C., Hattermann, T., Zhou, Q., Smedsrud, L.H., , Kovacs, K.M., Eddy overturning of the Antarctic Slope Front controls glacial melting in the Eastern Weddell Sea. Journal of Geophysical Research, Vol. 116(C11014) (2011):1–17, doi:10.1029/2011JC006965

O'Neill, B., Tebaldi, C., Van Vuuren, D.P., Eyring, V., Friedlingstein, P., Hurtt, G., et al., The Scenario Model Intercomparison Project (ScenarioMIP) for

CMIP6. Geoscientific Model Development, Vol. 9(9) (2016):3461–3482, doi:10.5194/gmd-9-3461-2016

Ong, E.Q.Y., Doddridge, E., Constantinou, N.C., Hogg, A.M., England, M.H., Intrinsically Episodic Antarctic Shelf Intrusions of Circumpolar Deep Water via Canyons. Journal of Physical Oceanography, Vol. 54 (2023):1195–1210, doi:10.1175/JPO-D-23-0067.1

Orsi, A.H., Whitworth, T., Nowlin, W.D., On the meridional extent and fronts of the Antarctic Circumpolar Current. Deep Sea Research Part I: Oceanographic Research Papers, Vol. 42 (1995)(5):641–673, doi:10.1016/0967-0637(95)00021-W

Ou, H., Watermass Properties of the Antarctic Slope Front: A Simple Model. Journal of Physical Oceanography, Vol. 37 (2007):50–59, doi:10.1175/JPO2981.1

Paul, S., Willmes, S., Heinemann, G., Long-term coastal-polynya dynamics in the southern Weddell Sea from MODIS thermal-infrared imagery. The Cryosphere, Vol. 9 (2015):2027–2041, doi:10.5194/tc-9-2027-2015

Pauthenet, E., Sallée, J.B., Schmidtko, S., Nerini, D., Seasonal variation of the antarctic slope front occurrence and position estimated from an interpolated hydrographic climatology. Journal of Physical Oceanography, Vol. 51 (2021):1539–1557, doi:10.1175/JPO-D-20-0186.1

Peña-Molino, B., McCartney, M.S., Rintoul, S.R., Direct observations of the Antarctic Slope Current transport at 113°E. Journal of Geophysical Research: Oceans, Vol. 121 (2016):7390–7407, doi:10.1002/2015JC011594

Pritchard, H.D., Ligtenberg, S.R., Fricker, H.A., Vaughan, D.G., Van Den Broeke, M.R., Padman, L., Antarctic ice-sheet loss driven by basal melting of ice shelves. Nature, Vol. 484 (2012)(7395):502–505, doi:10.1038/nature10968

Purich, A., Doddridge, E.W., Record low Antarctic sea ice coverage indicates a new sea ice state. Communications Earth and Environment, Vol. 4 (2023)(1):1–9, doi:10.1038/s43247-023-00961-9

Rackow, T., Goessling, H.F., Jung, T., Sidorenko, D., Semmler, T., Barbi, D., et al., Towards multi-resolution global climate modeling with ECHAM6-FESOM. Part II: climate variability. Climate Dynamics, Vol. 50(7-8) (2018a):2369–2394, doi:10.1007/s00382-016-3192-6

Rackow, T., Sein, D., Semmler, T., Danilov, S., Koldunov, N., Sidorenko, D.e.a., Sensitivity of deep ocean biases to horizontal resolution in prototype CMIP6 simulations with AWI-CM1.0. Geoscientific Model Development Discussions, Vol. 3 (2018b):1–25, doi:10.5194/gmd-2018-192

Rackow, T., Sein, D.V., Semmler, T., Danilov, S., Koldunov, N., Sidorenko, D., Wang, Q., , Jung, T., Sensitivity of deep ocean biases to horizontal resolution in

prototype CMIP6 simulations with AWI-CM1.0. Geosci. Model Dev., Vol. 12 (2019):2635–2656, doi:10.5194/gmd-12-2635-2019

Reeve, K.A., Boebel, O., Strass, V., Kanzow, T., , Gerdes, R., Horizontal circulation and volume transports in the Weddell Gyre derived from Arge float data. Progress in Oceanography, Vol. 175 (2019):263–283, doi:10.1016/j.pocean.2019.04.006

Reimann, L., Vafeidis, A.T., Honsel, L.E., Population development as a driver of coastal risk: Current trends and future pathways. Cambridge Prisms: Coastal Futures, Vol. 1 (2023), doi:10.1017/cft.2023.3

Renault, A., Provost, C., Sennéchael, N., Barré, N., , Kartavtseff, A., Two full-depth velocity sections in the Drake Passage in 2006 - Transport estimates. Deep-Sea Research Part II, Vol. 58 (2011):2572–2591, doi:10.1016/j.dsr2.2011.01.004

Renfrew, I.A., King, J.C., Markus, T., Coastal polynyas in the southern Weddell Sea: Variability of the surface energy budget. Journal of Geophysical Research: Oceans, Vol. 107 (2002), doi:10.1029/2000JC000720

Rignot, E., Jacobs, S., Mouginot, J., Scheuchl, B., Ice-shelf melting around antarctica. Science, Vol. 341 (2013)(6143):266–270, doi:10.1126/science.1235798

Rignot, E., Mouginot, J., Scheuchl, B., van den Broeke, M., van Wessem, M.J., Morlighem, M., Four decades of Antarctic Ice Sheet mass balance from 1979–2017. Preceedings of the National Academy of Science, Vol. 116 (2019):1095–1103, doi:10.1073/pnas.1812883116

Rintoul, S., Hughes, C., Olbers, D., The Antarctic Circumpolar Current System. International Geophysics, (2001):271–301, doi:10.1016/S0074-6142(01)80124-8

Ruddiman, W.F. (2014): Overview of Climate Science. W. H. Freeman and Company, New York

Ryan, S., Hattermann, T., Darelius, E., , Schröder, M., Seasonal cycle of hydrography on the eastern shelf of the Filchner Trough, Weddell Sea, Antarctica. Journal of Geophysical Research: Oceans, Vol. 122(8) (2017):6437–6453, doi:10.1002/2017JC012916

Ryan, S., Hellmer, H.H., Janout, M., Darelius, E., Vignes, L., Schröder, M., Exceptionally Warm and Prolonged Flow of Warm Deep Water Toward the Filchner-Ronne Ice Shelf in 2017. Geophysical Research Letters, Vol. 47(13) (2020):1–10, doi:10.1029/2020GL088119

Schmidtko, S., Heywood, K.J., Thompson, A.F., , Aoki, S., Multidecadal warming of Antarctic waters. Science, Vol. 346(6214) (2014):1227–1232, doi:10.1126/science.1256117

Schröder, M. (2010): Physical oceanography during POLARSTERN cruise ANT-XII/3. doi:10.1594/PANGAEA.742581

Schröder, M., , Wisotzki, A. (2014): Physical oceanography during POLARSTERN cruise PS82 (ANT-XXIX/9). doi:10.1594/PANGAEA.833299

Schröder, M., Ryan, S., Wisotzki, A. (2016): Physical oceanography during POLARSTERN cruise PS96 (ANT-XXXI/2 FROSN). doi:10.1594/PANGAEA.859040

Schröder, M., Ryan, S., Wisotzki, A. (2019): Physical oceanography and current meter data from mooring AWI254-2. doi:10.1594/PANGAEA.903317

Sein, D.V., Danilov, S., Biastoch, A., Durgadoo, J.V., Sidorenko, D., Harig, S.e.a., Designing variable ocean model resolution based on the observed ocean variability. Journal of Advances in Modeling Earth Systems, Vol. 8 (2016):904–916, doi:10.1002/2016MS000650

Sein, D.V., Koldunov, N.V., Danilov, S., Wang, Q., Sidorenko, D., Fast, I.e.a., Ocean Modeling on a Mesh With Resolution Following the Local Rossby Radius. Journal of Advances in Modeling Earth Systems, Vol. 9(7) (2017):2601–2614, doi:10.1002/2017MS001099

Sein, D.V., Koldunov, N.V., Danilov, S., Sidorenko, D., Wekerle, C., Cabos, W., et al., The Relative Influence of Atmospheric and Oceanic Model Resolution on the Circulation of the North Atlantic Ocean in a Coupled Climate Model. Journal of Advances in Modeling Earth Systems, Vol. 10(8) (2018):2026–2041, doi:10.1029/2018MS001327

Semmler, T., Danilov, S., Gierz, P., Goessling, H.F., Hegewald, J., Hinrichs, C.e.a., Simulations for CMIP6 With the AWI Climate Model AWI-CM-1-1. Journal of Advances in Modeling Earth Systems, Vol. 12(9) (2020):1–34, doi:10.1029/2019MS002009

Shepherd, A., Ivins, E.R., A, G., Bareletta, V.R., Bentley, M.J., Bettadpur, S., et al., A Reconciled Estimate of Ice-Sheet Mass Balance. Science, Vol. 338(6111) (2012):1183–1189, doi:10.1126/science.1228102

Shepherd, A., Ivins, E.R., Rignot, E., Smith, B., van den Broeke, M.R., Velicogna, I., Whitehouse, P.L., Briggs, K.H., Joughin, I., Krinner, G., Nowicki, S., Payne, T., Scambos, T.A., Schlegel, N., A, G., Agosta, C., Ahlstrøm, A., Babonis, G., Barletta, V., Blazquez, A., Bonin, J., Csatho, B., Cullather, R., Felikson, D., Fettweis, X., Forsberg, R., Gallee, H., Gardner, A., Gilbert, L., Groh, A., Gunter, B., Hanna, E., Harig, C., Helm, V., Horvath, A., Horwath, M., Khan, S., Kjeldsen, K.K., Konrad, H., Langen, P., Lecavalier, B., Loomis, B., Luthcke, S., McMillan, M., Melini, D., Mernild, S., Mohajerani, Y., Mass balance of the Antarctic Ice Sheet from 1992 to 2017. Nature, Vol. 558 (2018)(7709):219–222, doi:10.1038/s41586-018-0179-y

Sidorenko, D., Rackow, T., Jung, T., Semmler, T., Barbi, D., Danilov, S.e.a., Towards multi-resolution global climate modeling with ECHAM6–FESOM. Part I: model formulation and mean climate. Climate Dynamics, Vol. 44(3-4) (2015):757–780, doi:10.1007/s00382-014-2290-6

Smith, W., Barber, D. (2007): Chapter 13 Polynyas and Climate Change: A View to the Future. In: W.O. Smith, D.G. Barber (Hg.), Polynyas: Windows to the World, *Elsevier Oceanography Series*, Vol. 74, 411–419, Elsevier, doi:10.1016/S0422-9894(06)74013-2, URL https://www.sciencedirect.com/science/article/pii/S0422989406740132

Spence, P., Griffies, S.M., England, M.H., Hogg, A.M., Saenko, O.A., Jourdain, N.C., Rapid subsurface warming and circulation changes of Antarctic Coastal waters by poleward shifting winds. Geophysical Research Letters, Vol. 41 (2014):4601–4610, doi:10.1002/2014GL060613

Spence, P., Holmes, R.M., Hogg, A.M., Griffies, S.M., Stewart, K.D., England, M.H., Localized rapid warming of West Antarctic subsurface waters by remote winds. Nature Climate Change, Vol. 7 (2017):595–603, doi:10.1038/nclimate3335

Spreen, G., Kaleschke, L., Heygster, G., Sea ice remote sensing using AMSR-E 89 GHz channels. Journal of Geophysical Research, Vol. 113 (2008):C02S03, doi:10.1029/2005JC003384

St-Laurent, P., Klinck, J.M., Dinniman, M.S., On the role of coastal troughs in the circulation of warm circumpolar deep water on Antarctic shelves. Journal of Physical Oceanography, Vol. 43 (2013):51–64, doi:10.1175/JPO-D-11-0237.1

Steger, C., Bucchignani, E., Regional Climate Modelling with COSMO-CLM: History and Perspectives. Atmosphere, Vol. 11 (2020):1250, doi:10.3390/atmos11111250

Stevens, B., Giorgetta, M., Esch, M., Mauritsen, T., Crueger, T., Rast, S.e.a., Atmospheric component of the MPI-M earth system model: ECHAM6. Journal of Advances in Modeling Earth Systems, Vol. 5(2) (2013):146–172, doi:10.1002/jame.20015

Stewart, A., Thompson, A., Eddy-mediated transport of warm Circumpolar Deep Water cross the Antarctic Shelf Break. Geophysical Research Letters, Vol. 42 (2015a):432–440, doi:10.1002/2014GL062281

Stewart, A., Thompson, A., The Neutral Density Temporal Residual Mean overturning circulation. Ocean Modelling, Vol. 90 (2015b):44–56, doi:10.1016/j.ocemod.2015.03.005

Stewart, A., Klocker, A., Menemenlis, D., Acceleration and Overturning of the Antarctic Slope Current by Winds, Eddies, and Tides. Journal of Physical Oceanography, Vol. 49 (2019):2043–2074, doi:10.1175/JPO-D-18-0221.1

Stocker, T. (2011): Springer, New York

Stössel, A., Zhang, Z., Vihma, T., The effect of alternative real-time wind forcing on Southern Ocean sea ice simulations. Journal of Geophysical Research: Oceans, Vol. 116 (2011):1–19, doi:10.1029/2011JC007328

Stulic, L., Timmermann, R., Paul, S., Zentek, R., Heinemann, G., Kanzow, T., Southern Weddell Sea surface freshwater flux modulated by icescape and atmospheric forcing. Ocean Science, Vol. 192 (2023):1791–1808, doi:10.5194/os-19-1791-2023

Sverdrup, H., The Currents off the Coast of Queen Maud Land. Norsk Geografisk Tidsskrift - Norwegian Journal of Geography, Vol. 14 (1954), doi:10.1080/00291955308542731

Tamura, T., Ohshima, K.I., Nihashi, S., Mapping of sea ice production for Antarctic coastal polynyas. Geophysical Research Letters, Vol. 35 (2008):L07606, doi:10.1029/2007GL032903

Tamura, T., Ohshima, K.I., Fraser, A.D., Williams, G.D., Sea ice production variability in Antarctic coastal polynyas. Journal of Geophysical Research: Oceans, Vol. 121 (2016):2967–2979, doi:10.1002/2015JC011537

Teske, V., Timmermann, R., Nissen, C., Zentek, R., Semmler, T., Heinemann, G., Regime shift caused by accelerated density reorganization on the Weddell Sea continental shelf with high-resolution atmospheric forcing. EGUsphere, (2024a):1–24, doi:10.5194/egusphere-2024-2873, [preprint]

Teske, V., Timmermann, R., Semmler, T., Subsurface warming in the Antarctica's Weddell Sea can be avoided by reaching the 2°C warming target. Communications Earth & Environment, Vol. 5 (2024b):93, doi:10.1038/s43247-024-01238-5

Thompson, A.F., Stewart, A.L., Spence, P., Heywood, K.J., The Antarctic Slope Current in a Changing Climate. Reviews of Geophysics, Vol. 56 (2018):741–770, doi:10.1029/2018RG000624

Thompson, D.W., Solomon, S., Kushner, P.J., England, M.H., Grise, K.M., Karoly, D.J., Signatures of the Antarctic ozone hole in Southern Hemisphere surface climate change. Nature Geoscience, Vol. 4 (2011)(11):741–749, doi:10.1038/ngeo1296

Thompson, D.W.J., Wallace, J.M., Annular Modes in the Extratropical Circulation. Part I: Month-to-Month Variability. Journal of Climate, Vol. 13 (2000):1000–1016, doi:10.1175/1520-0442(2000)013<1000:AMITEC>2.0.CO;2

Thompson, D.W.J., Wallace, J.M., Hegerl, G.C., Annular Modes in the Extratropical Circulation. Part II: Trends. Journal of Climate, Vol. 13 (2000):1018–1036, doi:10.1175/1520-0442(2000)013<1018:AMITEC>2.0.CO;2

Timmermann, R., Goeller, S., Response to Filchner-Ronne Ice Shelf cavity warming in a coupled ocean-ice sheet model - Part 1: The ocean perspective. Ocean Science, Vol. 13(5) (2017):765–776, doi:10.5194/os-13-765-2017

Timmermann, R., Hellmer, H.H., Southern Ocean warming and icreased ice shelf basal melting in the twenty-first and twenty-second centuries based on coupled ice-ocean finite-element modelling. Ocean Dynamics, Vol. 63(9-10) (2013):1011–1026, doi:10.1007/s10236-013-0642-0

Timmermann, R., Wang, Q., Hellmer, H., Ice-shelf basal melting in a global finite-element sea-ice/ice-shelf/ocean model. Ann. Glaciol., Vol. 53 (2012):303–314, doi:10.3189/2012AoG60A156

Turner, J., Anderson, P., Lachlan-Cope, T., Colwell, S., Phillips, T., Kirchgaessner, A., Marshall, G.J., King, J.C., Bracegirdle, T., Vaughan, D.G., Lagun, V., Orr, A., Record low surface air temperature at Vostok station, Antarctica. Journal of Geophysical Research: Atmospheres, Vol. 114 (2009):1–14, doi: 10.1029/2009JD012104

Turner, J., Marshall, G.J., Clem, K., Colwell, S., Phillips, T., Lu, H., Antarctic temperature variability and change from station data. Geophysical Research Letters, Vol. 40 (2020):2986–3007, doi:doi.org/10.1002/joc.6378

Turner, J., Lu, H., King, J., Marshall, G.J., Phillips, T., Bannister, D., Colwell, S., Extreme temperatures in the Antarctic. Journal of Climate, Vol. 34 (2021)(7):2653–2668, doi:10.1175/JCLI-D-20-0538.1

van Aken, H.M. (2007): The Oceanic Thermohaline Circulation: An introduction. Springer, New York

van den Broeke, M.R., On the interpretation of Antarctic temperature trends. Journal of Climate, Vol. 13 (2000)(21):3885–3889, doi:10.1175/1520-0442(2000)013<3885:OTIOAT>2.0.CO;2

Van Lipzig, N.P.M., King, J.C., Lachlan-Cope, T.A., van den Broeke, M.R., Precipitation, sublimation, and snow drift in the Antarctic Peninsula region from a regional atmospheric model. Journal of Geophysical Research, Vol. 109 (2004):D24106, doi: 10.1029/2004JD004701

Van Wessem, J.M., Reijmer, C.H., van de Berg, W.J., van den Broeke, M.R., J., C.A., van Ulft, L.H.E., van Meijgaard, E., Temperature and Wind Climate of the Antarctic Peninsula as Simulated by a High-Resolution Regional Atmospheric Climate Model. Journal of Climate, Vol. 28 (2015):1831–1844, doi:10.1175/JCLI-D-15-0060.1

Wang, Q., Danilov, S., Sidorenko, D., Timmermann, R., Wekerle, C., Wang, X.e.a., The Finite Element Sea Ice-Ocean Model (FESOM) v.1.4: Formulation of an ocean general circulation model. Geoscientific Model Development, Vol. 7(2) (2014):663–693, doi:10.1175/JCLI-D-16-0420.1

Wang, X., Zhang, Z., Wang, X., Vihma, T., Zhou, M., Yu, L., Uotila, P., Sein, D.V., Impacts of strong wind events on sea ice and water mass properties in Antarctic coastal polynyas. Climate Dynamics, Vol. 57 (2021):3505–3528, doi:10.1007/s00382-021-05878-7

Wei, Z., Zhang, Z., Vihma, T., Wang, X., Chen, Y., An overview of antarctic polynyas: Sea ice production, forcing mechanisms, temporal variability and water mass formation. Advances in Polar Science, Vol. 32 (2021):292–308, doi:10.13679/j.advps.2021.0026

Young, I.R., Ribal, A., Multiplatform evaluation of global trends in wind speed and wave height. Science, Vol. 364 (2019)(6440):548–552, doi:10.1126/science.aav9527

Zentek, R., Heinemann, G., Verification of the regional atmospheric model CCLM v5.0 with conventional data and Lidar measurements in Antarctica. Geosci. Model Dev, Vol. 13 (2020):1809–1825, doi:10.5194/gmd-13-1809-2020

Zhang, P., Duan, A., Connection between the Tropical Pacific and Indian Ocean and Temperature Anomaly across West Antarctic. npj Climate and Atmospheric Science, Vol. 6 (2023)(1):49, doi:10.1038/s41612-023-00381-8

APPENDIX

# A

# SUPPLEMENTARY MATERIAL TO CHAPTER 4

**Table A.1: Phase transitions in different simulations.** This table shows the beginning year of the Phases II and III for each simulation, defined by the criteria described in section "Three phases of climate change".

| | II | III | | II | III |
|---|---|---|---|---|---|
| hist1/SSP1-2.6 | 1997 | - | hist3/SSP3-7.0_3 | 2018 | 2059 |
| hist1/SSP2-4.5 | 1997 | 2097 | hist4/SSP3-7.0_4 | 2012 | 2068 |
| hist1/SSP3-7.0_1 | 1997 | 2075 | hist5/SSP3-7.0_5 | 1974 | 2074 |
| hist2/SSP3-7.0_2 | 2016 | 2070 | hist1/SSP5-8.5 | 1997 | 2075 |

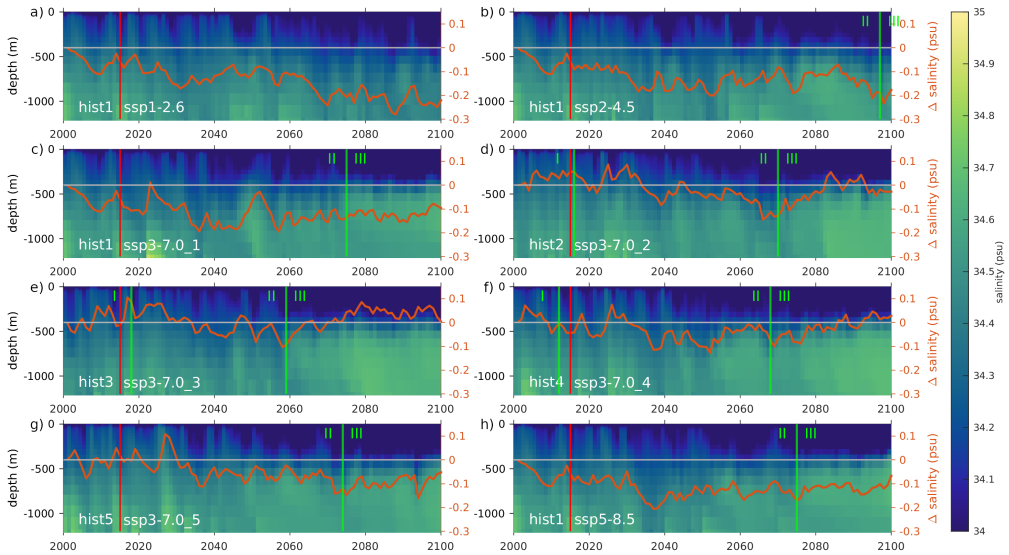


**Figure A.1: Simulated salinity evolution in Filchner Trough for four climate scenarios.** Hovmoeller plot of the yearly mean salinity in the Filchner Trough from the year 2000 to 2100, with the average salinity change in the Filchner Trough relative to 2000. The vertical red lines divide the timeline into the historical simulations (before 2015) and the future climate scenarios (from 2015 onward). Green lines mark the phase boundaries. For exact values see Supplementary Table 1.

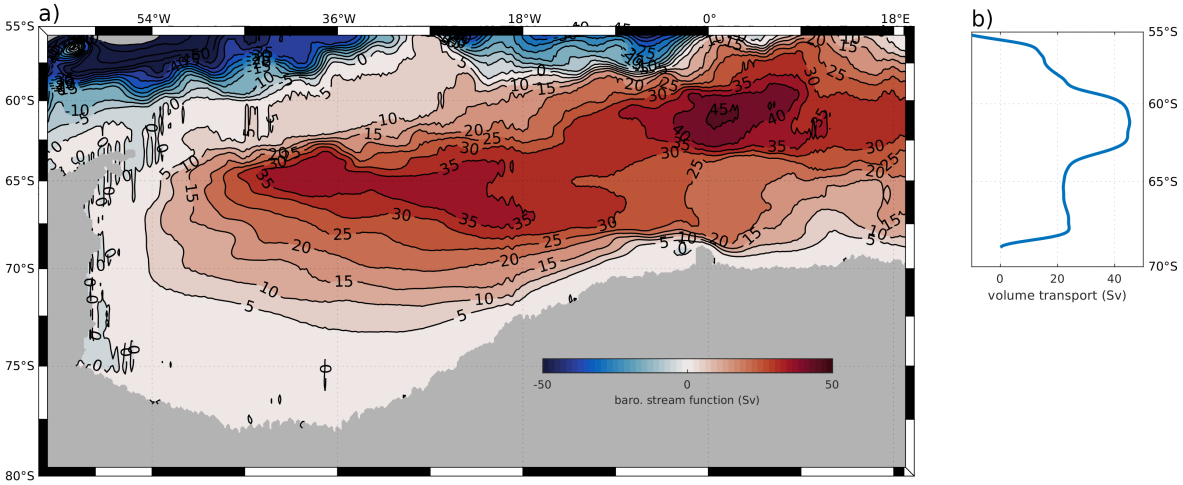


**Figure A.2: Volume transport in the historical simulation.** a) Volume transport in the Weddell Gyre. b) Cumulative volume transport along the prime meridian. The data contains the average of the last 15 years of the historical simulation *hist1* (from 2000 to 2014).

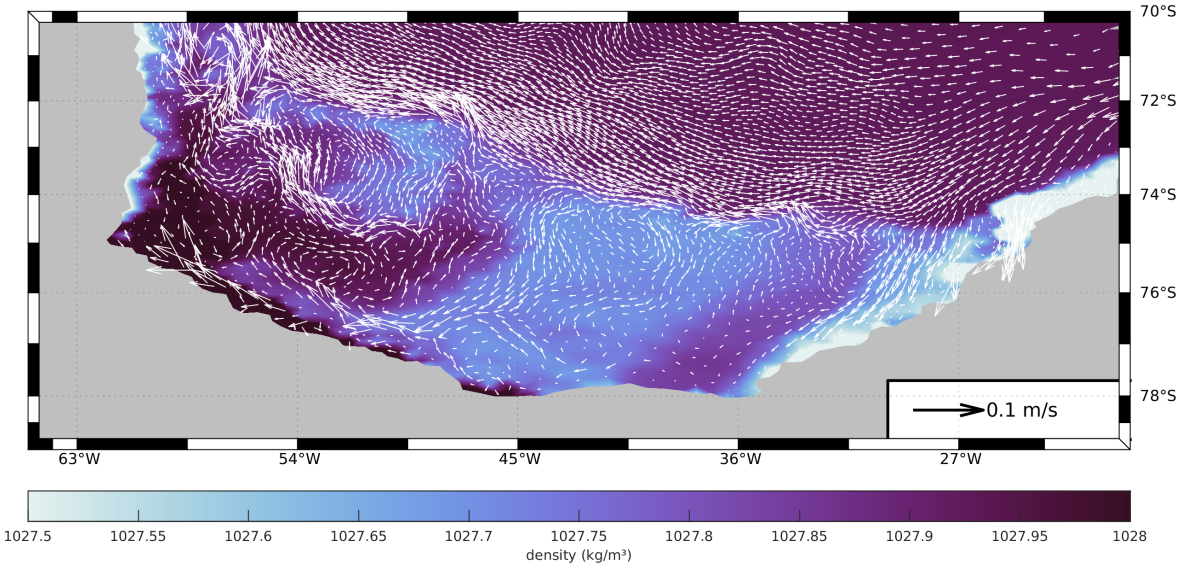


**Figure A.3: Bottom density and mean velocity in the historical simulation.** The bottom density is presented as the background color. The vertically averaged velocity is shown as white arrows on top. The data contains the average of the last 15 years of the historical simulation *hist1* (from 2000 to 2014).

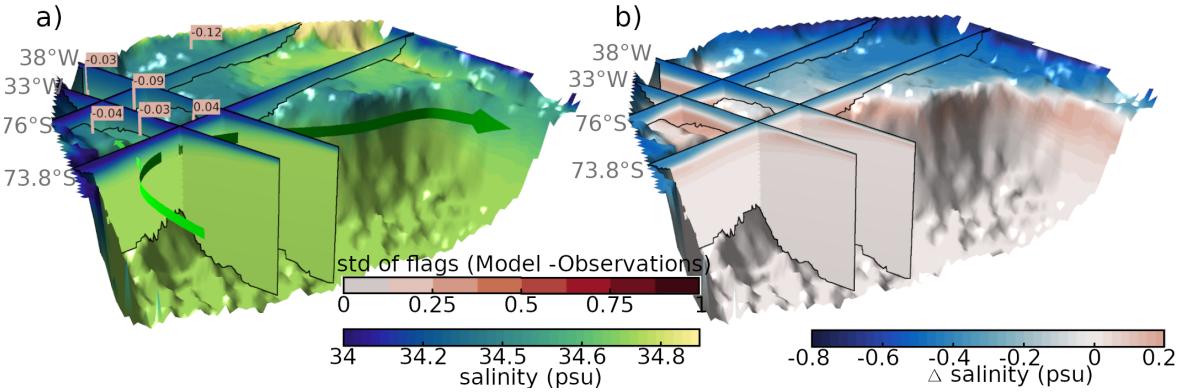


**Figure A.4: Simulated salinity distribution and evolution in the southern Weddell Sea.** (a) Salinity in a 15-year average of the ensemble mean of the historical scenario (2000 to 2014) at sections 33°W, 38°W, 73.8°S and 76°S with differences to observational data (values on flags) and the standard deviation within each key area (color of flags). Arrows show main slope current of WDW and mWDW flowing along the continental shelf break and onto the shelf (Color of the arrow does not represent salinity of the water mass). (b) Change in salinity in the 15-year average 2086 to 2100 to (a) in the ensemble mean of SSP3-7.0.

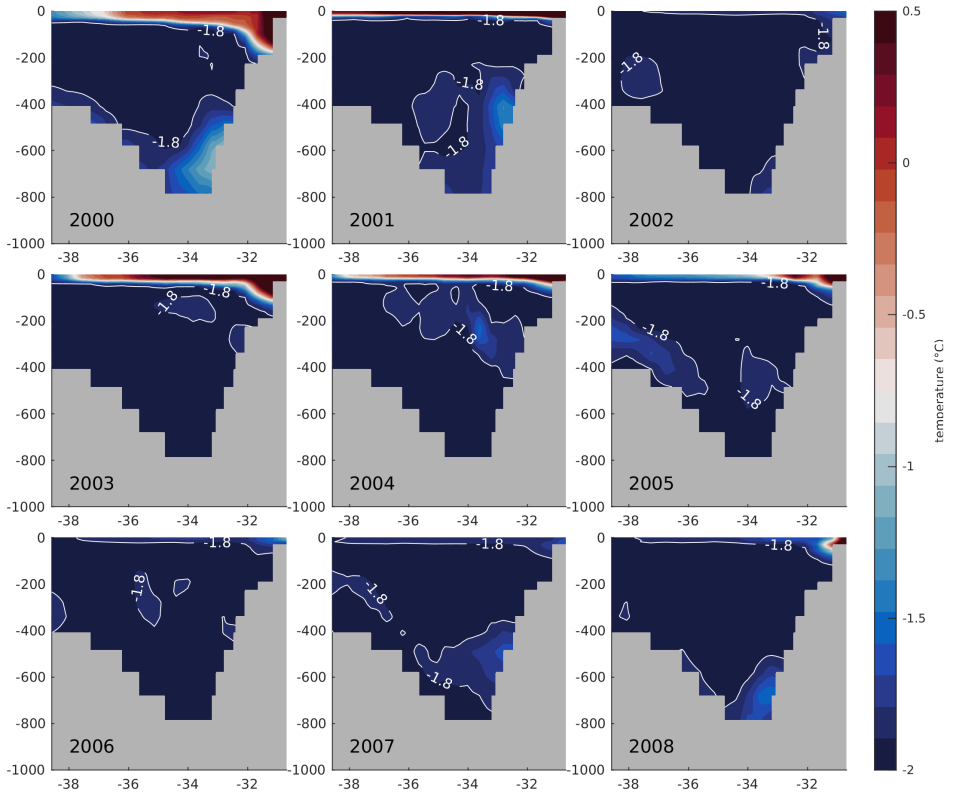


**Figure A.5: Potential temperature along section A.** Monthly averaged potential temperature along section A through the Filchner Trough in the historical simulation *hist1* for February from 2000 to 2008 (White lines at -1.8°C).

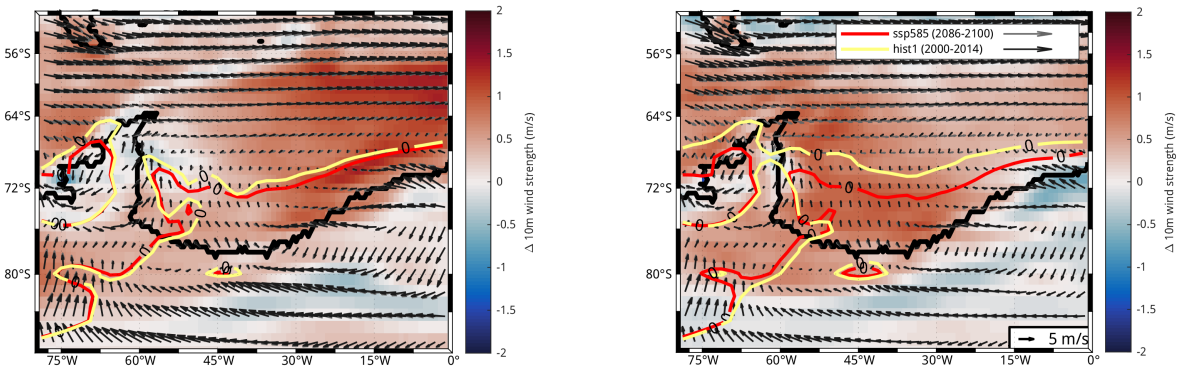


**Figure A.6: Change in the wind field.** a) Shaded area shows the wind speed difference in winter (June to August) between the 15-year mean of the historical period in hist1 from 2000 to 2014, and the last 15 years of the SSP5-8.5 scenario (2086-2100). Arrows depict the average wind direction per 15 years; their length indicates the vector mean wind speed. Discrepancies between differences in the vector mean and the wind speed mean indicate a higher variability in SSP5-8.5. The red and yellow line show the transition line between wind from the east and wind from the west. b) Same as a) but for summer (January to March).

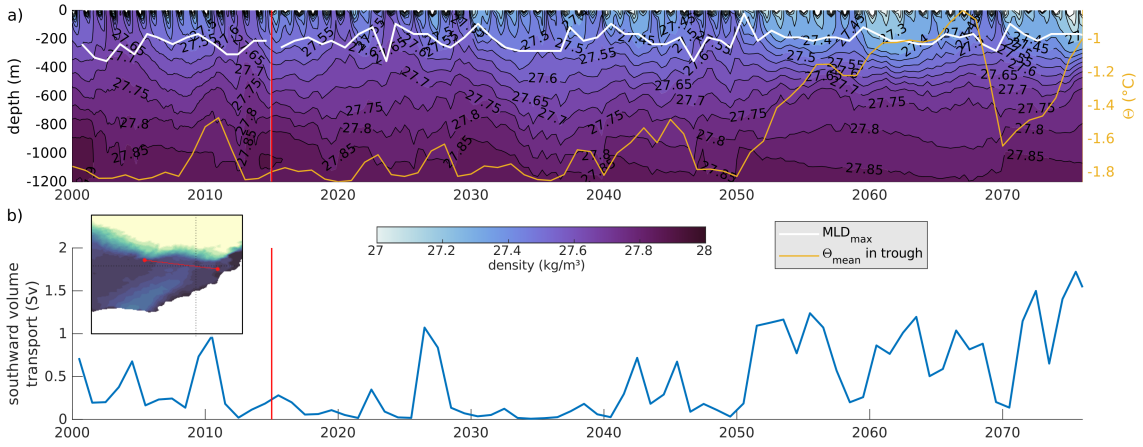


**Figure A.7: Density, transport and mixed layer depth on the continental shelf in SSP5-8.5.** a) Average density in the Filchner Trough and on the eastern continental shelf. White line shows the maximum Mixed Layer Depth for each year. The yellow curve shows the mean potential temperature in the Filchner Trough as defined in Fig. 1 of the manuscript. b) Yearly averaged southward volume transport of water masses with $\Theta > -1°C$ across the Filchner Sill as shown in the insert.

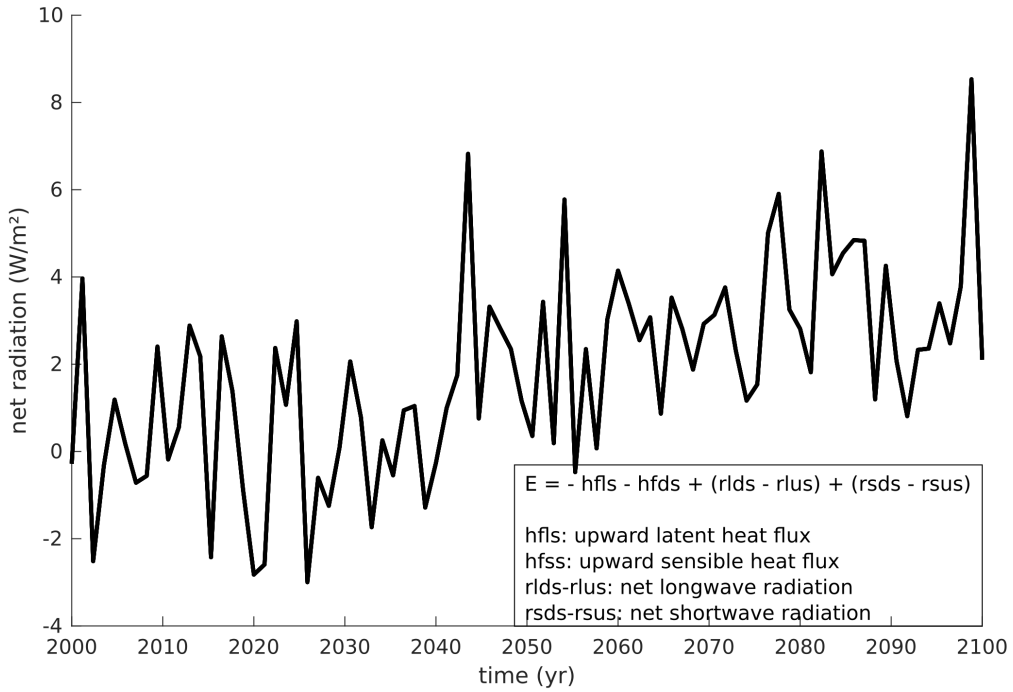


**Figure A.8: Net surface heat flux (SSP5-8.5).** Time series of yearly averaged net heat flux at the ocean surface (or the sea ice surface, wherever present), averaged over the Weddell Sea between 65°W and 0°W, and 80°S and 60°S.

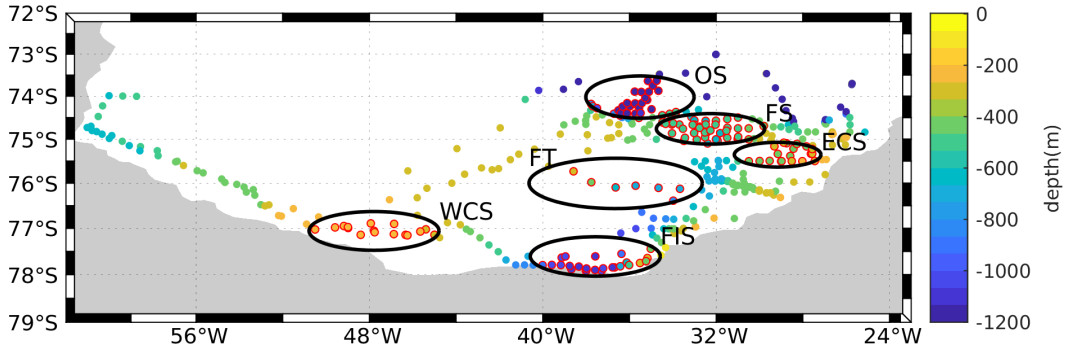


**Figure A.9: Coordinates and depth of temperature data used for validation.** Key areas: central Filchner Trough (FT), Filchner Sill (FS), Filchner Trough at the Filchner ice shelf edge (FIS), Eastern Continental Shelf east of the Filchner Trough (ECS), Western Continental Shelf west of the Filchner Trough (WCS), and Off-Shore north of the continental shelf (OS). Data points over which the average value difference between observational data and model data has been calculated per area have been outlined in red.

APPENDIX

# B

## SUPPLEMENTARY MATERIAL TO CHAPTER 5

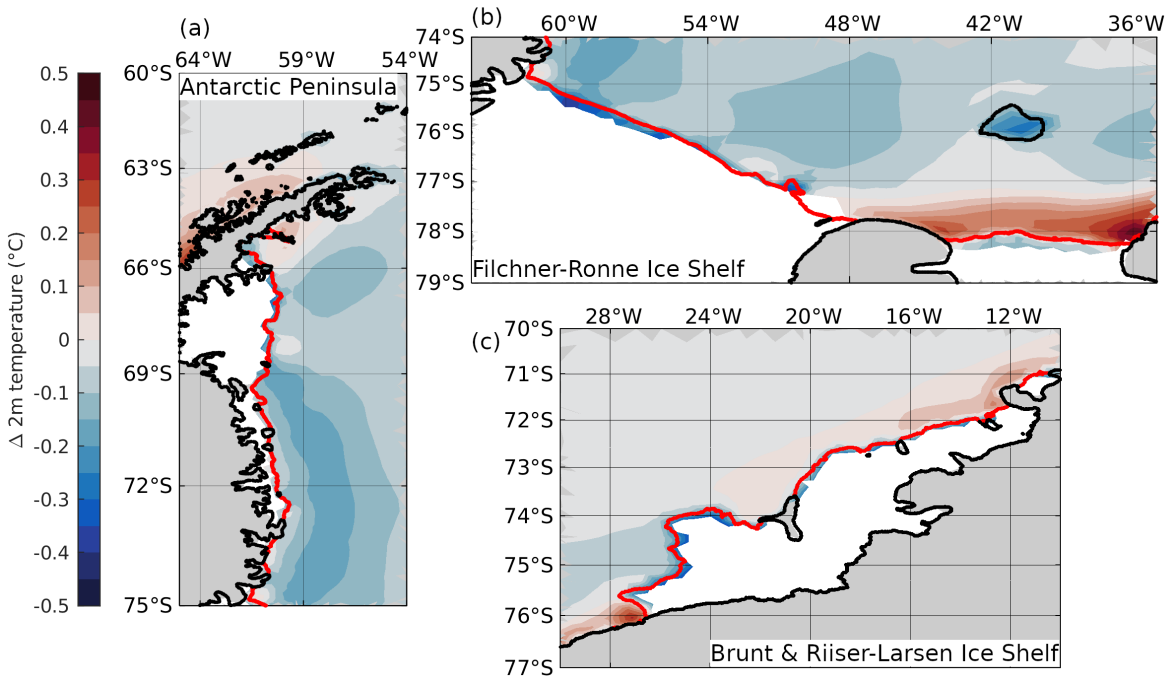


**Figure B.1:** Mean 2m temperature difference FECO-REF for 2000-2014 in the regions of (a) the Antarctic Peninsula, (b) The Filchner Ronne Ice Shelf front, and (c) the Brunt and Riiser-Larsen Ice Shelf front. The black line shows the position of the coast line in CCLM, the red line the position of the ice shelf mask in CCLM. Gray shows the position of the land and white the ice shelves in AWI-CM.

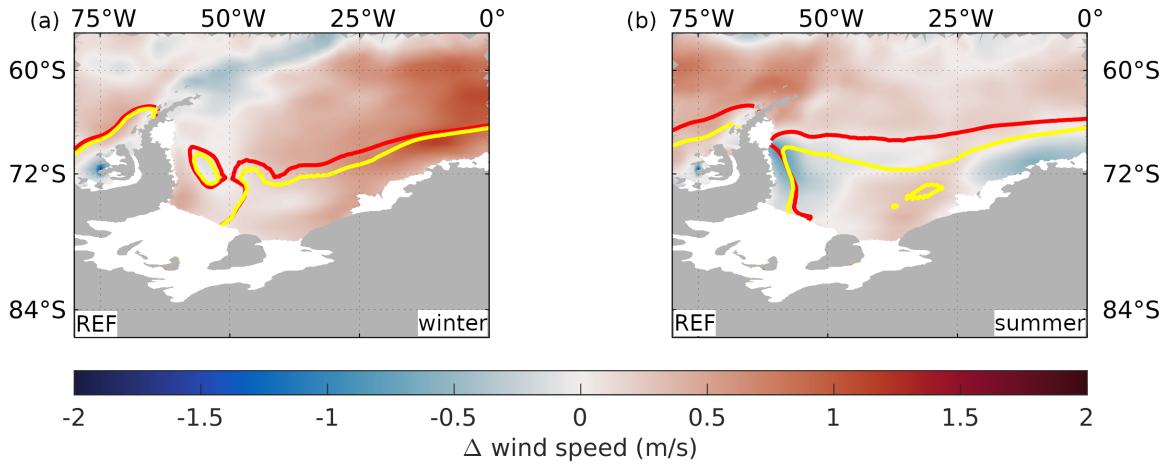


**Figure B.2:** a) Difference between the wind speed in the 5 year means of 2096-2100 to 2010-2014 in REF in winter and b) in summer. Red (yellow) line shows the position of the boundary between easterly and westerly winds in the 2010-2014 (2096-2100) mean.

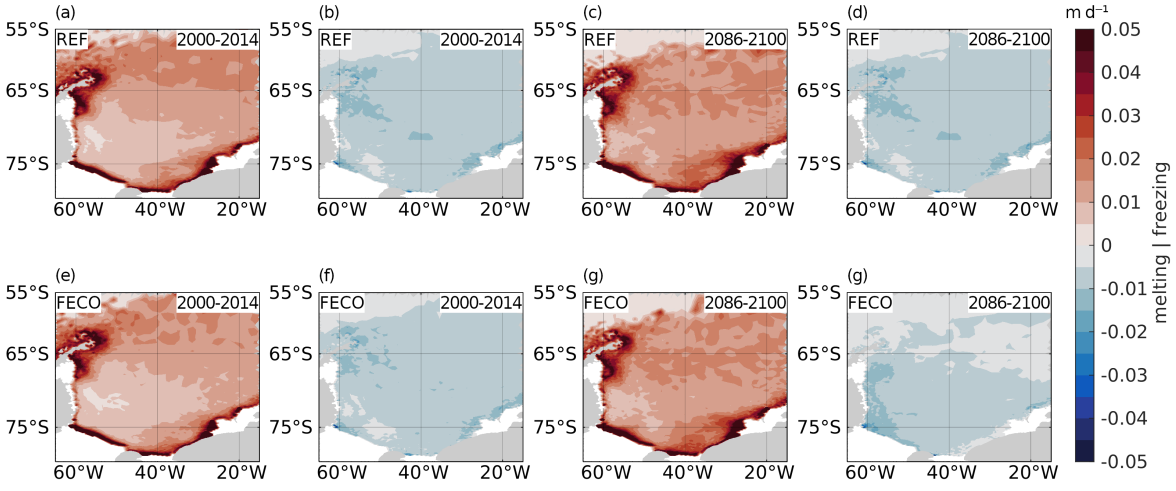


**Figure B.3:** Average sea ice freezing (a) and melting (b) distribution of the sea ice in REF in the 2000-2014 mean and (c) and (d) for 2086-2100. (e) to (h) show the same as (a) to (d) but for FECO.

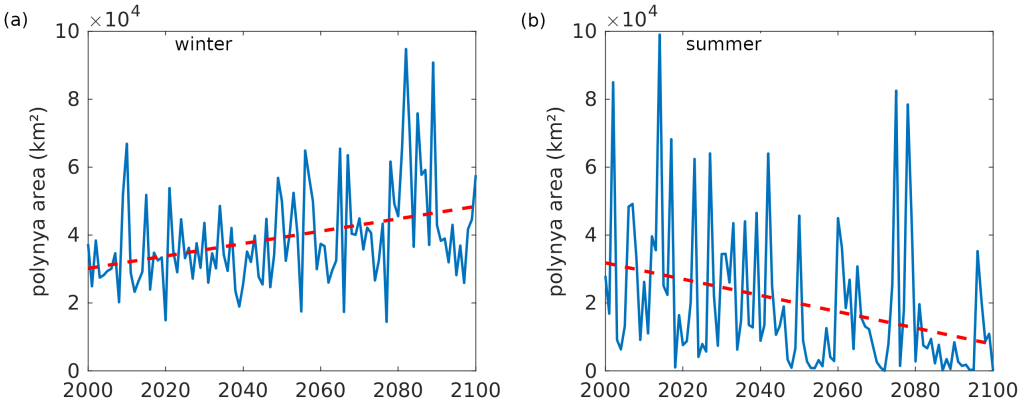


B:PolArea

**Figure B.4:** (a) Yearly mean winter time polynya area in the Weddell Sea (averaged over May to September) with trend line in red. (b) is the same as (a) but for summer (December to February).

APPENDIX

# C

# SUPPLEMENTARY MATERIAL TO CHAPTER 6

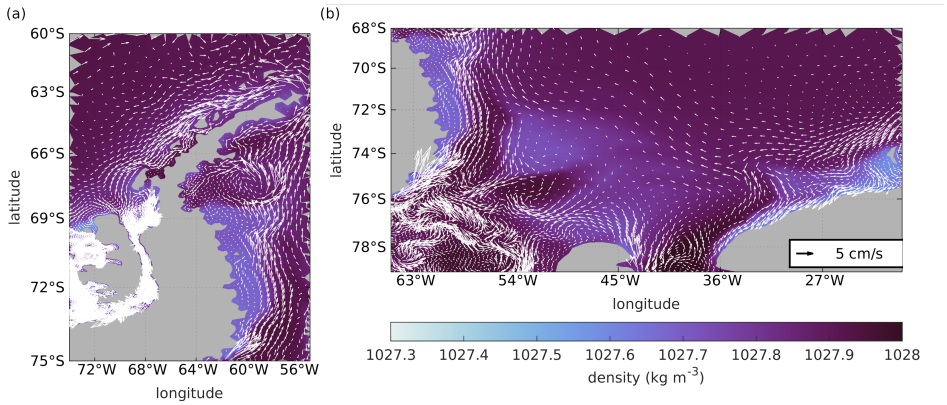


**Figure C.1:** Bottom density and mean ocean velocity (whole water column) in REF (2010-2014) at the Antarctic Peninsula (a) and on the southern Weddell Sea continental shelf (b).

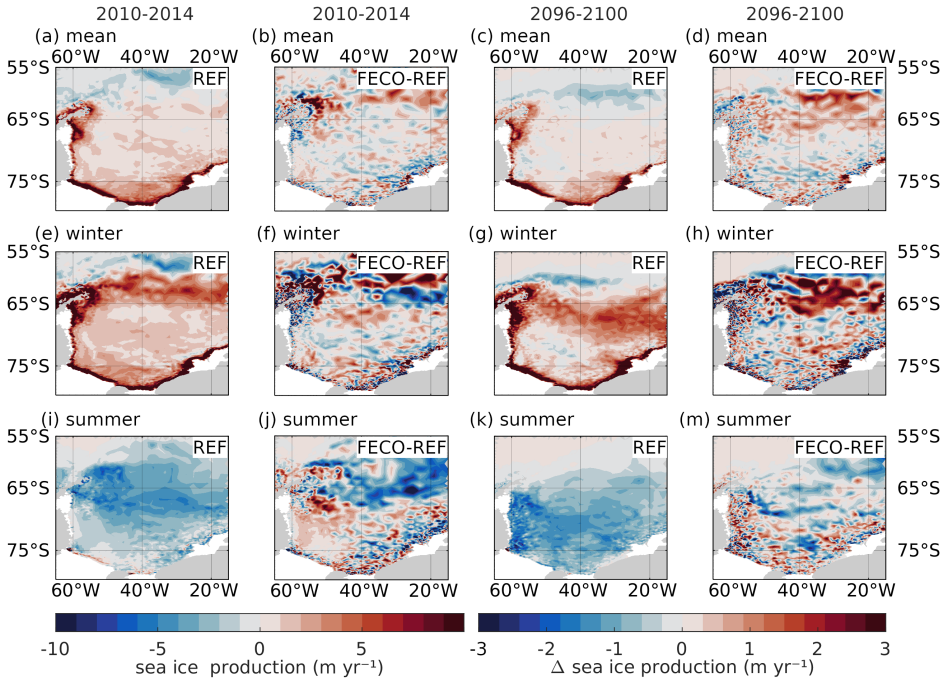


**Figure C.2:** Mean sea-ice formation by thermodynamic processes in REF for (a) 2010-2014, and (c) 2096-2100. Mean sea-ice formation difference between FECO and REF in (b) 2010-2014 and (d) 2096-2100. (e)-(h) same as (a)-(d) but only for summer means (December-February), and (i)-(m) for winter means (June-August).

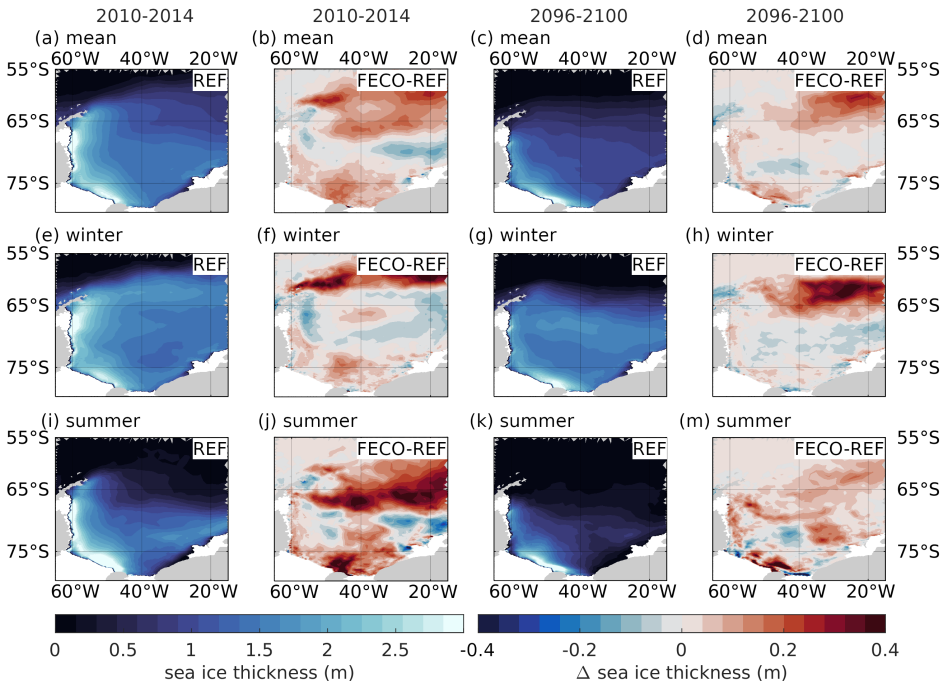


**Figure C.3:** Mean sea-ice thickness in REF for (a) 2010-2014, and (c) 2096-2100. (b) Mean sea-ice thickness difference between FECO and REF in (b) 2010-2014 and (d) 2096-2100. (e)-(h) same as (a)-(d) but only for summer means (December-February), and (i)-(m) for winter means (June-August).

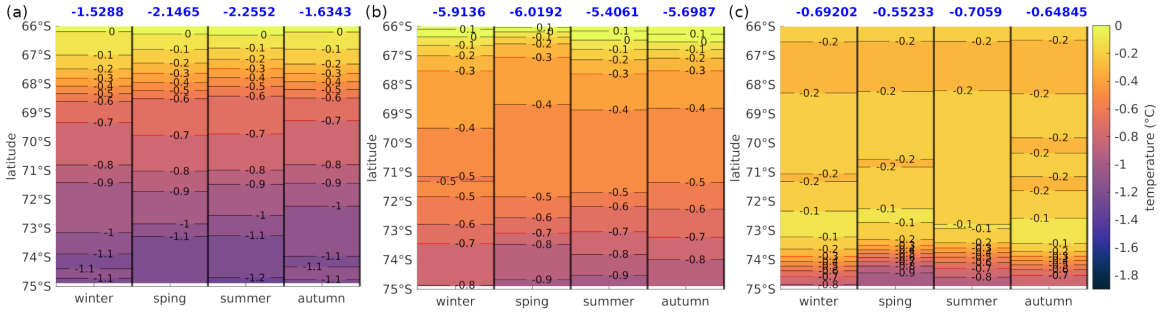


**Figure C.4:** Temperature at 300 m depth zonally averaged along the Filchner Trough section between 75°S and 66°S (see Fig. 1) in REF (2010-2014) with the distance between the -0.3°C and -0.7°C isotherms (marked in red) in degree in blue for (a) REF (2010-2014), (b) REF (2096-2100), and FECO (2096-2100).

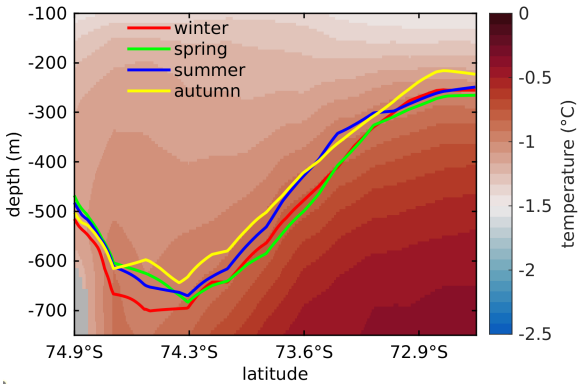


**Figure C.5:** Potential mean temperature in 2010-2014 in REF. Colored lines show the position of the 27.4 kg m$^{-3}$ isopycnal during the four seasons.

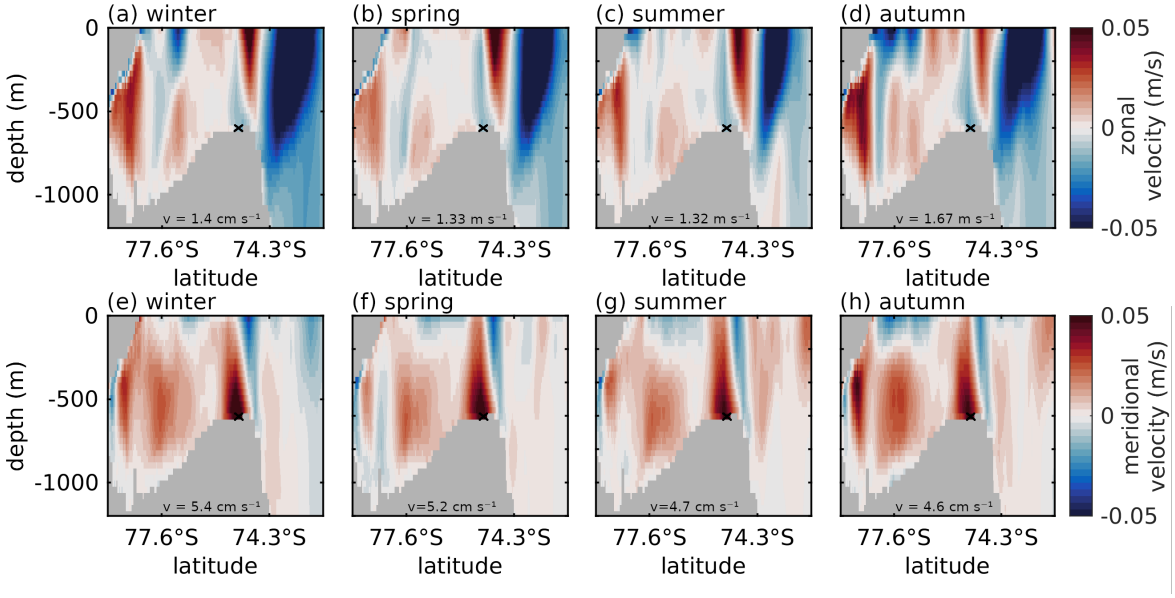


**Figure C.6:** Zonal velocity in ms$^{-1}$ along the Filchner Trough section (see Fig. 1) for (a) winter, (b) spring, (c) summer, and (d) autumn in REF (2010-2014). Positive values describe eastward velocity. The black x marks the spot where the velocity was determined and the location of the DSW exporting current. (e)-(h) same as (a)-(d) but for meridional velocity. Positive values describe northward velocity.

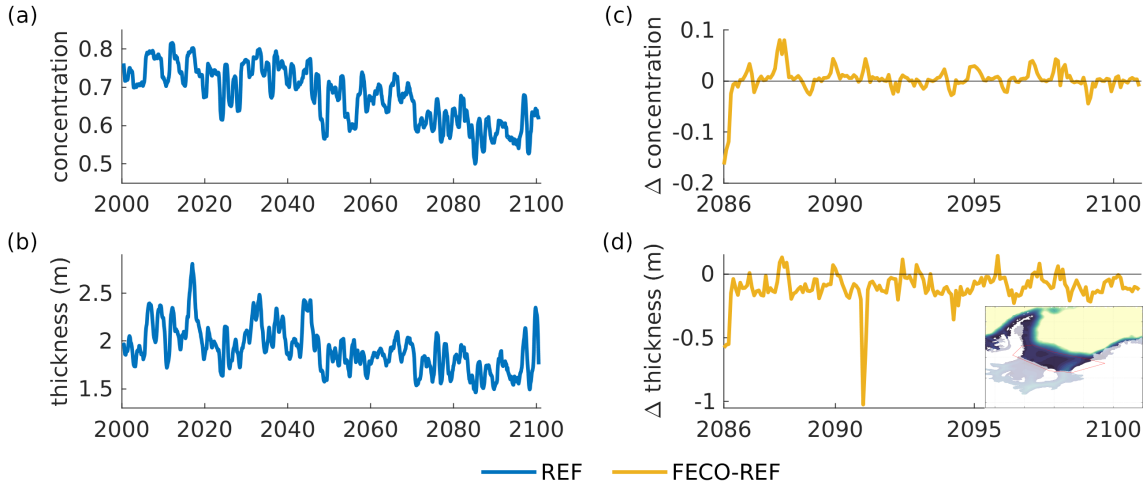


**Figure C.7:** a) Mean sea ice concentration in Filchner trough (running mean of 12 months) in REF (blue) and FECO (red) on the southern Weddell Sea continental shelf. b) Same but for mean sea ice thickness. c) Difference in monthly mean sea ice concentration FECO-REF. d) Same as c) but for sea ice thickness.

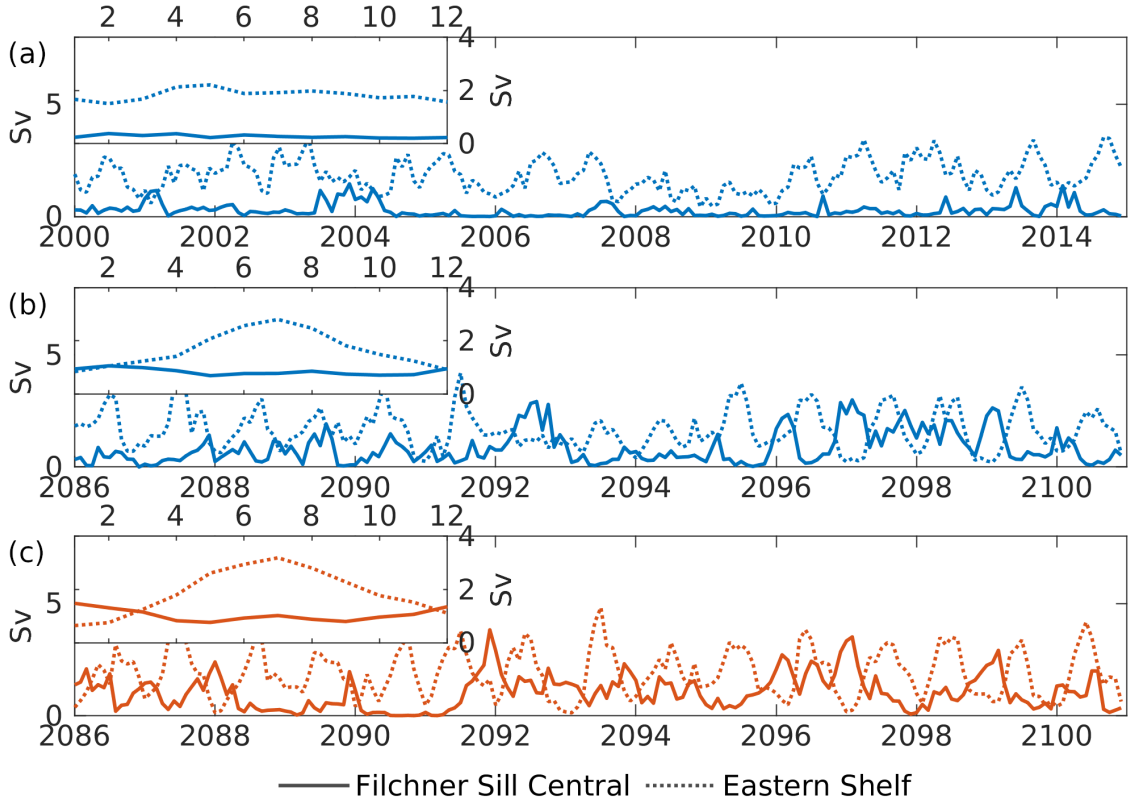


**Figure C.8:** Southward volume transport of water masses with $\Theta > -1.5$°C across the Filchner Sill and the Eastern Shelf in (a) REF (2000-2014), (b) REF (2086-2100), and (c) FECO (2086-2100). Insets show monthly averages.

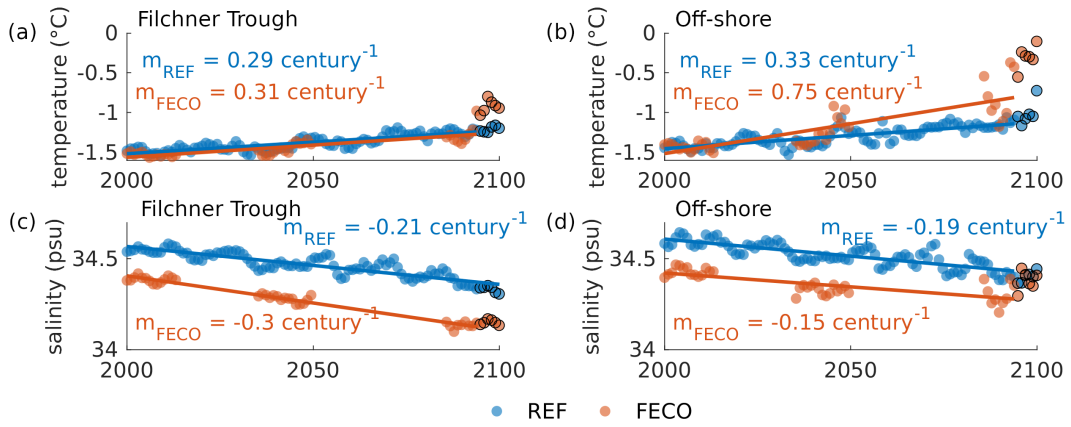


**Figure C.9:** Lineare regression of mean temperature in Filchner Trough (a) and north of the Filchner Trough sill at 636 m depth (b). c)-d) same as a)-b) but for salinity. Data points outlined in black were excluded from the linear regression due to the regime shift in 2093.

APPENDIX

# D

# PUBLISHED ARTICLES

## D.1 Teske et al. (2024b)

Vanessa Teske, Ralph Timmermann, and Tido Semmler, Communications Earth & Environment, 5, 93 (2024). https://doi.org/10.1038/s43247-024-01238-5

communications earth & environment

ARTICLE

https://doi.org/10.1038/s43247-024-01238-5 OPEN

# Subsurface warming in the Antarctica's Weddell Sea can be avoided by reaching the 2°C warming target

Vanessa Teske [1]✉, Ralph Timmermann[1] & Tido Semmler [1,2]

Recently, seasonal pulses of modified Warm Deep Water have been observed near the Filchner Ice Shelf front in the Weddell Sea, Antarctica. Here, we investigate the temperature evolution of subsurface waters in the Filchner Trough under four future scenarios of carbon dioxide emissions using the climate model AWI-CM. Our model simulates these warm intrusions, suggests more frequent pulses in a warmer climate, and supports the potential for a regime shift from cold to warm Filchner Trough in two high-emission scenarios. The regime shift is governed in particular by decreasing local sea ice formation and a shoaling thermocline. Cavity circulation is not critical in triggering the change. Consequences would include increased ice shelf basal melting, reduced buttressing of fast-flowing ice streams, loss of grounded ice and an acceleration of global sea level rise. According to our simulations, the regime shift can be avoided and the Filchner Trough warming can be restricted to 0.5 °C by reaching the 2 °C climate goal.

[1] Alfred Wegener Institute for Polar and Marine Research, D-27570 Bremerhaven, Germany. [2] Met Éireann, 65-67 Glasnevin Hill, D09 Y921 Dublin, Ireland. ✉email: vanessa.kolatschek@awi.de

Sea-level rise is one of the pressing topics of future climate change. The Antarctic ice sheet holds an ice volume equivalent to 58 m of sea level rise[1], but loses mass at an accelerating rate[2]. Melting of the Antarctic ice sheet is dominated by melting at the base of the ice shelves, bodies of ice fringing the ice sheet and floating on the Southern Ocean[3]. While most of the ice sheet mass loss currently occurs in the Amundsen Sea[4,5], where the cavities are filled with relatively warm water of deep-ocean origin[6,7], it has been suggested that a tipping point with a regime shift from cold to warm waters in the cavity and a dramatic increase of melt rates may exist for Filchner Ronne Ice Shelf in the Weddell Sea[8].

The continental shelf of the Weddell Sea is one of the main areas of dense shelf water production which is a precursor of Antarctic Bottom Water (AABW) and an important part of the global ocean circulation[9]. Any changes to the water masses on the continental shelf can therefore have far-reaching consequences not only for the global sea level, but also for the global overturning circulation.

If such a regime shift occurs, basal melting is bound to increase substantially, causing a reduction of buttressing to the flow of grounded ice[10] and an additional contribution to global sea-level rise. Model simulations with ocean/ice shelf models and prescribed atmospheric boundary conditions suggest that the occurrence of this regime shift and the magnitude of the anomaly are sensitive to the evolution of the future atmosphere[11,12]. Pulses of warm water[8,11] and a freshening of the continental shelf and Filchner-Ronne ice shelf cavity have been suggested to be precursors of the eventual tipping.

The circulation in the southern Weddell Sea is dominated by the Antarctic Coastal Current transporting Warm Deep Water (WDW; 0 °C to 0.8 °C) westwards along the continental shelf break. Mixing with overlying Winter Water (WW) forms modified Warm Deep Water (mWDW; $\Theta < 0$ °C). At 74.5°S, the current branches, one arm following the shelf break and the other flowing onto the continental shelf, for example at 28°W[13], 32°W[9,14], and 44°W[15], thereby entering the Filchner Trough. At the Filchner Sill, Dense Shelf Water (DSW), formed by brine rejection through sea ice formation above the continental shelf, and Ice Shelf Water (ISW) originating from the Filchner ice shelf cavity, leave the continental shelf[9]. They mix with overlying WW and mWDW while sinking along the continental slope. The water masses formed on the way down are Weddell Sea Deep Water (WDSW) and Weddell Sea Bottom Water (WSBW[16]; Fig. 1). WSBW remains in the Weddell Sea, confined by the ocean ridges fringing the Weddell Basin. WSDW, in contrast, leaves the Weddell Sea towards the north, feeding the Antarctic Bottom Water in the process[17].

The mWDW flux onto the continental shelf experiences seasonal variability. It is strongest at the shelf break in summer and autumn (February - April) and weakens in winter[13]. The mWDW current then follows the eastern slope of the Filchner Trough southward. March to June, it reaches 76°S[18], and only a short time later 77°S and 78°S[19]. By that time its temperature has been reduced to -1.6 °C. Observations, limited as they are, have until now only shown mWDW to be present on the continental shelf seasonally[9,13,14], however increased shoaling of the WDW in the southern Weddell Sea[20], and unprecedented variations in the Weddell Sea sea ice[21] might cause changes in the future.

In 2013, mWDW was observed at 78°S near the calving front of the Filchner Ice Shelf[19], which was then attributed to an uplift of the thermocline at the continental shelf break and an unusually strong coastal current. During the period of extended inflow of mWDW from February to October in 2017, the maximum temperature of the mWDW current was higher by approximately 0.5 °C compared to temperatures previously observed at the eastern flank of the Filchner Trough[22].

In numerical model studies, pulses of warm water on the continental shelf and mWDW reaching the ice shelf front have been identified as precursors to a regime shift in the Weddell Sea. They become more frequent in a warming climate and may at some point irreversibly enter the continental shelf and fill the Filchner Ice Shelf cavern, drastically increasing basal melt rates[8,11,12,23]. This situation compared to the situation in the past is schematically shown in Fig. 1. Ice shelf mass loss reduces the buttressing effect of the ice shelf and enhances the flow of grounded ice towards the ocean[10], thus contributing to global sea level rise. Another precursor that has recently been identified is freshening of the continental shelf due to reduced sea ice production and increased local sea ice melting[12]. This flips the

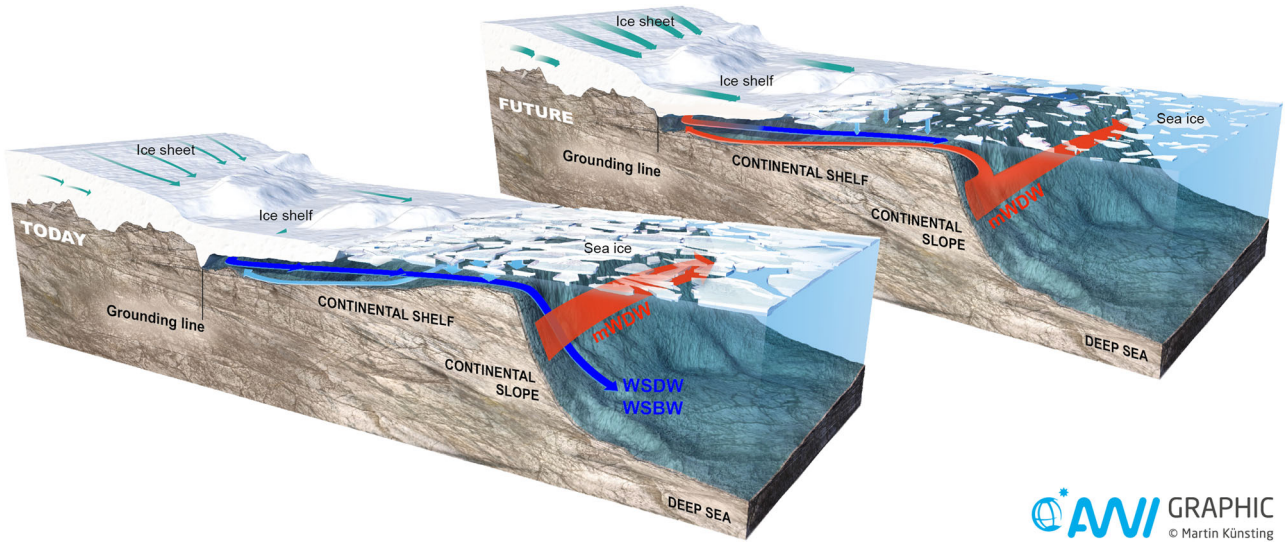


**Fig. 1 Present and potential future circulation on the continental shelf.** Schematic representation of circulation patterns in the Filchner Trough and the Filchner Ronne Ice Shelf cavity illustrating the regime shift assessed in this study. Today: Trough and cavity are filled with cold shelf water masses. Future: mWDW branches of the slope current, warming the trough and cavity. Graphic created by Alfred Wegener Institute and Martin Künsting. The Alfred Wegener Institute provides permission to reuse it (source: Alfred-Wegener-Institut / Martin Künsting (CC-BY 4.0)).

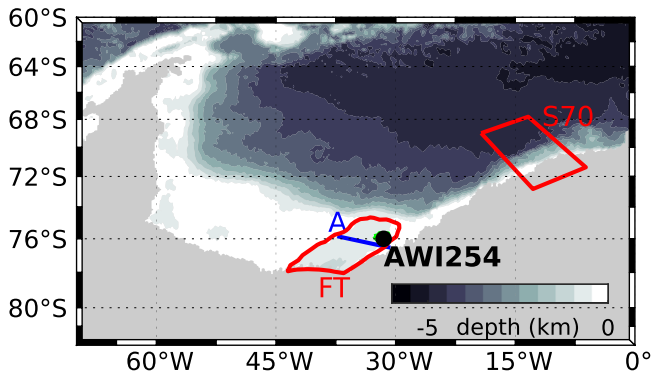


**Fig. 2 Study area.** Model topography and the outlines of the Filchner Trough (FT) and the area around 70°S (S70) that have been used for mean calculations. The blue line represents section A. While the definition of S70 uses a simple latitude/longitude criterion, a polygon of surface grid nodes is used as a perimeter for the FT area. The bold black dot at 31.5°W 76°S indicates the location of the mooring AWI254 that is referred to in Fig. 6[36]. The green area contours the grid nodes over which temperature was averaged for the comparison to AWI254 in Fig. 6.

density gradients between the DSW in the Ronne Depression and the Filchner Ronne Ice Shelf cavity, as well as between the mWDW at the continental shelf break and the ISW leaving the ice shelf cavity. The changes lead to a reverse of the flow direction in the cavity. In these previous studies, this phenomenon has been simulated in regional and/or uncoupled model configurations considering ice shelf cavities and/or with idealised forcing scenarios.

While the connection between the flow of mWDW in Filchner Trough and the increase of basal melt rates in the ice shelf cavity is well understood[8], if and when the mWDW actually enters the trough has so far been only weakly constrained. This is the gap that we aim to fill. In this study, we analyse a suite of simulations performed with the AWI Climate Model (AWI-CM) for the Coupled Model Intercomparison Project (CMIP6) of the 6th Assessment Report of the Intergovernmental Panel on Climate Change (IPCC)[24,25]. AWI-CM is a global coupled climate model with an eddy-permitting ocean component. The simulations were specifically designed to make projections of possible future climate evolution[26] rather than for specific case studies. Like other CMIP6 models, AWI-CM does not include ice shelf cavities or tides, but it features a horizontal ocean resolution of around 10 km in parts of the Southern Ocean, which is one of the highest in the CMIP6 model suite. The simulations include an ensemble of five historical simulations (hist1 to hist5, 1850–2014), and four climate scenarios with forcing derived from Shared Socioeconomic Pathways[27](SSP1-2.6, SSP2-4.5, SSP3-7.0, SSP5-8.5) covering 2015 to 2100. SSP3-7.0 also has five ensemble members.

We evaluate the distribution of mWDW in the southern Weddell Sea (Fig. 2) between 2000 and 2014 in the historical simulations, and we examine seasonal and long-term changers in the transport patterns of mWDW in Filchner Trough and attribute their divergent evolution to the spread between the different climate scenarios. We also show that for high-emission scenarios the Filchner Trough experiences a regime shift where the mean temperature in the trough can rise by 2 °C until 2100. However, the regime shift can be avoided by limiting global warming to 2 °C or below.

## Results

**Three phases of climate change**. The analysis of the historical simulation and the four different climate scenarios shows the occurrence of pulses of warm mWDW similar to contemporary observations. The pulses have changing characteristics that allow for the definition of three phases. The beginning of each individual phase depends on the climate scenario (Supplementary Table 1).

I. During the historical simulations (e.g. *hist1* in Fig. 3a), the Filchner Trough is filled with cold, dense shelf water with regular phases of weak warming during winter due to a seasonally enlarged (but still weak) inflow of mWDW.
II. The beginning of the second phase is defined as the point in time when the mean temperature in Filchner Trough rises above the long-term mean of 1850-2014, i.e. when the annual mean temperature in the trough lies above the mean plus the standard deviation from phase I for longer than two consecutive years. Over the course of this phase, temperature in the Filchner Trough is increasingly dominated by pulses of mWDW (Fig. 3a), while salinity in the trough slowly declines (Fig. 3b).
III. The last phase begins when the mean temperature in the trough rises permanently above −1 °C. In this state, the trough is mostly filled with mWDW and the seasonal signal has vanished. The mitigation scenario SSP1-2.6 is the only scenario that does not reach this state (Fig. 4, Supplementary Fig. 1).

During Phase I, the average temperature in Filchner Trough stays low near −1.8 °C and only shows seasonal warming by typically less than 0.25 °C relative to the 1850-1900 mean, reaching no higher than −1.5 °C (Fig. 4). During Phase II, the average maximum temperature of the current reaching the Filchner Trough over all scenarios is increased to −0.41 °C ± 0.36 °C (sampled at transect A, see Fig. 2). The longer the pulse lasts, the warmer the water that is registered in the trough, e.g the pulse in hist1 lasting from 2008 to 2012 reaches a peak temperature that is 0.68 °C warmer (potential temperature of −0.19 °C) compared to 2007 at its core along transect A. Most shorter warm water pulses show a lower temperature than this and remain below the temperature increase of 0.5 °C described by Ryan et al.[22]. All our climate projections show increasing numbers of mWDW pulses entering the Filchner Trough during the second phase (Fig. 4). The frequency of these pulses stays relatively constant until 2050.

In the second half of the 21st century, the multiyear intrusions of mWDW increase in length and frequency depending on the forcing scenario. While SSP1-2.6 remains in Phase II and returns to its DSW-filled state after each pulse (Fig. 4a), the SSP2-4.5 scenario transitions into Phase III during the last four years of the simulation with a warmer state than the SSP1-2.6 but colder than the temperatures reached in SSP3-7.0 or SSP5-8.5 (Fig. 4b). It is unclear if the warm state would be maintained or the trough would return to a colder temperature if the scenario continued beyond the year 2100. In the SSP3-7.0 ensemble and in SSP5-8.5, the trough clearly shifts to a consistently warmer state (Fig. 4c–h). In these two higher-emission climate projections, the Filchner Trough in Phase III stays warm and is filled with mWDW. For this particular aspect, results from the SSP5-8.5 lie within the spread of the SSP3-7.0 ensemble.

The observation of an especially warm and prolonged mWDW presence on the continental shelf during 2017[22] suggests that the Filchner Trough in reality is either on the brink of transitioning or it has already transitioned into Phase II.

### Evaluation of circulation characteristics

*Present mean state*. A particular feature of our climate model simulations is that for a global coupled climate model, many aspects of the results of the historical simulations for the period

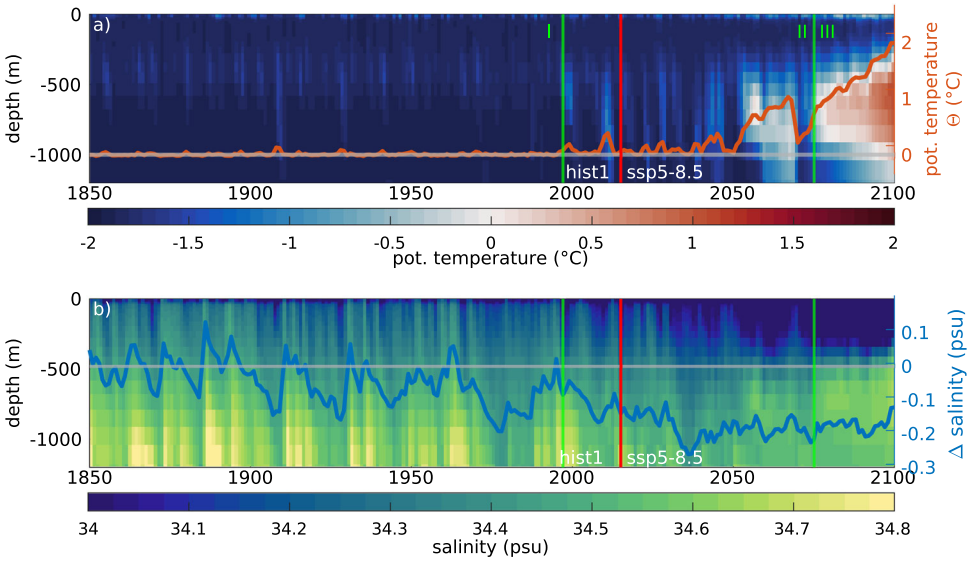


**Fig. 3 Simulated temperature evolution in Filchner Trough in SSP5-8.5. a** Hovmoeller plot of the yearly mean potential temperature in Filchner Trough for the historical simulation hist1 and the scenario SSP5-8.5, and the average temperature change (orange) relative to the 1850-1900 mean (gray). The red line marks the transition from historical to scenario simulation. The green lines mark the phase boundaries. **b** same as **a** but for salinity.

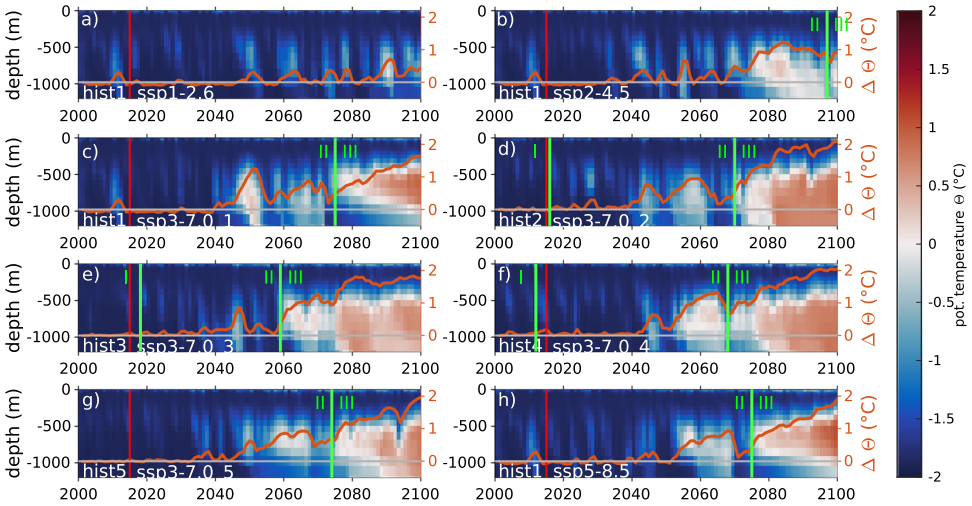


**Fig. 4 Simulated potential temperature evolution in Filchner Trough for four climate scenarios.** Hovmoeller plots of the yearly mean potential temperature in Filchner Trough from the year 2000 to 2100, with the average temperature change in the Filchner Trough relative to 2000 shown in orange, for the climate scenarios: **a** SSP1-2.6, **b** SSP2-4.5, **c**–**g** SSP3-7.0 (five ensemble members) and **h** SSP5-8.5. The vertical red lines divide the timeline into the historical simulations (before 2015) and the future climate scenarios (from 2015 onward). Green lines mark the phase boundaries.

2000-2014 are in remarkably good agreement with observations in key areas around the Filchner Trough (Fig. 5a, Supplementary Fig. 4a, for the definition of key areas see Methods and Supplementary Fig. 9). Due to the high variability of the water mass properties on the continental shelf and the fact that model years in a climate model do not reflect the actual year-to-year evolution, a direct comparison of the model results with hydrographic measurements taken as a snapshot or over a short period of time is difficult. The position and strength of the modeled mWDW current shows a strong interannual variability (Supplementary Fig. 5) that can cover the true variations only with regard to their statistical properties. However, the temperature and salinity distributions in key areas show a similar pattern in the model results as in observations, indicating that the model can reproduce the main features and processes that define the circulation in the Weddell Sea, even without ice shelf cavities (Fig. 5, Supplementary Fig. 4a). The most important water masses and circulation features in the western Weddell Sea, except for Ice Shelf Water (ISW), can be clearly identified. The simulations do not produce ISW due to the absence of ice shelf cavities in the model grid. The coldest water mass in the Filchner Trough has in-situ surface freezing temperature (approx. −1.9 °C). However, all other water mass properties compare well with observations even quantitatively (Fig. 5a, Supplementary Fig. 4a).

Large-scale circulation features two cyclonic cells forming the Weddell Gyre (Supplementary Fig. 2a) as has been suggested by earlier model studies[28]. The volume transport of the simulated Weddell Gyre is 46 Sv at the Prime Meridian and thus similar to observational data[29,30] (Supplementary Fig. 2b). Transport by the ACC across 60°W amounts to 170 Sv and is therefore on the high side of observation-based estimates (e.g., 107-161 Sv in Drake Passage[31,32]). The Antarctic Slope Current transports mWDW with a potential temperature $\theta > 0$ °C along the continental slope southward (Fig. 5a). The main current turns west at about 74°S

and follows the continental slope towards the Antarctic Peninsula (Supplementary Fig. 3). A side current branches off and cooler mWDW flows onto the continental shelf east of Filchner Trough and along the trough's eastern slope, indicated by a warm signature with temperatures between −0.5 °C and 0 °C on the eastern continental shelf, and approximately −1.5 °C over the eastern slope of Filchner Trough (Fig. 5a), similar to the observations described by[9]. In the 15-year mean, this southern branch can be traced south to 76°S (Fig. 5a). The simulation reproduces WSDW and WSBW in the Weddell Sea with temperatures between −0.8 °C and 0 °C, and Antarctic surface water with temperatures below −1.5 °C and the lowest salinity values in the central Weddell Sea (S < 34.3; Fig. 5a, Supplementary Fig. 4a).

The ensemble mean of the historical simulation is a close match for observational data in key areas in and around Filchner Trough[33–38]. In the central Filchner Trough (FT), at the Filchner ice shelf front (FIS), on the continental shelf west of the trough (WCS) and off-shore over the continental slope (OS), the mean ensemble temperature deviates by 0.06 °C or less from observation data (flags in Fig. 5a). The standard deviation in each of the key region shows that the largest variations in the deviation between model and observations are found at the off-shore location, caused by a varying depth of the ASF. The largest positive temperature bias can be found on the eastern shelf and on the eastern slope of the Filchner Trough, areas that are subject to strong annual and interannual variability due to the varying mWDW flux. This area is 0.36 ± 0.36 °C warmer in the model average than in the observations. The bottom salinity of the ensemble mean ranges from 34.33 on the Berkner Shelf to 34.58 in the Filchner Trough and deviates by 0.12 ± 0.06 psu from observations (Supplementary Fig. 4a). The model trough is filled with DSW with a minimum simulated temperature of −1.9 °C. Generally, the model results are slightly warmer and fresher on the continental shelf than observational data suggest.

The circulation on the shelf agrees well with observed patterns in most areas outside of the ice shelf cavities[9,14]. We identify three major areas of dense water overflow: the Filchner Sill, the center of the southern Weddell Sea continental shelf at approx. 47°W, and north of the Ronne Trough (Supplementary Fig. 3). Because of the lack of an ice shelf cavity, High Salinity Shelf Water/DSW produced in the Ronne Trough flows northward towards the Antarctic Peninsula and not through the cavity towards the Filchner Trough[39,40].

*Seasonality*. Phase I (as defined above) is characterized by a seasonal influx of varying length of mWDW into Filchner Trough, which increases the mean temperature in the trough during winter. The model results show the main transport of mWDW into the Filchner Trough taking place via the continental shelf east of the Filchner Trough (Fig. 5a, Supplementary Fig. 3), while occasionally smaller currents enter the trough over the central and western depression (Supplementary Fig. 5), reproducing observed patterns[13,14,41]. The warm water takes several months to travel from the slope southward before going west, down the slope into the trough.

The seasonal influx of mWDW onto the shelf east of Filchner Trough and along the eastern slope of the trough was reported to be the strongest during February to June and weaker during the spring and summer months[13,18,19,42]. Mooring data (AWI254) from 31.5°W 76°S shows the warming onset caused by mWDW during late March, early April (Fig. 6a,[36]). However, Ryan et al.[18]

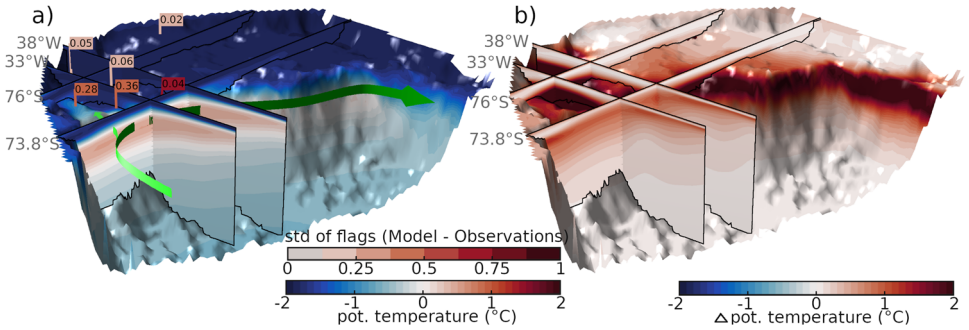


**Fig. 5 Simulated potential temperature distribution and evolution in the southern Weddell Sea. a** Potential temperature in a 15-year average of the ensemble mean of the historical scenario (2000 to 2014) at the sea floor and at sections along 33°W, 38°W, 73.8°S and 76°S with differences to observational data (flags,[33–37]). Arrows indicate the slope current of WDW and mWDW flowing along the continental shelf break and onto the shelf. Upper colorbar: standard deviation of difference of model data to observational data in averaged key areas (flag color), lower colorbar: potential temperature along sections and sea floor. **b** Change in potential temperature in the 15-year average 2086 to 2100 compared to a) in the ensemble mean of SSP3-7.0.

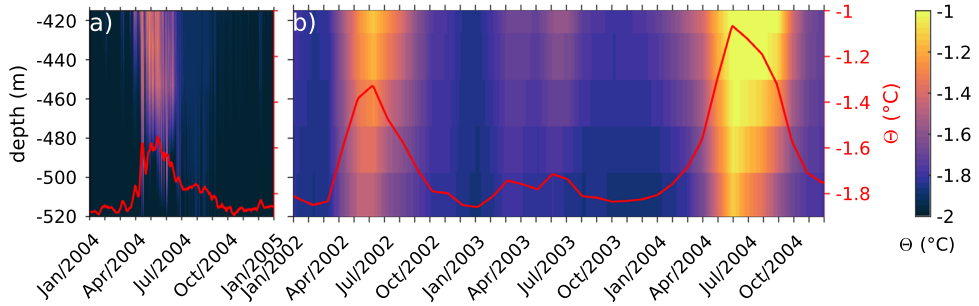


**Fig. 6 Hovmoeller diagrams of potential temperature at mooring AWI254 (31.5°W 76°S). a** Mooring data from January 2016 to December 2016[36], **b** Model output for the area outlined in green in Fig. 2 for 2002–2004. The red lines indicate the temperature averaged between 410 m and 520 m. In **a** a five-days running mean was applied to the vertically averaged temperature data. The temperature and depth scales are valid for both panels.

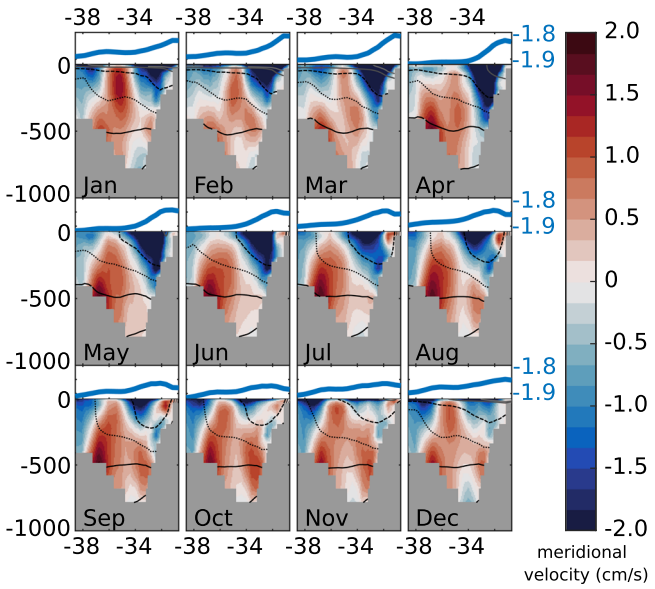


**Fig. 7 Mean seasonal cycle across Transect A.** The line plot in blue shows the sea surface elevation (ssh in m). The panel below shows the meridional velocity component (m/s) as background color, with isopycnals (black: 27.7 kg/m$^3$, dotted: 27.6 kg/m$^3$, dashed: 27.5 kg/m$^3$, gray: <27.5 kg/m$^3$) for the simulated monthly means of 2000-2014. Positive numbers for the velocity (i.e. reddish colors) indicate northward flow.

reported the presence of mWDW at 31°W already starting in January. To compare the model output to the mooring observations, we compute an area-weighted temperature average over the area outlined in Fig. 2. We see similar behaviour in the simulation as in the observations (Fig. 6b). MWDW generally starts to arrive at 76°S during March, however as the examples show, the onset can vary by several months and in strength. The timing of the maximum temperature varies between February and June[18,22], and so does the timing in the simulations.

During April to August the model results show an intensification of the northbound transport of DSW along the western slope of the Filchner Trough (Fig. 7), caused by a higher sea ice production over Berkner Shelf in autumn and winter. Morrison et al.[43] proposed that northward DSW transport in a canyon or trough leads to a gradient in sea surface height due to the replacement of less dense water along the western canyon slope with DSW. This creates a barotropic pressure gradient which drives more lighter AASW and mWDW from the northeast into the trough[43](their schematic in Fig. 5A). Given that our model results show similar characteristics in the density distribution across the Filchner Trough and a difference in sea surface height between eastern and western slope of the trough (Fig. 7), we conclude that the mechanism proposed by Morrison et al.[43] offers a plausible explanation for the timing and structure of the seasonal mWDW inflow both in the model and in reality. The intensification of the north-bound transport and the simultaneously increased presence of denser water in autumn strengthen the pressure gradient across the trough and bring more mWDW into the trough, leading to the observed seasonal increase in temperature.

As an additional component, the depth of the thermocline at the continental slope also shows a weak seasonal oscillation. It rises during spring and summer, and deepens during autumn and winter. This facilitates the flow of mWDW onto the continental shelf during summer, when the thermocline is at its shallowest. The mWDW then takes two to three months to reach the Filchner Trough.

**Future evolution**. During the climate projections for the 21st century, the characteristics of the water mass filling the Filchner Trough change significantly. Some of these changes can already be observed at the end of the historical simulations when the Filchner Trough reaches Phase II. Causes for these changes can be found in the local sea ice formation as well as upstream, and in the position and temperature of the Antarctic Slope Current. The mechanism behind the increased presence of mWDW on the shelf is different from the one responsible for the seasonal variation. It will be described in the following.

*Changes in Filchner Trough*. In the emission scenario SSP3-7.0, the mean water temperature in Filchner Trough is warmer by approx. 2 °C (Fig. 8a) and saltier by less than 0.2 psu (Supplementary Figs. 1c-g and 4b) by the end of the century, showing the permanent presence of mWDW. Salinity of near-surface water on the continental shelf, however, has decreased by up to 0.8 psu, following a decrease in sea ice formation (Fig. 8a). Further changes occur along the continental slope, where the slope current warms by up to 1 °C (Figs. 5b and 8a). The high-emission scenario SSP5-8.5 shows similar warming patterns with an even further increase in bottom temperature on the continental shelf at the Berkner Bank and north of the Ronne Trough (temperature anomaly between 1.5 °C and 1.8 °C). The mitigation scenarios SSP1-2.6 and SSP2-4.5 show a similar distribution of warming water, but the temperature rise in Filchner Trough is limited to 1 °C or less. The average salinity in Filchner Trough increases in SSP3-7.0 and SSP5-8.5 where mWDW, with a higher salinity than the fresher DSW, is registered permanently in the Filchner Trough (Fig. 3b, Supplementary Figs. 1c-h and 4b).

In all scenarios, the increase of the average temperature in the Filchner Trough accelerates during Phase II. During the 2030s, the average temperature in the trough for the ensemble mean of SSP3-7.0 rises from −1.75 °C to −1.6 °C (thick red line in Fig. 8a), while the temperature in SSP1-2.6 (thin red line in Fig. 8a) decreases slightly. Starting from 2040, the average temperature in the Filchner Trough in SSP3-7.0 rises quickly and reaches 0.3°C in 2100, 2 °C warmer compared to 2000. This goes hand in hand with a strong decrease of sea-ice formation in the area of Filchner Trough beginning in the early 2030s (thick dark blue line in Fig. 8a). In 2000, the model produces on average approx. 2.4 m/yr of sea ice at the Filchner Trough. Towards the end of the century, this reduces to 1.6 m/yr. Changes in the mean temperature in Filchner Trough in the lowest-emission scenario SSP1-2.6 are comparably small. Compared to 2000, mean temperature in SSP1-2.6 increases by 0.15 °C until 2050 similar to the higher-emission scenarios, but in contrast to those, the temperature rises only by 0.5 °C compared to 2000 until 2100. Sea ice formation in the Filchner Trough area does not decrease at all in SSP1-2.6 (thin dark blue line in Fig. 8a).

*Changes upstream of Filchner Trough*. While the temperature in Filchner Trough begins to rise in the 2030s and is scenario-sensitive with regard to magnitude and timing of the warming, the temperature of the slope current upstream of the Filchner Trough transporting mWDW towards the southern continental shelf increases over the whole simulation, independent of the climate scenario (orange lines in Fig. 8a). In all four scenarios, the average temperature at the bottom of the slope current at about 70°S increases from −0.45 °C in 2000 to −0.1 °C in 2100 (0.03°C per decade), which is a smaller trend than the CDW warming of approx. 0.05 °C per decade that was observed in the Weddell Sea from 1980 to 2010[20]. However, the shoaling of the thermocline is scenario-dependent with 10 m per decade in SSP3-7.0 and 7 m per decade in SSP1-2.6 (black lines in Fig. 8c).

The shoaling of the thermocline is consistent with observations, but the rate is lower than the 30 m per decade suggested from observations in the Weddell Sea[20]. The change in depth of the thermocline relates directly to the reduced down-welling at the continental slope (more negative average surface stress curl, gray line in Fig. 8c), caused by weakening Easterlies and a southward displacement of the transition zone between Westerlies and Easterlies above the Weddell Sea during January to March (Supplementary Fig. 6a). The wind field above the Weddell Sea gains strength during July to August (Supplementary Fig. 6b), while during January to March, the 15-year average wind speed above the continental shelf east of 15°W is reduced by 0.5 m/s between 2000–2014 and 2086–2100.

The decreasing sea ice formation over the Filchner Sill and growing differences between the climate projections become visible in the sea ice extent during the second half of the 21st century (Figs. 8 and 9). Until 2050, the spread between the different scenarios (Fig. 9a, b) is not larger than the spread between the different ensemble members for the SSP3-7.0 scenario (Fig. 9c, d).

In SSP5-8.5, summer sea ice shrinks until only a small area in the southwestern Weddell Sea remains ice-covered. Average summer sea ice thickness reduces in the Weddell Sea by up to 1.3 m. In contrast to the other scenarios, SSP1-2.6 shows no further area loss in summer sea ice after 2050 (Fig. 9a). While the sea ice extent in the southeastern Weddell Sea reaches 73°S for 2000 to

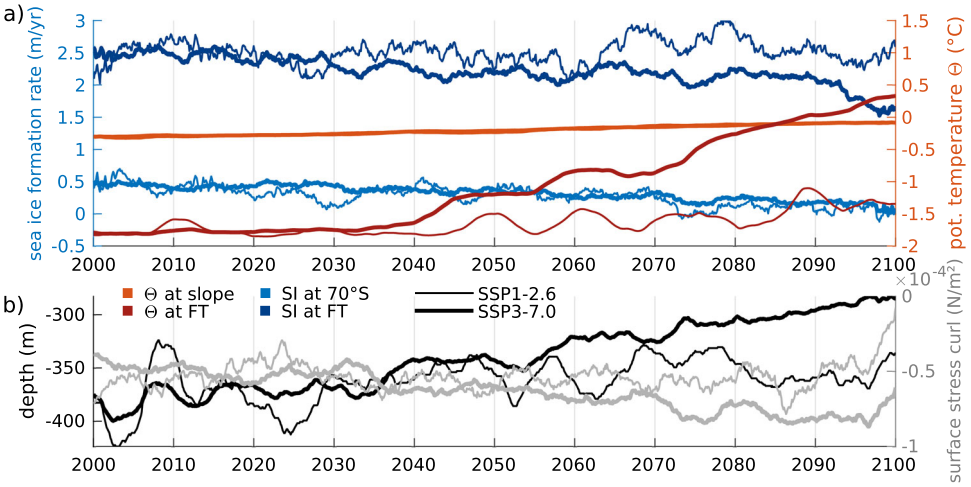


**Fig. 8 Evolution of temperature, sea ice formation, thermocline depth, and surface-stress curl in the Filchner Trough and upstream. a** 10-year running mean of yearly mean temperature and sea ice formation rate at the slope at S70 (Fig. 2) and in the Filchner Trough for SSP1-2.6 and the ensemble mean of SSP3-7.0. Mean temperature (hues of red) was calculated for Filchner Trough and the bottom layer at the slope at S70. Mean sea ice formation rate (hues of blue) was calculated for Filchner Trough and at S70. **b** Depth of the thermocline at the shelf break (black) and area average of surface stress curl (gray) at S70 in SSP1-2.6 and the ensemble mean of SSP3-7.0.

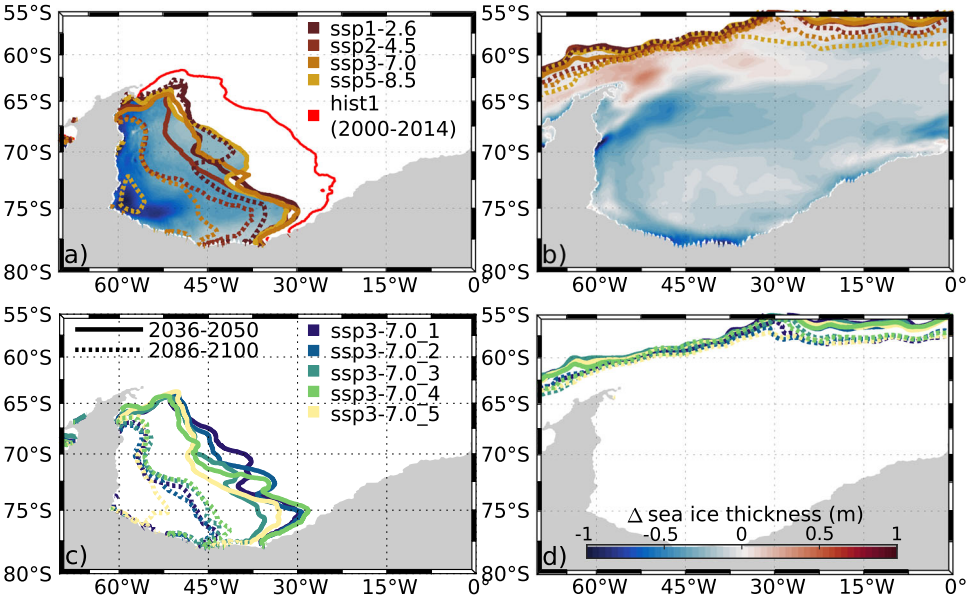


**Fig. 9 Sea ice extent (threshold: 15 % sea ice concentration per area) and thickness difference in the historical simulations and for the four different climate scenarios in two 15-year averages. a** March and **b** September sea ice extent in the Weddell Sea, with results from the historical simulations and SSP3-7.0 being averaged over all five ensemble members (line plots). Shading in the background of **a** and **b** shows sea ice thickness difference between the 15-year averages of hist1 (2000-2014) and SSP5-8.5 (2086-2100). **c** and **d** same as **a** and **b**, but all ensemble members of SSP3-7.0 shown individually.

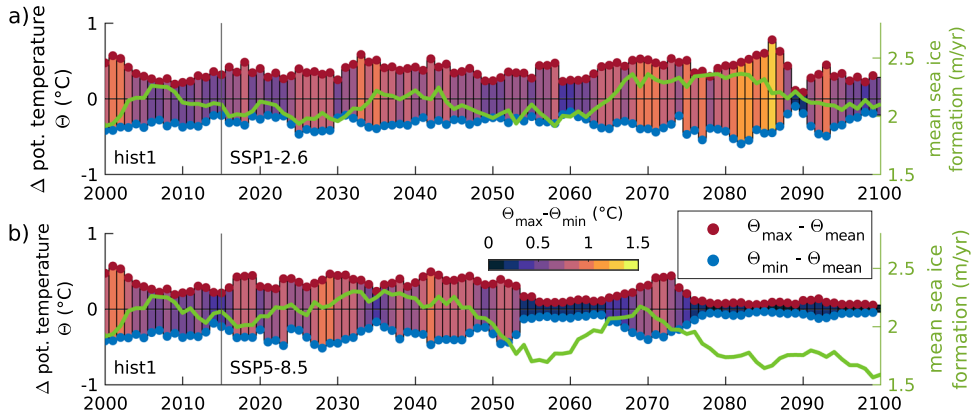


**Fig. 10 Development of the seasonality of the spatial maximum temperature below 200 m depth along section A. a** for SSP1-2.6 and **b** for SSP5-8.5. Red (blue) dots depict the difference between the temporal and spatial maximum (minimum) of the area to the temporal mean of the spatial maximum along the transect in the Filchner Trough (Fig. 8). The bars illustrate the seasonal variation. The green line represents the sea ice formation in the Filchner Trough.

2014, ice coverage reduces with increasingly warmer climate until the sea-ice cover in the southern Weddell Sea is confined in summer to south of 74°S by 2050 (Fig. 9). Summer sea ice extent reduces in SSP5-8.5 by ≈76% in the Weddell Sea from $3.69 \times 10^6$ km$^2$ to $0.88 \times 10^6$ km$^2$. The sea ice opens first along the eastern coast of the Weddell Sea, clearing the Filchner Trough of summer sea ice. By the end of the projected time period, the Filchner Trough is only partly ice-covered (SSP1-2.6, SSP2-4.5) or completely ice-free in summer (SSP3-7.0, SSP5-8.5). The winter sea ice extent by contrast shows far less variability. The largest changes in September sea ice occur in SSP5-8.5 towards the end of the century. But even though the sea ice extends as far north during the period of 2086 to 2100 as it did in the beginning of the simulation, sea ice freezing rates during winter are much lower, causing a decrease in sea ice thickness by up to 1 m in September compared to the historical period and reducing the amount of sea ice melting in summer.

*Changes of seasonality*. Over the course of Phase II after 2050, the seasonal variation in Filchner Trough temperature decreases more or less strongly, depending on the climate scenario (Fig. 10). The weaker seasonal signal is particularly pronounced in SSP3-7.0 and SSP5-8.5 (Fig. 10), but it can also be found during a brief period in 2089 and 2090 in SSP1-2.6 (Fig. 10a). The connection of the seasonality and the local sea ice formation becomes only clear when the sea ice formation is particularly low. In SSP5-8.5, this is the case 2050 onward Fig. 10b). Before that, a decrease in sea ice formation rate does not coincide with lower seasonality. The permanent loss of the seasonal signal marks the transition from Phase II to Phase III as defined above.

## Discussion and Conclusions

The present study shows that over the course of this century strong changes in the hydrography of the Filchner Trough are imminent. Already in the present climate, warm water pulses reach the Filchner ice shelf front both in the model simulations presented here and according to observations[19,22,41]. The comparability between the historical simulations and observations gives confidence into our model projections for the future climate evolution.

It should be noted that in the current simulations ice shelf cavities are not considered. Previous specialized ocean model simulations with ice shelf cavities (e.g.[8,12]) showed the same three modes as our CMIP6 simulations: seasonal warm water only in Phase I, intermittent warm water pulses in Phase II (and in present-day climate), and persistent warm water in Phase III, occurring in future climate scenarios with strong emission of greenhouse gases. This implies that cavity circulation is not a critical component in triggering the simulated changes in the Filchner Trough hydrography. Instead, reduced sea ice formation and changing wind fields play a major role. This concurs with the results from Naughten et al.[12], who showed that the intrusion of mWDW into the ice shelf cavity can only happen after the density on the continental shelf has reduced to a critical value, therefore sea ice formation on the shelf has a larger direct impact on the mWDW flux than any processes below the ice shelves.

The amount of heat that reaches the Filchner Trough depends on two factors: The amount of southward transport of (m)WDW onto the continental shelf and the grade of modification of the WDW by vertical mixing through DSW formation (Supplementary Fig. 7). Of these two, the first factor depends on the density gradient between the continental shelf waters and the slope current, and on the depth of the ASF at the continental slope. The grade of modification depends on the depth and intensity of convection and thus primarily on the rate of sea ice formation. However, DSW formation also influences the density gradient at the shelf edge and thus the on-shelf transport. A clear separation between the two processes is therefore not possible, but we conclude that sea ice formation plays a dominant role in governing the mWDW transport into the trough.

As a caveat, we note that in reality density of the water masses on the continental shelf is clearly influenced by the ISW outflow from under the ice shelf, which may have an impact on the timing of the regime shift we find in the high-emission scenarios. Given that ice shelf melting is a source of freshwater, it could be argued that adding ice shelves to our simulation would reduce the density of water masses on the continental shelf, potentially accelerating the regime shift towards a warm continental shelf. But then, given the very low temperatures of ISW, the mixing product of ISW and (m)WDW is a very dense water mass known to contribute to WSBW formation. A denser watermass on the shelf would potentially delay the regime shift. Which of these effects dominates is not obvious to us, but we note that they counteract each other, which mitigates a potential bias caused by the missing ice shelves in our simulations. A similar case can be made for the fact that we neglect the freshwater input from the ice shelves in the eastern Weddell Sea, upstream of Filchner Trough. In the presence of these ice shelf cavities, we would expect a stronger stratification over the shelf break, strengthening the Antarctic Slope Front (ASF) and reducing the mWDW flux onto the shelf. However, increased freshening of the shelf water masses might also a) cause baroclinic instabilities and thus an uplift of the

thermocline[44,45] and b) reduce the density gradient between the continental shelf and the Filchner-Ronne ice shelf cavity. Whether the ice shelves in the eastern Weddell Sea rather facilitate or inhibit the flow of warm water into the Filchner Trough is therefore not clear and needs to be addressed in a follow-up study.

While sea ice is the main driver behind the variations of mWDW transport onto the shelf and into the Filchner Trough, the model underestimates summer sea ice extent in the Antarctic, but slightly overestimates the winter sea ice extent[25]. The smaller sea ice area in summer might increase heat uptake during the warmest part of the year, creating a feedback loop of warmer sea surface temperatures decreasing and delaying sea ice formation. This would decrease the modification of WDW so that water closer in temperature to WDW reaches the trough and might cause an overestimation of simulated warming in Filchner Trough in SSP3-7.0 and SSP5-8.5. On the other hand, a reduced summer sea ice extent leads to additional sea ice formation in fall and thus additional salt input (similarly to the processes in coastal polynyas), potentially compensating or even overcompensating for the effect of too strong heat uptake in summer.

Despite the caveats outlined above, and given that the sign of the bias each of them could create is not obvious in all cases, we are confident that our main findings are robust. We find a decrease of ASF depth over the course of the high-emission scenario simulations that might facilitate the warm water influx to the Filchner Trough, notably in combination with pronounced density changes on the shelf. The receding sea ice and reduced freezing rates on the continental shelf in a warming climate cause the DSW in the Filchner Trough to freshen, reducing the intensity of vertical mixing between DSW and the underlying mWDW. A decline in density on the shelf weakens the density gradient at the continental shelf break and allows mWDW to flow into the trough[11,46]. This effect is especially large in the high-emission scenarios. Because the sea ice formation mostly depends on atmospheric processes, the differences in forcing in the SSP scenarios heavily impact changes in sea ice formation rates in the Weddell Sea.

The uplift of the ASF above the continental shelf in turn is caused by changing wind fields, reducing downwelling at the continental slope by lessening the coastward Ekman transport by easterly winds from January to March. Stronger westerly winds above the central Weddell Sea and a southward shift of the transition zone between Westerlies and Easterlies further decrease areas of downwelling along the coast. The wind above the continental shelf east and north of the Filchner Trough has a much higher westward component during the summer months of the high-emission scenarios SSP3-7.0 and SSP5-8.5 in 2086-2100 compared to 2000-2014. Even though the lower sea ice concentration in the high emission scenarios should increase the wind stress on the ocean, the effect is balanced by weaker wind during summer, a northwest-going wind field during the following months promoting upwelling along the coast, and reduced erosion of mWDW on the continental shelf by sea ice formation during the following autumn and winter.

There is a clear seasonality in the mWDW influx both in our model simulations and according to Darelius et al.[19] as well as Ryan et al.[18,22]. While Ryan et al.[22] attribute the seasonal inflow of mWDW to an inflow of freshened shelf waters from the coast of Dronning Maud Land, causing baroclinic instabilities and lifting the thermocline, we mainly attribute this seasonal inflow to the autumn maximum in local sea-ice production. According to Morrison et al.[43], sea ice formation causes increased DSW production and northbound transport in the Filchner Trough and establishes a pressure gradient across the trough that fosters the near-surface inflow of mWDW.

The sea ice decrease towards the end of the century in the high-emission scenarios, especially in thickness, is caused by the increased heat flux from the atmosphere. Higher $CO_2$-concentration in the atmosphere escalates the greenhouse gas effect and changes the heat flux in the western Weddell Sea from net heat loss to heat gain (Supplementary Fig. 8), warming the ocean and reducing sea ice formation. The southward displacement of the wind belt, stronger variability of the wind fields and strengthening of the wind field increase the off-shore sea ice transport and cause stronger sea ice deformation, which could potentially increase sea ice formation rates. However, weakening easterlies above the continental shelf in the eastern Weddell Sea during summer and a stronger heat flux towards the ocean counteract this effect, increase sea surface temperature and lead to thinning of the sea ice in the Weddell Sea. The driving factor behind the reduced sea ice formation is therefore not the wind but the increased heat flux at the surface during the climate scenarios.

Towards the end of the century, the general decrease in sea ice formation in the simulations leads to a decrease in the strength of the seasonal signal of the mWDW. The reduction of the density of the DSW outflow along the western slope of the Filchner Trough causes a weakening of the across-trough pressure gradient during winter. The reduced sea ice production weakens the convection in winter, when in the present state the flow of mWDW is eroded by deep vertical mixing triggered by sea ice formation. Together with the uplift of the thermocline above the continental shelf break (Fig. 8b), the weaker winds during the following summer months prolong the time where mWDW intrusions are possible, leading to a year-round presence of mWDW on the shelf. A regime shift occurs when DSW production in the Filchner Trough and surrounding continental shelf is not sufficient anymore to erode the inflow of mWDW into the trough during winter and spring. This point is reached between 2070 and 2080 in the high-emission scenarios SSP3-7.0 and SSP5-8.5, confirming the timing suggested by previous numerical model simulations with different, prescribed atmospheric forcing[8,10,11,23,46].

An important finding in our model results is that sea ice formation and extent, temperature in Filchner Trough and depth of the ASF all really start to differentiate between the different SSP scenarios in the 2040s. The slope current temperature even does not vary between the scenarios at all until 2100. This indicates that any endeavors to change the course of the current and future climate development will only start to show results in 20 to 30 years or later. If we as humanity do not change our habit of emitting greenhouse gases soon, the pulses of warm water reaching the continental shelf could be replaced by a permanent warm water flow (according to the strong emission scenarios SSP3-7.0 and SSP5-8.5). The presence of this warm water is bound to increase ice shelf basal melt, leading to a thinning of the ice shelf, a reduced buttressing to the ice flow, and additional sea-level rise. If a marine ice sheet instability is triggered, this process is self-sustained and can accelerate even if the original perturbation (here: the warm water inflow) is removed. If we do make the effort to restrict greenhouse gas emissions substantially, we could preserve the state of intermittent pulses of warm water reaching the continental shelf and possibly restrict ice shelf melting. According to our findings, a regime shift towards a warm cavity under Filchner Ronne Ice Shelf with strongly increased basal melt rates and an increased contribution to global sea-level rise can only be sustainably avoided by reaching the 2 °C (SSP1-2.6) climate goal. With the SSP2-4.5 scenario, restricting the global warming to 3 °C, no regime shift to a permanent warm inflow occurs in our simulation until 2100, but the water in Filchner Trough still warms by 1 °C in this scenario. Whether this

may still trigger a marine ice sheet instability or leads to the crossing of any tipping point with a large impact on global sea-level rise is a topic of ongoing research.

## Methods

**Model**. The simulations were performed with the AWI Climate Model (AWI-CM). It is a coupled model consisting of the Finite Element Sea ice-Ocean Model (FESOM v.1.4) and the atmospheric model ECHAM6, developed by the Max Planck Institute for Meteorology in Hamburg. The components are coupled via the OASIS3-MCT coupler. The ocean-sea ice model FESOM uses unstructured meshes which allow for a variable grid resolution in highly dynamic regions. More information on FESOM is provided by Wang et al.[47]. ECHAM6 is a spectral atmospheric model[48], which was used without any additional modifications or tuning. For more information on the performance of AWI-CM see ref. [25,49,50].

The ocean grid 'MR' used in the simulations has a medium resolution with a resolution distribution following the strategy proposed by Sein et al.[51,52]. The resolution is locally increased in areas of high sea surface height variability derived from satellite data and ranges between 8 km and 80 km[53–55]. The horizontal resolution in the Weddell Sea varies between 12 km and 40 km. While eddy transport is not resolved, the eddy parameterization has been proven to work well with the mesh resolution used here, producing isopycnals very similar to atlas data[56]. The grid has 46 unevenly spaced layers with a minimum layer thickness of 10 m near the surface and a maximum spacing of 250 m at the bottom. The mesh does not include ice shelf cavities. Tides are not explicitly calculated, but the effect of barotropic tides is included in the calculation of the Richardson number as proposed by[47,57].

The atmosphere component uses the resolution of T127L95. T127 stands for the spectral truncation of wave number 127, which corresponds to approximately 100 km horizontal resolution in the tropics and higher resolution towards the poles. The atmosphere has 95 unevenly spaced layers with lower spacing of the levels near the surface and wider spacing towards the top of the atmosphere.

AWI-CM participated in the sixth round of the Coupled Model Intercomparison Project (CMIP6). The simulations include a historical forcing simulation and four subsequent climate simulations with forcing derived from Shared Socioeconomic Pathways (SSP)[24,27]. For the historical scenario, five ensemble members were simulated. Preceding the start of the historical simulations a spin-up period was computed. This includes 10 years ocean-only simulation, 500 years of pre-industrial control spin-up with constant pre-industrial forcing and 500 years of piControl from which the historical simulations were branched off in the years 150 (*hist1*), 175 (*hist2*), 200 (*hist3*), 225 (*hist4*) and 250 (*hist5*). The future climate simulations were performed for the scenarios SSP1-2.6, SSP2-4.5, SSP3-7.0 and SSP5-8.5. Only SSP3-7.0 has 5 ensemble members[25]. The scenarios SSP1-2.6, SSP2-4.5, SSP5-8.5 and the first member of SSP3-7.0 started from 2014 of *hist1*. The other ensemble members 2 to 5 of SSP3-7.0 were branched off the corresponding historical ensemble members.

**Validation**. To validate the model results we use a data set that has been compiled from in-situ observations by Mathias v. Caspel (pers. comm. 2022). The data set includes salinity and potential temperature from the years 1995[33], 2013[34,38], 2016[35,36] and 2018[37] at depths between 100 m and 1200 m in different areas of the southern Weddell Sea. We choose six key areas as shown in Supplementary Fig. 9 for validation: central Filchner Trough (FT), Filchner Sill (FS), the Filchner Trough at the Filchner ice shelf edge (FIS), the continental shelf east of the Filchner Trough (ECS), the continental shelf west of the Filchner Trough (WCS), and at 74°S off-shore of the continental shelf (OS). The locations were chosen to be representative for specific water masses.

We interpolated the model results vertically for temperature and salinity onto the greatest depth at each observation location, and interpolated between the three nearest horizontal grid points. The resulting temperature and salinity values were then compared to the observational data. From these differences we calculated the average difference and standard deviation in each key area, displayed in the flags of Fig. 5a and Supplementary Fig. 4a.

**Calculation of diagnostic properties**. The ASF is defined as the boundary between the continental shelf water masses and the denser and warmer (m)WDW of the slope current. To identify this boundary, we use the thermocline and pycnocline between the two water masses. The model data was selected for the area around 70°S as depicted in Fig. 8b. For each mesh layer, the data was then averaged in twelve equidistant bins approximately parallel to the coastline. The temperature and density gradients were calculated between the mesh layers, and the depth with the highest gradient between bins selected as the depth of the ASF. The temperature at the slope was calculated by averaging the temperature of the bottom bins. As this includes the surface layer and the bottom temperature at greater depth, the result underestimates the real slope current temperature.

To calculate a measure for the seasonal variability of the mWDW influx into the Filchner Trough, we choose section A approximately perpendicular to the main axis of the Filchner Trough, ranging from 75.95°S 37.31°W to 76.54°S 30.66°W (Fig. 2). Along this profile, the spatial maximum of the monthly mean temperature was selected. The seasonal variability was then computed as the difference between the temporal maximum and temporal minimum of the spatial maximum temperature per year.

## Data availability

All data are available on the Earth System Grid Federation (ESGF): http://esgf-data.dkrz.de/search/cmip6-dkrz/?mip_era=CMIP6&activity_id=CMIP&institution_id=AWI&source_id=AWI-CM-1-1-MR[58]. A processed minimum data set can be accessed under https://doi.org/10.5281/zenodo.10552405.

## Code availability

The code for AWI-CM can be accessed from the esm-tool at https://github.com/esm-tools/esm_tools after registration with the MPI-ESM user forum (last access 16.09.2022). The Matlab codes used for the analysis of the model output will be made available upon request to the corresponding author.

Received: 8 September 2022; Accepted: 24 January 2024;
Published online: 27 February 2024

## References

1. Fretwell, P. et al. Bedmap2: improved ice bed, surface and thickness datasets for antarctica. *Cryosphere* **7**, 375–393 (2013).
2. The IMBIE team. Mass balance of the antarctic ice sheet from 1992 to 2017. *Nature* **558**, 219–222 (2018).
3. DeConto, R. & Pollard, D. Contribution of antarctica to past and future sea-level rise. *Nature* **531**, 591–597 (2016).
4. Shepherd, A. et al. A reconciled estimate of ice-sheet mass balance. *Science* **338**, 1183–1189 (2012).
5. Mouginot, J., Rginot, E. & Scheuchl, B. Sustained increase in ice discharge form the amundsen sea embayment, west antarctica, from 1973 to 2013. *Geophys. Res. Lett.* **41**, 1576–1584 (2014).

6. Arneborg, L., Wåhlin, A. K., Björk, G., Liljebladh, B. & Orsi, A. H. Persistent inflow of warm wate ronto the central amundsen shelf. *Nat. Geosci.* **5**, 876–880 (2012).
7. Jacobs, S. et al. The amundsen sea and the antarctic ice sheet. *Oceanography* **25**, 154–163 (2012).
8. Hellmer, H. H., Kauker, F., Timmermann, R., Determann, J. & Rae, J. Twenty-first-century warming of a large antarctic ice-shelf cavity by a redirected coastal current. *Nature* **485**, 225–228 (2012).
9. Foldvik, A., Gammelsrø d, T. & Torresen, T. Circulation and water masses on the southern weddell sea shelf. *Oceanol. Antarctic Continent. Shelf* **43**, 5–20 (1985).
10. Timmermann, R. & Goeller, S. Response to filchner-ronne ice shelf cavity warming in a coupled ocean-ice sheet model - part 1: The ocean perspective. *Ocean Sci.* **13**, 765–776 (2017).
11. Timmermann, R. & Hellmer, H. H. Southern ocean warming and icreased ice shelf basal melting in the twenty-first and twenty-second centuries based on coupled ice-ocean finite-element modelling. *Ocean Dynam.* **63**, 1011–1026 (2013).
12. Naughten, K. A. et al. Two-timescale response of a large antarctic ice shelf to climate change. *Nat. Commun.* **12**, 1–10 (2021).
13. Årthun, M., Nicholls, K.-W., Makinson, K., Fedak, M.-A. & Boehme, L. Seasonal inflow of warm water onto the southern weddell sea continental shelf, antarctica. *Geophys. Res. Lett.* **39**, 2–7 (2012).
14. Nicholls, K., Østerhus, S., Makinson, K., Gammelsrød, T. & Fahrbach, E. Ice-ocean processes over the continental shelf of the southern weddell sea, antarctica: A review. *Rev. Geophys.* **47**, 1–23 (2009).
15. Nicholls, K. W., Boehme, L., Biuw, M. & Fedak, M. A. Wintertime ocean conditions over the southern weddell sea continental shelf, antarctica. *Geophys. Res. Lett.* **35**, L21605 (2008).
16. Foldvik, A. et al. Ice shelf water overflow and bottom water formation in the southern weddell sea. *J. Geophys. Res.* **109**, C02015 (2004).
17. Naveira Garabato, A. C., McDonagh, E. L., Stevens, D. P., Heywood, K. J. & Sanders, R. J. On the export of antarctic bottom water from the weddell sea. *Deep-Sea Res. Part II: Topical Studies Oceanography* **49**, 4715–4742 (2002).
18. Ryan, S., Hattermann, T., Darelius, E. & Schröder, M. Seasonal cycle of hydrography on the eastern shelf of the filchner trough, weddell sea, antarctica. *J. Geophys. Res.: Oceans* **122**, 6437–6453 (2017).
19. Darelius, E., Fer, I. & Nicholls, K.-W. Observed vulnerability of filchner-ronne ice shelf to wind-driven inflow of warm deep water. *Nat. Commun.* **7**, 1–7 (2016).
20. Schmidtko, S., Heywood, K. J., Thompson, A. F. & Aoki, S. Multidecadal warming of antarctic waters. *Science* **346**, 1227–1232 (2014).
21. Turner, J. et al. Recent decrease of summer sea ice in the weddell sea, antarctica. *Geophys. Res. Lett.* **47**, e2020GL087127 (2020).
22. Ryan, S. et al. Exceptionally warm and prolonged flow of warm deep water toward the filchner-ronne ice shelf in 2017. *Geophys. Res. Lett.* **47**, 1–10 (2020).
23. Hellmer, H. H., Kauker, F., Timmermann, R. & Hattermann, T. The fate of the southern weddell sea continental shelf in a warming climate. *J. Clim.* **30**, 4337–4350 (2017).
24. Eyring, V. et al. Overview of the coupled model intercomparison project phase 6 (cmip6) experimental design and organization. *Geosci. Model Dev.* **9**, 1937–1958 (2016).
25. Semmler, T. et al. Simulations for cmip6 with the awi climate model awi-cm-1-1. *J. Adv. Model. Earth Syst.* **12**, 1–34 (2020).
26. O'Neill, B. C. et al. The scenario model intercomparison project (scenariomip) for cmip6. *Geosci Model Dev.* **9**, 3461–3482 (2016).
27. Meinshausen, M. et al. The shared socio-economic pathway (ssp) greenhouse gas concentrations and their extensions to 2500. *Geosci. Model Dev.* **13**, 3571–3605 (2020).
28. Beckmann, A., Hellmer, H. H. & Timmermann, R. A numerical model of the weddell sea: Large-scale circulation and water mass distribution. *J. Geophys. Res.* **10**, 375–391 (1999).
29. Klatt, O., Fahrbach, E., Hoppema, M. & Rohardt, G. The transport of the weddell gyre across the prime meridian. *Deep-Sea Res. Part II* **52**, 513–528 (2005).
30. Reeve, K. A., Boebel, O., Strass, V., Kanzow, T. & Gerdes, R. Horizontal circulation and volume transports in the weddell gyre derived from arge float data. *Progress Oceanograp.* **175**, 263–283 (2019).
31. Renault, A., Provost, C., Sennéchael, N., Barré, N. & Kartavtseff, A. Two full-depth velocity sections in the drake passage in 2006 - transport estimates. *Deep-Sea Res. Part II* **58**, 2572–2591 (2011).
32. Koenig, Z., Provost, C., Ferrari, R., Sennéchael, N. & Rio, M.-H. Volume transport of the antarctic circumpolar current: Production and validation of a 20 year long time series obtained from in situ and satellite observations. *J. Geophys. Res.: Oceans* **119**, 5407–5433 (2014).
33. Schröder, M. Physical oceanography during polarstern cruise ant-xii/3 https://doi.org/10.1594/PANGAEA.742581 (2010).
34. Schröder, M. & Wisotzki, A. Physical oceanography during polarstern cruise ps82 (ant-xxix/9) https://doi.org/10.1594/PANGAEA.833299 (2014).
35. Schröder, M., Ryan, S. & Wisotzki, A. Physical oceanography during polarstern cruise ps96 (ant-xxxi/2 frosn) https://doi.org/10.1594/PANGAEA.859040 (2016).
36. Schröoder, M., Ryan, S. & Wisotzki, A. Physical oceanography and current meter data from mooring awi254-2 https://doi.org/10.1594/PANGAEA.903317 (2019).
37. Janout, M. A., Hellmer, H. H., Schröoder, M. & Wisotzki, A. Physical oceanography during polarstern cruise ps111 (ant-xxxiii/2) https://doi.org/10.1594/PANGAEA.897280 (2019).
38. Darelius, E. & Fer, I. Physical oceanography from ctd in the filchner depression (weddell sea, antarctica) during ernest shackleton cruise es060 https://doi.org/10.1594/PANGAEA.846962 (2015).
39. Foldvik, A. & Gammelsrød, T. Notes on southern ocean hydrography, sea-ice and bottom water formation. *Palaeograp. Palaeoclimatol. Palaeoecol.* **67**, 3–17 (1988).
40. Nicholls, K. W., Østerhus, S., Makinson, K. & Johnson, M. R. Oceanographic conditions south of berkner island, beneath filchner-ronne ice shelf, antarctica. *J. Geophys Res.* **106**, 11481–11492 (2001).
41. Janout, M. et al. Fris revisited in 2018: On the circulation and water masses at the filchner and ronne ice shelves in the southern weddell sea. *J. Geophys. Res.: Oceans* **126**, e2021JC017269 (2021).
42. Darelius, E. et al. On the seasonal signal of the filchner overflow, weddell sea, antarctica. *J. Phys Oceanograp.* **44**, 1230–1243 (2014).
43. Morrison, A. K., Hogg, A. M., England, M. H. & Spence, P. Warm circumpolar deep water transport toward antarctica driven by local dense water export in canyons. *Sci. Adv.* **6**, eaav2516 (2020).
44. Hatterman, T. Antarctic thermocline dynamics along a narrow shelf with easterly winds. *J. Phys Oceanograp.* **48**, 2419–2443 (2018).
45. Nøst, O. et al. Eddy overturning of the antarctic slope front controls glacial melting in the eastern weddell sea. *J. Geophys. Res.* **116**, 1–17 (2011).
46. Daae, K. et al. Necessary conditions for warm inflow toward the filchner ice shelf, weddell sea. *Geophys. Res. Lett.* **47**, e2020GL089237 (2020).
47. Wang, Q. et al. The finite element sea ice-ocean model (fesom) v.1.4: Formulation of an ocean general circulation model. *Geosci. Model Dev.* **7**, 663–693 (2014).
48. Stevens, B. et al. Atmospheric component of the mpi-m earth system model: Echam6. *J. Adv. Model. Earth Syst.* **5**, 146–172 (2013).
49. Sidorenko, D. et al. Towards multi-resolution global climate modeling with echam6-fesom. part i: model formulation and mean climate. *Clim. Dynam.* **44**, 757–780 (2015).
50. Rackow, T. et al. Towards multi-resolution global climate modeling with echam6-fesom. part ii: climate variability. *Clim. Dynam.* **50**, 2369–2394 (2018).
51. Sein, D. V. et al. Designing variable ocean model resolution based on the observed ocean variability. *J. Adv. Model Earth Syst.* **8**, 904–916 (2016).
52. Sein, D. V. et al. Ocean modeling on a mesh with resolution following the local rossby radius. *J. Adv. Model. Earth Syst.* **9**, 2601–2614 (2017).
53. Rackow, T. et al. Sensitivity of deep ocean biases to horizontal resolution in prototype cmip6 simulations with awi-cm1.0. *Geosci Model Dev. Discuss.* **3**, 1–25 (2018).
54. Sein, D. V. et al. The relative influence of atmospheric and oceanic model resolution on the circulation of the north atlantic ocean in a coupled climate model. *J. Adv. Model. Earth Syst.* **10**, 2026–2041 (2018).
55. de la Vara, A. et al. On the impact of atmospheric vs oceanic resolutions on the representation of the sea surface temperature in the south eastern tropical atlantic. *Clim. Dyna.* **54**, 4733–4757 (2020).
56. Rackow, T. et al. Sensitivity of deep ocean biases to horizontal resolution in prototype cmip6 simulations with awi-cm1.0. *Geosci. Model Dev.* **12**, 2635–2656 (2019).
57. Lee, H. C., Rosati, A. & Spelman, M. J. Barotropic tidal mixing effects in a coupled climate model: oceanic conditions in the northern atlantic. *Ocean Model.* **11**, 464–477 (2006).
58. Semmler, T. et al. Awi awi-cm 1.1 mr model output prepared for cmip6 cmip. earth system grid federation https://doi.org/10.22033/esgf/cmip6.359 (2018).


## Acknowledgements

This work was funded by Deutsche Forschungsgemeinschaft SPP 1158 under grants SE2901/2, HE2740/33 and TI296/9. AWI-CM computing time was provided by DKRZ. The research was also supported by the European Union's Horizon 2020 research and innovation program under grant agreement no. 820575 (TiPACCs). We thank M. van Caspel for providing the data for the hydrographic validation. Thanks also go to Günther Heinemann, Rolf Zentek, Cara Nissen, Thomas Jung, Hartmut Hellmer and Svein Østerhus for the scientific discourse. We acknowledge support by the Open Access Publication Funds of Alfred-Wegener-Institut Helmholtz-Zentrum für Polar- und Meeresforschung.

## Author contributions

TS ran the AWI-CM simulations. VT conducted the analyses and prepared the figures. VT, TS and RT contributed to the interpretation of the results and writing of the manuscript.

## Funding

Open Access funding enabled and organized by Projekt DEAL.

## Competing interests

The authors declare no competing interests.

## Additional information

**Supplementary information** The online version contains supplementary material available at https://doi.org/10.1038/s43247-024-01238-5.

**Correspondence** and requests for materials should be addressed to Vanessa Teske.

**Peer review information** : *Communications Earth & Environment* thanks the anonymous reviewers for their contribution to the peer review of this work. Primary Handling Editor: Aliénor Lavergne. A peer review file is available.

## D.2 Teske et al. (2024a)

Teske, V., Timmermann, R., Nissen, C., Zentek, R., Semmler, T., and Heinemann, G., EGUsphere [preprint],(2024). https://doi.org/10.5194/egusphere-2024-2873.

https://doi.org/10.5194/egusphere-2024-2873
Preprint. Discussion started: 26 September 2024


# Regime shift caused by accelerated density reorganization on the Weddell Sea continental shelf with high-resolution atmospheric forcing

Vanessa Teske[1], Ralph Timmermann[1], Cara Nissen[2], Rolf Zentek[4], Tido Semmler[1,3], and Günther Heinemann[4]

[1]Alfred Wegener Institute for Polar and Marine Research, D-27570 Bremerhaven, Germany
[2]Department of Atmospheric and Oceanic Sciences and Institute of Arctic and Alpine Research, University of Colorado, Boulder, Boulder, Colorado, USA
[3]Met Éireann, 65-67 Glasnevin Hill, D09 Y921 Dublin, Ireland
[4]Department of Environmental Meteorology, University of Trier, D-54286 Trier, Germany

**Correspondence:** Vanessa Teske (vanessa.kolatschek@awi.de)

**Abstract.**

The strong Antarctic Slope Front in the southern Weddell Sea limits the present-day transport of modified Warm Deep Water onto the continental shelf and is associated with a characteristic V-shape in the density structure all along the continental slope. The mechanisms controlling today's V-shape are well studied, but its future development is not yet well constrained. In this study, we run ocean model simulations for a 21st-century Shared Socio-economic Pathways (SSP) 3-7.0 emission scenario forced with atmospheric model output from simulations with a global climate model and from a higher-resolved regional atmospheric model, respectively. We find that the resolution of the atmospheric model component influences the simulated future transport of modified Warm Deep Water onto the continental shelf through differences in the evolution of the depth and symmetry of the V-shape over the 21st century. In both simulations, reduced sea-ice formation and weakened Ekman downwelling reduce the depth of the V-shape and increase the sensitivity of its position above the slope to seasonal variations in sea-ice production and in the wind field. Using data from an atmosphere model with higher resolution leads to an acceleration of the density redistribution on the continental shelf, provoking a regime shift from cold to warm Filchner Trough through a cross-slope current before the end of the 21st century. As cross-slope currents disturb the continuity of the V-shape, we define a grade of connectivity to quantify the lateral integrity of the V-shape along the continental slope. We find that the integrity of the V-shape reduces with a delay of 3 months after a strong cross-slope current of modified Warm Deep Water enters Filchner Trough. Our results also indicate that the SSP3-7.0 climate scenario may have a higher potential for a regime shift than other ocean simulations for the same scenario but with lower atmospheric resolution suggest. Atmospheric downscaling increases the potential for a regime shift, dominated by warmer summer air temperatures. The Antarctic Slope Front is temporarily disturbed by cross-slope currents but the primary reason for the regime shift is the cross-slope density gradient.

https://doi.org/10.5194/egusphere-2024-2873
Preprint. Discussion started: 26 September 2024


## 1 Introduction

The Filchner Trough on the continental shelf in the southern Weddell Sea, Antarctica (Fig. 1), is one of the key regions of Dense Shelf Water (DSW) export and therefore plays an important role in the global ocean circulation (Heywood et al., 2014). However, the Filchner Trough is also a region where a southward current of modified Warm Deep Water (mWDW), the local cooler derivative of Circumpolar Deep Water, may reach the Filchner ice shelf cavity and significantly increase melt rates (Darelius et al., 2016; Ryan et al., 2020). Future climate projections for different warming scenarios have shown that a regime shift from a cold DSW-dominated to a warm mWDW-dominated Filchner Trough is possible during the 21st century (Timmermann and Hellmer, 2013; Daae et al., 2020; Haid et al., 2023; Nissen et al., 2023; Teske et al., 2024). Numerous studies have demonstrated that the density ratio between the continental shelf and the open ocean is critical in controlling the on-shelf transport of relatively warm off-shore water (Daae et al., 2020; Haid et al., 2023; Nissen et al., 2023). While a higher density of shelf waters prevents a warm inflow onto the shelf, projections have shown the potential for a reversal of the density ratio (Haid et al., 2023; Nissen et al., 2023), allowing for mWDW transport onto the continental shelf.

North of Filchner Trough above or near the continental shelf break sits the Antarctic Slope Front (ASF), the frontal zone between coastal and open-ocean waters which is associated with strong subsurface temperature and salinity gradients. Around Antarctica, the structure of the ASF varies depending on hydrographic properties over the continental shelf and shelf break, and can be classified into three groups: fresh shelf, warm shelf, and dense shelf (Thompson et al., 2018). With its DSW production and export, the continental shelf of the southern Weddell Sea is an example for a dense shelf. For dense shelves, density surfaces tilt down southward towards the continental slope, but shoal again above the DSW layer. This creates a characteristic V-shape running perpendicular to the continental slope (see also Fig. 2a) which has been described in many studies (e.g., Gill, 1973; Ou, 2007; Baines, 2009; Thompson et al., 2018).

Variability in the V-shape has been linked to variability in both DSW export and on-shelf transport of mWDW. While the northern arm of the V-shape is formed by Ekman downwelling (Sverdrup, 1954), the southern arm of the V-shape is formed by entrainment of overlying surface water to the descending flow of DSW (Gill, 1973; Baines, 2009). The V-shape shows seasonal variability in depth that has been associated with variations in the along-shore wind strength (Graham et al., 2013). For example, a peak in wind strength in the southeastern Indian Ocean in April 2009 led to increased mixing, on-shore Ekman transport and convergent downwelling on the continental shelf near 113°E. Similar behaviour was observed in 2010 and 2011 (Peña-Molino et al., 2016). Kida (2011) showed in a numerical model experiment with an idealized set-up of the Filchner Trough and the southern Weddell Sea that enhanced winds lead to a deepening of the V-shape and a decrease of the ocean stratification near the continental shelf break. The larger amount of lighter surface water at greater depth increases the density gradient across the shelf break and enhances the overflow transport. In contrast, three-dimensional eddy-resolving simulations by Stewart & Thompson (Stewart and Thompson, 2015a, b) showed nearly no sensitivity of the DSW export to wind strength. Reanalysis of ship-based observations, argo floats and data from marine mammals showed a steepening of the angle of the northern arm of the V-shape in the southern Weddell Sea in winter and a flattening in summer (Pauthenet et al., 2021; Le Paih et al., 2020). The seasonal variability of the V-shape and the associated thermocline at the continental slope leads to seasonal

https://doi.org/10.5194/egusphere-2024-2873
Preprint. Discussion started: 26 September 2024


pulses of mWDW flowing into the Filchner Trough (Årthun et al., 2012; Hellmer et al., 2017). Several studies have shown that an intensification of these seasonal pulses is a precursor for an impending regime shift in the Filchner Trough (Hellmer et al., 2017; Naughten et al., 2021; Teske et al., 2024).

Despite its importance for the on-shelf supply of heat governing Antarctic ice shelf melting, only comparatively few studies with global ocean or climate models have focused on the Antarctic Slope Current or the ASF due to the high resolution requirements to adequately resolve coastal ocean dynamics (Mathiot et al., 2011; Stewart et al., 2019; Beadling et al., 2022; Huneke et al., 2022). While only Beadling et al. (2022) concentrated on possible responses of the ocean to changes in the wind field and meltwater input in a future climate, their model resolution of 100 km to 200 km is relatively coarse. Mathiot et al. (2011) showed that a downscaling of the atmospheric forcing to 40 km in a hindcast scenario increases katabatic winds and increases the strength of the seasonal cycle in the wind and temperature fields. While modeling studies on different aspects that affect the Antarctic Slope Current, like freshwater input or changes in the wind strength and direction are more abundant, they often use idealized set-ups, regional models, or are only coarsely resolved (Kida, 2011; Nøst et al., 2011; Dinniman et al., 2012; St-Laurent et al., 2013; Hattermann et al., 2014; Lockwood et al., 2021; Ong et al., 2023). Previous studies have described a possible regime shift in the Filchner Trough, but less attention has been paid to the consequences that a shift in the current regime might have for the density structure at the continental slope which is controlling the mWDW inflow into Filchner Trough (Hellmer et al., 2012; Timmermann and Hellmer, 2013; Naughten et al., 2021; Nissen et al., 2022, 2023, 2024). The sensitivity of the ocean processes in response to the atmospheric forcing was demonstrated by Hattermann et al. (2014), Haid et al. (2015) and Dinniman et al. (2015). This leads us to the hypothesis that resolved mesoscale atmospheric processes may intensify the seasonality of the V-shape, the on-shore mWDW transport and the export of DSW in the Weddell Sea. Additionally, a finer atmospheric resolution produces more detailed and more pronounced temperature and wind speed gradients mostly related to katabatic winds and foehn wind (Van Lipzig et al., 2004; Mathiot et al., 2011; Van Wessem et al., 2015; Elvidge et al., 2014; Cape et al., 2015).

The aim of this study is to explore the evolution of the V-shaped ASF in the southwestern Weddell Sea in a warming climate (for study area see Fig. 1). By using ocean model simulations forced with data from two atmosphere models with different grid resolutions, we assess the processes governing the structure of the ASF and the transport of mWDW onto the continental shelf. To reach that goal, we analyse (i) how the cross-slope structure of the V-shape at the Filchner Trough sill develops in a high-emission climate scenario for the 21st century in Chapters 3.2 and 3.3, (ii) the change in seasonal atmospheric variability and its influence on the symmetry and structure of the V-shape (Chapters 3.4 and 3.5), and (iii) the longitudinal integrity of the V-shape as an indicator for the stability of the ASF and a possible regime shift in the Filchner Trough in a warming climate (Chapter 3.6).

https://doi.org/10.5194/egusphere-2024-2873
Preprint. Discussion started: 26 September 2024


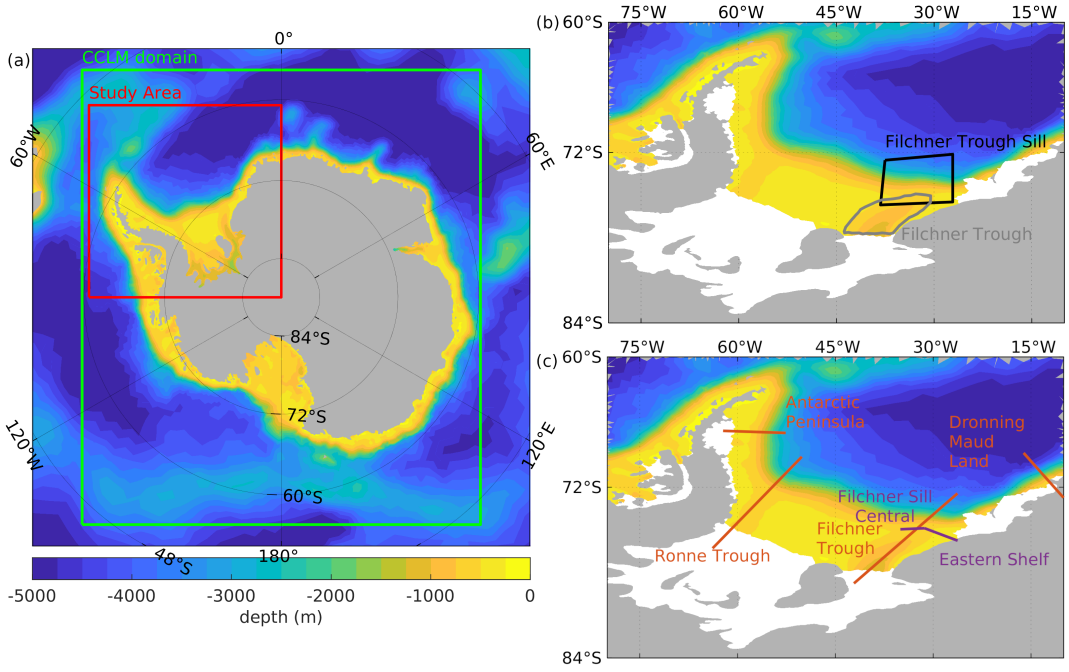


**Figure 1.** a) FESOM bottom topography in the Southern Ocean, study area in the Weddell Sea (red line) and perimeter of the COSMO-Climate Model (CCLM) domain (green line). b) Location of areas and c) sections used in the analysis of this study. Areas shaded in white represent ice shelves.

## 2 Methods

### 2.1 The ocean model FESOM

For this study, we performed ocean model simulations with the Finite Element Sea-ice Ocean Model FESOM-1.4 (Wang et al., 2014). FESOM is a global ocean general circulation model based on unstructured-mesh methods coupled with a dynamic-thermodynamic sea ice component, also including a representation of ice-shelf cavities (Timmermann et al., 2012; Wang et al., 2014; Danilov et al., 2015). The interaction between the ocean and ice shelves is governed by the three-equation system that describes the flux of heat and fresh water through an exchange-controlling boundary layer (Hellmer and Olbers, 1989; Holland and Jenkins, 1999). The variable horizontal resolution of the ocean mesh ranges from (minimum) 4 km around Antarctica and its adjacent ice shelf cavities, via 25 km at 75°S in the Weddell Sea, to 250 km at the equator. In the vertical, the mesh has 99 depth levels (z-levels) of varying thickness (Gurses et al., 2019; Nissen et al., 2023). Here, we perform two ocean model simulations forced with atmospheric data from either a global climate model ("REF" simulation throughout the paper) or a higher-resolved regional atmospheric model (referred to as the "FECO" simulation) which will be described in more detail in the following section.

https://doi.org/10.5194/egusphere-2024-2873
Preprint. Discussion started: 26 September 2024


### 2.2 The atmospheric forcing data

The FESOM reference simulation (REF) is forced with global atmospheric data created with the AWI Climate Model (AWI-CM), a coupled global climate model using FESOM1.4 as the ocean model and ECHAM6.3.04p1 as the atmospheric model component, as a contribution to phase 6 of the Coupled Model Intercomparison Project (CMIP6; Semmler et al., 2020). The atmospheric data resolution ranges from approx. 27 km to 52 km in zonal direction and corresponds to approx. 100 km in meridional direction. Our ocean model simulation is initialized in the year 2000 with FESOM output from Nissen et al. (2023) and is driven by 3-hourly atmospheric output of the historical AWI-CM simulation for the period 2000 to 2014 and of the future Shared Socio-economic Pathways (SSP) 3-7.0 emission scenario (Meinshausen et al., 2020) projection for 2015 to 2100, identical to Nissen et al. (2023).

The FESOM FECO simulation is forced with a regional atmospheric forcing data set which was created with the COnsortium for Small-scale MOdeling - CLimate Mode model (COSMO-CLM or CCLM; Steger and Bucchignani, 2020; Zentek and Heinemann, 2020), a regional non-hydrostatic atmospheric model with terrain-following vertical coordinates at a horizontal resolution of 15 km. The used CCLM is a polar-adapted version including improved parameterizations for sea ice and the stable boundary layer (see Heinemann et al., 2022, for more details). The model is used in a forecast mode with daily re-initialization and a spin-up of 12 hours. The CCLM domain reaches the northernmost corners at approx. 50°S (Fig. 1a). At its lateral boundaries, it is driven by the global AWI-CM data sets described above. Sea ice concentration and thickness are initially taken from FESOM data of the AWI-CM simulation, but are modified by the parameterizations of grid-scale and sub-grid-scale ice in leads and polynyas. For use as forcing for the global ocean model FESOM, the CCLM output is merged with the global AWI-CM atmospheric output. The merging follows the procedure from Haid et al. (2015) and uses a transition zone of 2° to linearly interpolate between the global AWI-CM data and the regional CCLM data. South of this 2° boundary only CCLM data is applied as forcing, while only AWI-CM data is used outside the CCLM domain. Inside the transition zone, the weighted average depending on the distance to the CCLM domain boundary is used. CCLM data are available for the three timeslices 2000-2014, 2036-2050, and 2086-2100. The following quantities are used from the downscaled CCLM simulations: 2m-temperature, 10m-wind, downward longwave and shortwave radiation at the ocean surface, mean sea level pressure, 2m specific humidity and total precipitation. We ran FESOM simulations forced with CCLM (henceforth called FECO) for each of the three time slices, each preceded by 10 years of spin-up, already driven by the CCLM data (2000-2009, 2036-2045, and 2086-2095, respectively). The spin-ups were branched off the REF simulation in 2000, 2036, and 2086, respectively.

### 2.3 Grade of Connectivity

We define the grade of connectivity (GOC) as a metric describing the coherency of the V-shape along the continental slope in a selected sector (here the Filchner Trough Sill, see Fig 1b). Motivated by the link between the V-shape and DSW export from the Weddell Sea continental shelf (Gill, 1973; Baines, 2009; Nissen et al., 2022) and on-shelf mWDW transport (Nøst et al., 2011; Stewart and Thompson, 2015a; Thompson et al., 2018), this metric quantifies the modification (or erosion) of the V-shape structure in response to cross-slope currents. The GOC is defined as the normalized zonal mean of the north-south

https://doi.org/10.5194/egusphere-2024-2873
Preprint. Discussion started: 26 September 2024


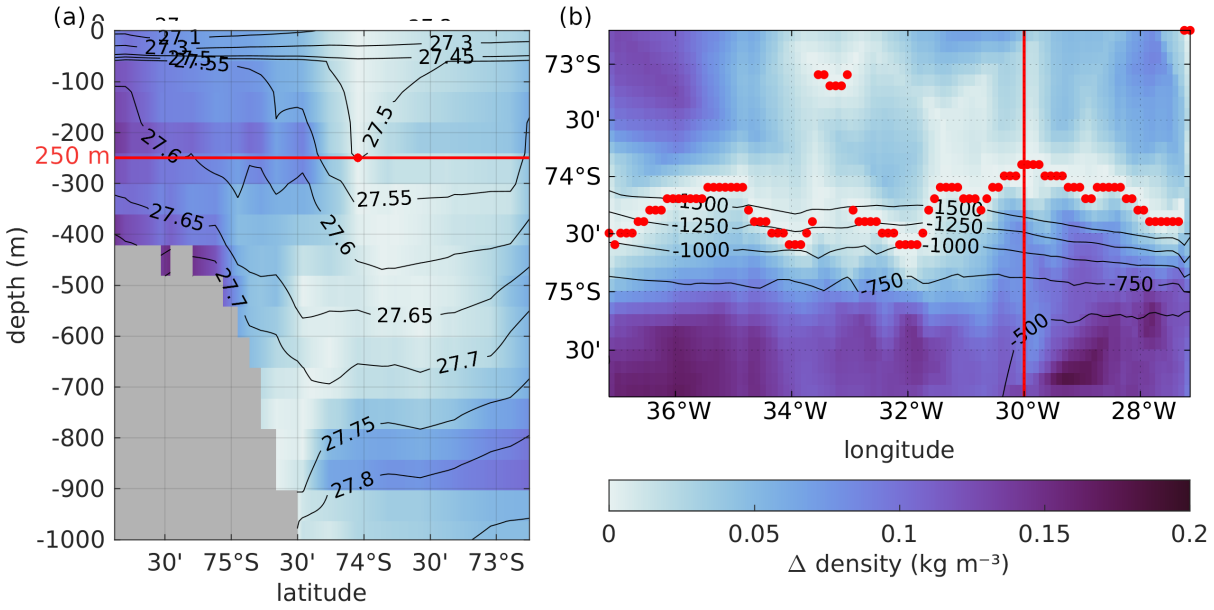


**Figure 2.** Section across Filchner Trough sill of the horizontal potential density distribution relative to the level-wise horizontal minimum density in December 2000 to illustrate the connection between the V-shaped density distribution and the grade of connectivity as defined in section 2.3. Isolines depict the potential density in kg m$^{-3}$ relative to 1000 kg m$^{-3}$. The red dot marks the location of the minimum density difference at 250 m depth, the horizontal line the position of the level presented in (b). (b) Horizontal projection of the density difference at 250 m depth with bottom isobaths. Red dots mark the location of the meridional minimum in longitudinal increments of 0.1°. The red line marks the location of the section shown in panel (a).

variations of the deepest point of the V-shape in a horizontal plane. To calculate the GOC, we first interpolate the model data from the unstructured grid to a regular grid with a resolution of 0.1° through linear interpolation between FESOM grid points. As a second step, to find the meridional position $y_n$ of the deepest point of the V-shape for each longitude coordinate, we find the horizontal density minimum at the chosen depth by searching for the maximum density difference at 250 m depth compared to the northern border of the selected area (here 72.69°S; Fig. 2). $\Delta y_n$ then denotes the absolute meridional distance from the neighboring $y_n$. The average GOC is then calculated from monthly mean model output as

$$GOC = \frac{1}{n} \sum_{n} \begin{cases} 1, & if\ \Delta y_n \leq d_L \\ \frac{d_L}{\Delta y_n}, & if\ \Delta y_n > d_L \end{cases} \tag{1}$$

where $n$ is the number of grid cells in zonal direction, and the distance threshold $d_L = 0.2°$ is the maximum distance that counts two neighbouring density minima as connected. In summary, the GOC is defined as the normalized zonal mean of the north-south variations of the deepest point of the V-shape in a horizontal plane. We normalize by $n$ so that it gives a number between 0 and 1, with lower values indicating a less coherent V-shape along the continental slope and a value of 1 indicating a

https://doi.org/10.5194/egusphere-2024-2873
Preprint. Discussion started: 26 September 2024


V-shape without disruptions in longitudinal direction. As such, the GOC allows for a quantitative description of the slope front stability and a quantitative assessment of how this relates to, e.g., on-shelf transport of mWDW.

## 3 Results

### 3.1 Present-day V-shape in the Weddell Sea (REF simulation)

The reference simulation REF shows a distinct wedge structure of the isopycnals above the continental slope for the period 2010-2014, but details vary substantially across different sectors of the Weddell Sea (Fig. 3). In the following, the potential density is always given relative to 1000 kg $m^{-3}$. At the coast of Dronning Maud Land (DML) in the eastern Weddell Sea, a fresh-shelf region, the narrow continental shelf prevents the accumulation of large amounts of DSW. Cold, fresh surface water is pushed towards the coast and subducted, pressing down on the isopycnals of greater density (Fig. 3a). The planes of equal density dip towards the continental shelf and the coast, forming only the northern arm of a V-shape. The section at Filchner Trough (Fig. 3b), a dense-shelf region, shows a strongly pronounced V-shape in which the 27.7 kg $m^{-3}$ isopycnal is found at approx. 500 m greater depth above the continental slope than on the continental shelf. The southern arm of the V-shape is pronounced in the Filchner Trough, as this is an area of DSW overflow (Fig. S1). Further to the west at the Ronne Trough (Fig. 3c), water of colder temperature reaches deeper than at the Filchner Trough. However, the V-shape is less pronounced in the upper open ocean, i.e., the region displays a less pronounced northern arm, due to the deepening of the slope current along its path following the continental slope. At the Antarctic Peninsula in the western Weddell Sea (Fig. 3d), a V-shape in the isolines is clearly visible only in the temperature field and for the 27.7 kg $m^{-3}$ isopycnal and higher-density but not for lower-density isopycnals. In addition, mWDW at temperatures around -1°C can be found on the continental Shelf and in the Larsen Ice Shelf cavity originating from Ronne Trough and following the coast northward (Fig. S1a). The Filchner Trough has previously been shown to be an entrance point for mWDW to reach the Filchner Ronne ice shelf (e.g. Foldvik et al., 1985; Ryan et al., 2017). Because of its particular relevance, we will focus on the Filchner Trough in our further analysis.

### 3.2 Present-day seasonality of the V-shape at Filchner Trough (REF simulation)

Previous studies have shown that seasonal variations in the density distribution at the continental shelf break control the on-shore flow of mWDW (e.g. Teske et al., 2024). During the historical 2010-2014 time period in REF, the depth and steepness of the V-shape shows seasonal variations (Fig. 4). More intense sea-ice formation on the continental shelf leads to thicker sea-ice above the continental shelf (Fig. S3) and stronger DSW export in winter and spring than in summer and autumn, which pushes down the isopycnals at the continental slope by approx. 50 m (Fig. 4 a, b). This is consistent with observed variations in the thermocline depth at the Filchner Trough sill (Hattermann, 2018), though with a smaller amplitude than in the observations. Sea-ice melting during summer reduces the steepness of the arm of the V-shape above the continental shelf (Fig. 4c). Subsequently, stronger densification over the continental shelf through sea-ice formation in autumn strengthens the southern arm again (Fig. 4d). Sea-ice formation in winter is particularly pronounced along the coasts of the Weddell Sea

https://doi.org/10.5194/egusphere-2024-2873
Preprint. Discussion started: 26 September 2024


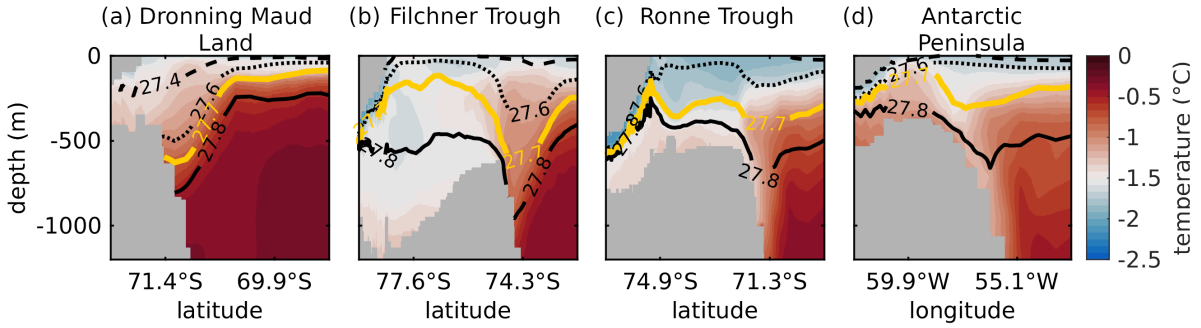


**Figure 3.** Potential temperature sections across the continental slope in the southern Weddell Sea with isopycnals shown relative to 1000 kg $m^{-3}$ for 27.4, 27.6 27.7 (orange) and 27.8 kg $m^{-3}$ for the average over 2010-2014 in REF. a) Dronning Maud Land, b) Filchner Trough, c) Ronne Trough, and d) Antarctic Peninsula. The continent and ice shelves (marked in grey) are on the left-hand side for all panels. See Figure 1 for the exact locations of the transects.

(Fig. S2e), while in summer most of the Weddell Sea is dominated by sea-ice melting (Fig. S2i). Only a small band along the Filchner-Ronne Ice Shelf edge produces sea ice year round, which - together with sea-ice deformation by tides and variable winds - leads to a band of exceptionally thick sea ice north of Ronne Ice Shelf in summer (Fig. S3i).

The rise of the thermocline in summer also enables seasonal pulses of mWDW to flow onto the continental shelf (see also Ryan et al., 2020; Teske et al., 2024). The horizontal temperature gradient in 300 m depth is strongest during winter - which is consistent with observations (Fig. S4; Pauthenet et al., 2021) - however the northern arm of the V-shape has its steepest angle during summer (blue line in Fig. S5). During summer, reduced DSW export (Fig. S6) and weakened Ekman downwelling (see also Fig. 7) reduce the depth of the V-shape compared to winter (Fig. 4c). The main mechanisms behind the seasonal variations are thus the seasonal production of DSW and seasonally varying Ekman downwelling. These mechanisms as found in the simulation agree with observations and previous modelling studies (Peña-Molino et al., 2016; Le Paih et al., 2020; Pauthenet et al., 2021; Ryan et al., 2020).

### 3.3 Effect of a warming climate on the seasonally varying V-shape geometry (REF simulation)

Over the 21st century, increased summer sea-ice melting and reduced freezing rates in winter above the continental shelf (Fig. S2) lead to freshening of the continental shelf and to a density redistribution in the Filchner Trough and across the continental slope. While the geometry of the V-shaped density distribution is mostly symmetrical in 2010-2014 (Fig. 4), it becomes lopsided towards the end of the century in the REF simulation (Fig. 5). A reduction of the density over large parts of the water column in Filchner Trough by up to 0.2 kg $m^{-3}$ between 2000 and 2100 reduces the vertical extent of the southern arm of the V-shape. In addition, a shoaling of the slope current over the course of the century reduces the depth of the V-shape so that the yearly mean depth of the 27.8 kg $m^{-3}$ isopycnal lifts from approx. 992 m to 791 m between 2010-2014 and 2096-2100 (dotted and dashed horizontal lines in Fig. 5, respectively). Of all seasons, the V-shape reaches its deepest position in summer by the end of the century (Fig. 5c), as opposed to in winter for the 2010-2014 period (Fig. 4).

https://doi.org/10.5194/egusphere-2024-2873
Preprint. Discussion started: 26 September 2024


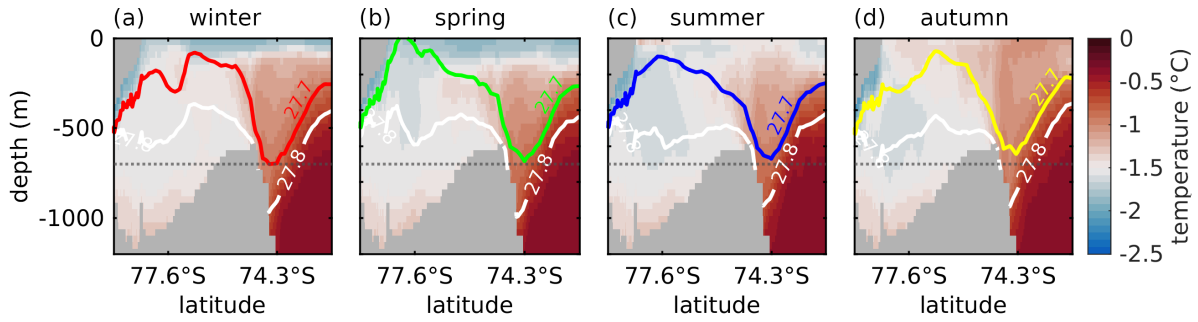


**Figure 4.** Potential temperature in the 2010-2014 mean of the Filchner Trough section in REF for winter (June-August), spring (September-November), summer (December-February), and autumn (March-May). The colored (white) lines show the position of the 27.7 kg m$^{-3}$ (27.8 kg m$^{-3}$) isopycnal in the respective season. Horizontal dotted line shows the maximum depth of the 27.7 kg m$^{-3}$ isopycnal in winter. The continent and ice shelves (marked in grey) are on the left-hand side for all panels. See Figure 1 for the exact locations of the transects.

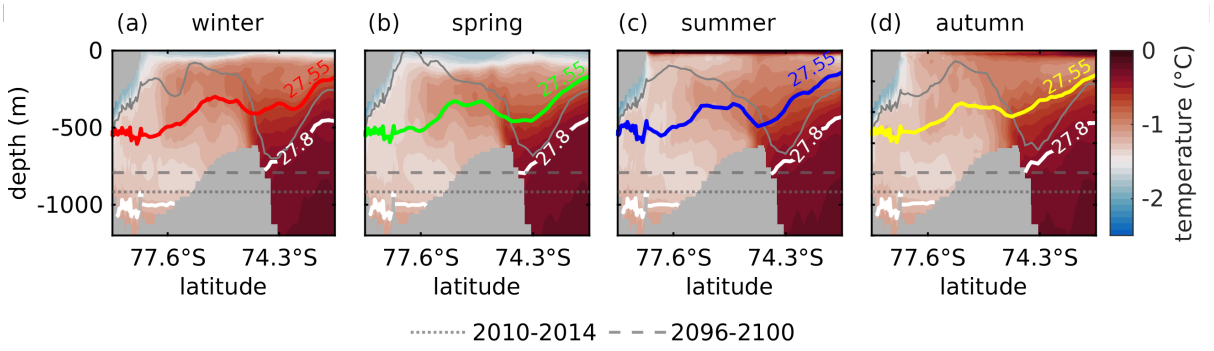


**Figure 5.** Potential temperature in the 2096-2100 mean of the Filchner Trough section in REF for a) winter (June-August), b) spring (September-November), c) summer (December-February), and d) autumn (March-May). The colored lines show the position of the 27.55 kg m$^{-3}$ isopycnal in the respective season, the white line the 27.8 kg m$^{-3}$ isopycnal. The gray line shows the position of the 27.7 kg m$^{-3}$ from Fig. 4. The dotted (dashed) horizontal gray line shows the mean depth of the 27.8 kg m$^{-3}$ isopycnal in the multi-year mean of 2010-2014 (2096-2100).

The change in sea-ice thickness and concentration (Fig. S7a & b) during the 21st century does not only lead to freshening of shelf waters, but also influences how the wind field impacts the ocean surface. To isolate the relative effects of wind speed changes and changes in sea-ice properties, we compute the wind stress curl from the 2m wind field assuming a constant drag coefficient over ocean ($C_{AO}$=1.00e-3) and sea ice ($C_{AI}$=1.32e-3), weighted by sea ice concentration per grid cell. We find that an intensification of the wind field towards the end of the century enhances existing wind stress curl patterns in winter (Fig. 6a-d), while qualitatively the patterns remain largely unchanged. In contrast, considering the ocean surface stress, i.e. taking the effect of the sea-ice cover into account, we find an alternating pattern of negative and positive surface stress curl, corresponding to alternating areas of up- and downwelling, respectively (Fig. 6e). With a reduction of winter sea-ice thickness by up to 80%

https://doi.org/10.5194/egusphere-2024-2873
Preprint. Discussion started: 26 September 2024


compared to at the beginning of the century, some of the up- and downwelling areas are redistributed. Regional variability is slightly reduced so that the surface stress curl resembles the wind stress curl more closely at the end of the century. Similar changes in the wind stress curl can be seen in spring and autumn (Fig. 6 b/d vs. f/h). In summer, when the sea-ice thickness (Fig. S2) and concentration (not shown) in the Filchner Trough is already low between 2010 and 2014, a southward shift of the wind field increases areas of downwelling above the continental slope. The impact of sea ice on the surface stress curl is especially visible in autumn where in the 5-year average for March to May, the Filchner Trough is covered approximately halfway by sea ice. South of approx. 76°S, sea ice creates alternating patterns of positive and negative surface stress curl, while north of this, surface stress curl closely resembles the wind stress curl (Fig. 6 d, h).

From the fact that in the comparison between 2096-2100 and 2010-2014 we find modified patterns of spatial variability in the ocean surface stress curl (lower panels in Fig. 6) much more pronounced than in the wind stress curl (upper panels in Fig. 6), we conclude that the long-term trend in up- and downwelling patterns is created by trends in the sea ice cover rather than in the wind field. The combination of reduced DSW export in winter and spring and the enhanced wind stress impact on the ocean is then responsible for the change in the seasonal variations of the V-shape.

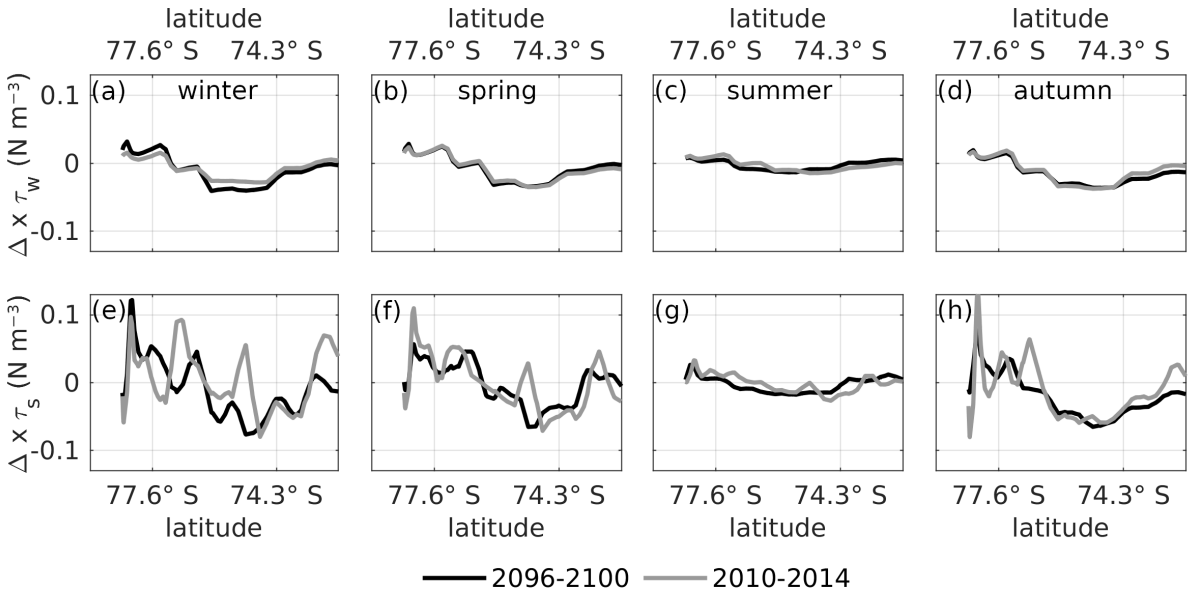


**Figure 6.** Wind stress curl (N m$^{-3}$), estimated from the 2m-wind field, in the 5-year means of 2096-2100 (black line) and 2010-2014 (gray line) in REF above the Filcher Trough section (see Fig. 1) for (a) winter (June-August), (b) spring (September-November), (c) summer (December-February), and (d) autumn (March-May). (e)-(h) Same as (a)-(d) but for surface stress curl on the liquid ocean from overlying atmosphere and sea ice. Positive curl corresponds to downwelling.

https://doi.org/10.5194/egusphere-2024-2873
Preprint. Discussion started: 26 September 2024


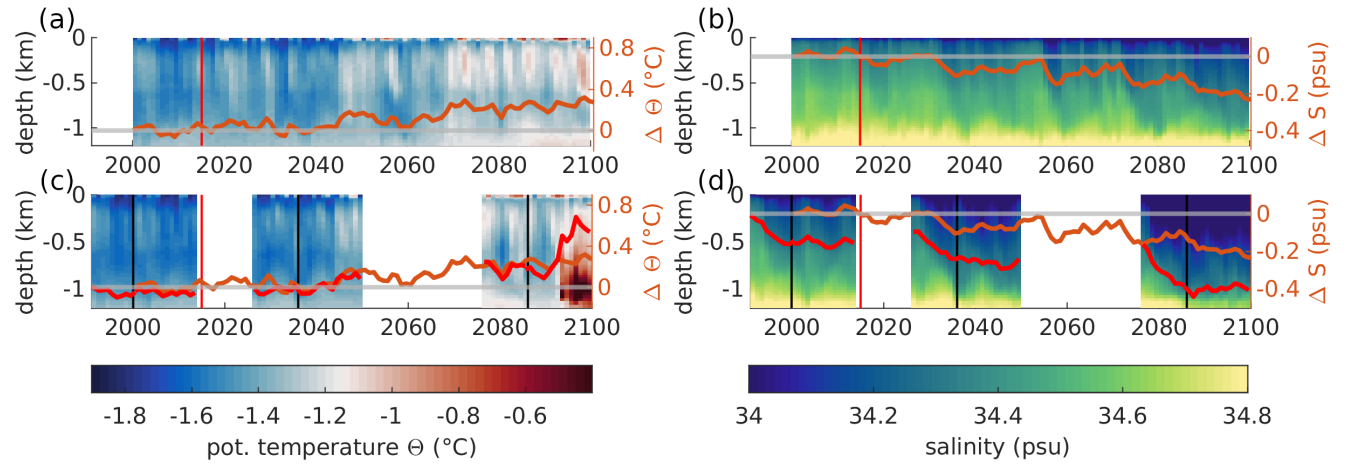


**Figure 7.** Hovmöller diagram of the yearly mean temperature in Filchner Trough (see Fig. 1) for (a) REF and (c) FECO. Colored lines show the relative temperature change of the horizontally and vertically averaged temperature of the whole water column compared to 2000. (b) & (d) Same as (a) & (c) but for salinity. Orange lines in (c) and (d) are the same as the orange lines in (a) and (b), respectively. Red line marks the relative change of the average temperature/salinity in FECO. Red vertical line: boundary between historical and future climate scenario. Black vertical lines: boundary between transition time and experiment in FECO.

### 3.4 Sensitivity of the Filchner Trough circulation to atmospheric forcing

The application of the regional higher-resolved CCLM forcing in FECO affects the transport of mWDW onto the continental shelf. Reduced freezing rates along the coasts in winter and higher melt rates in summer (Fig. S2) due to higher air temperatures (not shown) compared to REF lead to an additional decrease of the Filchner Trough mean salinity by up to 0.2 psu over the course of 10 years of transition time, converging to a new mean state for all three time slices (Fig. 7d). Additionally, lower wind speeds in most of the southern Weddell Sea reduce the wind stress on sea ice and ocean, except for some areas at the eastern Ronne Ice Shelf Front and the Filchner Ice Shelf, where stronger off-shore winds dominate. In contrast to the salinity, the mean potential temperature does not appear to be sensitive to the forcing change (Fig. 7c) in the transition time. In the FECO experiment, the circulation across the Filchner Trough sill and in the trough experiences a regime shift that REF does not. In 2093, mWDW enters the Filchner Trough as a near-bottom current across the sill, strongly increasing the temperature in the trough (Fig. 7c). This is not the first occasion for mWDW to influence the temperature of the Filchner Trough. Over the course of the 21st century, REF shows increasingly stronger seasonal pulses of mWDW crossing into the Filchner Trough across the shelf east of Filchner Trough and along the eastern slope of the trough (Fig. S8). Over the course of the reference simulation, we find an increase in the temperature of the mWDW pulses, originating in a warming of the slope current. The slope current shows a warming trend of approx. 0.053°C per decade between 2000 and 2100. This agrees well with the 0.05°C per decade that were observed between 1980 and 2010 (Schmidtko et al., 2014). Previous studies have suggested that warmer and longer-lasting pulses can be a precursor for a regime shift in the Filchner Trough from a DSW-dominated to a mWDW

https://doi.org/10.5194/egusphere-2024-2873
Preprint. Discussion started: 26 September 2024


dominated state (Timmermann and Hellmer, 2013; Timmermann and Goeller, 2017; Ryan et al., 2020; Nissen et al., 2023; Teske et al., 2024), but despite the increase in the mean temperature and the visible mWDW pulses, no sudden warming of the trough occurs in REF.

Before the regime shift in FECO, the reduced density of the upper 1000 m in the open ocean leads to changes in the position and symmetry of the V-shape above the continental slope (Fig. 8). The comparison of the seasonal positions of the deepest point of the 27.4 kg m$^{-3}$ isopycnal in FECO for 2088-2092 (Fig. 8b) - chosen for its position at depth above the continental slope at all times, but nearly no intersection with the surface in REF - yields an additional horizontal component to the seasonal depth variation seen in REF (Fig. 8a). This horizontal movement displaces the V-shape by approx. 50 km between summer, when the deepest point of the V-shape is at its southernmost point, and winter. The deepest point of the V-shape is closest to the sill in summer and furthest away in winter (Fig. 8b). In addition, the V-shape reaches its deepest position in spring and summer, while REF reaches the deepest point in winter and spring. The fresher water masses on the continental shelf in FECO cause the southern arm of the V-shape to be very flat and to vanish during autumn (Fig. 8b, yellow curve). Stronger Ekman downwelling in autumn, but a late onset of the freezing season lead to a situation that temporarily resembles fresh-shelf regions like the Dronning Maud Land section (Fig. 3d), though sea-ice formation in winter regularly restores the V-shape.

### 3.5 Accelerated density redistribution with high-resolution atmospheric forcing

The high-resolution atmospheric forcing does not only affect the slope front symmetry and seasonality, but also accelerates the reduction of density over the 21st century compared to REF (Fig. 9). The differences in the density evolution between REF and FECO are particularly large in Filchner Trough (Fig 9a). Here, the application of CCLM forcing leads to a negative density trend between 2000 and 2092 that is 1.47 times larger than in REF. Values after 2092 were excluded from the calculation due to the impact the regime shift has on the density of the Filchner Trough. In contrast, above the continental slope north of the Filchner Trough sill, the trend is slightly smaller in FECO than in REF (-1.5 kg m$^{-3}$ century$^{-1}$ as compared to -1.6 kg m$^{-3}$ century$^{-1}$; Fig. 9b). Separately assessing the trends in temperature and salinity reveals that the density trend on the continental shelf is driven by freshening, while the trend in the slope current is driven by a combination of warming and freshening (Fig. S9). From this we conclude that reduced sea-ice formation is not the only factor influencing the density distribution across the continental slope, but the dominating one for the existence of the V-shape.

### 3.6 Influence of cross-slope currents on the V-shaped density distribution

With the onset of the near-bottom current of mWDW entering the Filchner Trough in FECO in 2093, the V-shaped density distribution at the continental slope experiences pronounced structural changes that lead to the loss of the southern arm of the V-shape. Visible as a sudden increase in the average temperature in the Filchner Trough (Fig. 7c), the inflow of mWDW in FECO in 2093 brings the bottom density in the Filchner Trough closer to that of the slope current. This has the effect of increasing the stratification of the water column. In combination with low sea-ice formation rates and reduced mixing (not shown) during the freezing season, the seasonal variations in the southern arm of the V-shape vanish at depths below approx. 450 m (Fig. 8d), in contrast to REF, where the V-shape is formed also at greater depths (Fig. 8c). Seasonal variations of the depth of the V-shape

https://doi.org/10.5194/egusphere-2024-2873
Preprint. Discussion started: 26 September 2024


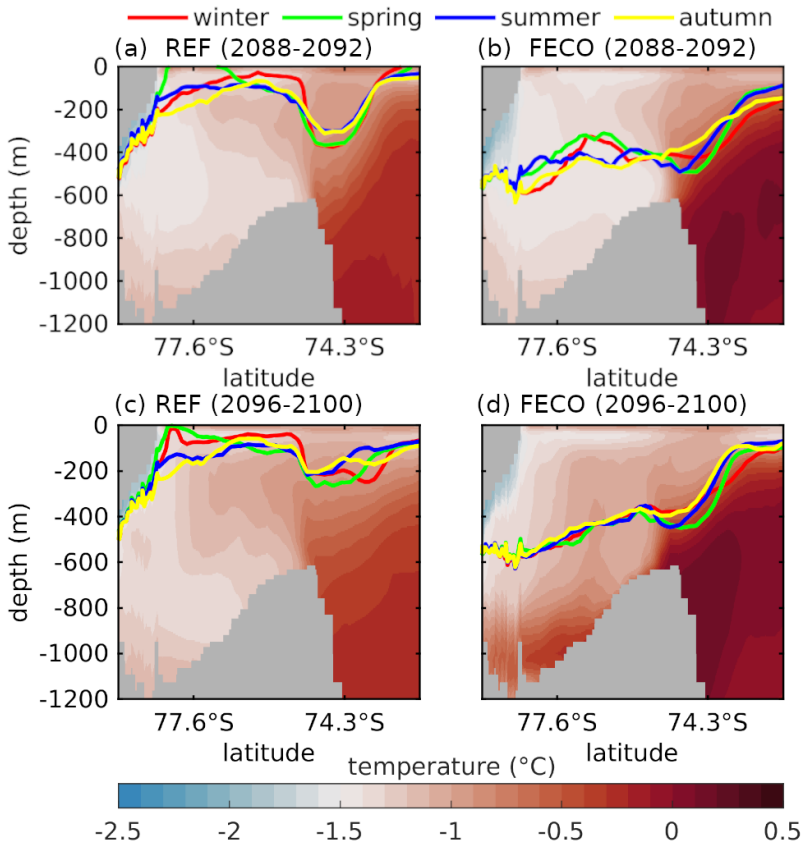


**Figure 8.** Potential temperature in the 2088-2092 mean (5 years before regime shift in FECO) in a) REF and b) FECO. Colored lines show the position of the 27.4 kg m$^{-3}$ isopycnal. c) and d) same as a) and b) but for 2096-2100.

and the position of the northern arm remain, however, the southern arm of the V-shape decreases strongly in vertical extent. From a height difference in spring of approx. 200 m between the deepest point of the V-shape and the shallowest point above the continental shelf, the 27.4 kg m$^{-3}$ isopycnal position reduces to a vertical range of approx. 80 m after the bottom current onset. With the near-bottom inflow of mWDW into the trough, the sensitivity of the southern arm of the V-shape to sea ice formation is reduced, while the northern arm, which is created by the wind, remains.

The timing of the intensified mWDW flux in FECO can be related directly to the density gradient across the Filchner Sill and the depth of the thermocline at the sill. In FECO, the thermocline remains above the Filchner Trough sill depth throughout the 15-year FECO simulation and stays between 400 m to 600 m depths, while the thermocline in REF rises from approx. 1000 m in 2000 to 600 m depth over the course of the 21st century (last 15 years shown in Fig. 10a). The sill depth of approx. 600 m (horizontal gray line in Fig. 10a) is only crossed occasionally and never for an extended period of time. Despite the thermocline in FECO already reaching above the sill from the beginning of the time slice 2086-2100, the warm near-bottom current is still only developing at a later date. This agrees with the conclusions presented by Haid et al. (2023) suggesting that another key

https://doi.org/10.5194/egusphere-2024-2873
Preprint. Discussion started: 26 September 2024


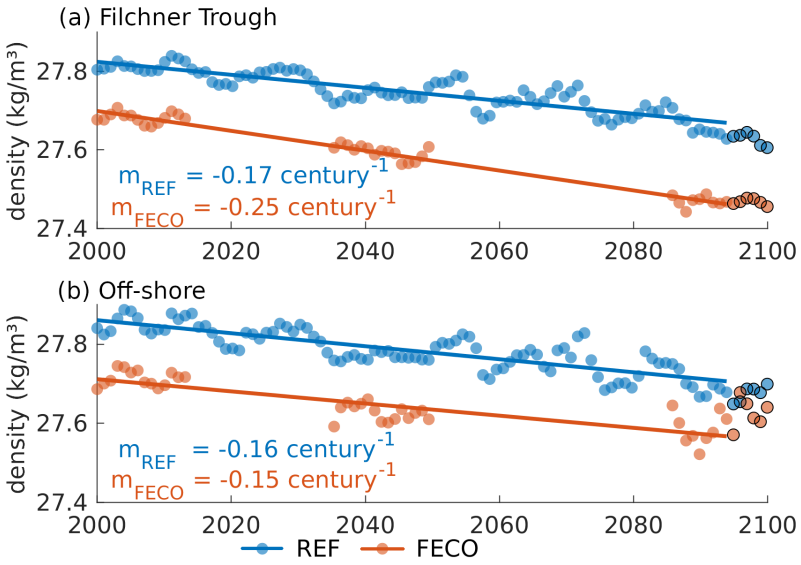


**Figure 9.** Linear regression of the annual mean potential density relative to 1000 kg $m^{-3}$ over time in a) the Filchner Trough and b) at the Filchner Trough Sill at 636 m depth for REF in blue and FECO in red. The slope of each linear fit is given in the figure. Data points outlined in black were excluded from the calculation due to the regime shift in 2093. The areas over which properties are averaged for the time series are indicated in Fig. 1.

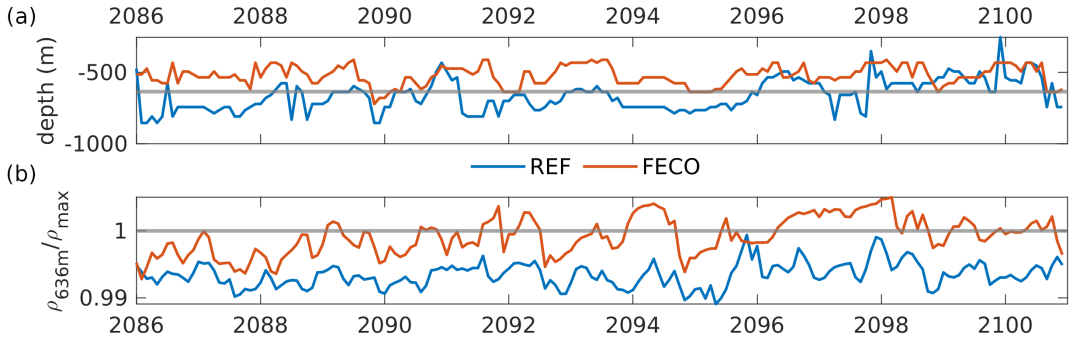


**Figure 10.** a) Depth of the thermocline at the Filchner Sill (horizontal line: sill depth at 636 m) and b) density ratio between the maximum density in Filchner Trough ($\rho_{max}$) and the mean density at the Filchner Trough sill (see Fig. 1) at 636 m depth ($\rho_{636m}$).

factor for or against an inflow of mWDW onto the continental shelf in addition to the depth of the mWDW at the slope is the density ratio between the dense water on the shelf and the slope current (see also Nissen et al., 2023).

The inflow of mWDW onto the continental shelf is not only visible in the cross-slope density structure, but also as a disruption of the V-shape in along-slope direction. In both simulations, the GOC at the Filchner Sill shows multiple minima between 2086 and 2100, demonstrating phases of instability of the Antarctic Slope Front where the barrier across the sill is weakened

https://doi.org/10.5194/egusphere-2024-2873
Preprint. Discussion started: 26 September 2024


(Fig. 11). However, not all of the recognised events of a minimum GOC are related to an increased flow of mWDW into the Filchner Trough. The comparison of the southward mWDW (Θ >-0.8°C) transport in the Filchner trough across the central Filchner Trough sill with the GOC in FECO shows a significant correlation with a lag of 3 months (p=0.0005, r=0.35) between the maximum mWDW transport and a minimum of the GOC after 2093 (Fig. 11). In REF, there is not only a lagged correlation between the inflow of mWDW with the GOC (p=7e-7, r=0.36) but also weakly between the outflowing DSW (Θ <-0.8°C) and the GOC (p=0.0001, r=0.29), while FECO does not show this correlation (p=0.27, r=0.08). The calculation of the GOC was performed for 250 m depth, where the V-shape is present at all times, even when it is less pronounced. The changing circulation patterns associated with the density reorganization on the shelf in FECO decouple the weak correlation between the water export and GOC that can be found in REF.

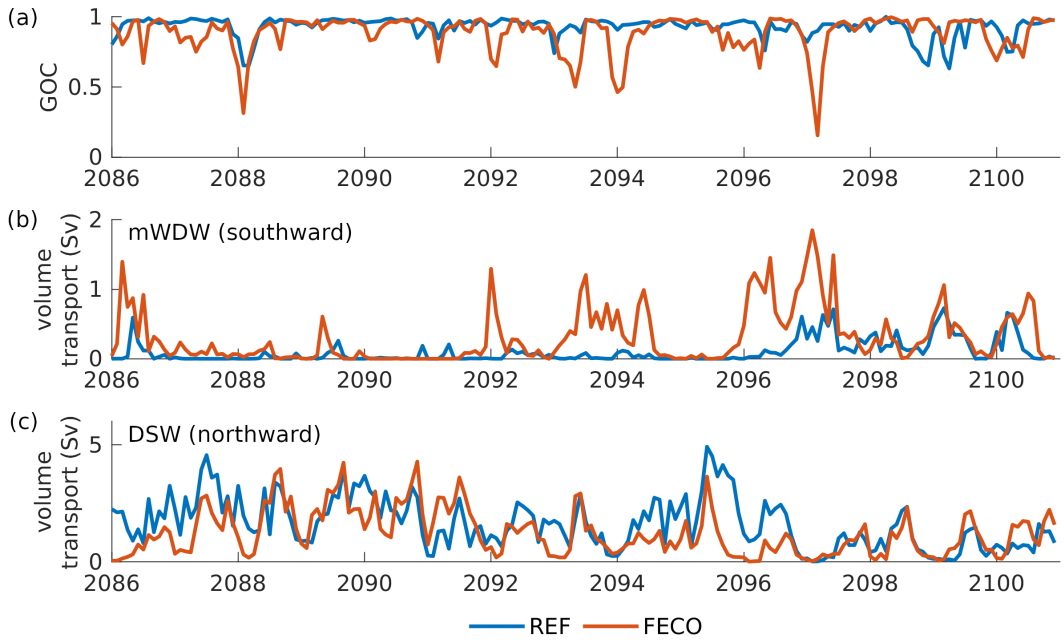


**Figure 11.** a) Time series of the grade of connectivity (GOC) of the V-shaped density structure above the continental slope at the Filchner Trough sill for REF (in blue) and FECO (in red; for area outline see Fig. 1; for calculation see section 2.3). b) Southward volume transport in Sv across Filchner Sill Central (see Fig. 1) of water masses mWDW with a potential temperature of Θ>-0.8°C and c) northward volume transport of DSW (Θ<-0.8°C).

https://doi.org/10.5194/egusphere-2024-2873
Preprint. Discussion started: 26 September 2024


# 4 Discussion

## 4.1 Drivers of the accelerated density redistribution: wind speed and sea ice

Our results show that for the high-emission scenario SSP3-7.0, lower sea-ice production in a simulation with high-resolution atmospheric forcing data accelerate the density redistribution on the continental shelf of the southern Weddell Sea relative to a simulation with lower-resolution atmospheric forcing. Subsequently, the accelerated density redistribution induces a regime shift in the Filchner Trough area before the end of the 21st century. The regime shift from a DSW-dominated to a mWDW-dominated state is accompanied by the near-loss of the southern arm of the V-shaped density distribution at the continental slope that prominently separates the shelf from the open ocean in today's climate.

The main factors controlling the circulation regime in Filchner Trough are the wind field and sea-ice production (Teske et al., 2024), which directly influence the density distribution on the shelf. The on-shore transport of mWDW, which intensifies in the case of a regime shift, strongly depends on the density ratio across the continental slope at the Filchner Trough sill. This ratio changes faster in FECO than in REF, driven by an accelerated freshening of the continental shelf in response to higher summer temperatures and weaker wind speeds in CCLM. Higher summer air temperatures in FECO compared to REF lead to a stronger decline and local melting of summer sea-ice. Since multi-year mean air temperatures are actually lower in FECO than in REF, this emphasizes the importance of the seasonal cycle.

Weaker wind speeds may have two effects: (i) smaller heat loss to the atmosphere, and (ii) less wind-driven sea-ice transport. Both effects tend to reduce sea-ice production and thus winter brine release in regions that are dominated by freezing and export of sea ice. In contrast, stronger off-shore winds at the Filchner Ice Shelf front in FECO increase the occurrence and width of coastal polynyas that locally cause higher sea-ice production rates. While this could counteract some of the freshening of the Filchner Trough, the net effect appears to be dominated by the weaker off-shore winds in the high-resolution atmosphere model.

In the historical time period between 2010 and 2014, REF produces a steeper, narrower temperature and density gradient across the ASF at 300 m depth during winter than during summer, which agrees with the assessment of the ASF by Pauthenet et al. (2021). According to their study, the ASF forming the northern arm of the V-shape has the smallest meridional extent during winter months, which translates to a strong temperature gradient. The steepening is a result of stronger DSW export in winter. The entrainment of colder, fresher surface water suppresses the isopycnal and forces the isopycnal and thermocline into a steeper position. However, observational data for winter in the ice-covered southern Weddell Sea are scarce, leading to high uncertainties in the assessment of the position and extent of the ASF in the southern Weddell Sea. Additionally, Pauthenet et al. (2021) applied their analysis at 300 m at relatively shallow depths for the Weddell Sea, where the pycnocline extends deeper than 380 m (Thompson et al., 2018). As Fig. 4 has shown, the isopycnals are steeper in greater depth. It is therefore unclear if the shift in the minimum extent of 1.53° of the distance between the -0.7°C and -0.3°C isotherms at 300 m depth in winter during 2010-2014 of REF to a minimum extent of 5.41° in summer in 2096-2100 (Fig. S4b) is an effect of climate change and the shift in the front dynamics.

https://doi.org/10.5194/egusphere-2024-2873
Preprint. Discussion started: 26 September 2024


The decreasing wind strength over the 21st century in REF reduces the Ekman transport and downwelling above the continental shelf. Multiple studies have shown that a strengthening and poleward shift of the westerlies and a weakening of the easterly winds above the continental shelf will weaken the Ekman downwelling along the coast of the Weddell Sea (Spence et al., 2017; Naughten et al., 2021; Teske et al., 2024). The indirect influence of the wind strength on the flow of Antarctic Surface Water and mWDW onto the continental shelf has also been shown in previous studies (Hattermann et al., 2014; Dinniman et al., 2015; Haid et al., 2015; Hatterman, 2018). In particular, Hattermann et al. (2014) described the weakening of shallow and the strengthening of deep inflow towards the Fimbul ice shelf cavity in response to weaker easterly winds based on observations and modelling results. The projected reduced wind speed of the easterlies in our model towards the end of the 21st century and the southward shift of the mid-latitude westerlies, consistent with Spence et al. (2014) and Goyal et al. (2021), broaden the V-shaped density structure at the continental slope and reduce its depth in REF, as seen in Fig. 3. The uplift of the thermocline due to weakened downwelling lifts mWDW closer to the sill depth and slowly increases the amount of mWDW flowing into the Filchner Trough. A similar signature is found when comparing results from FECO with those from REF: The generally weaker wind speeds in the southern Weddell Sea in FECO than in REF weaken the Ekman downwelling further, reducing the V-shape depth in comparison to REF. The reduced density gradient weakens the barrier effect of the cross-slope gradient further and allows the strong cross-slope current to develop towards the end of the century that does not develop in REF.

### 4.2 Drivers of the accelerated density redistribution: cross-slope density gradient

One of the main criteria for the potential of the current system in the Filchner Trough to switch from a DSW-dominated state to the mWDW-dominated state is the density gradient across the Filchner Trough sill as has been previously shown (Ryan et al., 2017; Haid et al., 2023; Nissen et al., 2023). A near-bottom current of mWDW onto the continental shelf only develops once this gradient flattens out or reverses. Our results show that this on-shelf current disrupts the V-structure at the slope, reducing the V-shape to the upper 450 m of the water column and warming the Filchner Trough. The horizontal distance of the ASF (northern arm of the V-shape) to the continental slope varies over the year as shown in an analysis of observational data by Pauthenet et al. (2021). The introduction of the GOC provides a metric for the stability of the ASF in areas of cross-slope transport in dense-shelf areas. However, not all features of the V-shape of the ASF are included. The GOC is useful to detect strong changes in the cross-slope density distribution that remove the dip in the isopycnals or lead to a very large meridional displacement within the V-shape. What the GOC is not able to do, is to differentiate between a lot of small displacements that just exceed the distance threshold $d_L$ and few very large meridional distances. Also, the selection of $d_L$ as a maximum displacement before it reduces the GOC influences the result. A distance larger than ten times the grid size reduces the number of recognised events by 12.5% compared to a $d_L$ of two times the grid size; with $d_L$ 100 times the grid size, the number of recognised events decreases by 29.1%. The three-month delay between intensified cross-slope currents and a minimum event of the GOC at 250 m depth indicates a connection based on seasonal cross-slope water transport. Ryan et al. (2017) showed that during winter intensified DSW production and export suppress the isopycnals at the continental slope, reducing or stopping on-shore transport of mWDW. This conclusion is back up by the lack of correlation in FECO where DSW production is reduced

https://doi.org/10.5194/egusphere-2024-2873
Preprint. Discussion started: 26 September 2024


compared to REF. The lack of non-delayed correlation between cross-slope currents and the GOC indicates that an intensified bottom current does not destabilize the ASF in shallower than sill depth. This also implies that a (hypothetical) decreasing trend in the GOC cannot be regarded as an indicator that a cold-to-warm regime shift in Filchner Trough is about to occur in the near future.

### 4.3 Comparison to other studies

Considering our results in the context of other scenario simulations for the 21st century, it becomes clear that the choice of atmospheric forcing data has a strong impact on the susceptibility of Filchner Trough to undergo a regime shift before 2100. Previous future projections produced a tipping of the Filchner Trough circulation in very high-emission scenarios (e.g., SSP5-8.5 or similar; Timmermann and Hellmer, 2013; Nissen et al., 2023) or idealized scenarios (e.g., 1pctCO2 scenario; Naughten et al., 2021). Ocean simulations with lower emission scenarios generally did not produce a regime shift (Timmermann and Hellmer, 2013; Nissen et al., 2023), except in case of a coupled atmospheric component (Teske et al., 2024, regime shift in SSP3-7.0 and SSP5-8.5 scenarios). While our reference simulation for the emission scenario SSP3-7.0 does not produce a regime shift during the 21st century, downscaling of the atmosphere in FECO induces a strong mWDW inflow before the end of the 21st century. We therefore conclude that the potential for a regime shift in a warming climate in the SSP3-7.0 scenario might be higher than suggested by previous studies using relatively low-resolution atmospheric forcing (Nissen et al., 2023). With the currently implemented policies, global warming is projected to be between 2.2°C and 3.5°C by 2100, which corresponds to the warming projected for the SSP2-4.5 (2.1°C-3.5°C) and SSP3-7.0 (2.8°C-4.6°C) scenarios (Calvin et al., 2023). Our results thus highlight the importance of developing a better understanding of the potential implications for vulnerable climate components like the Antarctic Slope Front and the Filchner Trough in the current climate development.

### 4.4 Limitations and caveats

Several studies have suggested that eddies play an important role in the transport of Circumpolar Deep Water across the continental shelf break (Nøst et al., 2011; Stewart and Thompson, 2015a). Our model is not eddy-resolving, but it has an eddy-permitting grid resolution on the Weddell Sea continental shelf (∼3-12 km). It has been proposed by Nøst et al. (2011) that freshening of the shelf can lead to increased eddy kinetic energy which drives onshore cross-ASF eddy transport. The resolution of approx. 12 km at the continental slope in our model grid might lead to an underrepresentation of eddies, the Rossby radius in the southern Weddell Sea being 2-5 km. With reduced eddy presence, the model might underestimate cross-slope volume transport. An underrepresentation of eddy-driven on-shore transport of mWDW would mean a greater depth of the V-shape as the lack of mesoscale eddies reduces the relaxation of the isopycnals above the continental slope (Dettling et al., 2024). As a result, the temperatures on the continental shelf would be underestimated. A shallower V-shape at the continental slope in a simulation with an adequate eddy representation might lead to an earlier regime shift of the Filchner Trough due to the lower density gradient into the shelf and the higher connectivity between the slope current and the Filchner Trough through the sloping isopycnals.

https://doi.org/10.5194/egusphere-2024-2873
Preprint. Discussion started: 26 September 2024


## 5 Conclusions

We have presented model results indicating the future evolution of the density distribution across the Filchner Trough sill, a key property of the Antarctic Slope Front in the Southern Weddell Sea. The reference simulation REF and the experiment simulation FECO with down-scaled atmospheric forcing both reproduce the typical V-shaped density distribution that is formed by interplay of Ekman downwelling and Dense Shelf Water export in the southern Weddell Sea. Sea ice loss in the warming climate of the SSP3-7.0 emission scenario decreases the density on the continental shelf and flattens the southern arm of the V-shape in REF and FECO. This causes an increased sensitivity of the density distribution on the continental shelf to seasonal wind speed variations. Using results from a regional, high-resolution atmosphere model as forcing, we find an acceleration of the density redistribution on the continental shelf, which leads to a regime shift with modified Warm Deep Water entering Filchner Trough before the end of the 21st century for the high emission scenario SSP3-7.0. Colder air temperatures in the multi-year mean are more than outweighed by the warmer summer air temperatures of the regionally down-scaled atmosphere, accelerating density loss on the continental shelf, which ultimately leads to a regime shift from a cold Dense Shelf Water dominated Filchner Trough to a warm, modified Warm Deep Water dominated trough in 2093. The criterion of spatial coherency of the V-shape along the continental slope, quantified by the grade of connectivity, is not usable as a tool to predict an imminent regime shift because the southward transport of modified Warm Deep Water is, contrary to our expectations, not a result of a weakening of the slope front, but instead leads to a temporary disturbance of the ASF and the associated V-shape. While the density minimum is completely restored after disruption in present-day climate, in a warming climate the distinct V-shape remains confined to the upper ocean. Due to the geostrophic nature of the Antarctic Slope Current, the flattening of the northern arm of the V-shape and stronger seasonality will affect the transport of the slope current and the transport of heat towards the peninsula and onto the continental shelf in the future.

The accelerated density redistribution by the high-resolution atmospheric data and the resulting regime shift show that the potential for a regime shift in the Filchner Trough in the SSP3-7.0 scenarios is higher than previously published ocean simulations of the same scenario suggest. With the current climate policies, the projected 21st-century global warming lies within the potential range of the SSP3-7.0 scenario, increasing the urgency to better understand and represent vulnerable climate components.

*Code and data availability.* The code for FESOM can be accessed from the esm-tool at https://github.com/esm-tools/esm_tools (last access 01.08.2024). The Matlab codes used for the analysis of the model output will be made available upon request to the corresponding author.

The CCLM model is available from the CCLM community website: https://clmcom.scrollhelp.site/clm-community (last access: 07 August 2024). CCLM data are available in the DKRZ long-term archive: https://hdl.handle.net/21.14106/cb44f718061ed8e9cdeb574d51113b64ec781564 (last access: 07 August 2024, (Zentek and Heinemann, 2023)).

https://doi.org/10.5194/egusphere-2024-2873
Preprint. Discussion started: 26 September 2024


*Author contributions.* VT ran the FESOM simulations, conducted the analyses, and prepared the figures. CN and VT prepared the FESOM model code. GH and RZ prepared the CCLM model code and ran the simulations. VT, RT and TS contributed to the interpretation of the results. All authors contributed to the writing and editing of the manuscript.

*Competing interests.* The authors declare no competing interests.

*Acknowledgements.* This work was funded by Deutsche Forschungsgemeinschaft SPP 1158 under grants SE2901/2, HE2740/33 and TI296/9. CCLM simulations used resources of the Deutsches Klimarechenzentrum (DKRZ) granted by its Scientific Steering Committee (WLA) under project ID bb0958.

https://doi.org/10.5194/egusphere-2024-2873
Preprint. Discussion started: 26 September 2024


## References

Årthun, M., Nicholls, K.-W., Makinson, K., Fedak, M.-A., and Boehme, L.: Seasonal inflow of warm water onto the southern Weddell Sea continental shelf, Antarctica, Geophysical Research Letters, 39(17), 2–7, https://doi.org/10.1029/2012GL052856, 2012.

Baines, P.: A model for the structure of the Antarctic Slope Front, Deep Sea Research Part II: Topcial Studies in Oceanography, 56, 859–873, 2009.

Beadling, R. L., Krasting, J. P., Griffies, S. M., Hurlin, W. J., Bronselaer, B., Russell, J. L., MacGilchrist, G. A., Tesdal, J., and Winton, M.: Importance of the Antarctic Slope Current in the Southern Ocean Response to Ice Sheet Melt and Wind Stress Change, Journal of Geophysical Research: Oceans, 127, e2021JC017 608, 2022.

Calvin, K., Dasgupta, D., Krinner, G., Mukherji, A., Thorne, P. W., Trisos, C., Romero, J., Aldunce, P., Barrett, K., Blanco, G., Cheung, W. W., Connors, S., Denton, F., Diongue-Niang, A., Dodman, D., Garschagen, M., Geden, O., Hayward, B., Jones, C., Jotzo, F., Krug, T., Lasco, R., Lee, Y.-Y., Masson-Delmotte, V., Meinshausen, M., Mintenbeck, K., Mokssit, A., Otto, F. E., Pathak, M., Pirani, A., Poloczanska, E., Pörtner, H.-O., Revi, A., Roberts, D. C., Roy, J., Ruane, A. C., Skea, J., Shukla, P. R., Slade, R., Slangen, A., Sokona, Y., Sörensson, A. A., Tignor, M., van Vuuren, D., Wei, Y.-M., Winkler, H., Zhai, P., Zommers, Z., Hourcade, J.-C., Johnson, F. X., Pachauri, S., Simpson, N. P., Singh, C., Thomas, A., Totin, E., Alegría, A., Armour, K., Bednar-Friedl, B., Blok, K., Cissé, G., Dentener, F., Eriksen, S., Fischer, E., Garner, G., Guivarch, C., Haasnoot, M., Hansen, G., Hauser, M., Hawkins, E., Hermans, T., Kopp, R., Leprince-Ringuet, N., Lewis, J., Ley, D., Ludden, C., Niamir, L., Nicholls, Z., Some, S., Szopa, S., Trewin, B., van der Wijst, K.-I., Winter, G., Witting, M., Birt, A., and Ha, M.: IPCC, 2023: Climate Change 2023: Synthesis Report. Contribution of Working Groups I, II and III to the Sixth Assessment Report of the Intergovernmental Panel on Climate Change [Core Writing Team, H. Lee and J. Romero (eds.)]. IPCC, Geneva, Switzerland., Tech. rep., Intergovernmental Panel on Climate Change, https://doi.org/10.59327/IPCC/AR6-9789291691647, 2023.

Cape, M. R., Vernet, M., Skvarca, P., Marinsek, S., Scambos, T., and Domack, E.: Foehn winds link climate-driven warming to ice shelf evolution in Antarctica, Journal of Geophysical Research: Atmosphere, 120, https://doi.org/10.1002/2015JD023465, 2015.

Daae, K., Hattermann, T., Darelius, E., Mueller, R., Naughten, K. A., and Timmermann, R. e. a.: Necessary Conditions for Warm Inflow Toward the Filchner Ice Shelf, Weddell Sea, Geophysical Research Letters, 47(22), e2020GL089 237, https://doi.org/10.1029/2020GL089237, 2020.

Danilov, S., Wang, Q., Timmermann, R., Iakovlev, N., Sidorenko, D., Kimmritz, M., Jung, T., and Schröter, J.: Finite-Element Sea Ice Model (FESIM), version 2, Geoscientific Model Development, pp. 1747–1761, 2015.

Darelius, E., Fer, I., and Nicholls, K.-W.: Observed vulnerability of Filchner-Ronne Ice Shelf to wind-driven inflow of warm deep water, Nature Communications, 7, 1–7, https://doi.org/10.1038/ncomms12300, 2016.

Dettling, N., Losch, M., Pollmann, F., and Kanzow, T.: Toward Parameterizing Eddy-Mediated Transport of Warm Deep Water across the Weddell Sea Continental Slope, Journal of Physical Oceanography, 54, 2024.

Dinniman, M., Klinck, J., Bai, L.-S., Bromwich, D., Hines, K. M., and Holland, D.: The effect of atmospheric forcing resolution on the delivery of ocean heat to the Antarctic floating ice shelves, Journal of Climate, pp. 6067–6085, https://doi.org/10.1175/JCLI-D-14-00374.1, 2015.

Dinniman, M. S., Klinck, J. M., and Hofmann, E. E.: Sensitivity of Circumpolar Deep Water Transport and Ice Shelf Basal Melt along the West Antarctic Peninsula to Changes in the Winds, Journal of Climate, 2012, 4799–4816, 2012.

Elvidge, A., Renfrew, I., King, J., Orr, A., and Lachlan-Cope, T.: Foehn warming distributions in non-linear and linear flow regimes: A focus on the Antarctic Peninsula, Quarterly Journal of the Royal Meteorological Society, 142, https://doi.org/10.1002/qj.2489, 2014.

https://doi.org/10.5194/egusphere-2024-2873
Preprint. Discussion started: 26 September 2024


Foldvik, A., Gammelsrø d, T., and Torresen, T.: Circulation and Water Masses on the Southern Weddell Sea Shelf, Oceanology of the Antarctic Continental Shelf, 43, 5–20, 1985.

Gill, A.: Circulation and bottom water production in the Weddell Sea, Deep-Sea Research and Oceanographic Abstracts, 20, 111–140, 1973.

Goyal, R., Sen Gupta, A., Jucker, M., and England, M. H.: Historical and Projected Changes in the Southern Hemisphere Surface Westerlies, Geophysical Research Letters, 48, 1–13, 2021.

Graham, J., Heywood, C., Chavanne, C. P., and Holland, P. R.: Seasonal variability of water masses and transport on the Antarctic continental shelf and slope in the southeastern Weddell Sea, Journal of Geophysical Research: Oceans, 118, 2201–2214, 2013.

Gurses, O., Kolatschek, V., Wang, Q., and Rodehacke, C. B.: Brief communication: A submarine wall protecting the Amundsen Sea intensifies melting of neighboring ice shelves, The Cryosphere, 13, 2317–2324, https://doi.org/10.5194/tc-13-2317-2019, 2019.

Haid, V., Timmermann, R., Ebner, L., and Heinemann, G.: Atmospheric forcing of coastal polynyas in the southwestern Weddell Sea, Antarctic Science, 27, 388–402, https://doi.org/10.1017/S0954102014000893, 2015.

Haid, V., Timmermann, R., Gurses, O., and Hellmer, H. H.: On the drivers of regime shifts in the Antarctic marginal seas, exemplified by the Weddell Sea, Ocean Science, 19, 1529–1544, https://doi.org/10.5194/os-19-1529-2023, 2023.

Hatterman, T.: Antarctic thermocline dynamics along a narrow shelf with easterly winds, Journal of Physical Oceanography, 48(10), 2419–2443, https://doi.org/10.1175/JPO-D-18-0064.1, 2018.

Hattermann, T.: Antarctic thermocline dynamics along a narrow shelf with easterly winds, Journal of Physical Oceanography, 48, 2419–2443, 2018.

Hattermann, T., Smedsrud, L. H., Nøst, O. A., Lilly, J. M., and Galton-Fenzi, B. K.: Eddy-resolving simulations of the Fimbul Ice Shelf cavity circulation: Basal melting and exchange with open ocean, Ocean Modelling, 82, 28–44, 2014.

Heinemann, G., Schefczyk, L., Willmes, S., and Shupe, M. D.: Evaluation of simulations of near-surface variables using the regional climate model CCLM for the MOSAiC winter period, Elementa: Science of the Anthropocene, 10, 1–22, 2022.

Hellmer, H. H. and Olbers, D. J.: A two-dimensional model for the thermohaline circulation under an ice shelf, Antarctic Science, 1, 325–336, https://doi.org/10.1017/S0954102089000490, 1989.

Hellmer, H. H., Kauker, F., Timmermann, R., Determann, J., and Rae, J.: Twenty-first-century warming of a large Antarctic ice-shelf cavity by a redirected coastal current, Nature, 485(7397), 225–228, https://doi.org/10.1038/nature11064, 2012.

Hellmer, H. H., Kauker, F., Timmermann, R., , and Hattermann, T.: The fate of the Southern Weddell sea continental shelf in a warming climate, Journal of Climate, 30(12), 4337–4350, https://doi.org/10.1175/JCLI-D-16-0420.1, 2017.

Heywood, K. J., Schmidtko, S., Heuzé, C., Kaiser, J., Jickells, T. D., Queste, B. Y., Stevens, D. P., Wadley, M., Thompson, A. F., Fielding, S., Guihen, D., Creed, E., Ridley, J. K., and Smith, W.: Ocean processes at the Antarctic continental slope, Philosophical Transactions of the Royal Society A, 372, 20130 047, https://doi.org/10.1098/rsta.2013.0047, 2014.

Holland, D. M. and Jenkins, A.: Modeling Thermodynamic Ice–Ocean Interactions at the Base of an Ice Shelf, Journal of Physical Oceanography, 29, 1787–1800, https://doi.org/10.1175/1520-0485(1999)029<1787:MTIOIA>2.0.CO;2, 1999.

Huneke, W. G. C., Morrison, A. K., and Hogg, A. M.: Spatial and Subannual Variability of the Antarctic Slope Current in an Eddying Ocean–Sea Ice Model, Journal of Physical Oceanography, 52, 347–361, 2022.

Kida, S.: The impact of open oceanic processes on the Antarctic Bottom Water outflows, Journal of Physical Oceanography, 41, 1941–1957, 2011.

Le Paih, N., Hattermann, T., Boebel, O., Kanzow, T., Lüpkes, C., Rohardt, G., Strass, V., and Herbette, S.: Coherent Seasonal Acceleration of the Weddell Sea Boundary Current System Driven by Upstream Winds, Journal of Geophysical Research: Oceans, 125, 1–20, 2020.

https://doi.org/10.5194/egusphere-2024-2873
Preprint. Discussion started: 26 September 2024


Lockwood, J. W., Dufour, C. O., Griffies, S. M., and Winton, M.: On the Role of the Antarctic Slope Front on the Occurrence of the Weddell Sea Polynya under Climate Change, Journal of Climate, 34, 2529–2548, 2021.

Mathiot, P., Goosse, H., Fichefet, T., Barnier, B., and Gallée, H.: Modelling the seasonal variability of the Antarctic Slope Current, Ocean Science, 7, 455–470, 2011.

Meinshausen, M., Nicholls, Z. R., Lewis, J., Gidden, M. J., Vogel, E., and Freund, M. e. a.: The shared socio-economic pathway (SSP) greenhouse gas concentrations and their extensions to 2500, Geoscientific Model Development, 13(8), 3571–3605, https://doi.org10.5194/gmd-13-3571-2020, 2020.

Naughten, K. A., De Rydt, J., Rosier, S. H. R., Jenkins, A., Holland, P. R., and Ridley, J. K.: Two-timescale response of a large Antarctic ice shelf to climate change, Nature Communications, 12(1), 1–10, https://doi.org/10.1038/s41467-021-22259-0, 2021.

Nissen, C., Timmermann, R., Hoppema, M., Gürses, Ö., and Hauck, J.: Abruptly attenuated carbon sequestration with Weddell Sea dense waters by 2100, Nature Communications, 13, 2022.

Nissen, C., Timmermann, R., Hoppema, M., and Hauck, J.: A regime shift on Weddell Sea Continental Shelves with Local and Remove Physical and Biogeochemical Implications is Avoidable in a 2°C Scenario, Journal of Climate, 36, 6613–6630, 2023.

Nissen, C., Timmermann, R., van Caspel, M., and Wekerle, C.: Altered Weddell Sea warm- and dense-water pathways in response to 21st-century climate change, Ocean Science, 20, 85–101, https://doi.org/10.5194/os-20-85-2024, 2024.

Nøst, O., Biuw, M., Tverberg, V., Lydersen, C., Hattermann, T., Zhou, Q., Smedsrud, L. H., , and Kovacs, K. M.: Eddy overturning of the Antarctic Slope Front controls glacial melting in the Eastern Weddell Sea, Journal of Geophysical Research, 116(C11014), 1–17, https://doi.org.de/10.1029/2011JC006965, 2011.

Ong, E. Q. Y., Doddridge, E., Constantinou, N. C., Hogg, A. M., and England, M. H.: Intrinsically Episodic Antarctic Shelf Intrusions of Circumpolar Deep Water via Canyons, Journal of Physical Oceanography, 54, 1195–1210, 2023.

Ou, H.: Watermass Properties of the Antarctic Slope Front: A Simple Model, Journal of Physical Oceanography, 37, 50–59, 2007.

Pauthenet, E., Sallée, J. B., Schmidtko, S., and Nerini, D.: Seasonal variation of the antarctic slope front occurrence and position estimated from an interpolated hydrographic climatology, Journal of Physical Oceanography, 51, 1539–1557, 2021.

Peña-Molino, B., McCartney, M. S., and Rintoul, S. R.: Direct observations of the Antarctic Slope Current transport at 113°E, Journal of Geophysical Research: Oceans, 121, 7390–7407, 2016.

Ryan, S., Hattermann, T., Darelius, E., , and Schröder, M.: Seasonal cycle of hydrography on the eastern shelf of the Filchner Trough, Weddell Sea, Antarctica, Journal of Geophysical Research: Oceans, 122(8), 6437–6453, https://doi.org/10.1002/2017JC012916, 2017.

Ryan, S., Hellmer, H. H., Janout, M., Darelius, E., Vignes, L., and Schröder, M.: Exceptionally Warm and Prolonged Flow of Warm Deep Water Toward the Filchner-Ronne Ice Shelf in 2017, Geophysical Research Letters, 47(13), 1–10, https://doi.org/10.1029/2020GL088119, 2020.

Schmidtko, S., Heywood, K. J., Thompson, A. F., , and Aoki, S.: Multidecadal warming of Antarctic waters, Science, 346(6214), 1227–1232, https://doi.org/10.1126/science.1256117, 2014.

Semmler, T., Danilov, S., Gierz, P., Goessling, H. F., Hegewald, J., and Hinrichs, C. e. a.: Simulations for CMIP6 With the AWI Climate Model AWI-CM-1-1, Journal of Advances in Modeling Earth Systems, 12(9), 1–34, https://doi.org/10.1029/2019MS002009, 2020.

Spence, P., Griffies, S. M., England, M. H., Hogg, A. M., Saenko, O. A., and Jourdain, N. C.: Rapid subsurface warming and circulation changes of Antarctic Coastal waters by poleward shifting winds, Geophysical Research Letters, 41, 4601–4610, 2014.

Spence, P., Holmes, R. M., Hogg, A. M., Griffies, S. M., Stewart, K. D., and England, M. H.: Localized rapid warming of West Antarctic subsurface waters by remote winds, Nature Climate Change, 7, 595–603, 2017.

https://doi.org/10.5194/egusphere-2024-2873
Preprint. Discussion started: 26 September 2024


St-Laurent, P., Klinck, J. M., and Dinniman, M. S.: On the role of coastal troughs in the circulation of warm circumpolar deep water on Antarctic shelves, Journal of Physical Oceanography, 43, 51–64, 2013.

Steger, C. and Bucchignani, E.: Regional Climate Modelling with COSMO-CLM: History and Perspectives, Atmosphere, 11, 2020.

Stewart, A. and Thompson, A.: Eddy-mediated transport of warm Circumpolar Deep Water cross the Antarctic Shelf Break, Geophysical Research Letters, 42, 432–440, 2015a.

Stewart, A. and Thompson, A.: The Neutral Density Temporal Redidual Mean overturning circulation, Ocean Modelling, 90, 44–56, 2015b.

Stewart, A., Klocker, A., and Menemenlis, D.: Acceleration and Overturning of the Antarctic Slope Current by Winds, Eddies, and Tides, Journal of Physical Oceanography, 49, 2043–2074, 2019.

Sverdrup, H.: The Currents off the Coast of Queen Maud Land, Norsk Geografisk Tidsskrift - Norwegian Journal of Geography, 14, 1954.

Teske, V., Timmermann, R., and Semmler, T.: Subsurface warming in the Antarctica's Weddell Sea can be avoided by reaching the 2°C warming target, Communications Earth & Environment, 5, 93, 2024.

Thompson, A. F., Stewart, A. L., Spence, P., and Heywood, K. J.: The Antarctic Slope Current in a Changing Climate, Reviews of Geophysics, 56, 741–770, 2018.

Timmermann, R. and Goeller, S.: Response to Filchner-Ronne Ice Shelf cavity warming in a coupled ocean-ice sheet model - Part 1: The ocean perspective, Ocean Science, 13(5), 765–776, https://doi.org/10.5194/os-13-765-2017, 2017.

Timmermann, R. and Hellmer, H. H.: Southern Ocean warming and icreased ice shelf basal melting in the twenty-first and twenty-second centuries based on coupled ice-ocean finite-element modelling, Ocean Dynamics, 63(9-10), 1011–1026, https://doi.org/10.1007/s10236-013-0642-0, 2013.

Timmermann, R., Wang, Q., and Hellmer, H.: Ice-shelf basal melting in a global finite-element sea-ice/ice-shelf/ocean model, Ann. Glaciol., 53, 303–314, 2012.

Van Lipzig, N. P. M., King, J. C., Lachlan-Cope, T. A., and van den Broeke, M. R.: Precipitation, sublimation, and snow drift in the Antarctic Peninsula region from a regional atmospheric model, Journal of Geophysical Research, 109, D24 106, https://doi.org/10.1029/2004JD004701, 2004.

Van Wessem, J. M., Reijmer, C. H., van de Berg, W. J., van den Broeke, M. R., J., C. A., van Ulft, L. H. E., and van Meijgaard, E.: Temperature and Wind Climate of the Antarctic Peninsula as Simulated by a High-Resolution Regional Atmospheric Climate Model, Journal of Climate, 28, 1831–1844, 2015.

Wang, Q., Danilov, S., Sidorenko, D., Timmermann, R., Wekerle, C., and Wang, X. e. a.: The Finite Element Sea Ice-Ocean Model (FESOM) v.1.4: Formulation of an ocean general circulation model, Geoscientific Model Development, 7(2), 663–693, https://doi.org/10.1175/JCLI-D-16-0420.1, 2014.

Zentek, R. and Heinemann, G.: Verification of the regional atmospheric model CCLM v5.0 with conventional data and Lidar measurements in Antarctica, Geosci. Model Dev, 13, 1809–1825, 2020.

Zentek, R. and Heinemann, G.: COSMO-CLM REDOCCA Simulation (Version 2), https://hdl.handle.net/21.14106/cb44f718061ed8e9cdeb574d51113b64ec781564, 2023.

**Acknowledgements**

First and foremost I would like to thank my supervisors Ralph Timmermann and Tido Semmler for their unwavering support over the last years. Without them I surely would have given up on more than a few occasions. Thank you for the time spent bug hunting, discussing scientific and not so scientific questions, and just talking about life, the universe and all the rest.

A huge thank you goes also to Prof. Thomas Jung for giving me the opportunity to be part of the Climate Dynamics section and for the often needed reminder to keep the big picture in mind, when I was lost in the nitty-gritty details (again). I would also like to thank Prof. Günther Heinemann and Rolf Zentek for many fruitful discussions about local and regional atmospheric phenomena and polynya processes. And for a nice evening in Trier.

Thanks as well to Cara Nissen, Claudia Wekerle, Verena Haid and all the others who were always available when I had a small or large question, or just wanted someone to talk to. Thanks to the RIO people who gave ideas and help when needed, and the whole Climate Dynamics section for their support.

And special thanks to my wonderful wife Fiona for putting up with me when I could only talk about the latest bug bugging me.